Genetic and molecular mechanisms underlying spinocerebellar ataxias

Jezierska, Justyna

Genetic and molecular mechanisms underlying spinocerebellar ataxias

Justyna Jezierska

Phd thesis – Department of Genetics

University Medical Center Groningen, University of Groningen

Groningen, The Netherlands

This study was financially supported by University of Groningen and Research Institute GUIDE.

Cover design and book layout:  Lovebird design and printing solutions (www.lovebird-design.com)

Printed by: EIKON

Printing of the thesis was financially supported by University of Groningen, GUIDE and Department of Genetics, UMCG.

RIJKSUNIVERSITEIT GRONINGEN

Genetic and molecular mechanisms underlying spinocerebellar ataxias

Proefschrift

ter verkrijging van het doctoraat in de
Medische Wetenschappen
aan de Rijksuniversiteit Groningen
op gezag van de
Rector Magnificus, dr. E. Sterken,
in het openbaar te verdedigen op
maandag 23 september 2013
om 11.00 uur

door

Justyna Jezierska

geboren op 10 april 1985

te Warszawa, Polen

Promotores:	Prof. dr R. Sinke
	Prof. dr H.H. Kampinga
Co-Promotor:	Dr. D.S. Verbeek
Beoordelingscommissie:	Prof.dr H. van Bokhoven
	Prof.dr H.P.H. Kremer
	Prof.dr O.C.M. Sibon

ISBN: 978-90-367-6373-8

CONTENTS

CHAPTER 1:

General introduction and outline of the thesis 7

CHAPTER 2:

SCA14 mutation V138E leads to partly unfolded PKCγ associated with an exposed C-terminus, altered kinetics, phosphorylation and enhanced insolubilization 27

CHAPTER 3:

Mutations in potassium channel KCND3 cause spinocerebellar ataxia type 19 45

CHAPTER 4:

Prodynorphin mutations cause the neurodegenerative disorder spinocerebellar ataxia type 23 63

CHAPTER 5:

Identification and characterization of novel PDYN mutations in dominant cerebellar ataxia cases 81

CHAPTER 6:

Elevated Dynorphin A levels lead to Purkinje cell loss in spinocerebellar ataxia type 23 mice 91

CHAPTER 7:

SCA23-mutant Dynorphin A peptides cause cell death via non-opioid excitotoxic mechanisms 101

CHAPTER 8:

Conclusions, General Discussion and Future Perspectives 129

PODSUMOWANIE 141

SAMENVATTING 146

SUMMARY 149

ACKNOWLEDGEMENTS 152

List of Abbreviations

AD = Alzheimer's disease
ADCA = autosomal dominant ataxia
ALS = amyotrophic lateral sclerosis
AMPAR = α-amino-3-hydroxy-5-methyl-4-isoxazolepropionic acid receptor
Ca^{2+} = calcium
CF = climbing fiber
DAG = diacylglycerol
Dyn = dynorphin
EAAT = excitatory amino acid transporter
ER = endoplasmic reticulum
ERAD = endoplasmic reticulum-associated degradation
GC = granule cell
HD = Huntington's disease
IP_3 = inositol-triphosphate
IP_3R = inositol-triphosphate receptor
iPS = induced pluripotent
KChIP = K_v channel-interacting protein
KOR = kappa-opioid receptor
K_v = voltage-gated potassium channel
LTD= long-term depression
LTP = long-term potentiation
mGluR = Group I metabotropic glutamate receptors
ML = molecular layer
NAc = nucleus accumbens
NGS = next-generation sequencing
NMDAR = *N*-methyl-$_D$-aspartate receptor
NSC = neuronal stem cell
PC = Purkinje cell
PD = Parkinson's disease
PDK1 = Phosphoinositide-dependent kinase-1
PDYN = prodynorphin
PF = parallel fiber
PFC = prefrontal cortex
PI = propidium iodide
PKC = protein kinase C
PKCγ = protein kinase C gamma
PLC = phospholipase C
polyQ = polyglutamine
SCA = spinocerebellar ataxia
UTR = untranslated region
WT = wild type

CHAPTER 1

General introduction and outline of the thesis

Spinocerebellar ataxias

Neurodegenerative disorders, such as Alzheimer's disease (AD), Parkinson's disease (PD), Huntington's disease (HD), amyotrophic lateral sclerosis (ALS), and spinocerebellar ataxias (SCAs), are a group of diseases that remain incurable despite the enormous research effort into the underlying pathological mechanisms. The pathology includes progressive neuronal cell death, hence the name "neurodegeneration", but the underlying cause is still mainly unknown.

SCAs are autosomal dominant disorders that lead to the atrophy of Purkinje cells (PCs) in the cerebellar cortex and successive neuronal loss in spinocerebellar tracks. The disease pathology is characterized by cerebellar ataxia, which means unsteady gait, clumsiness and eye movement defects (dysarthria). This ataxic disorder can be accompanied by various other symptoms including cognitive impairment, epilepsy, peripheral neuropathy or psychiatric problems, correlated with neuronal loss in other brain regions. Onset of the disease symptoms is usually in third or fourth decade of life [1].

The first neurological ataxic phenotype classification was proposed by Harding and it divides the autosomal dominant ataxias (ADCA) into three clinical subgroups (ADCA I-III; **Table 1**) [1]. This classification is sometimes still used, but it is not that useful as not all SCA phenotypes fit exactly into the three defined subgroups. Additionally, the genetic mechanisms underlying particular types of SCA do not correlate with Harding's classification. For instance, the ADCA I subgroup comprises SCA types caused by coding and non-coding repeat expansions and conventional mutations. The current classification of the SCAs is therefore based on the underlying genetic defect and the definitive diagnosis relies on the outcome of the genetic analysis.

Table 1 The autosomal dominant cerebellar ataxia (ADCA) classification of Harding (1982) [2]

	SCA type	Clinical manifestations
ADCA I	1-4, 8, 10, 12-23, 25, 27, 28, DRPLA	Complex (spinal cord syndromes, peripheral nerve disease, cognitive impairment, ophthalmologic signs, psychiatric problems and seizures)
ADCA II	7	Pigmentary maculopathy
ADCA III	5, 6, 11, 26, 29, 30, 31	"Pure" cerebellar

SCA is genetically a very heterogeneous group of diseases (**Fig. 1**), and to date 32 different subtypes of SCA have been recognized (SCA9 and SCA33 are unassigned, SCA15 and 16 were proved to be allelic, also SCA19 and 22 were linked to the same gene, and SCA24 was proved to be recessively inherited) (**Table 2**). The disease gene has been identified for 22 SCA types. Phenotypically similar SCAs are not only caused by mutations in various genes, but the mutation mechanism can also be different, including coding and non-coding repeat expansions, missense and nonsense mutations, deletions and duplications.

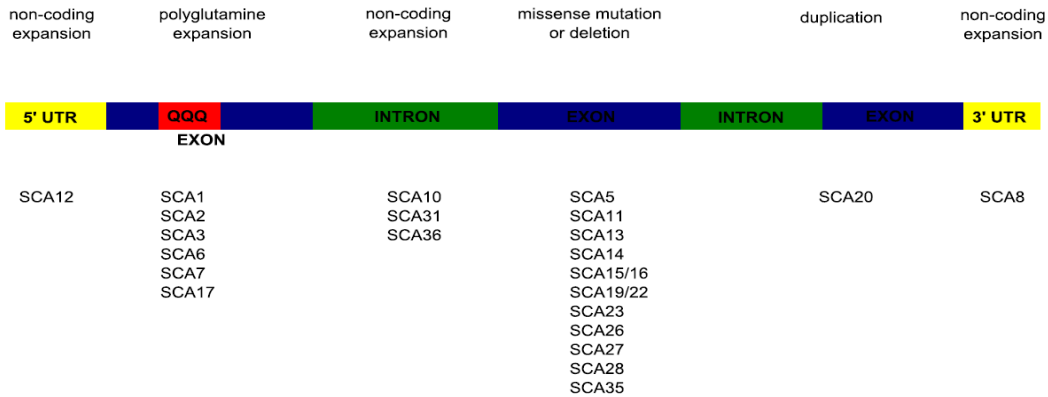

Fig. 1 Localization of various spinocerebellar ataxias-associated mutations in different gene regions.

Despite the recent advances in genetic techniques, the genetic diagnosis for SCA remains problematic. Screening of the more common SCA genes (SCA types 1-3, 6, 7, 12, 14, and 17) yields mutations in only 60-70% of the cases. Additionally, the identification of new disease genes is not always straightforward, as even after the disease locus has been mapped, the disease genes cannot always be found in the linkage regions. These loci are often large and contain too many candidate genes, which cannot be screened individually as this is too costly and labour-intensive. The development of deep sequencing technologies has greatly advanced the search for mutations and led to the identification of new genes in which mutations are responsible for SCAs, including SCA19/22 (**Chapter 3**), SCA26 [3], and SCA35 [4].

SCAs caused by polyglutamine repeat expansions

The most common genetic cause of SCA is the expansion of a coding CAG trinucleotide repeat tract resulting in abnormally long polyglutamine (polyQ) stretches in the corresponding proteins. This expansion is associated with SCA1-3, 7, 6, and 17 (and occurs in exons of the genes encoding for ataxin-1, 2, 3 and 7, $Ca_V2.1$, and TBP, respectively) [5-11].

These SCA types are therefore considered to be polyQ diseases, just like HD, spinal and bulbar muscular atrophy (SBMA), and dentatorubral pallidoluysian atrophy (DRPLA) [12]. In polyQ diseases, the expansion of the CAG repeat tract has to surpass a certain threshold to become pathological (reviewed in [13]). The size of the CAG repeat tract and age of disease onset are negatively correlated (when the repeat tract is not interrupted) [1], with longer repeat tracts associated with earlier disease onset. Another feature of polyQ diseases is genetic anticipation (with paternal transmission), which means that in each subsequent generation, the disease onset occurs earlier and with more severe symptoms, and this is correlated with longer CAG repeat tracts [1]. Discrepancies in these correlations (between severity of the symptoms and CAG repeat length) were reported, caused by alternate codons disrupting the expanded CAG repeat tract (interrupted alleles) [14].

Table 2 Overview of the genes and mutation effects in different types of SCAs

SCA	Locus	Gene	Type of mutations	References
SCA1	6p22.3	ATXN1	Coding CAG expansion	[5]
SCA2	12q24.13	ATXN2	Coding CAG expansion	[6]
SCA3/MJD	14q32.12	ATXN3	Coding CAG expansion	[8]
SCA4	16q22.1	unknown	-	[91]
SCA5	11q13.2	SPTBN2	Deletion, missense mutation	[35]
SCA6	19p13.13	CACNA1A	Coding CAG expansion	[9]
SCA7	3p14.1	ATXN7	Coding CAG expansion	[92]
SCA8	13q21	ATXN8	3' UTR repeat expansion	[93]
SCA10	22q13.31	ATXN10	intronic repeat expansion	[18], [94]
SCA11	15q14-21.3	TTBK2	Deletion*, nonsense mutation	[95], [96]
SCA12	5q32	PPP2R2B	5' UTR repeat expansion	[19]
SCA13	19q13.33	KCNC3	Missense mutation	[37]
SCA14	19q13.42	PRKCG	Missense mutation	[38]
SCA15/16	3q24.2-pter	ITPR1	Deletion, missense mutation	[97], [98]
SCA17	6q27	TBP	Coding CAG expansion	[99]
SCA18	7q31-32	unknown	-	[100]
SCA19/22	1p21-q21	KCND3	Missense mutation	[101], [102], [103], [104]
SCA20	11p11.2	unknown	Duplication	[40]
SCA21	7p21.3-15.1	unknown	-	[105]
SCA23	20p13-12.2	PDYN	Missense mutation	[106]
SCA25	2p21-15	unknown	-	[107]
SCA26	19p13.3	EF2	Deletion, missense mutation	[108], [3]
SCA27	13q13.1	FGF14	Missense mutation	[109]
SCA28	18p11.21	AFG3L2	Missense mutation	[110], [54]
SCA29	3p26-pter	unknown	-	[111]
SCA30	4q34.3-q35.1	unknown	-	[112]
SCA31	16q22.1	TK2, BEAN	Intronic insertion of repeats	[20]
SCA32	7q32	unknown	-	
SCA34#	6q12.3-q16.2	unknown	-	[113]
SCA35	20p13-12.2	TGM6	Missense mutation	[44]
SCA36	20p13	NOP56	Intronic repeat expansion	[21]
SCA37	1p32	unknown	-	[114]

* leading to premature codon stop and expression of truncated protein #Reserved lately, not yet published [57]

The coding CAG repeat expansion is thought to be a toxic gain-of-function mutation, as proteins with expanded polyQ stretches show pathological interactions with other proteins, are prone to aggregate, and subsequently form cytoplasmic or intranuclear inclusions [15]. Although the precise mechanisms by which these expanded proteins exert toxicity is still unknown, the aggregates are known to sequester important proteins for cell function, such as transcription factors, chaperones and members of degradation systems (i.e. proteasomes and ubiquitin ligases), leading to depletion of these factors in the cell [12]. The trapped chaperones and proteasomes can no longer perform their function, what induces further accumulation of misfolded and un-degraded proteins. Sequestration of transcription factors results in dysregulation of important pathways and subsequent cell death (reviewed in [16] and [12]). The protein aggregates may also physically disrupt intracellular membranes, leading to mitochondrial dysfunction, or hinder axonal transport (reviewed in [12]), and as such impair neuronal

functioning and cause degeneration.

The toxic structure of the aggregated polyQ proteins is not sufficient to explain the selective neurodegeneration of specific brain areas and neuronal populations. Despite the fact that many of the disease-related proteins are ubiquitously expressed through the whole central nervous system, specific subpopulations of neurons are affected, for example, striatal neurons in HD, and PCs in SCA. Therefore, other, context-dependent factors probably trigger the disease-related neurodegeneration.

SCAs caused by non-coding repeat expansions

Besides coding expansions, other SCA types such as SCA8, 10, 12, 31 and 36 (**Table 2**) are caused by non-coding repeat expansions, leading to the transcription of abnormally long RNA molecules [16-21]. SCA8 and SCA12 are caused by triplet (CTG/CAG) repeat expansions in the 3' untranslated region (UTR) of the *SCA8* gene of unknown function and 5' UTR of the *PPP2R2B* gene encoding for brain-specific regulatory subunit of phosphatase PP2A, respectively [22, 23]. SCA10 is caused by a very long expansion of the pentanucleotide repeat ATTCT in intron 9 of *ATXN10* (also of unknown function). SCA31 is caused by a pentanucleotide TGGAA repeat insertion in intron of overlapping genes *BEAN* (brain-expressed gene associated with Nedd4) and *TK2* (encoding for thymidine kinase 2) which are transcribed in opposite directions [20]. SCA36 is caused by large expansions of a GGCCTG repeat tract in the first intron of the *NOP56* gene, encoding for nucleolar protein 56 involved in biogenesis of ribosomal RNA [24].

In SCA10 and 31 the repeat length negatively correlates with the age of disease onset, while anticipation with paternal transmission was reported for SCA31 [18, 20]. In SCA8, 12 and 36 there is no clear correlation between the repeat length and age of onset or severity of the disease [23-25].

For non-coding repeat expansion-associated SCAs, a toxic RNA-gain-of-function mechanism was proposed, in which the repeat expansions are toxic on the RNA level. Abnormally long RNA molecules often accumulate in RNA foci, as has been described in SCA8, 10, 31, and 36 [20, 21, 26]. However, how and if these RNA foci cause neuronal dysfunction and subsequent cell death is still unclear and needs to be determined. One of the hypotheses is that these RNA foci sequester important RNA-binding proteins leading to transcription and splicing dysregulation, which might contribute to disease pathogenesis [20]. For example, the expanded ATXN10 RNA accumulates in PCs and binds to heteronuclear ribonuclear protein K (hnRNP K) causing loss of its function and subsequent cell death [16, 27]. In SCA8, the SCA8 transcript is an antisense RNA to Kelch-like protein-1 gene (*KLHL1*) [28] and controls the expression of KLHL1 protein, which is suggested to be important for stabilizing calcium (Ca^{2+}) channels on the neuronal membrane. Expansion in SCA8 RNA causes *KLHL1* silencing [29, 30]. Moreover, the SCA31 insertion contains a paracentromeric satellite sequence of a pentanucleotide TGGAA repeat that might have an essential role in the maintenance of chromatin conformation [20]. It has also been proposed that this mutation alters the expression of other, neighbouring genes by inducing structural changes in DNA structure, leading to a conformational change that is hardly recognizable by transcription factors, such as non-B DNA [20].

SCA8 and 12 are unique among the SCAs caused by the non-coding expansions. In SCA8, the bidirectional

transcription through the repeat region results in two overlapping mechanisms: a toxic RNA gain-of-function and a toxic protein gain-of-function through polyQ expanded protein (reviewed in [31]). However, some controversy exists about the pathogenicity of this non-coding repeat expansion, as expanded SCA8 alleles have been found to be more common in patients suffering from other types of SCAs, including SCA1 and 6 [32, 33]. In SCA12, the pathology does not seem to be associated with the RNA, but only with the protein. The SCA12-associated repeat expansion results in overexpression of the PP2A phosphatase regulatory subunit that is important for mitochondria fusion-fission homeostasis [34].

SCA types caused by missense mutations and chromosomal rearrangements (conventional mutations)

Historically, SCAs were thought to be caused only by (tri-)nucleotide repeat expansions. However, the more recently identified SCA mutations are mainly either missense mutations or chromosomal rearrangements, such as deletions or duplications, that can be found in SCA5, 11, 13, 14, 15/16, 19/22 (**Chapter 3**), 20, 23 (**Chapter 4**), 26, 27, 28 and 35 (**Table 2**), causing changes in the function of the corresponding proteins [3, 35-44].

In most cases, neuronal signalling pathways are compromised due to mutations in the genes encoding for potassium channels ($K_v3.3$ in SCA13 and $K_v4.3$ in SCA19/22), Ca^{2+} transporters (IP_3R in SCA15/16), proteins responsible for stabilizing receptors/channels on plasma membrane (βIII-spectrin in SCA5 and FGF14 in SCA27), proteins involved in intracellular signal transduction (TTBK2, PKCγ, and FGF14 in SCA11, SCA14, and SCA27, respectively), or proteins involved in mitochondrial energy pathways (AFG3L2 in SCA28). Since the disease proteins implicated in this subgroup have been identified only relatively recently and they show a fair degree of functional diversity, not much is known yet about the underlying pathomechanisms.

Loss-of-function and haploinsufficiency was proposed as the underlying cause of SCA5 [45, 46], SCA15/16 [47-49] and SCA28 [50]. In SCA28, partial loss of mitochondrial metalloproteinase AFG3L2 can result in respiratory chain dysfunction leading to PC death due to oxidative stress [50]. In SCA5, haploinsufficiency/loss of βIII-spectrin, which is important for stabilizing membrane proteins, causes alterations in glutamatergic transmission and subsequent Ca^{2+} imbalance due to loss of functioning glutamate receptors and transporters on the plasma membrane [45, 46]. SCA15/16-associated missense mutations in *ITPR1* encoding for inositol-triphosphate receptor (IP_3R) subunit were shown to cause loss of function of this transporter resulting in motor coordination problems in flies [48]. However, enhanced Ca^{2+} conductance of wild type subunits was observed in the presence of the SCA15/16-mutant subunits [47, 49], suggesting a gain-of-function mechanism or dominant negative effect. Moreover, SCA13-mutant potassium channel subunit $K_v3.3$ was shown to have a dominant-negative effect on wild type subunits and reduced neuronal excitability leading to locomotor dysfunction [51]. In SCA14, it was also proposed that mutant protein kinase C gamma (PKCγ) has a dominant-negative effect on wild type PKCγ molecules, leading to dysregulation of oxidative homeostasis, caspase activation and PCs degeneration [52].

Together, this evidence shows that SCAs caused by conventional mutations do not seem to have a directly identical underlying genetic mechanism.

Prevalence of SCAs

SCA is a rare disorder that occurs between 1 and 3 per 100,000 people in Europe [2]. However, the prevalence of particular SCA types can vary drastically in different populations, probably due to founder effects. For instance, SCA3 frequency was calculated to be ~1.5% of all SCA cases in South Africa, but ~60% in Brazil and Portugal [53]. Worldwide the polyQ-related SCAs are more common (**Fig. 2**), with SCA3 as the most frequent type, representing 44% of all SCA cases in Europe [1]. The incidence of the more recently identified SCA types caused by conventional mutations also seems to be highly variable based on geographical location/population, but it is difficult to establish accurately due to the low numbers of affected families and family members. The worldwide prevalence is only known for three SCA types: for SCA14 it was calculated to be 1.5% of all SCA cases (<1% in Europe [1]), for SCA15/16 1% (3% in Europe [1]), and for SCA28 3% (1.5% in Europe [54]) (see www.internaf.org).

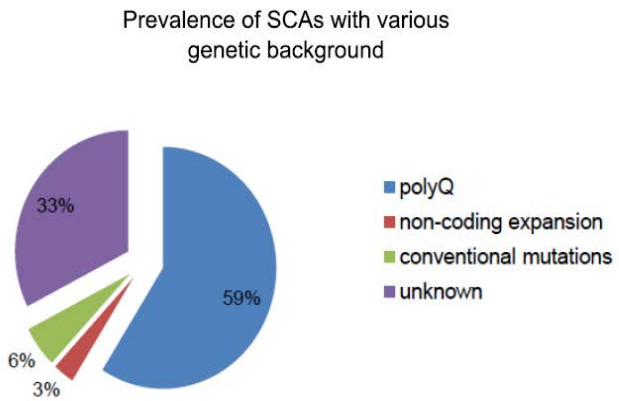

Fig. 2 Worldwide prevalence of spinocerebellar ataxias with different underlying genetic mechanisms (according to [1] and www.internaf.org).

Pathology of SCAs

The different SCA mutations seem to be correlated with slightly different disease manifestations [1, 55-57]. In SCAs caused by coding repeat expansions, the ataxic phenotype was accompanied by additional pathological features like peripheral neuropathy in SCA3 or retinal degeneration in SCA7, and, in addition to the pronounced cerebellar degeneration, it also displayed widespread brain degeneration (**Fig. 3**). In contrast, the SCAs caused by conventional mutations showed much purer cerebellar ataxia, with a slower disease progression and often later disease onset (**Table 3**) [1, 55-57]. Additionally, in these SCAs the neurodegeneration seems to be restricted to the cerebellum (**Fig. 3**).

Table 3

Difference in SCA caused by coding expansions and conventional mutations

	Coding expansions	Conventional mutations	Exceptions
Types of SCA	1, 2, 3, 6, 7, and 17	5, 11, 13, 14, 15/16, 19/22, 20, 23, 26, 27, 28, 35	
Prevalence	Common	Rare	
Anticipation	Yes	No	
Relative onset of symptoms	Earlier onset	Late onset	SCA6 (late); SCA11, SCA13 (earlier)
Disease progression	Fast	Slow	SCA6 (slow)
Relative severity of symptoms	More severe	Milder	
Neuropathology	Widespread	Isolated/global cerebellar	
Additional symptoms to cerebellar ataxia	Yes	No	SCA14, 15/16, 19/22, 20, 23, 27, 28 (yes)

[55, 56]

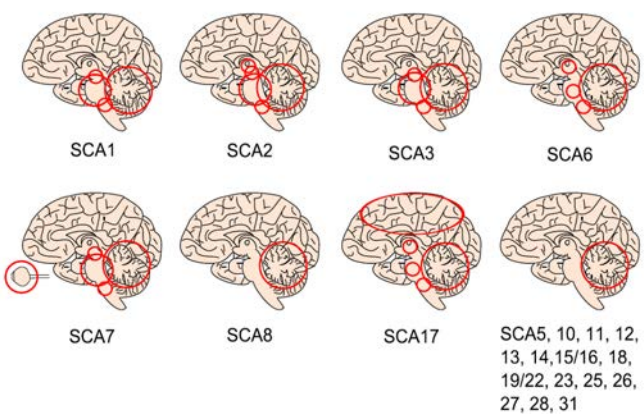

Fig. 3 Brain neurodegeneration regions in various types of SCAs.

Illustrations represent midsaggittal sections through the cerebrum, cerebellum and brainstem of human brain. Red circles indicate regions of neuronal loss in SCA1, 2, 3, 6, 7, 8, 17, and pure cerebellar SCAs, including loss in the cerebral cortex, thalamus, cerebellum and brainstem. Figure adapted with permission from [57].

The wide functional range of genes implicated in SCA indicate that multiple pathways can cause degeneration of PCs and induce the cerebellar dysfunction underlying the ataxic phenotype (**Table 4**). However, common pathomechanisms leading to SCA were also suggested [12, 13, 16, 58]. The pure cerebellar phenotype of SCAs associated with conventional mutations offers the rare opportunity to study the PC pathophysiology

underlying ataxia without the additional pathological features involved in other, repeat expansion-related SCA types. Why SCA pathology is restricted primarily to PCs is still an open question and will be discussed below.

Table 4 Pathomechanisms underlying different types of SCAs

	SCA types associated with:		
	Coding expansions	Non-coding expansions	Conventional mutations
Protein aggregation	SCA1, 2, 3, 7, 17	SCA8	-
RNA foci	-	SCA8, 10, 31, 36	-
Transcription dysregulation and RNA alterations	SCA1, 2, 3, 7, 17	SCA8, 10, 31, 36	-
Disturbance of calcium homeostasis	SCA2, 6	SCA12	SCA5, 13, 14, 15/16, 27
Problems with synaptic transmission	SCA1, 3, 7, 17	-	SCA5
Mitochondrial dysfunction	SCA2, 6, 7	SCA12	SCA28
Axonal transport deficits	-	-	SCA5, 11
Channelopathy	SCA6	-	SCA13, 19/22

[1, 55, 56]

Purkinje cell signalling

PCs represent the sole inhibitory output of the motor cortex, thus a functional deficit of these cells is directly associated with the impairment of motor coordination, as observed in SCA patients [59]. PCs form a one-cell layer in the cerebellum localized between the granule cell (GC) layer and molecular layer (ML, **Fig. 4**). They play a critical role in integrating cortical signals in the regulation of motor function and motor learning [60]. PCs receive stimulating glutamate-mediated input from parallel fibers (PFs, the axons of GCs) and climbing fibers (CFs, axons from inferior olive; **Fig. 4**). Stimulation of ionotropic glutamate receptors leads to ion fluxes and depolarization of the PC membranes, which subsequently activates voltage-dependent Ca^{2+} channels (**Fig. 5**) [59, 61, 62]. The major Ca^{2+} channel that takes part in this step of glutamate/Ca^{2+} signalling belongs to the P/Q-type channel family ($Ca_v2.1$, a subunit of this channel, is directly associated with SCA6). Activation of P/Q-type channels results in a local increase in intracellular Ca^{2+} concentration, which is important for local signalling [60, 61, 63]. Glutamate-mediated stimulation of Group I metabotropic glutamate receptors (mGluR1 and 5) provides a signal for activation of phospholipase C (PLC), which produces diacylglycerol (DAG) and inositol-triphosphate (IP_3). DAG is known to activate protein kinase C (PKCγ; SCA14) and IP_3 binds to its receptor (IP_3R; SCA15/SCA16) that acts as a signal for release of Ca^{2+} from the endoplasmic reticulum (ER) [60, 61]. Ca^{2+} signalling regulates the inhibitory activity of PCs and is also important for the formation of the specific, fast-repetitive, firing patterns of these neurons [60].

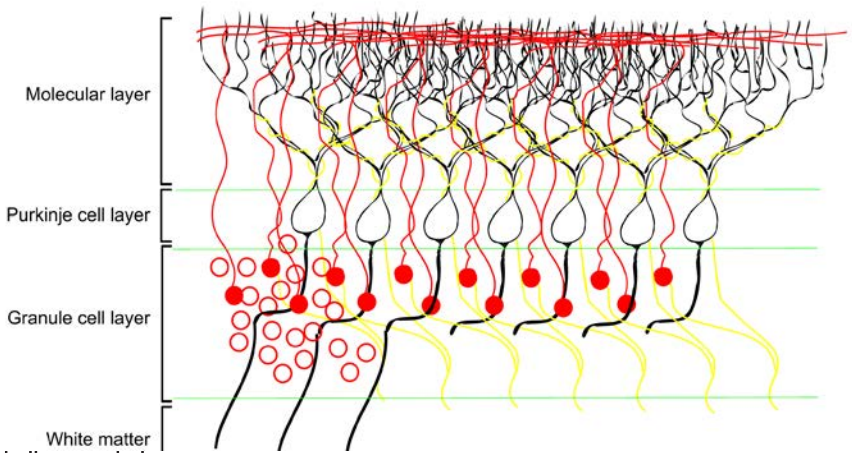

Fig. 4 Cerebellar morphology.

Like the cerebrum, the cerebellum has an outer cortex, an inner white matter, and deep nuclei below the white matter. The illustration shows layers of cerebellar folds: molecular layer (dendritic trees of Purkinje cells), Purkinje cell layer (cell bodies of Purkinje cells), granule cell layer, and white matter.

Neuronal calcium homeostasis and excitotoxicity

Neuronal Ca^{2+} influx is regulated via two distinct mechanisms (from extracellular space or intracellular ER stores [64-67]) and neurons tightly regulate these mechanisms to maintain low intracellular Ca^{2+} concentrations in the resting or almost inactive state (30-100 nM) [68]. Excitation will lead to a rise in cytoplasmic Ca^{2+}, ranging from highly localized, transient Ca^{2+} levels to long-lasting and more global alterations in the neuron [69]. Ca^{2+} has a wide range of downstream targets and signalling pathways, the activation of which depends on the source, timing, synchronicity, localization, and the final concentration of Ca^{2+} in the cytosol. The control of intracellular Ca^{2+} levels is thus crucial for neurons that are, therefore, equipped with pumps, exchangers, cytoplasmic Ca^{2+}-binding proteins, and display ER and mitochondrial Ca^{2+} sequestration [70-72]. Ca^{2+} imbalance is cytotoxic and marked alterations in Ca^{2+} homeostasis underlie neuronal cell death (reviewed in [73]). Marked increase in cytoplasmic Ca^{2+} levels triggers various neurotoxic pathways, including uncoupling of mitochondrial electron transfer from ATP synthesis, and activation of proteases, such as calpains, and other enzymes, including nitric oxide synthases, calcineurin or endonucleases [74]. These processes may all lead to energy loss, protein damage, oxidative stress or DNA fragmentation.

Excitotoxicity is suggested to be one of the common pathomechanisms leading to PC loss in SCA, by which excessive synaptic release of glutamate leads to dysregulation of intracellular Ca^{2+} homeostasis and cell death (reviewed in [73]). Postsynaptic ionotropic glutamate receptors, such as α-amino-3-hydroxy-5-methyl-4-isoxazolepropionic acid receptors (AMPARs) or *N*-methyl-$_D$-aspartate receptors (NMDARs) control PC Ca^{2+} signalling [74-76]. Activation of these receptors may lead to excitotoxicity through enhanced permeability for Ca^{2+} ions, causing intracellular Ca^{2+} overload and subsequently selective and progressive neuronal loss (reviewed in [74]). The alterations in glutamatergic/Ca^{2+} signalling have been reported in SCA1 [77], SCA5 [45, 46], SCA6

[78], and SCA15/16 [47]. Although Ca^{2+} dysregulation has been clearly linked to neurodegeneration, the exact mechanisms by which alterations in intracellular Ca^{2+} levels lead to selective PC death in SCA still remain unclear.

Purkinje cells vulnerability for calcium changes

PCs are the biggest cells in the brain, with large dendritic trees that receive massive excitatory input. One PC forms hundreds of thousands synapses with PFs and multiple synapses with CF, which are thought to be one of the strongest connections in human brain [63]. PCs are exposed to large amounts of intracellular Ca^{2+}, which can rise up to concentrations of 400 μM upon stimulation [79], while other neuronal cells show Ca^{2+} concentrations around 1 μM [79]. It was suggested earlier that PCs are specifically vulnerable for CF-hyperexcitability and die earlier than other neurons due to excitotoxicity, microglia activation, or axonal degeneration [80, 81].

The PC-specific excitatory amino acid transporter, EAAT4, could play an important role in PC excitotoxicity, as its main function is to remove excessive glutamate from the synaptic cleft and prevent sustained PC excitation and Ca^{2+} influx. Thus, EAAT4 has a neuroprotective role [82]. Notably, loss or altered trafficking of EAAT4 seem to be a common deficit in various SCA types [35, 83, 84]. This strengthens the hypothesis that excitotoxicity may be one of the major pathomechanisms underlying SCA disease.

Some SCA proteins are directly involved in Ca^{2+} signalling pathways, such as $Ca_v2.1$ in SCA6, and IP_3R in SCA15/16, or indirectly influence this pathway by stabilizing EAAT4, which controls the glutamate concentration in synaptic clefts, such as βIII-spectrin in SCA5, or by controlling the potassium flux that leads to suppression of the glutamate/Ca^{2+} signal, such as $K_v3.3$ in SCA13 (**Fig. 5**). Other SCA proteins are involved in intracellular signal transduction and synaptic transmission, including TTBK2 in SCA11, PKCγ in SCA14, and FGF14 in SCA27, or in mitochondrial homeostasis, such as AFG3L2 in SCA28 (**Fig. 5**). Clearly, alterations in intracellular Ca^{2+} concentrations contribute to the pathology of various SCA types, and this implies that deficits in Ca^{2+} homeostasis underlie PC degeneration.

Different models for SCA and their contribution to unravelling the pathways underlying the disease pathogenesis

Experimental model systems are used to study specific functional aspects of genes or proteins (often of unknown function) identified in neurodegenerative diseases. In general, such studies are carried out in cell culture, slices and organotypic cultures, and *in vivo*. Whilst the *in vitro* studies give insight into cellular and molecular mechanisms, experiments in whole living animals would reflect the human disease more closely, providing insights into physiological and phenotypical aspects of the disease. The best animal models are those which mimic the human disease in symptoms and development over time. However, in most cases, these models reflect only some aspects of the disease and provide only partial insight into the pathophysiology. For a full understanding of the pathomechanisms of SCA disease, studies on various models will be needed to provide complementary information that can be integrated into a satisfactory model of disease pathology.

To study the underlying mechanisms of neurodegenerative diseases including SCA, the *in vitro* models usually include neuronal cells (for a comparison of different model systems see **Table 5**), either immortalized

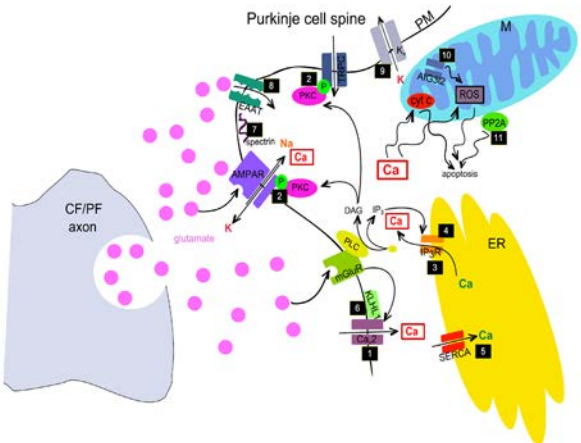

Fig. 5 Neuronal signalling on postsynaptic membrane of Purkinje cell.

The illustration shows various routes of Ca2+ entry and its further signalling after excitatory stimulation of ionotropic glutamate receptors (i.e. AMPAR) or metabotrobic glutamate receptors (mGluR1). The numbers indicate proteins involved in SCA pathology: 1) mutations in the gene encoding for Cav2.1 cause SCA6, 2) mutations in the gene encoding for PKCγ cause SCA14, 3) mutations in the gene encoding for IP3R cause SCA15/16, 4) changes in Ca2+ permeability of IP3R were reported in SCA2 and 3, 5) down-regulation of the gene encoding for Ca2+ pump SERCA1 is a hallmark of SCA1, 2, and 3, 6) the down-regulation of KLHL1, a protein stabilizing P/Q-type Ca2+ channels was reported in SCA8, 7) mutations in the gene encoding for βIII-spectrin, a protein stabilizing glutamate transporters on membrane, cause SCA5, 8) membrane deficits of EAAT4 are common in the pathology of SCA1, 5, and 23, 9) mutations in genes encoding for potassium channels cause SCA13 and SCA19/22, 10) mutations in metalloproteinase AFG3L2 cause SCA28 and disrupt fusion-fission balance of mitochondria, and 11) mutations in phosphatase PP2A cause SCA12 leading to excessive mitochondrial fission.

neuronal cell lines or primary cultures differentiated into neurons. Cell lines provide long-lasting and easy to manipulate tools, but they are genetically modified and hardly reflect the physiological situation. Primary cultures are more physiologically relevant, but the genetic manipulation is harder (transduction with viruses), the lifespan is limited, and the cells are not of human origin. Although improvements are still necessary in order to produce a reliable *in vitro* model that accurately reproduces the cellular mechanisms of neurodegeneration, the induced pluripotent (iPS) cells derived from SCA patients and differentiated into neurons seem to be the most relevant. This recently developed technique is not yet well established, but will probably be used more often in the future. The latest iPS cells derived from SCA2 patients offer means to study the concept of disease neuronal specificity, as SCA2 neuronal stem cells (NSCs) showed decreased levels of ataxin-2 and a shorter lifespan than control NSCs or SCA2 fibroblasts [85].

The *in vivo* models provide a more complex, tissue-dependent background of the disease and usually involve worms (*Caenorhabditis elegans*), fruit flies (*Drosophila melanogaster*), zebrafish (*Danio rerio*), or mice (*Mus musculus*), but they can be used only when the disease-associated protein and corresponding pathways are evolutionarily conserved. Worms, flies and zebrafish are easier to breed and have a higher number of progeny (summarized in **Table 5**). Moreover, worm- and zebrafish embryos are transparent, making *in situ* imaging easier. Worms and flies are well-established models for polyQ diseases, including SCA [86, 87], and provide a means of

validating genetic findings and of screening for genetic modifiers or chemical compounds that prevent or reduce disease symptoms [47, 48, 88]. The latter is usually obtained by monitoring the apparent signs of neurotoxicity in these models (motor phenotype impairment in both models; aggregation in worms, and retina degeneration in flies).

Table 5 Advantages of various models to study neurodegeneration

	In vitro		In vivo			
	Neuronal cell lines	iPS cells	Worms	Fruit flies	Zebrafish	Mice
Low relative cost	Yes		Yes	Yes	Yes	
Generation/ culturing/ breeding	Easy, short		Easy, short	Easy, short	Easy, short	
Manipulation	Easy		Easy	Easy	Easy	
Number of cells/ progeny	Many	Many	Many	Many	Many	
Variability	No/less	No/less				Yes
Lifespan			Short	Short	Short	Relative*
Vertebrates	-	-	No	No	Yes	Yes
Other		Patient-derived	Transparent	Big eyes	External development, transparent embryos	Mammals

* Physiologically-relative lifespan, the human disease span can be mimicked.

Although zebrafish are normally used to study developmental aspects of pathophysiology of diseases *in vivo* due to their relatively short lifespan and their transparent embryos and external development, recent studies on SCA13 [89] showed that this animal model can also be used for SCA research and that it is suitable for performing all types of experimental studies, including electrophysiological characterization, motor phenotyping, and protein tracking during and after embryonic development [51].

Mouse models are thought to be the most relevant for human disease studies, because they are not only vertebrates, but also mammals, and therefore closer to humans. Knock-out mice are relatively easier to obtain and were developed, for example, for SCA5 [46] and SCA6 [90], reflecting the disease symptoms seen in humans, including impaired motor coordination, changes in cerebellar and brain morphology, PC degeneration, and alterations in glutamatergic signalling. However, in the case of gain-of-function or dominant-negative mutations, the simple knock-out models are not sufficient. To study neurodegenerative diseases such as SCAs,

usually the knock-in or conditional transgenic animals are generated. Mice also offer the opportunity to study the disease in the context of population variability and provide a way of identifying disease dependence on tissue or cell types.

To study all the complexity of neurodegenerative diseases such as SCAs, one has to choose models that offer the best possibility of establishing valid correlations between molecular and cellular alterations and motor behaviour (the advantages of different models are summarized in **Table 5**).

Aim and overview of the thesis

The aim of this thesis was to unravel the genetic and molecular mechanisms underlying different types of SCA, with the main focus being on SCA23 and the pathology of the Dynorphin A peptide.

In Chapter 2, "**SCA14 mutation V138E leads to partly unfolded PKCγ associated with an exposed C-terminus, altered kinetics, phosphorylation and enhanced insolubilization**", I present the molecular mechanism underlying SCA14, in which the V138E mutation in PKCγ kinase causes an open protein, resulting in its aberrant maturation and processing. In Chapter 3, "**Mutations in voltage-gated potassium channel *KCND3* cause spinocerebellar ataxia type 19**", I describe the identification of the mutations/gene responsible for SCA19 and discuss the underlying molecular mechanism. In Chapter 4, "**Prodynorphin mutations cause the neurodegenerative disorder spinocerebellar ataxia type 23**", we found that the causative mutations for SCA23 are localized to the *PDYN* gene, which encodes for the precursor protein for opioid peptides. In Chapter 5, "**Identification and characterization of novel *PDYN* mutations in dominant cerebellar ataxia cases**", we studied the *PDYN* gene and sequenced 371 European ataxia patients in order to identify other mutations underlying SCA23. In Chapter 6, "**Elevated Dynorphin A levels lead to Purkinje cell loss in spinocerebellar ataxia type 23 mice**", I present the generation and characterization of our unique conditional transgenic mouse model for SCA23, which gives insights into the pathology underlying this disease, and, in Chapter 7, "**SCA23-mutant Dynorphin A peptides cause cell death via non-opioid excitotoxic mechanisms**", I discuss the molecular mechanisms of SCA23-mutant Dynorphin A action that lead to neurotoxicity. Finally, in Chapter 8, "**Conclusions, General Discussion and Future Perspectives**", I summarize and discuss the outcomes of the work on the different types of SCA caused by conventional mutations and the future perspectives for studying the pathology of SCAs. This work may eventually lead to new therapies to treat these devastating and incurable diseases.

References

1. Durr A. Autosomal dominant cerebellar ataxias: polyglutamine expansions and beyond. *Lancet Neurol* 2010; 9: 885-94.
2. Harding AE. The clinical features and classification of the late onset autosomal dominant cerebellar ataxias. A study of 11 families, including descendants of the 'the Drew family of Walworth'. *Brain* 1982; 105(Pt 1): 1-28.
3. Hekman KE, Yu GY, Brown CD et al. A conserved eEF2 coding variant in SCA26 leads to loss of translational fidelity and increased susceptibility to proteostatic insult. *Hum Mol Genet* 2012; 21: 5472-5483.
4. Wang JL, Yang X, Xia K et al. TGM6 identified as a novel causative gene of spinocerebellar ataxias using exome sequencing. *Brain* 2010; 133: 3510-3518.
5. Orr HT, Chung MY, Banfi S et al. Expansion of an unstable trinucleotide CAG repeat in spinocerebellar ataxia type 1. *Nat Genet* 1993; 4: 221-6.
6. Imbert G, Saudou F, Yvert G et al. Cloning of the gene for spinocerebellar ataxia 2 reveals a locus with high sensitivity to expanded CAG/glutamine repeats. *Nat Genet* 1996; 14: 285-91.
7. Pulst SM, Nechiporuk A, Nechiporuk T et al. Moderate expansion of a normally biallelic trinucleotide repeat in spinocerebellar ataxia type 2. *Nat Genet* 1996; 14: 269-76.
8. Kawaguchi Y, Okamoto T, Taniwaki M et al. CAG expansions in a novel gene for Machado-Joseph disease at chromosome 14q32.1. *Nat Genet* 1994; 8: 221-8.
9. Zhuchenko O, Bailey J, Bonnen P et al. Autosomal dominant cerebellar ataxia (SCA6) associated with small polyglutamine expansions in the alpha 1A-voltage-dependent calcium channel. *Nat Genet* 1997; 15: 62-9.
10. David G, Abbas N, Stevanin G et al. Cloning of the SCA7 gene reveals a highly unstable CAG repeat expansion. *Nat Genet* 1997; 17: 65-70.
11. Nakamura K, Jeong SY, Uchihara T et al. SCA17, a novel autosomal dominant cerebellar ataxia caused by an expanded polyglutamine in TATA-binding protein. *Hum Mol Genet* 2001; 10: 1441-8.
12. Takahashi T, Katada S, Onodera O. Polyglutamine diseases: where does toxicity come from? what is toxicity? where are we going? *J Mol Cell Biol* 2010; 2: 180-191.
13. Matilla-Duenas A, Sanchez I, Corral-Juan M, Davalos A, Alvarez R, Latorre P. Cellular and molecular pathways triggering neurodegeneration in the spinocerebellar ataxias. *Cerebellum* 2010; 9: 148-66.
14. Chung MY, Ranum LP, Duvick LA, Servadio A, Zoghbi HY, Orr HT. Evidence for a mechanism predisposing to intergenerational CAG repeat instability in spinocerebellar ataxia type I. *Nat Genet* 1993; 5: 254-258.
15. Koeppen AH. The pathogenesis of spinocerebellar ataxia. *Cerebellum* 2005; 4: 62-73.
16. La Spada AR, Taylor JP. Repeat expansion disease: progress and puzzles in disease pathogenesis. *Nat Rev Genet* 2010; 11: 247-258.
17. Koob MD, Moseley ML, Schut LJ et al. An untranslated CTG expansion causes a novel form of spinocerebellar ataxia (SCA8). *Nat Genet* 1999; 21: 379-84.
18. Matsuura T, Yamagata T, Burgess DL et al. Large expansion of the ATTCT pentanucleotide repeat in spinocerebellar ataxia type 10. *Nat Genet* 2000; 26: 191-4.
19. Holmes SE, O'Hearn EE, McInnis MG et al. Expansion of a novel CAG trinucleotide repeat in the 5' region of PPP2R2B is associated with SCA12. *Nat Genet* 1999; 23: 391-392.
20. Sato N, Amino T, Kobayashi K et al. Spinocerebellar ataxia type 31 is associated with "inserted" penta-nucleotide repeats containing (TGGAA) n. *Am J Hum Genet* 2009; 85: 544-57.
21. Kobayashi H, Abe K, Matsuura T et al. Expansion of intronic GGCCTG hexanucleotide repeat in NOP56 causes SCA36, a type of spinocerebellar ataxia accompanied by motor neuron involvement. *Am J Hum Genet* 2011; 89: 121-130.
22. Handa V, Yeh HJ, McPhie P, Usdin K. The AUUCU repeats responsible for spinocerebellar ataxia type 10 form unusual RNA hairpins. *J Biol Chem* 2005; 280: 29340-29345.
23. Holmes SE, O'Hearn E, Margolis RL. Why is SCA12 different from other SCAs? *Cytogenet Genome Res* 2003; 100: 189-197.
24. Ikeda Y, Ohta Y, Kobayashi H et al. Clinical features of SCA36: a novel spinocerebellar ataxia with motor neuron involvement (Asidan). *Neurology* 2012; 79: 333-341.
25. Gupta A, Jankovic J. Spinocerebellar ataxia 8: variable phenotype and unique pathogenesis. *Parkinsonism Relat Disord* 2009; 15: 621-626.

26. Daughters RS, Tuttle DL, Gao W et al. RNA gain-of-function in spinocerebellar ataxia type 8. *PLoS Genet* 2009; 5: e1000600.

27. White MC, Gao R, Xu W et al. Inactivation of hnRNP K by expanded intronic AUUCU repeat induces apoptosis via translocation of PKCdelta to mitochondria in spinocerebellar ataxia 10. *PLoS Genet* 2010; 6: e1000984.

28. Nemes JP, Benzow KA, Moseley ML, Ranum LP, Koob MD. The SCA8 transcript is an antisense RNA to a brain-specific transcript encoding a novel actin-binding protein (KLHL1). *Hum Mol Genet* 2000; 9: 1543-1551.

29. He Y, Zu T, Benzow KA, Orr HT, Clark HB, Koob MD. Targeted deletion of a single Sca8 ataxia locus allele in mice causes abnormal gait, progressive loss of motor coordination, and Purkinje cell dendritic deficits. *J Neurosci* 2006; 26: 9975-9982.

30. Aromolaran KA, Benzow KA, Koob MD, Piedras-Renteria ES. The Kelch-like protein 1 modulates P/Q-type calcium current density. *Neuroscience* 2007; 145: 841-850.

31. Merienne K, Trottier Y. SCA8 CAG/CTG expansions, a tale of two TOXICities: a unique or common case? *PLoS Genet* 2009; 5: e1000593.

32. Sulek A, Hoffman-Zacharska D, Zdzienicka E, Zaremba J. SCA8 repeat expansion coexists with SCA1--not only with SCA6. *Am J Hum Genet* 2003; 73: 972-974.

33. Izumi Y, Maruyama H, Oda M et al. SCA8 repeat expansion: large CTA/CTG repeat alleles are more common in ataxic patients, including those with SCA6. *Am J Hum Genet* 2003; 72: 704-709.

34. Dagda RK, Merrill RA, Cribbs JT et al. The spinocerebellar ataxia 12 gene product and protein phosphatase 2A regulatory subunit Bbeta2 antagonizes neuronal survival by promoting mitochondrial fission. *J Biol Chem* 2008; 283: 36241-36248.

35. Ikeda Y, Dick KA, Weatherspoon MR et al. Spectrin mutations cause spinocerebellar ataxia type 5. *Nat Genet* 2006; 38: 184-90.

36. Houlden H, Johnson J, Gardner-Thorpe C et al. Mutations in TTBK2, encoding a kinase implicated in tau phosphorylation, segregate with spinocerebellar ataxia type 11. *Nat Genet* 2007; 39: 1434-6.

37. Waters MF, Minassian NA, Stevanin G et al. Mutations in voltage-gated potassium channel KCNC3 cause degenerative and developmental central nervous system phenotypes. *Nat Genet* 2006; 38: 447-51.

38. Chen DH, Brkanac Z, Verlinde CL et al. Missense mutations in the regulatory domain of PKC gamma: a new mechanism for dominant nonepisodic cerebellar ataxia. *Am J Hum Genet* 2003; 72: 839-49.

39. van de Leemput J, Chandran J, Knight MA et al. Deletion at ITPR1 underlies ataxia in mice and spinocerebellar ataxia 15 in humans. *PLoS Genet* 2007; 3: e108.

40. Knight MA, Hernandez D, Diede SJ et al. A duplication at chromosome 11q12.2-11q12.3 is associated with spinocerebellar ataxia type 20. *Hum Mol Genet* 2008; 17: 3847-53.

41. Bakalkin G, Watanabe H, Jezierska J et al. Prodynorphin Mutations Cause the Neurodegenerative Disorder Spinocerebellar Ataxia Type 23. *Am J Hum Genet* 2010.

42. van Swieten JC, Brusse E, de Graaf BM et al. A mutation in the fibroblast growth factor 14 gene is associated with autosomal dominant cerebellar ataxia [corrected]. *Am J Hum Genet* 2003; 72: 191-9.

43. Di BD, Lazzaro F, Brusco A et al. Mutations in the mitochondrial protease gene AFG3L2 cause dominant hereditary ataxia SCA28. *Nat Genet* 2010; 42: 313-321.

44. Wang JL, Yang X, Xia K et al. TGM6 identified as a novel causative gene of spinocerebellar ataxias using exome sequencing. *Brain* 2010; 133: 3510-3518.

45. Stankewich MC, Gwynn B, Ardito T et al. Targeted deletion of betaIII spectrin impairs synaptogenesis and generates ataxic and seizure phenotypes. *Proc Natl Acad Sci U S A* 2010; 107: 6022-6027.

46. Perkins EM, Clarkson YL, Sabatier N et al. Loss of beta-III spectrin leads to Purkinje cell dysfunction recapitulating the behavior and neuropathology of spinocerebellar ataxia type 5 in humans. *J Neurosci* 2010; 30: 4857-4867.

47. Srikanth S, Wang Z, Hasan G, Bezprozvanny I. Functional properties of a pore mutant in the Drosophila melanogaster inositol 1,4,5-trisphosphate receptor. *FEBS Lett* 2004; 575: 95-98.

48. Banerjee S, Lee J, Venkatesh K, Wu CF, Hasan G. Loss of flight and associated neuronal rhythmicity in inositol 1,4,5-trisphosphate receptor mutants of Drosophila. *J Neurosci* 2004; 24: 7869-7878.

49. Srikanth S, Banerjee S, Hasan G. Ectopic expression of a Drosophila InsP(3)R channel mutant has dominant-negative effects in vivo. *Cell Calcium*

2006; 39: 187-196.

50. Maltecca F, Magnoni R, Cerri F, Cox GA, Quattrini A, Casari G. Haploinsufficiency of AFG3L2, the gene responsible for spinocerebellar ataxia type 28, causes mitochondria-mediated Purkinje cell dark degeneration. *J Neurosci* 2009; 29: 9244-9254.

51. Issa FA, Mazzochi C, Mock AF, Papazian DM. Spinocerebellar ataxia type 13 mutant potassium channel alters neuronal excitability and causes locomotor deficits in zebrafish. *J Neurosci* 2011; 31: 6831-6841.

52. Zhang Y, Snider A, Willard L, Takemoto DJ, Lin D. Loss of Purkinje cells in the PKCgamma H101Y transgenic mouse. *Biochem Biophys Res Commun* 2009; 378: 524-528.

53. Schols L, Bauer P, Schmidt T, Schulte T, Riess O. Autosomal dominant cerebellar ataxias: clinical features, genetics, and pathogenesis. *Lancet Neurol* 2004; 3: 291-304.

54. Cagnoli C, Stevanin G, Brussino A et al. Missense mutations in the AFG3L2 proteolytic domain account for approximately 1.5% of European autosomal dominant cerebellar ataxias. *Hum Mutat* 2010; 31: 1117-1124.

55. Whaley NR, Fujioka S, Wszolek ZK. Autosomal dominant cerebellar ataxia type I: a review of the phenotypic and genotypic characteristics. *Orphanet J Rare Dis* 2011; 6: 33.

56. Fujioka S, Sundal C, Wszolek ZK. Autosomal dominant cerebellar ataxia type III: a review of the phenotypic and genotypic characteristics. *Orphanet J Rare Dis* 2013; 8: 14.

57. Seidel K, Siswanto S, Brunt ER, den DW, Korf HW, Rub U. Brain pathology of spinocerebellar ataxias. *Acta Neuropathol* 2012; 124: 1-21.

58. Carlson KM, Andresen JM, Orr HT. Emerging pathogenic pathways in the spinocerebellar ataxias. *Curr Opin Genet Dev* 2009; 19: 247-253.

59. Llinas RR. Inferior olive oscillation as the temporal basis for motricity and oscillatory reset as the basis for motor error correction. *Neuroscience* 2009; 162: 797-804.

60. Eilers J, Plant T, Konnerth A. Localized calcium signalling and neuronal integration in cerebellar Purkinje neurones. *Cell Calcium* 1996; 20: 215-226.

61. Knopfel T, Grandes P. Metabotropic glutamate receptors in the cerebellum with a focus on their function in Purkinje cells. *Cerebellum* 2002; 1: 19-26.

62. Lamont MG, Weber JT. The role of calcium in synaptic plasticity and motor learning in the cerebellar cortex. *Neurosci Biobehav Rev* 2012; 36: 1153-1162.

63. Hartmann J, Konnerth A. Determinants of postsynaptic Ca2+ signaling in Purkinje neurons. *Cell Calcium* 2005; 37: 459-466.

64. Schiller J, Schiller Y, Clapham DE. NMDA receptors amplify calcium influx into dendritic spines during associative pre- and postsynaptic activation. *Nat Neurosci* 1998; 1: 114-118.

65. Dunlap K, Luebke JI, Turner TJ. Exocytotic Ca2+ channels in mammalian central neurons. *Trends Neurosci* 1995; 18: 89-98.

66. Yuzaki M, Mikoshiba K. Pharmacological and immunocytochemical characterization of metabotropic glutamate receptors in cultured Purkinje cells. *J Neurosci* 1992; 12: 4253-4263.

67. Neher E, Marty A, Fukuda K, Kubo T, Numa S. Intracellular calcium release mediated by two muscarinic receptor subtypes. *FEBS Lett* 1988; 240: 88-94.

68. Sabatini BL, Oertner TG, Svoboda K. The life cycle of Ca(2+) ions in dendritic spines. *Neuron* 2002; 33: 439-452.

69. Yang SNGJ, Tang YGF, Tanaka K. Local calcium signaling in neurons. *Neuron* 1999; 40: 331-346.

70. Paschen W, Mengesdorf T. Endoplasmic reticulum stress response and neurodegeneration. *Cell Calcium* 2005; 38: 409-415.

71. Puzianowska-Kuznicka M, Kuznicki J. The ER and ageing II: calcium homeostasis. *Ageing Res Rev* 2009; 8: 160-172.

72. Rasheva VI, Domingos PM. Cellular responses to endoplasmic reticulum stress and apoptosis. *Apoptosis* 2009; 14: 996-1007.

73. Arundine M, Tymianski M. Molecular mechanisms of calcium-dependent neurodegeneration in excitotoxicity. *Cell Calcium* 2003; 34: 325-337.

74. Szydlowska K, Tymianski M. Calcium, ischemia and excitotoxicity. *Cell Calcium* 2010; 47: 122-129.

75. Brorson JR, Manzolillo PA, Gibbons SJ, Miller RJ. AMPA receptor desensitization predicts the selective vulnerability of cerebellar Purkinje cells to excitotoxicity. *J Neurosci* 1995; 15: 4515-4524.

76. Piochon C, Levenes C, Ohtsuki G, Hansel C. Purkinje cell NMDA receptors assume a key role in synaptic gain control in the mature cerebellum. *J Neurosci* 2010; 30: 15330-15335.

77. Skinner PJ, Vierra-Green CA, Clark HB, Zoghbi HY, Orr HT. Altered trafficking of membrane proteins in purkinje cells of SCA1 transgenic mice. *Am J Pathol* 2001; 159: 905-913.

78. Saito H, Okada M, Miki T et al. Knockdown of Cav2.1 calcium channels is sufficient to induce neurological disorders observed in natural occurring Cacna1a mutants in mice. *Biochem Biophys Res Commun* 2009; 390: 1029-1033.

79. Dove LS, Nahm SS, Murchison D, Abbott LC, Griffith WH. Altered calcium homeostasis in cerebellar Purkinje cells of leaner mutant mice. *Nat Rev NeurosciJ Neurophysiol* 2000; 84: 513-524.

80. Potts MB, Adwanikar H, Noble-Haeusslein LJ. Models of traumatic cerebellar injury. *Cerebellum* 2009; 8: 211-221.

81. Park E, McKnight S, Ai J, Baker AJ. Purkinje cell vulnerability to mild and severe forebrain head trauma. *J Neuropathol Exp Neurol* 2006; 65: 226-234.

82. Sachs AJ, David SA, Haider NB, Nystuen AM. Patterned neuroprotection in the Inpp4a(wbl) mutant mouse cerebellum correlates with the expression of Eaat4. *PLoS One* 2009; 4: e8270.

83. Lin X, Antalffy B, Kang D, Orr HT, Zoghbi HY. Polyglutamine expansion down-regulates specific neuronal genes before pathologic changes in SCA1. *Nat Neurosci* 2000; 3: 157-163.

84. Custer SK, Garden GA, Gill N et al. Bergmann glia expression of polyglutamine-expanded ataxin-7 produces neurodegeneration by impairing glutamate transport. *Nat Neurosci* 2006; 9: 1302-1311.

85. Xia G, Santostefano K, Hamazaki T et al. Generation of Human-Induced Pluripotent Stem Cells to Model Spinocerebellar Ataxia Type 2 In vitro. *J Mol Neurosci* 2012.

86. Satyal SH, Schmidt E, Kitagawa K et al. Polyglutamine aggregates alter protein folding homeostasis in Caenorhabditis elegans. *Proc Natl Acad Sci U S A* 2000; 97: 5750-5755.

87. Ambegaokar SS, Roy B, Jackson GR. Neurodegenerative models in Drosophila: polyglutamine disorders, Parkinson disease, and amyotrophic lateral sclerosis. *Neurobiol Dis* 2010; 40: 29-39.

88. Lorenzo DN, Li MG, Mische SE, Armbrust KR, Ranum LP, Hays TS. Spectrin mutations that cause spinocerebellar ataxia type 5 impair axonal transport and induce neurodegeneration in Drosophila. *J Cell Biol* 2010; 189: 143-158.

89. Mock AF, Richardson JL, Hsieh JY, Rinetti G, Papazian DM. Functional effects of spinocerebellar ataxia type 13 mutations are conserved in zebrafish Kv3.3 channels. *BMC Neurosci* 2010; 11: 99.

90. Todorov B, Kros L, Shyti R et al. Purkinje cell-specific ablation of Cav2.1 channels is sufficient to cause cerebellar ataxia in mice. *Cerebellum* 2012; 11: 246-258.

91. Flanigan K, Gardner K, Alderson K et al. Autosomal dominant spinocerebellar ataxia with sensory axonal neuropathy (SCA4): clinical description and genetic localization to chromosome 16q22.1. *Am J Hum Genet* 1996; 59: 392-399.

92. David G, Giunti P, Abbas N et al. The gene for autosomal dominant cerebellar ataxia type II is located in a 5-cM region in 3p12-p13: genetic and physical mapping of the SCA7 locus. *Am J Hum Genet* 1996; 59: 1328-1336.

93. Koob MD, Moseley ML, Schut LJ et al. An untranslated CTG expansion causes a novel form of spinocerebellar ataxia (SCA8). *Nat Genet* 1999; 21: 379-384.

94. Matsuura T, Achari M, Khajavi M, Bachinski LL, Zoghbi HY, Ashizawa T. Mapping of the gene for a novel spinocerebellar ataxia with pure cerebellar signs and epilepsy. *Ann Neurol* 1999; 45: 407-411.

95. Houlden H, Johnson J, Gardner-Thorpe C et al. Mutations in TTBK2, encoding a kinase implicated in tau phosphorylation, segregate with spinocerebellar ataxia type 11. *Nat Genet* 2007; 39: 1434-1436.

96. Worth PF, Giunti P, Gardner-Thorpe C, Dixon PH, Davis MB, Wood NW. Autosomal dominant cerebellar ataxia type III: linkage in a large British family to a 7.6-cM region on chromosome 15q14-21.3. *Am J Hum Genet* 1999; 65: 420-426.

97. Knight MA, Kennerson ML, Anney RJ et al. Spinocerebellar ataxia type 15 (sca15) maps to 3p24.2-3pter: exclusion of the ITPR1 gene, the human orthologue of an ataxic mouse mutant. *Neurobiol Dis* 2003; 13: 147-157.

98. Miyoshi Y, Yamada T, Tanimura M et al. A novel autosomal dominant spinocerebellar ataxia (SCA16) linked to chromosome 8q22.1-24.1.

Neurology 2001; 57: 96-100.

99. Koide R, Kobayashi S, Shimohata T et al. A neurological disease caused by an expanded CAG trinucleotide repeat in the TATA-binding protein gene: a new polyglutamine disease? *Hum Mol Genet* 1999; 8: 2047-2053.

100. Devos D, Schraen-Maschke S, Vuillaume I et al. Clinical features and genetic analysis of a new form of spinocerebellar ataxia. *Neurology* 2001; 56: 234-238.

101. Verbeek DS, Schelhaas JH, Ippel EF, Beemer FA, Pearson PL, Sinke RJ. Identification of a novel SCA locus (SCA19) in a Dutch autosomal dominant cerebellar ataxia family on chromosome region 1p21-q21. *Hum Genet* 2002; 111: 388-393.

102. Chung MY, Lu YC, Cheng NC, Soong BW. A novel autosomal dominant spinocerebellar ataxia (SCA22) linked to chromosome 1p21-q23. *Brain* 2003; 126: 1293-1299.

103. Duarri A, Jezierska J, Fokkens M et al. Mutations in potassium channel kcnd3 cause spinocerebellar ataxia type 19. *Ann Neurol* 2012; 72: 870-880.

104. Lee YC, Durr A, Majczenko K et al. Mutations in KCND3 cause spinocerebellar ataxia type 22. *Ann Neurol* 2012; 72: 859-869.

105. Vuillaume I, Devos D, Schraen-Maschke S et al. A new locus for spinocerebellar ataxia (SCA21) maps to chromosome 7p21.3-p15.1. *Ann Neurol* 2002; 52: 666-670.

106. Verbeek DS, van de Warrenburg BP, Wesseling P, Pearson PL, Kremer HP, Sinke RJ. Mapping of the SCA23 locus involved in autosomal dominant cerebellar ataxia to chromosome region 20p13-12.3. *Brain* 2004; 127: 2551-2557.

107. Stevanin G, Bouslam N, Thobois S et al. Spinocerebellar ataxia with sensory neuropathy (SCA25) maps to chromosome 2p. *Ann Neurol* 2004; 55: 97-104.

108. Yu GY, Howell MJ, Roller MJ, Xie TD, Gomez CM. Spinocerebellar ataxia type 26 maps to chromosome 19p13.3 adjacent to SCA6. *Ann Neurol* 2005; 57: 349-354.

109. van Swieten JC, Brusse E, de Graaf BM et al. A mutation in the fibroblast growth factor 14 gene is associated with autosomal dominant cerebellar ataxia [corrected]. *Am J Hum Genet* 2003; 72: 191-199.

110. Cagnoli C, Mariotti C, Taroni F et al. SCA28, a novel form of autosomal dominant cerebellar ataxia on chromosome 18p11.22-q11.2. *Brain* 2006; 129: 235-242.

111. Dudding TE, Friend K, Schofield PW, Lee S, Wilkinson IA, Richards RI. Autosomal dominant congenital non-progressive ataxia overlaps with the SCA15 locus. *Neurology* 2004; 63: 2288-2292.

112. Storey E, Bahlo M, Fahey M, Sisson O, Lueck CJ, Gardner RJ. A new dominantly inherited pure cerebellar ataxia, SCA 30. *J Neurol Neurosurg Psychiatry* 2009; 80: 408-411.

113. Giroux JM, Barbeau A. Erythrokeratodermia with ataxia. *Arch Dermatol* 1972; 106: 183-188.

114. Serrano-Munuera C, Corral-Juan M, Stevanin G et al. New subtype of spinocerebellar ataxia with altered vertical eye movements mapping to chromosome 1p32. *JAMA Neurol* 2013; 70: 764-771.

CHAPTER 2

SCA14 mutation V138E leads to partly unfolded PKCγ associated with an exposed C-terminus, altered kinetics, phosphorylation and enhanced insolubilization

Justyna Jezierska[1], Joachim Goedhart[2], Harm H. Kampinga[3], Eric A. Reits[4] and Dineke S. Verbeek[1]

[1]Department of Genetics, University of Groningen, University Medical Center Groningen, Groningen, the Netherlands

[2]Section Molecular Cytology, van Leeuwenhoek Centre for Advanced Microscopy, Swammerdam Institute for Life Sciences, University of Amsterdam, Amsterdam, the Netherlands

[3]Department of Cell Biology, University Medical Center Groningen, University of Groningen, Groningen, the Netherlands

[4]Department of Cell Biology and Histology, Academic Medical Center, University of Amsterdam, Amsterdam, the Netherlands

Submitted

Abstract

The protein kinase C γ (PKCγ) undergoes multi-step activation and participates in various cellular processes in Purkinje cells. Perturbations in its phosphorylation state, conformation or localization can disrupt kinase signaling, such as in Spinocerebellar ataxia type 14 (SCA14) that is caused by missense mutations in *PRKCG* encoding for PKCγ. We previously showed that SCA14 mutations enhance PKCγ membrane translocation upon stimulation due to an "open" protein conformation. Since the faster translocation did not result in an increased function, we examined how SCA14 mutations induce this "open" conformation of PKCγ and what the consequences of this conformational change are on PKCγ life cycle. Here, we show that the SCA14-related PKCγ-V138E exhibits an exposed C-terminus as shown by FRET-FLIM microscopy in living cells. This conformational change was associated with faster PMA-induced translocation and accumulation of fully phosphorylated PKCγ in the insoluble fraction, which could be rescued by co-expressing PDK1 kinase, that normally triggers PKCγ autophosphorylation. We propose that the SCA14 mutation V138E causes unfolding of the C1B domain and exposure of the C-terminus of the PKCγ-V138E molecule, resulting in a decrease of functional kinase in the soluble fraction.

Introduction

The protein kinase C γ (PKCγ) is a brain-specific serine/threonine kinase that responds to calcium and diacylglycerol (DAG) and is important for development and function of Purkinje cells in the cerebellum [1]. It contains an N-terminal regulatory part and a catalytic domain on the C-terminus. The regulatory part includes a tandem of two C1 domains (C1A and C1B), which are responsible for DAG binding and translocation to the membrane (**Fig. 1a**) [2].

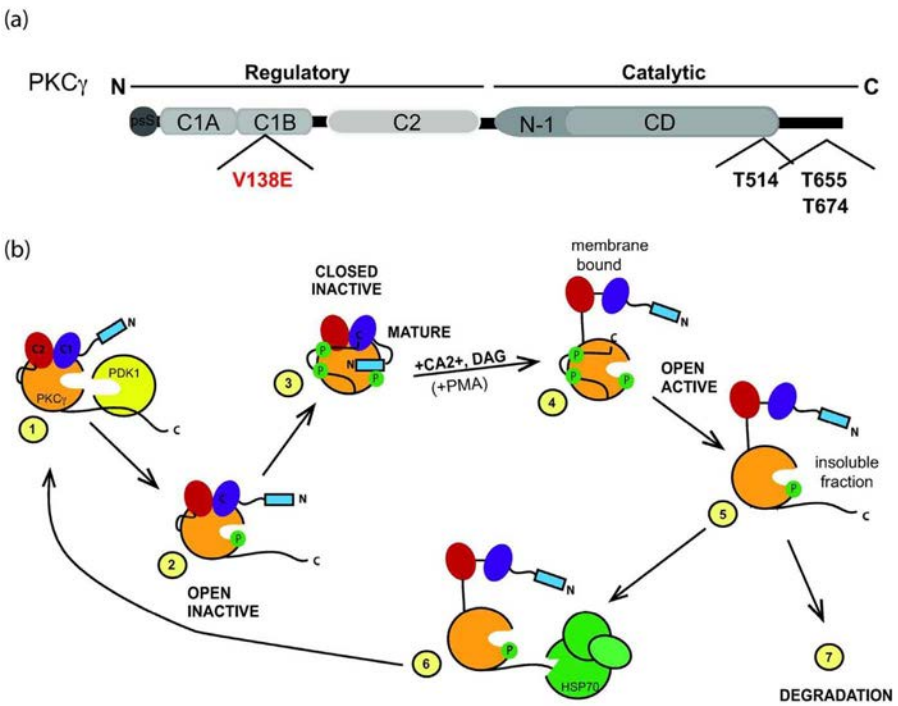

Fig. 1 Structure and lifecycle of PKCγ protein.

(a) Domain structure of the PKCγ protein. The regulatory part contains the pseudosubstrate sequence (psS), DAG-binding C1A and C1B domains and calcium-binding C2 domain. The catalytic part consists of the catalytic domain (CD) with the N-terminal lobe (N-l) and C-terminal extension (CT). The SCA14 mutation (V138E) and (auto)phosphorylation sites (T514, T655 and T674) used in this study are indicated. (b) Model of the life cycle of PKCγ. Inactive PKCγ protein is loosely tethered at the plasma membrane, where it binds kinase PDK1 (1). PDK1 phosphorylates PKCγ at T514, which allows 2 autophosphorylation events to occur at T655 and T674 (2). This results in a closed inactive, but mature, conformation of fully phosphorylated PKCγ (3). In response to calcium and DAG (or PMA in laboratory conditions) PKCγ translocates and binds to the plasma membrane, which triggers an open conformation (4). The open conformation makes PKCγ more susceptible for dephosphorylation and the proteins are targeted to the insoluble fraction upon dephosphorylation (5). Dephosphorylated proteins bind chaperones HSP70, which allow PKCγ recycling (6) or are degraded (7).

PKCγ undergoes a complicated lifecycle to become active and perform its kinase function (summarized in **Fig. 1b**). The first step in the lifecycle is phosphorylation at T514 by phosphoinositide-dependent protein kinase 1 (PDK1) [3]. This is followed by two autophosphorylation events at T655 and T674, which result in a closed conformation and mature PKCγ protein (reviewed in [4]). Once phosphorylated, PKCγ binds its second

messengers, calcium and DAG, and translocates to the plasma membrane, which subsequently causes an open active conformation of PKCγ that allows for kinase activity followed by phosphorylation of downstream targets. In this open conformation, PKCγ is more susceptible to dephosphorylation and the dephosphorylated PKCγ molecules are rapidly ubiquitinated and targeted for degradation [2].

Alterations in phosphorylation state, conformation or cellular localization of PKCγ can disrupt signaling pathways and lead to pathological states, such as spinocerebellar ataxia type 14 (SCA14). SCA14 is an autosomal dominant neurodegenerative disease, which is caused by missense mutations in *PRKCG* gene, encoding for PKCγ [5-11]. SCA14 patients suffer from a slowly progressive cerebellar ataxia accompanied by slurred speech and abnormal eye movements caused by degeneration of Purkinje cells in the cerebellum [12]. Interestingly, the majority of SCA14 mutations are localized in the region encoding for the C1B domain **(Fig. 1a)** [5-11]. Recently, the protein structure of full length PKCβII was resolved, which showed that the C1B domain, and not C1A, interacts directly with N-lobe and C-lobe of the catalytic domain, C-terminus, and C2 domain, forming the so-called C1B clamp [13]. This C1B clamp controls PKC protein conformation and activity, which can be affected by mutations in the C1B domain. In fact, we previously showed that SCA14 mutations in isolated C1B domains do not translocate in response to phorbol 12-myristate 13-acetate (PMA) stimulation, suggesting that the enhanced PMA translocation of the mutant PKCγ molecules is solely driven by more accessible C1A domains, due to an "open" PKCγ protein conformation [14]. Intriguingly, this "open" conformation did not result in a constitutively active kinase, but led to decreased kinase activity, causing aberrant downstream signaling in vitro [14]. This suggests that this "open" conformation of SCA14-mutant PKCγ is rather non-native, partly unfolded or misfolded, and does not reflect the physiological open state. Here, we examined the effect of the V138E mutation in the C1B domain in PKCγ in relation to the SCA14 disease pathology.

Materials and Methods

Materials

Phorbol 12-myristate 13-acetate (PMA) was purchased from Sigma-Aldrich (Milwaukee, WI, USA). The primary antibodies specific for the PKCγ (rabbit, 1:1,000) and GST (rabbit, 1:2,000) were obtained from Santa Cruz Biotechnology (Heidelberg, Germany), and for FLAG (mouse, 1:5,000) from Sigma-Aldrich. The anti-phosphorylation (p)-specific antibodies pT514-, pT655- and pT674-PKCγ (rabbit, 1:5,000), and anti-myc (mouse, 1:2,000) were acquired from Cell Signaling Technology (Leiden, the Netherlands). Living Colors for anti-GFP/CFP staining (mouse, 1:5,000) was purchased from Clontech (Saint-Germain-en-Laye, France).Secondary antibodies were conjugated with horseradish peroxidase (HRP) and used in 1:10,000 dilutions (Jackson Immunoresearch Inc., Suffolk, UK).

DNA constructs

Previously described constructs encoding for wild type (wt) PKCγ and SCA14-mutant PKCγ-V138E proteins fused to green flurorescent protein (GFP) were used for most experiments [14]. For intramolecular fluorescence

resonance energy transfer (FRET) experiments, mutations T655A or T674A were introduced into YFP-PKCγ-SCFP3A constructs described previously [14], using the Quickchange II Site-Directed Mutagenesis kit (Stratagene, La Jolla, CA, USA) and the following primer pairs: T655A-For 5'-GCGCCAGCGCTGGCCCCTCCAGACCG-3' and T655A-Rev 5'-CGGTCTGGAGGGGCCAGCGCTGGCGC-3', and T674A-For 5'-GATTTCCAGGGCTTCGCCTACGTGAACCCC-3' and T674A-Rev 5'-GGGGTTCACGTAGGCGAAGCCCTGGAAATC-3'.

For the GST pull-down experiments, PKCβII's C-terminus (CT-PKCβII-GST), PKCβII's catalytic domain (CD-PKCβII-GST), and myc-tagged PDK1 were kindly provided by Dr. A. Newton (University of California at San Diego, La Jolla, CA, USA) [15]. To generate wt-PKCγ-GST and PKCγ-V138E-GST, the wt-PKCγ cDNA sequence were cloned into backbone pEBB-C-GST/FLLG plasmid using the following primers: For 5'-GGATTCACCATGGCTGGTCTGGGCCCC-3' and Rev: 5'-GCGGCCGCCATGACGGGCACAGGCACTG-3', generating a BamHI site at the 5' end and a NotI site at the 3' end. The V138E mutation was introduced using the Quickchange II Site-Directed Mutagenesis kit and the primers described previously [14]. Moreover, a FLAG-tag (DYKDDDDK) was inserted on the C-terminus of both wt and V138E C1 domains of PKCγ. The C1 cDNAs were amplified from the corresponding PKCγ-GFP constructs by PCR using the following primers: For 5'-GGATTCACCATGCACAAGTTCACCGCTCGCTTC-'3 and Rev 5'-GCGGCCGCGCACAGGGAGGGCACGCT-3' generating a BamHI site at the 5' end and a NotI site at the 3' end. This facilitated cloning into the pEBB-C-FLAG plasmid.

All constructs were verified by sequencing.

Cell culture and transfection

HEK293T, HeLa and COS7 cells were cultured in high-glucose Dulbecco's modified Eagle's medium (DMEM, Gibco, Bleiswijk, the Netherlands) implemented with 10% fetal bovine serum and 5% penicillin (100 U/ml) and streptomycin (100 mg/ml). The cultures were maintained at 37°C in an atmosphere of 5% CO_2. The cells were detached using trypsinization and plated in six-well plates (for Western blotting or fractionation), 100x20 mm tissue culture dishes (BD Biosciences, Breda, the Netherlands) for GST pull-down experiments, or on to 24 mm glass coverslips (Fisher Scientific, Braunsweg, Germany) in a six-well plate for microscopy. The transient transfection was performed 24 h after plating using polyethylenimine (PEI; 0.6 µg/ml in serum-free medium).

Protein sample preparation and fractionation

Cells were harvested 48 h after transfection and lysed with ice-cold fractionation buffer (buffer A: 50 mM Na_2HPO_4, 1 mM $Na_4P_2O_7$, 20 mM NaF, 2mM EDTA, 2 mM EGTA, 1% Triton X-100, 1 mM DTT) supplemented with complete protease inhibitor cocktail (Roche, Woerden, the Netherlands) and phosphatase inhibitor cocktail (Sigma-Aldrich). For GST pull-down, cell lysates were incubated for 20 min on ice and centrifuged at 9,200 g for 15 min in 4°C for supernatant collection. For fractionation experiments, cell lysates were sonicated 2 x 5 s, incubated for 20 min on ice, and centrifuged at 9,200 g for 15 min in 4°C to obtain the Triton-insoluble fraction containing membranes and cytoskeleton proteins in the pellet. Protein concentrations in the soluble fractions were determined using the Pierce BCA Protein Assay Kit (Thermo Scientific, Etten-Leur, the Netherlands) and equal protein amounts were

loaded on SDS-PAGE gels (same volume for soluble and insoluble fractions of one sample).

GST pull-down

Pull-down was performed using GST-beads (Glutathione sepharose 48, GE Healthcare, Hoevelaken, the Netherlands), prepared according to the manufacturer's protocols. The cell lysates were incubated with the beads overnight. After centrifuging (1,300 g, 10 min, 4°C) and washing (4 times with buffer A), the beads and precipitates were dissolved in 2x Leammli buffer followed by boiling at 98°C for 5 min. The immunoprecipitates were loaded on 8% SDS-PAGE gels.

Western blotting

After electrophoresis, the proteins were transferred to the nitrocellulose membrane (Schleicher & Schuell, Dassel, Germany) and blocked with 5% milk in TBS-Tween. The blots were analyzed with primary antibodies according to manufacturer's protocol, followed by incubation with secondary antibody solution for 1 h in room temperature. The bands were visualized by enhanced chemiluminescence Western blotting detection system (LumiLight, Roche). The Fiji software (National Institutes of Health, http://fiji.sc/) was used to quantitatively analyze the protein levels.

Fluorescence resonance energy transfer and live cell microscopy

We used YFP-PKCγ-SCFP3A constructs (described previously [14]) encoding for PKCγ sandwiched between the FRET pair CFP and YFP. Fluorescence lifetime imaging microscopy (FLIM) was used to measure FRET efficiencies using untagged CFP as a control, in transiently transfected HeLa cells. Confocal imaging was performed as described previously [14]. Fluorescence lifetime imaging microscopy (FLIM) experiments and calculation of the FRET efficiency were performed as described before [16], with the exception that a 63x (NA 1.4) oil immersion objective was used.

Statistical analysis

All data are expressed as mean of at least three experiments ± standard error of the mean (SEM), unless stated otherwise. We used the unpaired, two-tailed Student's *t*-test or two-way ANOVA, followed by *post-hoc* Bonferroni correction for multiple testing, to determine the significance of the observed differences between the groups (considered statistically significant at $p < 0.05$).

Results

Exposed C-terminus of SCA14-mutant PKCγ-V138E proteins

We previously showed that SCA14-related mutations located in the C1B domain enhanced the membrane association kinetics of PKCγ, which is caused by a yet not understood induction of an "open" and more PMA-accessible protein conformation [14]. We therefore hypothesized that this altered protein conformation is at the basis of the etiology of SCA14 disease. Since mutant PKCγ-V138E showed the strongest effects [14], we continued with this particular mutant

by investigating how the V138E mutation alters the processing and structure of PKCγ.

Since previous reports showed that a negative charge on the C-terminus (autophosphorylation) is important for PKC protein conformation and intracellular localization [17-19], we started by examining the autophosphorylation levels of the SCA14-mutant PKCγ-V138E, which could still be phosphorylated at both autophosphorylation sites, the T655 and T674, although staining efficiency with phosphorylation-specific antibodies was reduced by about 20% when compared to wt-PKCγ (**Suppl. Fig. 1a and b**). We generated autophosphorylation site mutants (T655A and T674A) of wild type PKCγ (wt-PKCγ) and SCA14-mutant PKCγ-V138E that lack the phosphorylation pT655 or pT674, respectively. The PKCγ-T655A mutant could not be phosphorylated at position 655 as indicated by the loss of immunostaining with the pT655-specific antibody, and consequently also showed loss of pT674 (**Suppl. Fig. 1a**; [2]), similar to the double mutant PKCγ-V138E-T655A. The PKCγ-T674A did not display any pT674, but could still be phosphorylated at T655, in contrast to the double mutant PKCγ-V138E-T674A that could no longer be phosphorylated at T655. This data showed that the V138E mutation leads to reduced autophosphorylation levels and suggests that loss of pT674 on top of a (subtle) conformational change induced by the V138E mutation affects the accessibility of the C-terminus to the kinase active site.

To visualize these apparent effects on PKCγ protein conformation, we used intramolecular FRET to detect changes in the proximity of the N- and the C-terminus. PKCγ was tagged at its termini by the FRET pair CFP and YFP, as described before [14]. When the donor CFP and acceptor YFP moieties are in close proximity, this leads to a relative high FRET efficiency and a decrease in the lifetime of the donor (which is measured by Fluorescence Lifetime Imaging Microscopy or FLIM). Conversely, alterations in the protein conformation due to mutations that separate the donor from the acceptor fluorophore will result in a lower FRET efficiency and therefore a higher donor fluorescence lifetime.

We first examined the effect of loss of negative-charge on the C-terminus on PKC protein conformation. The autophosphorylation-deficient mutant PKCγ-T655A showed significantly lower FRET efficiency than wt-PKCγ (**Fig. 2**) similar to the control (unquenched CFP), reflecting an altered conformation, in which the C-terminus is dissociated from the kinase core and N-terminus [2]. PKCγ-T674A, that could still be phosphorylated at T655 (**Suppl. Fig. 1a**), did not display a markedly altered protein conformation, however, still significantly lower FRET was observed than in wt-PKCγ (**Fig. 2**). As published previously [14], PKCγ-V138E showed a lower FRET efficiency than wt-PKCγ, but the addition of either T655A and T674A mutations in PKCγ-V138E did not significantly further decrease the FRET efficiency compared to PKCγ-V138E (**Fig. 2**). This suggests that the mutation V138E induces a PKCγ molecule that already exhibits a C-terminus that is dissociated from the kinase core and N-terminus. Moreover, loss of FRET was not due to degradation of the mutant PKCγ proteins (**Suppl. Fig. 2**).

PDK1 interacts with the exposed and thus preferentially non-phosphorylated C-terminus of PKC, subsequently phosphorylating T514 and promoting PKC protein activation [15]. To confirm the exposed C-terminus of PKCγ-V138E, GST pull-down experiments were performed with PDK1 and various PKCγ proteins. Cell lysates of HEK293T were co-transfected with PDK1-myc and wt and mutant PKCγ-GST, or the isolated C-terminus of PKCβII (CT-PKCβII) as a positive control. As expected, a strong interaction was observed between PDK1 and CT-PKCβII

(a)

Construct	Tφ (ns)	Tm (ns)	n
CFP	2.67 ± 0.03	3.24 ± 0.06	20
PKCγ-WT	1.96 ± 0.03	2.62 ± 0.03	12
PKCγ-T665A	2.34 ± 0.06	2.98 ± 0.04	29
PKCγ-T674A	2.02 ± 0.05	2.66 ± 0.04	18
PKCγ-V138E	2.38 ± 0.12	2.97 ± 0.10	26
PKCγ-V138E-T665A	2.41 ± 0.05	3.05 ± 0.03	17
PKCγ-V138E-T674A	2.46 ± 0.08	3.05 ± 0.04	17

(b)

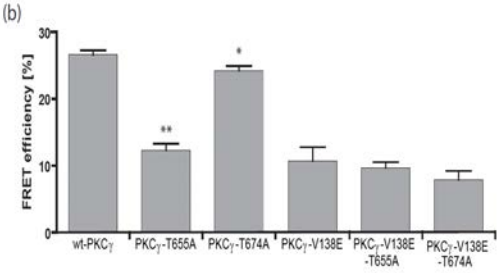

Fig. 2 Changes in PKCγ protein conformation corresponding to removal of negative charge on the C-terminus.

The tables summarize the average CFP phase and modulation lifetimes (± SD) of each construct. The number of cells measured is indicated by n. The FRET efficiencies (mean ± SEM) are calculated based on the CFP phase lifetimes relative to unquenched CFP lifetimes. (a) CFP lifetimes and FRET efficiencies of wt-PKCγ. Autophosphorylation-site mutant PKCγ-T655A showed lower FRET efficiency than wt-PKCγ indicating that removal of C-terminal phosphorylation causes an open protein conformation. Similarly PKCγ-T674 also displayed lower FRET efficiency, but only slightly, however, still statistically significant. (b) CFP lifetimes and FRET efficiencies of SCA14-mutant PKCγ-V138E. PKCγ-V138E already exhibits open conformation and additional mutations on the C-terminus do not decrease further the FRET efficiencies, suggesting that PKCγ-V138E already has an open C-terminus. (c) CFP lifetimes and FRET efficiencies of the known mutant PKCγ-A24E with an open N-terminus. Introduction of C-terminal autophosphorylation-site mutation causes further decrease in FRET efficiency of PKCγ-A24E, indicating that even in the presence of an open N-terminus the effect of T655A mutation on the C-terminus could be detected. Significant differences (unpaired *t*-test) from control values are indicated as * for $p < 0.05$ and ** for $p < 0.0001$.

(a)

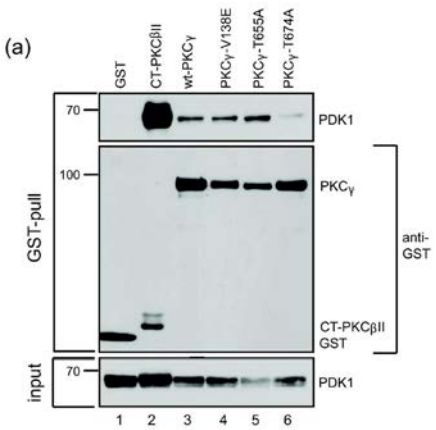

(b)

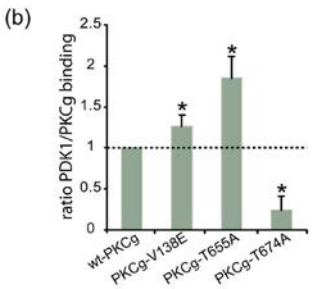

Fig. 3 PDK1 binding to the exposed C-terminus of SCA14-mutant PKCγ-V138E.

(a) Representative immunoblot of GST pull-down of PDK1-myc by different GST-fused PKCγ proteins, including wt-PKCγ (lane 3), PKCγ-V138E (lane 4), PKCγ-T655A (lane 5) and PKCγ-T674A (lane 6), analyzed with anti-myc and anti-GST antibodies, shows increased PDK1 affinity to the more open PKCγ mutants (PKCγ-V138E and PKCγ-T655A). The isolated C-terminus of PKCβII was used as a positive control (lane 2). (b) The relative PDK1/PKCγ ratio is presented (mean ± SEM). Significant differences (unpaired *t*-test) from control values, * $p < 0.05$.

(lane 2, **Fig. 3a**), and in line with our hypothesis, PDK1 preferentially interacted with proteins that exhibited exposed C-termini such as PKCγ-T655A and PKCγ-V138E, compared to wt-PKCγ and PKCγ-T674A (respectively: lane

4 and 5 versus lane 3 and 6; **Fig. 3b**). The weak interaction between PDK1 and PKCγ-T674A can be explained since T674 is located near the PDK1-binding site [15], and PKCγ-T674A showed only a slightly dissociated C-terminus shown in our FRET experiment (**Fig. 2a**). Altogether, these data are in agreement with our previous findings and confirm that the V138E mutation exposes the C-terminus of PKCγ, which favours the binding to PDK1.

Next, we examined whether the exposed C-terminus would affect the kinetics of PKCγ upon PMA activation in living cells as SCA14-mutant PKCγ showed enhanced PMA-induced translocation kinetics before (Verbeek et al., 2008). To do so, COS7 cells were transiently transfected with wt-PKCγ or PKCγ-V138E constructs with T655A or T674A mutations. These last mutant proteins were used as others have shown that the level of autophosphorylation can determine the subcellular localization of PKC and that lack of autophosphorylation alters the PMA-induced translocation kinetics of PKCα and β [17-19, 21]. Subsequently, PMA-induced translocation kinetics was investigated upon adding 400nM PMA. Mutation of either autophosphorylation site significantly increased the PMA-induced translocation kinetics of wt-PKCγ to the plasma membrane (**Fig. 4a**). However, both T655A and T674A mutations did not significantly alter the PMA-induced kinetics of PKCγ-V138E (**Fig. 4b**). This is in line with the observed FRET experiments, as the T655A and T674A mutations did not alter PKCγ-V138E FRET efficiencies (**Fig. 2b**), underscoring our model that primarily the exposed C-terminus accelerates PKCγ-V138E translocation kinetics due to more accessible PMA-binding sites in the C1A domain. It must be noted though that PKCγ-V138E might have an additional structural changes as the protein still translocates faster than either one of the autophosphorylation-site mutants.

Altogether these results strongly suggest that the V138E mutation results in a partially unfolded or misfolded PKCγ protein with an exposed C-terminus that drives enhanced PMA-induced translocation.

Accumulation of SCA14-mutant PKCγ-V138E proteins in the Triton-insoluble fraction

We next tested whether the presumably partially unfolded or misfolded PKCγ-V138E proteins are aggregation-prone and accumulate in the Triton-insoluble fraction like the other SCA14 mutants [22]. The lysates of HEK293T cells expressing the various wt and mutant PKCγ constructs were fractionated with Triton X-100 before or after stimulation with 400 nM PMA. Indeed, increased levels of PKCγ-V138E were detected in the Triton-insoluble fraction of HEK293T cells already without PMA stimulation (**Fig. 5a and b**), and these PKCγ-V138E proteins were more phosphorylated at T655 and T674 than wt-PKCγ proteins (**Fig. 5a and c**). PMA treatment targeted a large amount of the wt-PKCγ proteins to the Triton-insoluble fraction, but did not seem to cause further accumulation of PKCγ-V138E (**Fig. 5a and b**). Thus, as previously reported [23], PMA is able to promote the dephosphorylation of wt-PKCγ leading to accumulation in the Triton-insoluble fraction, but it does not act on PKCγ-V138E. These results show disrupted down-regulation of SCA14-mutant PKCγ-V138E and suggest that PKCγ-V138E proteins are resistant to PMA-induced dephosphorylation and therefore accumulate in insoluble fraction in phosphorylated state.

To investigate if the SCA14-mutant PKCγ-V138E proteins are resistant to dephosphorylation, HEK293T cells transiently transfected with either wt-PKCγ or PKCγ-V138E were stimulated with 400 nM PMA for 1, 3, 5, or 7 hours. Long-term PMA stimulation induces dephosphorylation of PKCγ via activation of various phosphatases,

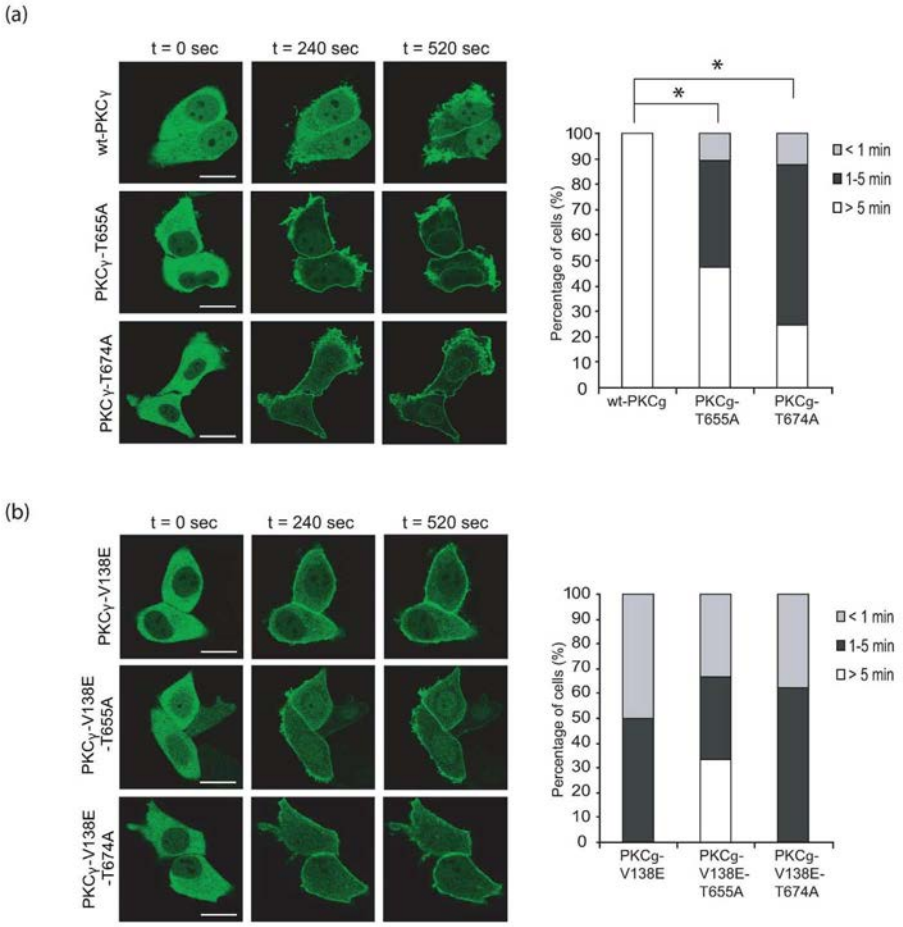

Fig. 4 The effect of an open C-terminus on PMA-induced translocation kinetics of PKCγ.

Confocal images of COS7 cells transfected with different PKCγ-GFP constructs (including wt-PKCγ, PKCγ-T655A, PKCγ-T674A, PKCγ-V138E, PKCγ-V138E-T655A, or PKCγ-V138E-T674A) were recorded prior to (t = 0), and 240 and 520 s after addition of 400 nM PMA. The scale bars are 5 μm. (a) Introduction of autophosphorylation mutations in wt-PKCγ causes faster translocation upon stimulation with PMA. (b) The additional T655A or T674A mutations in SCA14-mutant PKCγ-V138E have no effect on already faster (than wt- PKCγ) translocation kinetics. Changes were evaluated in at least 20 cells per condition by time-lapse imaging and the mean values are presented. Significant differences (unpaired *t*-test) are indicated as * ($p < 0.05$)

including membrane-associated protein phosphatase 2A (PP2A) [24]. Successive dephosphorylation of both T655 and T674 was observed in wt-PKCγ upon PMA stimulation, and at T655 only ±30% of the starting phosphorylation levels were detected after 7 hours of PMA treatment (left panel; **Fig. 6a and b**).Dephosphorylation of both T655 and T674 in PKCγ-V138E was (partially) delayed, still showing ±60% of pT655 7 hours after PMA treatment ($p < 0.05$; right panel; **Fig. 6a and b**). Also, over the entire time-course dephosphorylation kinetics were significantly different between wt-PKCγ and PKCγ-V138E (Two-way ANOVA: genotype x time; $F = 3,10$, $p < 0.01$), and both T655 and T674 phosphorylation could still be detected after overnight stimulation with PMA in PKCγ-V138E, but not in wt-PKCγ.

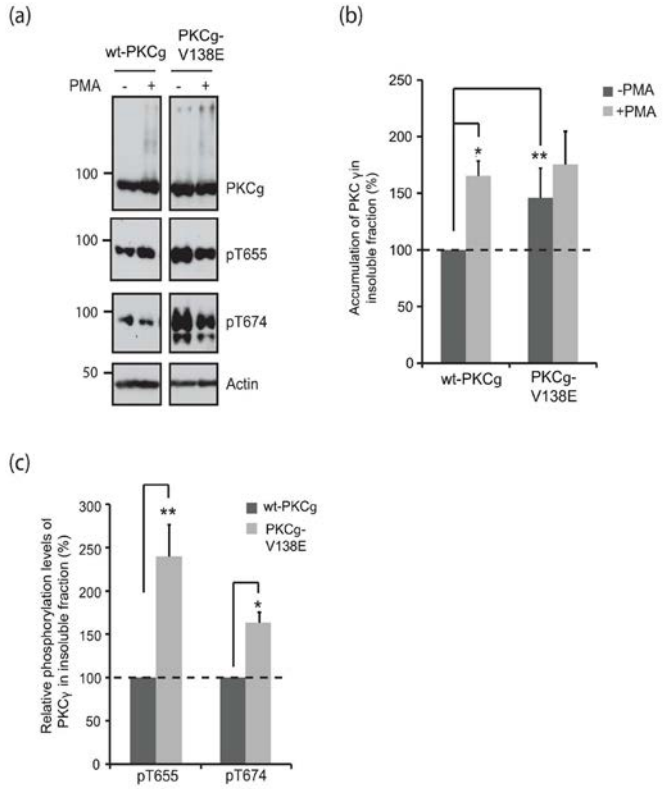

Fig. 5 Accumulation of phosphorylated PKCγ-V138E proteins in the Triton-insoluble fraction.

(a) Representative immunoblots of Triton-insoluble fractions of HEK293T cells transiently transfected with wt-PKCγ or PKCγ-V138E constructs and stimulated with 400 nM PMA were analyzed using anti-PKCγ and specific anti-phosphorylation (pT655 or pT675) antibodies. (b) Quantification graph of PKCγ-V138E accumulation in the Triton-insoluble fraction. (c) Quantification graph of autophosphorylation levels of PKCγ-V138E in the Triton-insoluble fraction. Data are presented as relative (to wt-PKCγ) mean ± SEM. Significant differences (unpaired *t*-test) from control values are indicated as * for $p < 0.05$ and ** for $p < 0.005$.

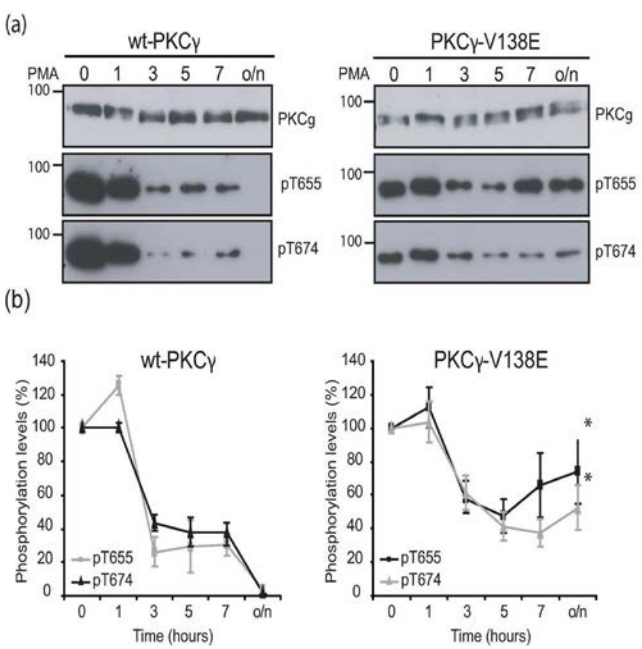

Fig. 6 Dephosphorylation of wt-PKCγ (left panel) and SCA14-mutant PKCγ-V138E (right panel) induced by PMA stimulation.

(a) Immunoblots showing the time-course of dephosphorylation of PKCγ proteins. Dephosphorylation analysis was conducted by stimulation with 400 nM PMA that induces endogenous phosphatases, including PP2A. Whole-cell lysate samples were collected before (0), and after 1, 3, 5, 7 hours and overnight stimulation. Representative immunoblots were analyzed using anti-PKCγ and anti-phosphorylation (pT655 or pT675) antibodies. (b) Quantification of the dephosphorylation in time. The starting point (at 0 hours) was set to 100%. Significance was assessed using two-way ANOVA (genotype x time) followed by Bonferroni multiple comparison tests and showed an overall significant effect for genotype ($F = 3.10$; $p < 0.01$), for time ($F = 4.74$; $p < 0.05$), and also for interaction ($F = 3.10$; $p < 0.05$). Data are presented as the mean ±SEM. Significant differences (*post-hoc t*-test) from control values, * $p < 0.05$.

To further examine this effect, we investigated whether PKCγ-V138E proteins could be dephosphorylated by type 1 protein phosphatase (PP1), known to dephosphorylate PKC at both autophosphorylation sites [25]. Wt-PKCγ or PKCγ-V138E proteins fused to GST were isolated from HEK293T cell lysates using GST pull-down and incubated with recombinant PP1 (5U). While both pT655 and pT674 were efficiently dephosphorylated in time in wt-PKCγ (left panels in **Suppl. Fig. 3a and b**), this was again significantly delayed in PKCγ-V138E, especially for pT655 (Two-way ANOVA: genotype x time; $F = 4{,}066$, $p < 0.05$ for genotype and interaction; right panels in **Suppl. Fig. 3a and b**). These data demonstrate that the partly unfolded and more "open" PKCγ-V138E molecules are less efficiently dephosphorylated by PP1 and PP2A.

Since the altered protein conformation of PKCγ-V138E seems to underlie the accumulation in the Triton-insoluble fraction, we investigated whether overexpression of heat shock proteins (HSPs) could prevent this event by facilitating the proper folding of PKCγ-V138E. However, overexpression of HSPs from various families, including HSP90, HSP70, HSP40, and small HSP did not yield any significant improvement in the solubility of PKCγ-V138E (data not shown). This indicates that SCA14-mutant PKCγ-V138E is rather partially unfolded and cannot be folded to its native conformation.

We next hypothesized whether PDK1 might be the natural chaperone that could prevent or rescue the accumulation of phosphorylated PKCγ-V138E from the Triton-insoluble fraction, as PDK1 has been shown to slow down the PKC processing rate [26, 27]. To explore this hypothesis, HEK293T cells were transiently transfected with PKCγ-V138E and PDK1, without or with PMA treatment (400 nM, 4 hours) followed by Triton-fractionation. Overexpression of PDK1 significantly decreased the levels of accumulated PKCγ-V138E in the Triton-insoluble fraction before and after PMA treatment (right panel; lanes 7 and 8 compared to lanes 5 and 6, **Fig. 7a and b**). Notably, the PKCγ-V138E proteins that were still detected in the Triton-insoluble fraction of cells co-expressing PDK1 showed decreased pT655 and pT674 levels compared to cells without PDK1 (**Fig. 7a and c**). These data suggest that PDK1 is able to prevent or rescue PKCγ-V138E protein insolubilization, as PDK1 seems to favour PKCγ dephosphorylation and subsequently enhance the degradation of the insoluble PKCγ-V138E proteins.

Discussion

In the present study, we aimed to reveal what deficits underlie the "open" PKCγ protein conformation and enhanced PMA-induced translocation kinetics of PKCγ -V138E, as we showed previously [14]. We demonstrated that the V138E mutation alters the native protein conformation of PKCγ leading to exposure of the C-terminus, affecting its proper processing and leading to accumulation of phosphorylated PKCγ molecules in the Triton-insoluble fraction.

Our work shows that quantitative FRET-FLIM measurements are uniquely suited to measure altered conformational states of PKC in single living cells. These measurements revealed that the V138E mutation, located in the C1B domain, results in an exposed C-terminus of PKCγ. This can be explained by the, recently reported, C1B clamp that plays a crucial role in keeping the proper protein conformation of PKC, as it makes extensive contacts with catalytic domain, C-terminus and C2 domain [13]. The Val138 is buried in the hydrophobic core

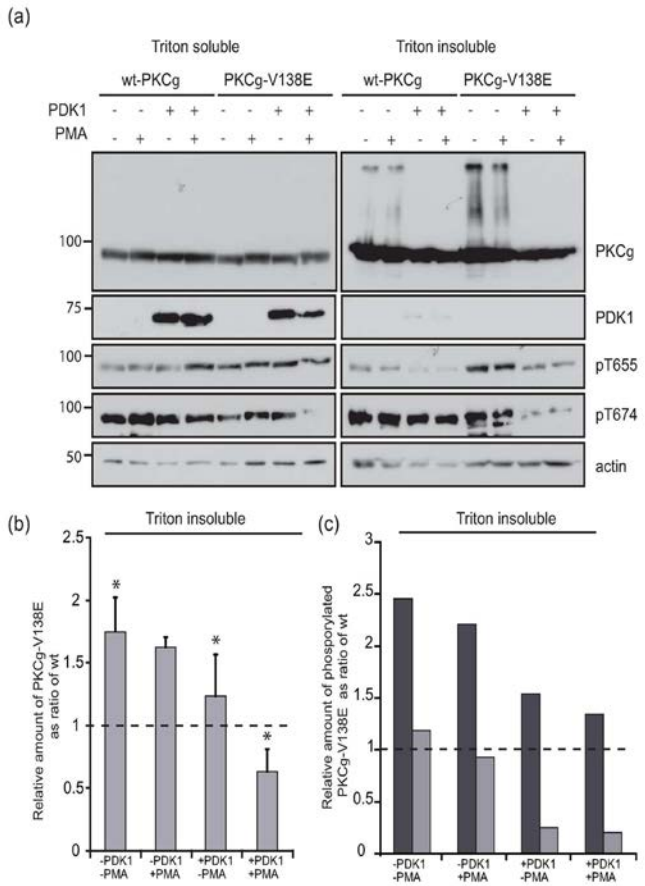

Fig. 7 The effect of PDK1 overexpression on the accumulation of SCA14-mutant PKCγ-V138E in Triton-insoluble fraction.

(a) Immunoblots of Triton-soluble (left panel) and Triton-insoluble (right panel) fractions of HEK293T cells transiently transfected with PDK1-myc and either wt-PKCγ or PKCγ-V138E with or without 400nM PMA stimulation. Immunoblots were analysed using anti-PKCγ, anti-myc, and specific anti-phosphorylation (pT655 or pT675) antibodies. (b) Quantification of the relative amount of PKCγ-V138E in Triton-insoluble fraction. (c) Quantification of relative amount of phosphorylated PKCγ-V138E in Triton-insoluble fraction. Data are expressed as relative (to wt-PKCγ) mean ± SEM. Significant differences (unpaired *t*-test) are indicated as * ($p < 0.05$).

in the native conformation of C1B domain of PKC [13], and therefore the V138E mutation would disrupt the domain folding by introducing a highly negative charge into the hydrophobic moiety. Therefore, we propose that the V138E mutation induces partial unfolding or misfolding of the C1B domain of PKCγ, leading to dissociation of the C-terminus from the kinase core. As a consequence, the PMA-binding sites of the C1 domains should have become more accessible, as PKCγ-V138E translocates faster than wt PKCγ. However, this translocation is probably solely driven by the C1A domain, as we previously showed that mutant C1B-V138E does not respond to PMA, lacking membrane translocation ability upon stimulation [14].

In addition, we showed that PKCγ-T655A, but not PKCγ-T674A, exhibited similar properties as PKCγ-V138E as both proteins demonstrated clearly dissociated C-termini and enhanced PMA-induced translocation kinetics. Thus, phosphorylation of T655 seems to be crucial to maintain PKCγ native protein conformation, as was suggested by the FRET and translocation assays. This would be consistent with published data on PKCβII in which phosphorylation of the same turn motif (T655 in PKCγ) was already found to be important for proper priming of PKCβII protein conformation and activity [19].

Our data suggest that alterations in the conformation of the C1B domain affect PKCγ-V138E autophosphorylation levels and may lead to decreased kinase activity, as reported before [14]. This conformational

changes caused by the V138E mutation did not enhance, but rather delayed, phosphatase sensitivity of PKCγ, despite the exposed C-terminus of PKCγ-V138E, and in turn, led to accumulation of highly phosphorylated PKCγ species in the Triton-insoluble fraction. Our work suggests that the V138E mutation affects the proper folding of the C1B domain, and proper (in-)activation and degradation of PKCγ, promoting its insolublization. In line with our work, SCA14-mutant PKCγ proteins were suggested before to be resistant to ubiquitine-proteasome system degradation [28], and phosphorylated PKC proteins could not be properly down-regulated [29]. These findings imply that proteasomes cannot handle phosphorylated PKCγ molecules, as was shown for PKCγ-V138E. Additionally, HSPs could not restore the native solubility of the PKCγ-V138E protein, whereas the "natural chaperone" of PKC, PDK1, did prevent PKCγ-V138E accumulation in the Triton-insoluble fraction by facilitating its processing and subsequent dephosphorylation that may lead to degradation. These results further support the hypothesis that the C1B domain in SCA14-mutant PKCγ-V138E is unfolded, and that is not recognized by HSPs or cannot be folded to its native conformation. Further investigation is required to clarify if PDK1 can rescue the accumulation of other SCA14-mutant PKCγ proteins harbouring mutations outside the C1B domain from the Triton-insoluble fraction.

In summary, the V138E may cause an unfolded C1B domain, which disrupts the C1B clamp, and results in a loss of C-terminus interaction with the kinase core. This exposed C-terminus leads to increased accessibility of the C1A domain for phorbol esters and induces enhanced translocation kinetics. This altered protein conformation very probably affects proper protein processing and degradation, leading to accumulation of the mutant proteins in the Triton-insoluble fraction. Molecules that can modify PKCγ processing, rather than modifying protein folding, like PDK1, are potential candidates to prevent the accumulation of phosphorylated PKCγ proteins in the Triton-insoluble fraction. Additional studies will be required to examine whether this is a general mechanism that will work for all SCA14 mutant proteins and whether overexpression of PDK1 will reduce PKCγ-related Purkinje cell death and ataxia.

Acknowledgements

This research was supported by a Rosalind Franklin Fellowship and University of Groningen. Confocal fluorescence imaging was performed at the UMCG Microscopy & Imaging Center (UMIC), which is supported by the Netherlands Organisation for Health Research and Development (ZonMW grant 40-00506-98-9021). The article edition was done by Jackie Senior Rogers. The authors declare that they have no conflict of interest.

References

1. Saito N, Shirai Y. Protein kinase C gamma (PKC gamma): function of neuron specific isotype. *J Biochem* 2002; 132**:** 683-687.
2. Newton AC. Protein kinase C: poised to signal. *Am J Physiol Endocrinol Metab* 2010; 298**:** E395-E402.
3. Balendran A, Hare GR, Kieloch A, Williams MR, Alessi DR. Further evidence that 3-phosphoinositide-dependent protein kinase-1 (PDK1) is required for the stability and phosphorylation of protein kinase C (PKC) isoforms. *FEBS Lett* 2000; 484**:** 217-223.
4. Newton AC. Regulation of the ABC kinases by phosphorylation: protein kinase C as a paradigm. *Biochem J* 2003; 370**:** 361-371.
5. van de Warrenburg BP, Verbeek DS, Piersma SJ et al. Identification of a novel SCA14 mutation in a Dutch autosomal dominant cerebellar ataxia family. *Neurology* 2003; 61**:** 1760-5.
6. Yabe I, Sasaki H, Chen DH et al. Spinocerebellar ataxia type 14 caused by a mutation in protein kinase C gamma. *Arch Neurol* 2003; 60**:** 1749-1751.
7. Chen DH, Brkanac Z, Verlinde CL et al. Missense mutations in the regulatory domain of PKC gamma: a new mechanism for dominant nonepisodic cerebellar ataxia. *Am J Hum Genet* 2003; 72**:** 839-849.
8. Giorgione J, Hysell M, Harvey DF, Newton AC. Contribution of the C1A and C1B domains to the membrane interaction of protein kinase C. *Biochemistry* 2003; 42**:** 11194-11202.
9. Verbeek DS, Warrenburg BP, Hennekam FA et al. Gly118Asp is a SCA14 founder mutation in the Dutch ataxia population. *Hum Genet* 2005; 117**:** 88-91.
10. Klebe S, Faivre L, Forlani S et al. Another mutation in cysteine 131 in protein kinase C gamma as a cause of spinocerebellar ataxia type 14. *Arch Neurol* 2007; 64**:** 913-914.
11. Adachi N, Kobayashi T, Takahashi H et al. Enzymological analysis of mutant protein kinase Cgamma causing spinocerebellar ataxia type 14 and dysfunction in Ca2+ homeostasis. *J Biol Chem* 2008; 283**:** 19854-19863.
12. Paulson HL. The spinocerebellar ataxias. *J Neuroophthalmol* 2009; 29**:** 227-237.
13. Leonard TA, Rozycki B, Saidi LF, Hummer G, Hurley JH. Crystal structure and allosteric activation of protein kinase C betaII. *Cell* 2011; 144**:** 55-66.
14. Verbeek DS, Goedhart J, Bruinsma L, Sinke RJ, Reits EA. PKC gamma mutations in spinocerebellar ataxia type 14 affect C1 domain accessibility and kinase activity leading to aberrant MAPK signaling. *J Cell Sci* 2008; 121**:** 2339-2349.
15. Gao T, Toker A, Newton AC. The carboxyl terminus of protein kinase c provides a switch to regulate its interaction with the phosphoinositide-dependent kinase, PDK-1. *J Biol Chem* 2001; 276**:** 19588-19596.
16. Kremers GJ, Goedhart J, van Munster EB, Gadella TW, Jr. Cyan and yellow super fluorescent proteins with improved brightness, protein folding, and FRET Forster radius. *Biochemistry* 2006; 45**:** 6570-6580.
17. Stensman H, Larsson C. Identification of acidic amino acid residues in the protein kinase C alpha V5 domain that contribute to its insensitivity to diacylglycerol. *J Biol Chem* 2007; 282**:** 28627-28638.
18. Stensman H, Raghunath A, Larsson C. Autophosphorylation suppresses whereas kinase inhibition augments the translocation of protein kinase Calpha in response to diacylglycerol. *J Biol Chem* 2004; 279**:** 40576-40583.
19. Edwards AS, Faux MC, Scott JD, Newton AC. Carboxyl-terminal phosphorylation regulates the function and subcellular localization of protein kinase C betaII. *J Biol Chem* 1999; 274**:** 6461-6468.
20. Pears CJ, Kour G, House C, Kemp BE, Parker PJ. Mutagenesis of the pseudosubstrate site of protein kinase C leads to activation. *Eur J Biochem* 1990; 194**:** 89-94.
21. Gysin S, Imber R. Replacement of Ser657 of protein kinase C-alpha by alanine leads to premature down regulation after phorbol-ester-induced translocation to the membrane. *Eur J Biochem* 1996; 240**:** 747-750.

22. Seki T, Adachi N, Ono Y et al. Mutant protein kinase Cgamma found in spinocerebellar ataxia type 14 is susceptible to aggregation and causes cell death. *J Biol Chem* 2005; 280: 29096-29106.

23. Huang FL, Yoshida Y, Cunha-Melo JR, Beaven MA, Huang KP. Differential down-regulation of protein kinase C isozymes. *J Biol Chem* 1989; 264: 4238-4243.

24. Hansra G, Bornancin F, Whelan R, Hemmings BA, Parker PJ. 12-O-Tetradecanoylphorbol-13-acetate-induced dephosphorylation of protein kinase Calpha correlates with the presence of a membrane-associated protein phosphatase 2A heterotrimer. *J Biol Chem* 1996; 271: 32785-32788.

25. Keranen LM, Dutil EM, Newton AC. Protein kinase C is regulated in vivo by three functionally distinct phosphorylations. *Curr Biol* 1995; 5: 1394-1403.

26. Sonnenburg ED, Gao T, Newton AC. The phosphoinositide-dependent kinase, PDK-1, phosphorylates conventional protein kinase C isozymes by a mechanism that is independent of phosphoinositide 3-kinase. *J Biol Chem* 2001; 276: 45289-45297.

27. Biondi RM. Phosphoinositide-dependent protein kinase 1, a sensor of protein conformation. *Trends Biochem Sci* 2004; 29: 136-142.

28. Seki T, Takahashi H, Adachi N et al. Aggregate formation of mutant protein kinase C gamma found in spinocerebellar ataxia type 14 impairs ubiquitin-proteasome system and induces endoplasmic reticulum stress. *Eur J Neurosci* 2007; 26: 3126-3140.

29. Gao T, Newton AC. Invariant Leu preceding turn motif phosphorylation site controls the interaction of protein kinase C with Hsp70. *J Biol Chem* 2006; 281: 32461-32468.

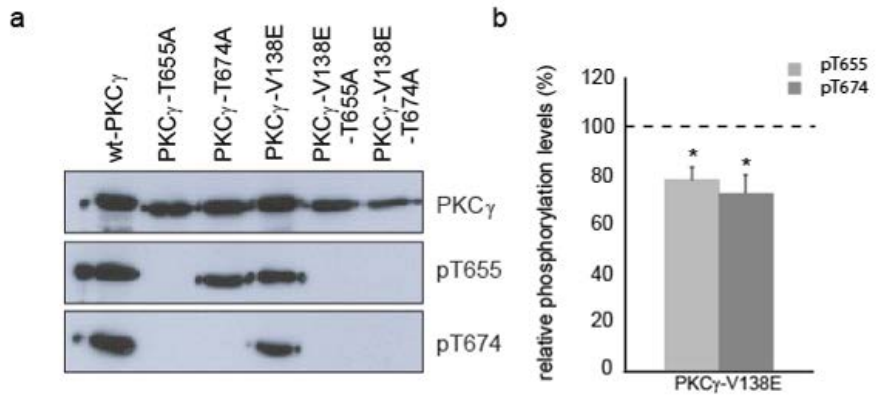

Suppl. Fig. 1 Phosphorylation levels of PKCγ.

(a) Representative immunoblot of whole-cell lysates of HEK293T transiently transfected with wt-PKCγ, PKCγ-T655A, PKCγ-T674A, PKCγ-V138E, PKCγ-V138E-T655A, or PKCγ-V138E-T674A and analyzed with anti-PKCγ and specific anti-phosphorylation (pT655 or pT675) antibodies. (b) Data are expressed as relative (to wt-PKCγ) mean ± SEM. Significant differences (unpaired *t*-test) from control values are indicated as * ($p < 0.05$).

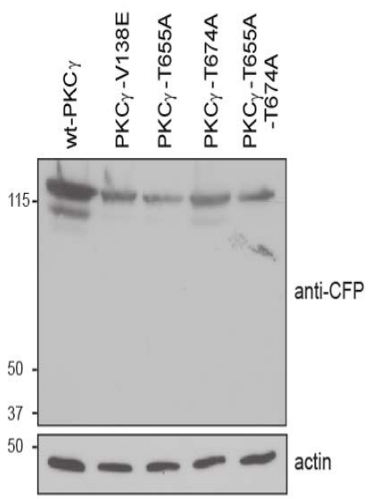

Suppl. Fig. 2

Immunoblot of HEK293T whole-cell lysates transiently transfected with YFP-PKCγ-CFP (including wt-PKCγ, PKCγ-T655A, PKCγ-T674A, or PKCγ-V138E) and analyzed with anti-CFP antibody, shows no protein degradation that could explain lower FRET efficiencies.

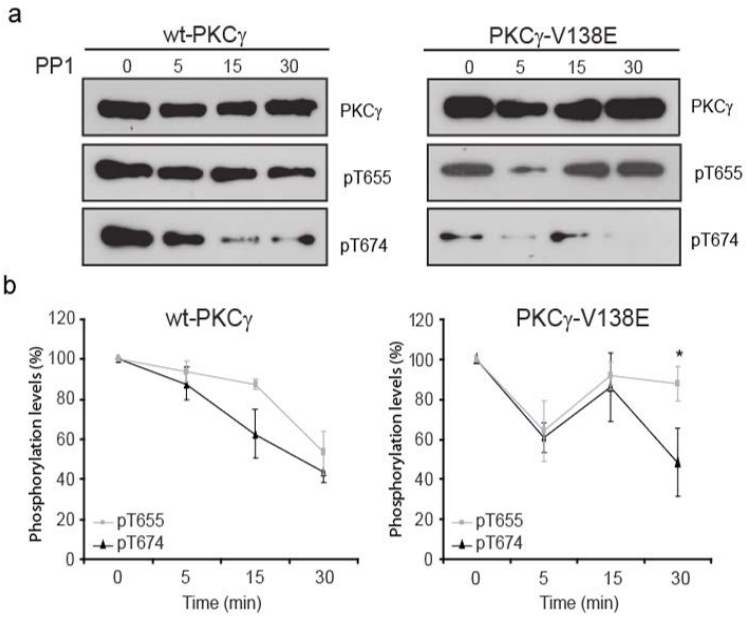

Suppl. Fig. 3 Dephosphorylation of PKCγ proteins by PP1 recombinant phosphatase in time.

Phosphorylation levels of wt-PKCγ (left panel) and PKCγ-V138E (right panel) were assessed before (0) and after 5, 15, and 30 minutes of treatment with recombinant PP1 phosphatase (5U) *in vitro*. (a) Representative immunoblots were analyzed using anti-PKCγ and anti-phosphorylation (pT655 or pT675) antibodies. (b) Time-course of dephosphorylation of PKCγ proteins by PP1 is presented as the mean ± SEM of each time-point. Two-way ANOVA (genotype x time) followed by Bonferroni multiple comparison tests showed overall significant effects for genotype ($F = 4.06$; pT655: $p < 0.05$; pT674: $p < 0.005$), but was not significant for time. The dephosphorylation in time was significantly different between wt and SCA14-mutant PKCγ for both pT655 and pT674 (interaction: $F = 4.06$; T655: $p < 0.05$; T674: $p < 0.01$). Significant difference from control values in the *post-hoc t*-test analysis is indicated as * ($p < 0.05$).

CHAPTER 3

Mutations in potassium channel *KCND3* cause spinocerebellar ataxia type 19

Anna Duarri, PhD,[1] Justyna Jezierska, MSc,[1] Michiel Fokkens, BSc,[1] Michel Meijer, BSc,[2] Helenius. J. Schelhaas, MD, PhD,[3] Wilfred F.A. den Dunnen, MD, PhD,[4] Freerk van Dijk, BSc,[5] Corien Verschuuren-Bemelmans, MD,[1] Gerard Hageman, MD, [6] Pieter van de Vlies, BSc,[1] Benno Küsters, MD, PhD[7] Bart P. van de Warrenburg, MD, PhD,[3] Berry Kremer, MD, PhD,[8] Cisca Wijmenga, PhD,[1] Richard J. Sinke, PhD,[1] Morris A. Swertz, PhD,[4] Harm H. Kampinga, PhD,[9] Erik Boddeke, PhD,[2] and Dineke S. Verbeek, PhD[1]

[1] Department of Genetics, University of Groningen, University Medical Center Groningen, Groningen, The Netherlands
[2] Department of Medical Physiology, University Medical Center Groningen, Groningen, The Netherlands.
[3] Department of Neurology, Donders Institute for Brain, Cognition and Behavior, Center for Neuroscience, Radboud University Nijmegen Medical Center, Nijmegen, The Netherlands
[4]Department Pathology & Medical Biology, University of Groningen, University Medical Center Groningen, Groningen, The Netherlands
[5] Genomics Coordination Center, Department of Genetics, University Medical Center Groningen & Groningen Bioinformatics Center, University of Groningen, Groningen, The Netherlands
[6] Department of Neurology, Medical Spectrum Twente, Enschede, The Netherlands
[7] Department of Pathology, Radboud University Nijmegen Medical Center, Nijmegen, The Netherlands
[8] Department of Neurology, University Medical Center Groningen, Groningen, The Netherlands
[9] Department of Cell Biology, Section of Radiation and Stress Cell Biology, University Medical Center Groningen, University of Groningen, Groningen, The Netherlands

Ann Neurol 2012; 72: 870-880

Abstract

Objective: To identify the causative gene for the neurodegenerative disorder spinocerebellar ataxia type 19 (SCA19) located on chromosomal region 1p21-q21.

Methods: Exome sequencing was used to identify the causal mutation in a large SCA19 family. We then screened two hundred and thirty ataxia families for mutations located in the same gene (*KCND3,* also known as Kv4.3) using high-resolution melting. SCA19 brain autopsy material was evaluated, and *in vitro* experiments using ectopic expression of wild-type and mutant Kv4.3 were used to study protein localization, stability and its channel activity by patch-clamping.

Results: We detected a T352P mutation in the third extracellular loop of the voltage-gated potassium channel *KCND3* that co-segregated with the disease phenotype in our original family. We identified two more novel missense mutations in the channel pore (M373I) and the S6 transmembrane domain (S390N) in two other ataxia families. T352P cerebellar autopsy material showed severe Purkinje cell degeneration, with abnormal intracellular accumulation and reduced protein levels of Kv4.3 in their soma. Ectopic expression of all mutant proteins in HeLa cells revealed retention in the endoplasmatic reticulum and enhanced protein instability, in contrast to wild-type Kv4.3 that was localized on the plasma membrane. The regulatory β subunit KChIP2 was able to rescue the membrane localization and the stability of two of the three mutant Kv4.3 complexes. However, this either did not restore the channel function of the membrane located mutant Kv4.3 complexes or only partially.

Interpretation: *KCND3* mutations cause SCA19 by impaired protein maturation and/or reduced channel function.

Introduction

Patients with a dominantly inherited spinocerebellar ataxia (SCAs) are characterized by a late-onset, progressive atrophy of the cerebellum, affecting their motor coordination, balance, speech, eye coordination movements, and with many other symptoms.[1] To date, 36 SCA loci have been described, for 21 of these the corresponding disease gene and causative mutation has been identified.[1-4] The majority of SCAs represent repeat expansion diseases, including a coding CAG repeat (SCA1–3, 6, 7, and 17) causing misfolding of the encoded protein due to the expanded polyglutamine tracts, or groups of non-coding CAG, CTG, ATTCT, and GGCCTG repeats (SCA8, 10, 12, and 36), or large TGGAA repeat insertions (SCA31) that induce RNA-mediated gain-of-function mechanisms.[1] The remaining known SCA types are caused by missense mutations or chromosomal rearrangements (SCA5, 11, 13–15, 20, 23, 27, 28, 31, and 35) in genes displaying a wide range of protein functions, often causing alterations in synaptic transmission via calcium, potassium and glutamate signaling.[1,5-7]

We previously mapped SCA19 in a large Dutch family (four generations with thirteen affected members) to a region of approximately 38 Mb located in chromosomal region 1p21-q21.[8] The SCA19 locus shows significant overlap with the SCA22 locus later reported in a single Chinese family,[9] suggesting that SCA19 and SCA22 might be caused by mutations in the same gene and lead to an ataxia type with a worldwide distribution.[10] Clinical investigation and magnetic resonance imaging of our SCA19 family revealed a relatively mild, cerebellar ataxic syndrome with cognitive impairment, pyramidal tract involvement, tremor and peripheral neuropathy, and mild atrophy of the cerebellar hemispheres and vermis.[11] The SCA19 locus comprises some five hundred genes and transcripts, but we could not identify the causative gene and mutation by candidate gene sequencing (data unpublished). We therefore applied exome sequencing to two affected family members and identified a novel missense mutation in *KCND3* (also known as Kv4.3) as causing SCA19 in our family.[8] Later, we identified two different missense mutations in this gene in two other families from our Dutch ataxia cohort. Kv4.3 is a Shal-related subfamily, voltage-gated potassium channel, involved in the transient outward A-type K+ current in the neurons. It is highly expressed in the cerebellum.[12-14] The three mutations in *KCND3* either impaired proper endoplasmatic reticulum (ER)-golgi-membrane trafficking and/or reduced Kv4.3 channel functioning. Together, our genetic and functional studies provide evidence that mutations in *KCND3* cause SCA19.

Material and Methods

Subjects

The participants of our original SCA19 family all gave informed written consent, as required by the Medical Ethics Committee of the University Medical Centre Utrecht, the Netherlands. The additional 230 ataxia patients screened in this study were obtained from the Genome analysis laboratory, Department of Genetics, University Medical Center Groningen. All extended DNA analyses were performed in a diagnostic setting (accredited diagnostic DNA lab). Only DNA samples from patients who were referred for genetic testing for SCA1-3, 6-12, 14, and 17 were used. The additional tests were thus performed in line with the original diagnostic request. Moreover, patients

were asked whether they agreed to their DNA being used for future (anonymous) studies to help develop or improve diagnostics. If they objected, this was indicated on the original "Request for DNA test" form and their DNA was not used. The unrelated 400 control individuals were obtained from the Dutch blood bank. DNA was extracted from peripheral blood by a routine salting-out procedure.

Exome sequencing and mutation screening

The genomic DNA samples (individuals IV:1 and II:10 marked by * in pedigree 1, **Suppl. Fig. 1A**) were randomly fragmented using nebulization. The resulting fragments were bar-coded, using the standard NEBNext DNA Library Prep Master Mix Set for Illumina (New England Biolabs, Ipswich, MA, USA). Fragments with an average insert size of 220 bp were amplified by PCR, and the quality was verified on an Experion machine (BioRad, Richmond, CA, USA). Exome capturing was performed using the Agilent SureSelect All exon V2 kit. After PCR amplification of the enriched products paired-end sequencing was performed on a HiSeq2000 (Illumina, San Diego, CA, USA) with 100 bp reads. Image files were processed using standard Illumina base-calling software and the generated reads were ready for downstream processing after de-multiplexing.

The reads were aligned to the human reference genome, build 37, using BWA software.[15] To clean the aligned data and perform variant calling, we applied Picard duplicate removal and the genome-analyzer toolkit (GATK)[16, 17] containing quality score recalibration, indel realignment, and an unified genotyper. Using snpEff (http://snpeff.sourceforge.net) the variants were annotated with information from dbSNP132, 1000 Genomes Project (phases 1, 2 and 3) and Ensembl, build 37.64. These programs are all integrated in our MOLGENIS Compute analysis pipeline developed by the Genomics Coordination Center, Department of Genetics, University of Groningen (http://wiki.gcc.rug.nl/wiki/GccStart).[18] Pathogenicity predictions for variants were obtained from PolyPhen 2.0, SIFT, and Align GVD.[19-23] Variations were validated by direct Sanger sequencing and analyzed using DNA Variant Analysis Software Mutation Surveyor. The high resolution melting technology with the LightScanner (Idaho Technologies, Salt Lake City, UT, USA) was used to identify additional mutations in *KCND3* according to the manufacturer's instructions. The primers used to amplify the amplicons are listed in **Suppl. Table 1**. Aberrant melting curves were checked by direct Sanger sequencing, and the sequences were aligned to reference sequence NM_172198.

Post-mortem human brain specimens

SCA19 cerebellar tissue (hemispheres and vermis) from the patient (Individual II:1 in pedigree 1 in **Suppl. Figure 1A**) with a T352P mutation and an age-matched, non-degenerative control subject were obtained from the University Medical Center St Radboud, Nijmegen, the Netherlands. The samples were collected with full clearance from their Medical Ethics Committee. The frozen brain tissue was used for Western blot, quantitative real-time PCR analysis and for making paraffin-embedded sections for histochemistry and immunohistochemistry tests.

Plasmids

Wild-type *KCND3* cDNA cloned into the pCMV6 plasmid (short isoform; 636 amino acids, NM_172198) was purchased from Origene (Rockville, MD, USA). The cDNA was amplified using primers (**Suppl. Table 2**) containing XhoI and EcoRI, or EcoR1 and EcoRV sites, to facilitate cloning into pcDNA3.1(-), and pIRES-EGFP/Cherry plasmids, respectively. The PCR product was first subcloned into pJET1.2/blunt (Fermentas, Vilnius, Lithuania). Mutations were introduced into the pJET-*KCND3* cDNA using side-directed mutagenesis (for primers see **Suppl. Table 3**) followed by further subcloning into pcDNA3.1(-) and pIRES-EGFP/Cherry. The pcDNA3.1-Kv4.3 plasmids were used for Western blot and immunohistochemistry and the pIRES-Kv4.3-EGFP/mCherry plasmids for patch-clamping. The constructs were checked for correctness by direct sequencing. The Emerald-C1 and Emerald-ratKChIP2b/c plasmids were kindly provided by Dr. K. Takimoto (Nagaoka University of Technology, Kamitomioka, Japan).[24]

Cell culture and transfection

HeLa and HEK293T cells were grown in DMEM medium (Invitrogen, Carlsbad, CA, USA) supplemented with 10 % FBS (Invitrogen) and 1% Pen/Strep (Gibco, Rockville, MD, USA) in a 37°C with 5% CO_2. Cells were grown in 6-well plates for Western blot or on glass cover slips in 12-well plates for immunohistochemisty and single cell patch clamping for 24 hours following transfection with PEI (Polysciences Inc., Warrington, PA, USA), according to the manufacturer's instructions.

Western blot

After 48 hours of transfection, cell extracts and human cerebella were homogenated using a 2% SDS/PBS buffer containing protease inhibitor cocktail (Roche Diagnostics, Indianapolis, IN, USA) and incubated for 1 hour at room temperature. Cell and tissue lysates were centrifuged for 10 minutes at 13,000 rpm. Proteins were quantified using the BCA kit (Thermo Fisher Scientific, Rockford, IL, USA) and the supernatant was mixed with loading sample buffer containing 10% β-mercaptoethanol and incubated for 5 minutes at 65°C.

For protein analysis 50 µg of cell extract or 200 µg of brain proteins was loaded on 10% SDS-PAGE gel followed by immunoblot analysis. Nitrocellulose membranes were incubated with mouse anti-Kv4.3 (K75/41, NeuroMab, Davis, CA UAS, 1:1000), mouse anti-Calbindin (Abcam, Cambridge, UK, 1:2500), mouse anti-Actin (MP Biochemicals, Solon, OH, USA, 1:5000), mouse anti-p53 (Santa Cruz, Santa Cruz, CA, USA, 1:1000), and mouse anti-KChIP2 (Abcam, Cambridge, UK, 1:1000). Final quantification was performed using the program Quantity One (Bio-Rad).

Immunochemistry and Sevier-Munger silver staining

After 48 hours of transfection, HeLa cells were used for immunocytochemisty as previously described but with some modifications.[26] Briefly, cells were fixed with PBS containing 4% paraformaldehyde for 15 minutes, permeabilized and blocked with 10% BSA 0.1% Triton X-100 in PBS for 1 hour at room temperature. Primary and secondary antibodies were diluted in blocking buffer and incubated overnight at 4°C and 1 hour at room

temperature, respectively. The antibodies used were: mouse anti-Kv4.3 (K75/41, NeuroMab, Davis, CA, USA, 1:250), rabbit anti-Calnexin (Sigma, Milwaukee, WI, USA, 1:200), goat anti-mouse FITC, goat antimouse Cy3 (all 1:500, Jackson ImmunoResearch, West Grove, PA, USA).

Cerebellar immunohistochemistry was performed on human cerebellar tissue 10 µm thick sections embedded in paraffin. After deparaffination, rehydratation, and antigen retrieval, tissues were blocked with 10% normal goat serum in TBS for 1 hour at room temperature. Primary and secondary antibodies were diluted in blocking buffer and incubated overnight at 4°C in a humidified chamber and for 2 hours at room temperature, respectively.

The antibodies used were: rabbit anti-Kv4.3 (Alomone labs, Jerusalem, Israel, 1:100) and mouse anti-Calbindin (Abcam, Cambridge, UK, 1:200), goat anti-mouse FITC and goat anti-rabbit Cy3 (1:500, Jackson ImmunoResearch, West Grove, PA, USA). All the slides were mounted in Vectashield medium with DAPI (Vector Laboratories, Burlingame, CA, USA). For the silver staining, after deparaffination and rehydration, the cerebellar slides were placed in a 20% solution of AgNO3 for 20 minutes at 60°C. After rinsing in distilled water, the slides were placed in a solution of 10% AgNO3 (to which ammonia was added until the precipitate was dissolved) + 1 ml of 25% sodium carbonate solution. While stirring, drops of 3.7% formalin were added until the slides stained gold-brown. After rinsing in distilled water, the slides were placed in 5% sodium thiosulphate solution for 2 minutes. Then the slides were rinsed again, followed by dehydration, xylene and mounting.

Membrane localization scoring assay

The percentage of transiently transfected HeLa cells with Kv4.3 membrane localization versus cells without membrane localization were scored using an IRB inverted fluorescent microscope (Leica, Mannheim, Germany). The scoring assay was de-coded and performed in triplicate by an independent scorer. On average a minimum of 250 cells were counted per experiment.

Electrophysiological measurements

Whole-cell patch clamp recording was used to quantify Kv4.3 potassium currents. All the experiments were performed at room temperature (22–24°C) using an Axopatch 200B amplifier, a Digidata 1320A interface, and pClamp version 8.2 software (Axon Instruments, Foster City, CA, USA). The extracellular (bath) solution contained (mmol/L) 140 NaCl, 4 KCl, 5 glucose, 2 $CaCl_2$, 1 $MgCl_2$, and 10 HEPES, and the pH was adjusted to 7.4 with NaOH. The pipette solution contained (mmol/L) 140 KCl, 10 EGTA, 1 $CaCl_2$, 1 $MgCl_2$ and 10 HEPES, and the pH was adjusted to 7.2 with KOH. Microelectrodes were made of GC120F-10 borosilicate glass (Harvard Apparatus, Holliston, MA, USA) and pulled on a P-87 puller (Sutter Instruments, Novato, CA, USA) having a final resistance of 4–5 MΩ. Series resistance was compensated by 80–85%. Currents were filtered at 5 kHz and digitized at 10 kHz. Data were analyzed using Clampfit (Axon Instruments, Sunnyvale, CA, USA) and Microsoft Excel software.

Results

In order to identify the causative gene for SCA19, the genomic DNA of two affected individuals from our large Dutch family (IV:1 and III:10 in pedigree 1 and indicated with * in **Suppl. Fig. 1A**) was analyzed by whole exome capturing. An average of 3 Gb of sequence was generated per individual, with an average coverage depth of 70x per targeted base. At least 85% of the total target region was covered more than 20x. The data were filtered for SNPs that were not previously reported to dbSNPv132 or found in the 1000 Genomes Project (phases 1, 2 and 3), yielding 4,382 and 5,830 novel SNPs per individual (**Suppl. Table 4**).

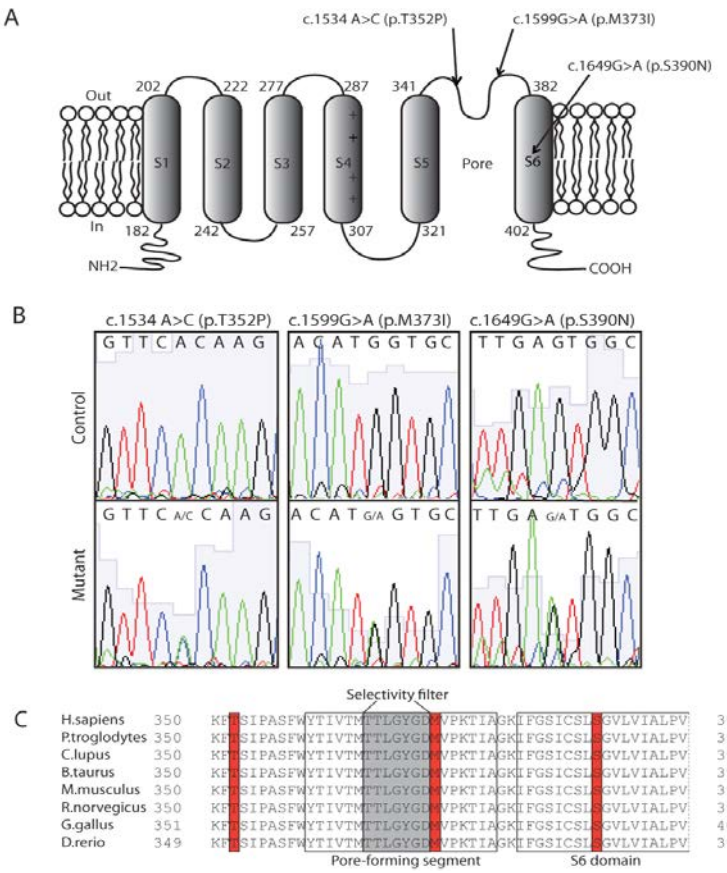

Figure 1 SCA19 mutations lead to amino acid substitutions in highly conserved parts and domains of Kv4.3.

A) Schematic representation of the Kv4.3 channel and the location of the three SCA19 mutations. Segments (S) 1-4 form the voltage sensor domain, and S5 and S6, together with the pore loop, form the ion-selective pore. Positively charged residues in S4 detect the voltage change. The numbers indicate the amino acid numbers defining the beginning and end of the transmembrane segments. The c.1054A>C; p.T352P mutation is located in the third extracellular loop, the c.1119G>A; p. M373I and c.1169G>A; p.S390 are located in the channel pore, and the S6 transmembrane domain, respectively. **B**) Electropherograms of the wild-type and mutant DNA sequences (NM_172198). **C**) Amino acid comparison of Kv4.3 channels across species reveals that amino acids T352, M373, and S390 are 100% conserved from human to fish.

Since the SCA19 disease gene had already been mapped to 1p21-q21, further analysis focused on those variations shared between the two SCA19 cases from the large Dutch pedigree and present within the linkage interval. This analysis resulted in a total of 33 shared SNPs not reported in any database (**Suppl. Table 5**). Of these, 25 SNPs were detected in a heterozygous state (**Suppl. Tables 6 and 7**). After exclusion of the non-coding variants, validation by Sanger sequencing, a co-segregation check with the disease phenotype in the original SCA19 family (**Suppl. Fig. 1A**) and, screening of 400 Dutch blood bank controls, only one heterozygous missense T>G variation located at chromosome 1: 112,524,295 remained unique for SCA19 (**Suppl. Table 7**). This variation led to a c.1054A>C

(p.T352P) substitution in the third extracellular loop of the voltage-gated potassium channel *KCND3*, also known as Kv4.3 (**Fig. 1A and B**).

To obtain further genetic evidence for *KCND3* as the gene underlying SCA19, we screened 230 Dutch ataxia cases with no mutation in the known SCA genes (SCA1-3, 6, 7, 14, 17, and 23) by high-resolution melting. This ataxia cohort contains 30 cases with an autosomal dominant (AD) inheritance pattern and 200 cases with an unknown family history. In the probands of two AD families (Pedigrees 2 and 3, **Suppl. Fig. 1B and C**), we identified two novel mutations, c.1119G>A; p. M373I and c.1169G>A; p.S390N, located in the channel pore, and the S6 transmembrane domain, (**Fig. 1A and B**), respectively. The c.1119G>A mutation was detected in two affected individuals and in one apparently asymptomatic carrier (**Suppl. Fig. 1B**). The segregation of the other mutation c.1169G>A could not be tested due to non-availability of family members (**Suppl. Fig. 1C**). All three mutated residues of human Kv4.3 are 100% conserved between different species (**Fig. 1C**). None of the *KCND3* mutations were found in 800 Dutch control chromosomes, nor in several genetic databases (dbSNPv132, 1000 Genomes Project, and Exome Variant Server (NHLBI Exome Sequencing Project, http://evs.gs.washington.edu/EVS/).

The M373I proband, (Pedigree 2: II:1; **Suppl. Fig. 1B**) had ambiguous neurological signs on testing at the age of 44. At the age of 52, he was re-examined but was found to be without neurological symptoms. His father (I:1) had a progressive gait disorder from age 55 onwards, including clear dysarthria, as well as ataxia of the arms and of gait. Computer tomography at that time demonstrated mild cerebellar atrophy. Comorbid conditions included hearing impairment and vascular atherosclerotic disease. He died at the age of 80. This paternal father was said to have had gait instability as well from about age of 60 onwards, deceasing at the age of 90. Of the proband's sisters, the eldest was found to have very mild gait impairment at the age of 64, with equivocal dysdiadochokinesia of the hands (II:3). The youngest sister was unaffected (II:2).

The S390N proband (Pedigree 3: II:1; **Suppl. Fig. 1C**) suffered from a slowly progressive, spastic ataxic syndrome, including dysarthria, saccadic eye movements and downbeat nystagmus, cognitive impairment, and hearing deficits. The disease symptoms started between 30-35 years of age. An MRI scan of the brain revealed cerebellar vermis atrophy. In addition, his brother and mother were diagnosed with the same disease.

Kv4.3 has been reported to be expressed in the cerebellum[14,27] and immunohistochemistry of autopsy material from control cerebellum revealed a weak, punctuated staining of the Purkinje cell (PC) bodies, whereas a more intense Kv4.3 signal in larger puncta was observed in the soma of T352P-mutant PCs (**Fig. 2A**). Sevier-Munger silver staining revealed many empty baskets indicative of PC loss (**Fig. 2B**; arrows). The anterior part of the vermis was most severely affected, followed by the posterior vermis and the cerebellar hemisphere. The PC loss in the hemisphere had a more patchy appearance. The cerebellar tonsils were the least affected. In this same order of PC loss, we observed degeneration/atrophy in both the molecular and internal granular layers. In the areas with remaining PCs, axonal torpedoes were observed (**Fig. 2B**; arrows). In addition, Kv4.3 protein levels in cerebellar lysates were lower in the patient's sample, which seemed to be the result of PC loss as shown by the reduced PC-specific marker Calbindin expression (**Fig. 2C-E**).

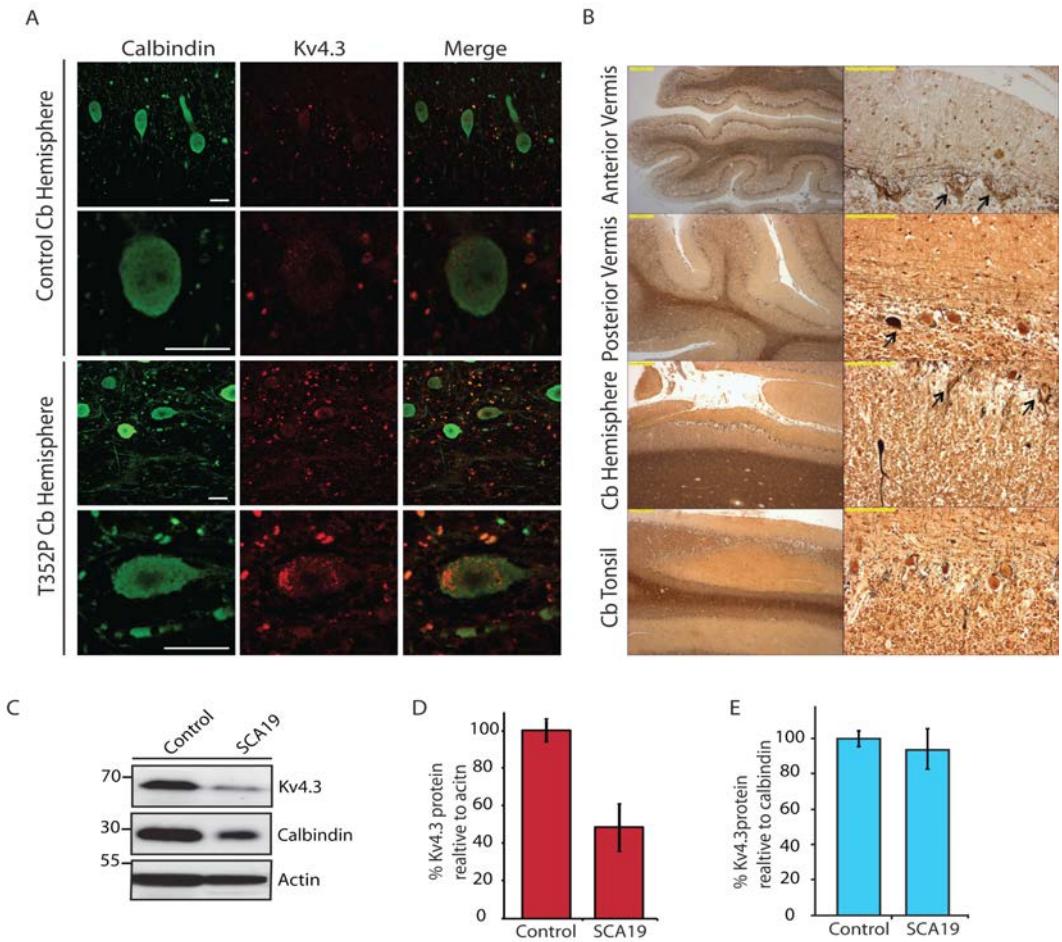

Figure 2 Immunocytochemistry, immunohistochemistry and Western blot analysis demonstrate the effect of the T352P mutation on Kv4.3 protein expression and cerebellar degeneration in human autopsy material.

A) Control cerebellar sections stained with Kv4.3 antibody (in red) and Calbindin (in green) showed punctuated staining of the Purkinje cell (PC) bodies. Stronger and more accumulated kv4.3 staining was observed in PCs soma of the SCA19 cerebellum of a T352P patient. (Scale bar: 25 µm) **B**) Micrographs of Sevier-Munger silver stainings showing overviews (left-hand side) and details (right-hand side) of degenerating cerebellar cortex. Note the atrophy of the folia in the vermis with empty baskets or torpedoes (arrows). The cerebellar hemisphere was less affected, although empty baskets and torpedoes (arrows) were still encountered. The cerebellar tonsils were least affected and showed relatively normal numbers of Purkinje cells. (Scale bars left: 500 µm and right: 100 µm) **C**) Western blot analysis of cerebellar protein extracts of control and T352 Kv4.3 mutant cerebella demonstrated markedly reduced Kv4.3 and Calbindin protein levels. **D**) Quantification of Kv4.3 protein levels in both control and the T352P mutant cerebella. Data is normalized against Actin levels using Quantity One. **E**) Data normalized against Calbindin levels.

In episodic ataxia type 2, missense mutations have already been reported as causing ER retention of the α-subunit $Ca_v2.1$ of the P/Q voltage activated calcium channel.[28] We therefore assessed whether the SCA19 missense mutations (T352P, M373I, and S390N) would also affect the subcellular localization/maturation of Kv4.3. Confocal microscopic analysis of transiently transfected HeLa cells revealed that, unlike wild-type Kv4.3

that was mainly located on the plasma membrane (74.5% ± 3.5; **Suppl. Fig. 2**), all three mutant proteins showed almost no or markedly reduced cell surface expression (T352P: 4.9% ± 0.6, M373I: 40.4% ± 6.7, and S390N: 5.0% ± 2.7; **Suppl. Fig. 2**), and rather accumulated in perinuclear foci (**Fig. 3A**). These data suggest that the SCA19 mutations cause ER retention of Kv4.3, causing impaired trafficking of the channel to the plasma membrane. Indeed, our studies showed perfect co-localization of the SCA19 mutant Kv4.3 foci and the ER marker Calnexin, but not with wild-type Kv4.3 (**Fig. 3B**). In addition, all the Kv4.3 mutants were more rapidly degraded, upon inhibition of protein synthesis, than wild-type Kv4.3 (**Fig. 3C and D**). The remaining Kv4.3 protein after 9 hours of cyclohexamide treatment was 54% ± 10 for wild-type versus 15% ± 3, 27% ± 10, and 16% ± 4 for T352P, M373I, and S390N mutant Kv4.3, respectively. The cycloheximide treatment led to an efficient translational block as was demonstrated using Western blot analysis against p53 (**Suppl. Figure 3**). This suggests that the SCA19 mutant proteins are recognized as misfolded proteins and are subsequently degraded, most likely via endoplasmatic reticulum-associated degradation (ERAD).

Functional channels do not comprise Kv4.3 alone, since tetrameric Kv4.3 complexes form a hetero-octamer complex together with the regulatory β subunits, Kv channel-interacting proteins (KChIPs), in which KChIPs drive the complex formation.[29,30] Since KChIPs are absent in HeLa cells, we wondered whether co-expression of Kv4.3 together with KChIP could improve the ER-golgi-plasma membrane trafficking of the Kv4.3 mutants as was seen for wild-type K4v.3 (**Fig. 4A**). When co-expressing KChIP2b, but not its inactive isoform KChIP2c, T352P and M373I (88.8% ± 1.5 and 82.6% ± 1.0) were detected at the plasma membrane like wild type Kv4.3 (87.8% ± 0.4 ; **Fig. 4B, C, and Suppl. Fig. 2**). However, the mislocalization of the S390N Kv4.3 mutant could not be rescued by co-expression of KChIP2b as only 21.2% ± 8.4 of the cells showed cell surface expression, but it rather trapped the regulatory β subunit in the same intracellular compartment (**Fig. 4D and Suppl. Fig. 2**). In addition, KChIPs not only drive the tetramerization of Kv4.3 subunits, but they also regulate Kv4.3 protein expression and stability.[31,32] KChIP2b co-expression led to increased protein expression for all Kv4.3 proteins (**Fig. 4D**) and also clearly improved the protein stability of wild-type, T352P and M373I-mutant Kv4.3 with the exception of S390N (**Fig. 4F and G**). The remaining Kv4.3 protein levels after 9 hours of cyclohexamide treatment were 96% ± 4 for wild-type Kv4.3 and 93% ± 20, 87% ± 3, and 13% ± 3 for T352P, M373I, and S390N, respectively. These data indicate that KChIP2b can ameliorate the folding defect of the SCA19 mutant proteins (except that of S390N) and thereby prevent protein degradation.

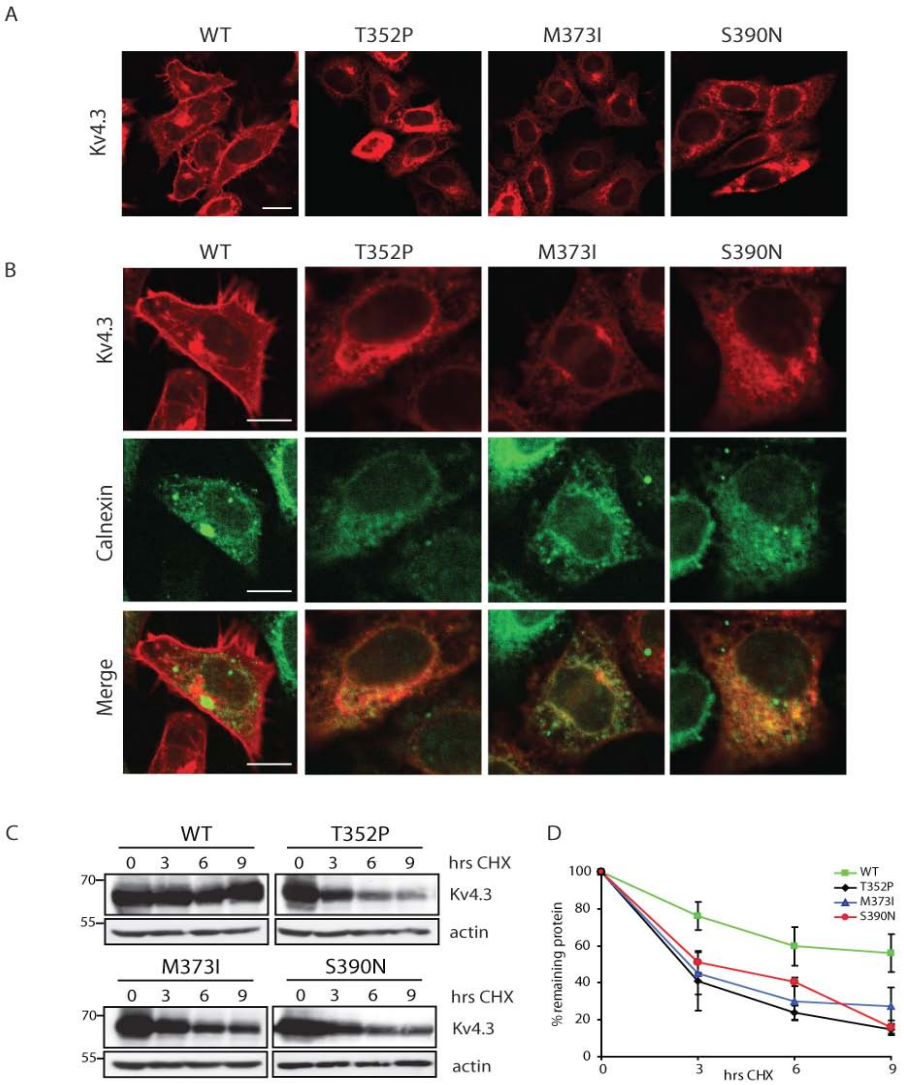

Figure 3 Endoplasmatic reticulum (ER) retention and enhanced protein degradation of SCA19 mutant Kv4.3.

A) Confocal images of HeLa cells expressing wild-type (WT) or T352P, M373I, and S390N mutant Kv4.3 subunits. All Kv4.3 mutants clearly showed intracellular retention in the perinuclear region with only 4.9 % (T352P), 40.4 % (M373I), and 5.0 % (S390N) membrane expressing cells, whereas the WT Kv4.3 channel was mainly expressed on the cell surface (74.5 % of the cells) detected using anti-Kv4.3 (in red). The quantification of the membrane localization is shown in Suppl. Fig. 2. **B**) Co-localization with the ER-marker Calnexin (in green) revealed that all three T352P, M373I and S390N mutant Kv4.3 proteins (in red) were retained in the ER, as was shown by the merged picture (in yellow). **C**) Time-course of protein degradation experiments were performed in HeLa cells transfected with either WT or T352P, M373I, and S390N mutant Kv4.3 treated with the protein synthesis inhibitor cyclohexamide (100 µg/ml) for the indicated time periods, and the existing cellular pool of all Kv4.3 were detected by Western blot. The pool of T352P, M373I and S390N mutant Kv4.3 proteins was degraded more rapidly than WT Kv4.3, which is a characteristic of misfolded ER-retained proteins. **D**) Quantification of the Western blot degradation experiment normalized by Actin, showing the % of remaining protein in time. The graphs show the average of three independent experiments and the error bars represent the Standard Deviation (SD) (Mean ± SD).

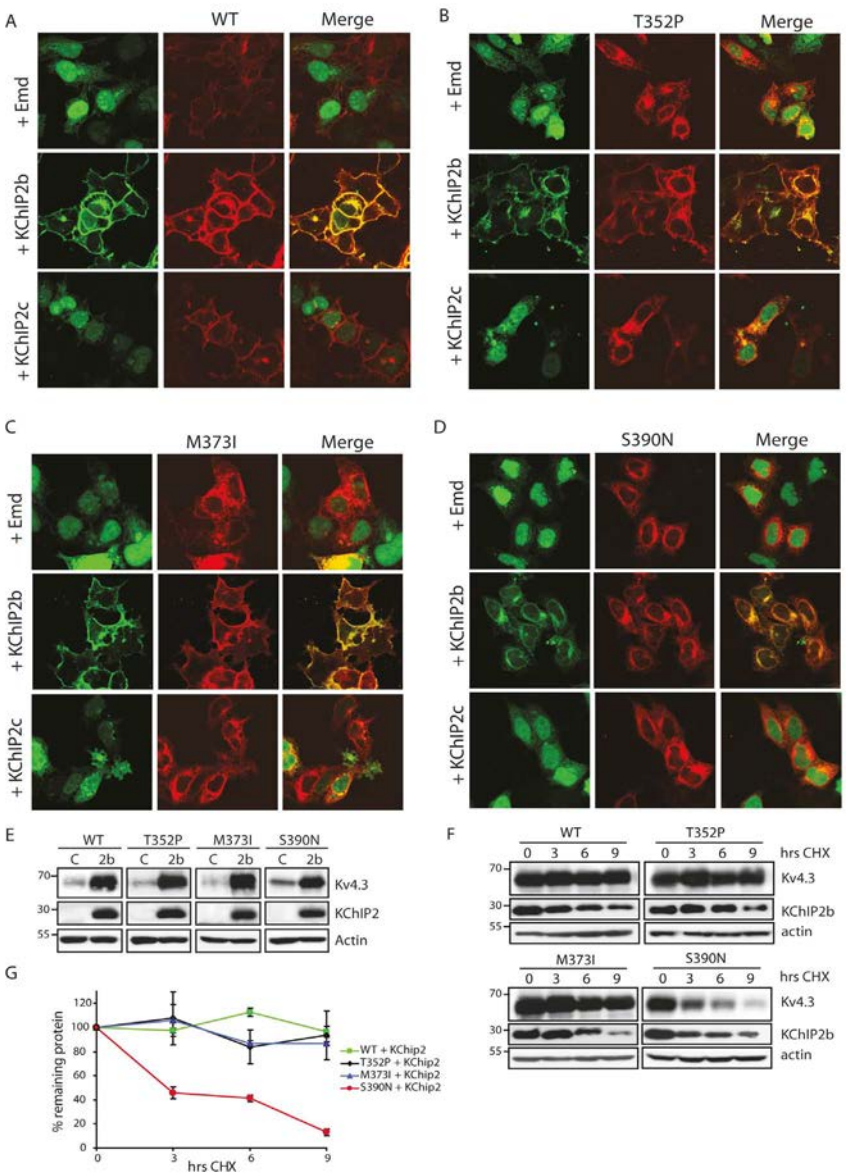

Figure 4 The regulatory β subunit, KChIP2b rescues the trafficking and stability of T352P and M373I mutant Kv4.3 channels.

A - D) Confocal images of HeLa cells expressing wild-type (WT) or T352P, M373I, and S390N mutant Kv4.3 subunits detected using anti-Kv4.3 antibody (in red), co-expressed with either empty control Emerald-C1 (Emd), KChIP2b or the non-functional isoform KChIP2c (in green) (Scale bar: 10 µm). Only KChIP2b expression resulted in a marked change in subcellular distribution of T352P (**B**) and M373I (**C**) mutant Kv4.3, as the remaining intracellular Kv4.3 pool was no longer associated with the endoplasmatic reticulum, but showed a significant increase in cell surface expression up to 88.8 % (T352P) and 82.6 % (M373I) of cells (merge in yellow). In contrast, almost no effect of KChIP2b on the subcellular distribution of S390N mutant Kv4.3 was detected as now only 21.2 % of cells showed Kv4.3 cell surface expression (**D**). The quantification of the membrane localization is shown in Suppl. Fig. 2. **E**) Western blot data showed that KChIP2b is able to regulate the expression levels of WT and all SCA19 mutant Kv4.3 proteins in HeLa cells, as for all Kv4.3 proteins increased Kv4.3 levels were detected in the presence of KChIP2b. C = empty control Emerald-C1 and 2b = KChIP2b. **F**) Time-course Kv4.3 protein degradation experiment. Western blot showed that co-expression of WT, T352P and M373I mutant Kv4.3 with KChIP2b resulted in a significant increase in protein stability (rescue up to almost 90% for WT, T352P, and M373I mutant Kv4.3) in HeLa cells during 9 hours of cyclohexamide treatment. This effect was not observed for S390N mutant Kv4.3. Here, co-expression with KChIP2b led to about 13% and thus a similar percentage of remaining S390N mutant Kv4.3 proteins levels without KChIP2b after 9 hours of cyclohexamide treatment. **G**) Quantification of the Kv4.3 protein degradation in the presence of KChIP2b normalized by Actin using Quantity One. The graphs show the average of three independent experiments and the error bars represent the Standard Deviation (SD) (Mean ± SD).

To test for Kv4.3 channel activity in the presence of KChIP2b, we recorded its K+ currents by patch clamping in HEK293T cells. Activation of the wild-type Kv4.3-KChIP2b complex was detected at approximately -40 mV followed by more positive potentials up to +28 mV (**Fig. 5A and E**). In contrast, almost no detectable channel activity was detected for T352P-KChIP2b and S390N- KChIP2b complexes (1% and 13% channel activity compared to wild type, 100%; **Fig. 5B, D, and E**), whereas strongly reduced activity (up to 75% of reduction) was measured for M373I-KChIP2b (**Fig. 5C and E**). All mutant Kv4.3 complexes showed significantly decreased current amplitude at 28mV from 4541 ± 599 (wild-type), to 44 ± 27 (T352P), 1150 ± 393 (M373I), and 571 ± 174 (S390N) (**Fig. 5F**). These results demonstrate that although T352P mutant Kv4.3 and the regulatory β subunit KChIP2b co-assemble and are present at the plasma membrane, the T352P-KChIP2b complex is not functional. The M373I-KChIP2b complex seem to be functional, but it produces Kv4.3 channels with marked reduced activity. Notably, very weak S390N-KChIP2b activity was detected, despite the fact that about all S390N-KChIP2b complexes are ER-retained as was observed by microscopy. Therefore, we speculate that probably a few S390N-KCHIP2b complexes escape the ER and reach the plasma membrane but still display almost no Kv4.3 channel activity. To confirm that the observed loss of channel activity is not due to enhanced T352P, M373I or S390N Kv4.3 protein degradation, the Kv4.3 expression levels were checked using Western blot. No differences in expression levels were observed between wild-type and all mutant Kv4.3 subunits (**Suppl. Fig. 4**).

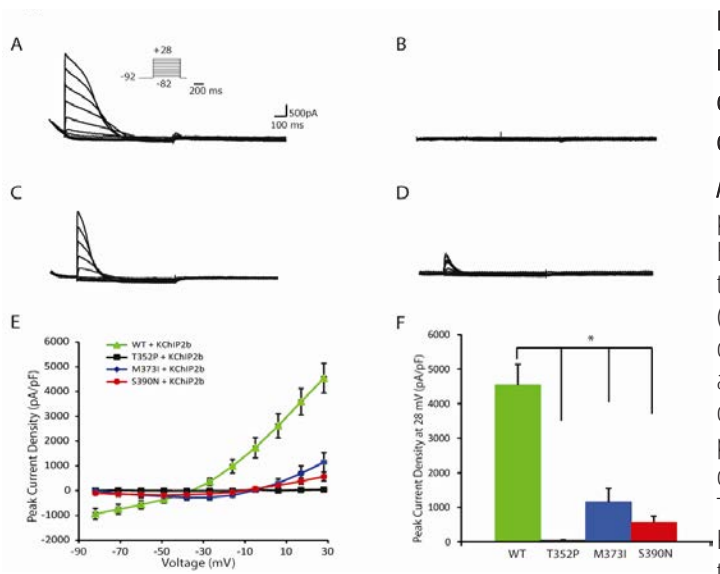

Figure 5 SCA19 mutations cause loss of the Kv4.3-KChIP2b channel complex activity and lead to reduced outward K+ currents.

A-D) Representative whole-cell potassium currents recorded in HEK293T cells transfected with wild-type (WT) (**A**), T352P (**B**), M373I (**C**), and S390N (**D**) mutant Kv4.3 co-expressing KChIP2b. The traces are generated by step depolarization of 200 ms duration from a holding potential of -82mV to +28mV. **E**) The current-voltage relationship for WT, T352P, M373I, and S390N mutant Kv4.3-KChIP2b complexes. Clearly, the T352P, M373I, and S390N mutant Kv4.3-KChIP2b complexes showed almost no or strongly reduced channel activity. All values shown in the graph are the average of at least 10 independent measurements and the error bars represent the Standard Error of the Mean (Mean ± SEM). **F**) The bar graph shows the mean peak current density at 28mV for WT, T352P, M373I, and S390N mutant Kv4.3-KChIP2b complexes. All mutant-KChIP2b complexes showed significant reduced peak current density at 28mV when compared to wild-type Kv4.3-KChIP2b. The significance was calculated using a Student's *t*-test, * = 0.05 (Mean ± SEM).

Discussion

Our studies provide evidence that missense mutations in *KCND3* cause SCA19 by either altering Kv4.3 ER-golgi-plasma membrane transport, leading to enhanced protein degradation suggestively by endoplasmatic reticulum associated degradation (ERAD), and/or by loss of Kv4.3 channel functioning. *KCND3* encodes for Kv4.3, a highly conserved ShaI-related subfamily, voltage-gated potassium channel, that is known to regulate cardiac and neuronal membrane excitability.[33] *KCND3* mRNA is highly expressed in cerebellum, including Purkinje cells, basket cells, stellate cells and deep neurons,[34] and is thought to be important for its development.[14,35] The Kv4 channel family consists of three pore-forming α subunits, Kv4.1, Kv4.2, and Kv4.3.[36] These α subunits form tetrameric channel complexes and bind regulatory β subunits, KChIPs, that change intracellular trafficking of the Kv4 channels from ER to plasma membrane and channel activity.[29,37] The neuronal Kv4 channel complex mediates the A-type K+ current, that are important for dendritic excitability, somatodentritic signal integration, and long-term potentiation (LTP).[33,38-42]

KCND3 knockout mice have already been generated but they do not display any neurological deficits,[43] probably due to redundancy of the other Kv4 family members. This implies that the SCA19 mutants described here must have a dominant negative effect on the maturation and/or function of the other complex members and cause a loss of Kv4.3 function. Indeed, our S390N mutant data support such a hypothesis as this mutant leads to the trapping of the regulatory β subunit in the ER.

The question remains how defects in a voltage-gated potassium channel can lead to cerebellar neurodegeneration. We are considering three potential mechanisms. First, altered dendritic excitability due to reduced A-type K+ currents and subsequent initiation and a longer duration of action potentials might lead to changes of intracellular calcium homeostasis that may trigger PC death.[44] Secondly, SCA19 mutations could induce LTP deficits at the PC synapse. This would affect one of the important tasks of the cerebellum – fine adjustment of motor coordination – that indeed requires intact long-term depression (LTD) and LTP processes.[45,46] Thirdly, the misfolded Kv4.3 channels may lead to a chronic form of ER stress and over-induction of the unfolded protein response, thereby activating pro-apoptotic factors leading to PC cell death.[47]

The different SCA19 mutations were found to affect Kv4.3 ER-golgi-plasma membrane maturation and channel activity differently, ranging from an almost complete inability to reach the plasma membrane (S390N), to almost complete absent (T352P), or only marked reduced (M373I) channel activity. This may, to some extent, explain the diverse disease phenotypes observed in the three SCA19 families. The patients with the T352P and S390N mutations showed more severe disease phenotypes than those with the M373I, given the presence of cognitive impairment, myoclonus, and tremor in most of the T352P patients, cognitive impairment and spasticity in the S390N case and the absence of these symptoms in M373I cases. In addition, the age of onset of the M373I family is relatively late (average of 55 years) compared to an average 30 or 35 years of age in the T352P and S390N cases.

Interestingly, the three different cellular phenotypes of the mutants are partially reminiscent of what is seen for mutations in the cAMP-regulated chloride channel (CFTR) that cause cystic fibrosis, in which both CFTR maturation defects and reduced channel activities were also found.[48] Different therapeutic strategies that

interfere with either the folding or degradation of maturation defective mutants or that stimulate channel opening of membrane-associated mutants with impaired function may also be of value for the Kv4.3 mutants and are currently being investigated.

Besides being expressed in brain, Kv4.3 is also expressed at relatively high levels in heart tissue. Although, the SCA19 cases have not (yet) been reported to exhibit cardiomyopathy, it is notable that rare genetic variations have been associated with a gain of Kv4.3 function that is associated with Brugada syndrome,[49] implying that Kv4.3 may well play a role in human heart disease.

In conclusion, our current findings significantly contributes to reveal the importance of voltage-gated potassium channels in cerebellar ataxias, including episodic ataxia type 1 and SCA13 [20,50] and show that mutations in *KCND3*, only required to prevent the fast repolarization of neurons, is sufficient to cause cerebellar neurodegeneration. We therefore speculate that more Kv4 family members or interacting proteins of Kv4.3 may also be involved in the etiology of other cerebellar ataxias.

Acknowledgments

We thank all the patients for their participation, Jackie Senior for editing the manuscript, Dr. K. Takimoto for providing the KChIP2 plasmids, and Dr. B. van de Sluis for critically reading the manuscript. This work was funded by a Rosalind Franklin Fellowship from the University of Groningen, the Prinses Beatrix Foundation (W.OR10-38) and NutsOhra (1101-042). Part of this work was performed at the UMCG Microscopy and Imaging Center (UMIC), which is sponsored by NWO (40-00506-98-9021 and 175-010-2009-023).

Supplementary Material available on: http://www.springer.com/medicine/neurology/journal/415

References

1. Durr A. Autosomal dominant cerebellar ataxias: polyglutamine expansions and beyond. Lancet Neurol 2010;9:885-994.
2. Bakalkin G, Watanabe H, Jezierska J, et al. Prodynorphin Mutations Cause the Neurodegenerative Disorder Spinocerebellar Ataxia Type 23. Am J Hum Genet 2010;12;87(5):593-603.
3. Wang JL, Yang X, Xia K, et al. TGM6 identified as a novel causative gene of spinocerebellar ataxias using exome sequencing. Brain 2010;133:3510-3518.
4. Kobayashi H, Abe K, Matsuura T, et al. Expansion of intronic GGCCTG hexanucleotide repeat in NOP56 causes SCA36, a type of spinocerebellar ataxia accompanied by motor neuron involvement. Am J Hum Genet 2011;89:121-130.
5. Carlson KM, Andresen JM, Orr HT. Emerging pathogenic pathways in the spinocerebellar ataxias. Curr Opin Genet Dev 2009;19:247-253.
6. Matilla-Duenas A, Sanchez I, Corral-Juan M, Davalos A, Alvarez R, Latorre P. Cellular and molecular pathways triggering neurodegeneration in the spinocerebellar ataxias. Cerebellum 9:148-166.
7. Schorge S, van de Leemput J, Singleton A, Houlden H, Hardy J. Human ataxias: a genetic dissection of inositol triphosphate receptor (ITPR1)-dependent signaling. Trends Neurosci 33:211-219.
8. Verbeek DS, Schelhaas JH, Ippel EF, Beemer FA, Pearson PL, Sinke RJ. Identification of a novel SCA locus (SCA19) in a Dutch autosomal dominant cerebellar ataxia family on chromosome region 1p21-q21. Hum Genet 2002;111:388-393.
9. Chung MY, Lu YC, Cheng NC, Soong BW. A novel autosomal dominant spinocerebellar ataxia (SCA22) linked to chromosome 1p21-q23. Brain 2003;126:1293-1299.
10. Schelhaas HJ, Verbeek DS, van de Warrenburg BP, Sinke RJ. SCA19 and SCA22: evidence for one locus with a worldwide distribution. Brain 2004;127:E6.
11. Schelhaas HJ, Ippel PF, Hageman G, Sinke RJ, van der Laan EN, Beemer FA. Clinical and genetic analysis of a four-generation family with a distinct autosomal dominant cerebellar ataxia. J Neurol 2001;248:113-120.
12. Serodio P, Kentros C, Rudy B. Identification of molecular components of A-type channels activating at subthreshold potentials. J Neurophysiol 1994;72:1516-1529.
13. Tsaur ML, Chou CC, Shih YH, Wang HL. Cloning, expression and CNS distribution of Kv4.3, an A-type K+ channel alpha subunit. FEBS Lett 1997;400:215-220.
14. Serodio P, Rudy B. Differential expression of Kv4 K+ channel subunits mediating subthreshold transient K+ (A-type) currents in rat brain. J Neurophysiol 1998;79:1081-1091.
15. Li H, Durbin R. Fast and accurate long-read alignment with Burrows-Wheeler transform. Bioinformatics 2010;26:589-595.
16. McKenna A, Hanna M, Banks E, et al. The Genome Analysis Toolkit: a MapReduce framework for analyzing next-generation DNA sequencing data. Genome Res 2010;20:1297-1303.
17. DePristo MA, Banks E, Poplin R, et al. A framework for variation discovery and genotyping using next-generation DNA sequencing data. Nat Genet 2011;43:491-498.
18. Adamusiak T, Parkinson H, Muilu J, et al. Observ-OM and Observ-TAB: Universal syntax solutions for the integration, search and exchange of phenotype and genotype information. Hum Mutat 2012; Epub ahead of print
19. Adzhubei IA, Schmidt S, Peshkin L, et al. A method and server for predicting damaging missense mutations. Nat Methods 2010;7:248-249.
20. Waters MF, Minassian NA, Stevanin G, et al. Mutations in voltage-gated potassium channel KCNC3 cause degenerative and developmental central nervous system phenotypes. Nat Genet 2006;38:447-451.
21. Kumar P, Henikoff S, Ng PC. Predicting the effects of coding non-synonymous variants on protein function using the SIFT algorithm. Nat Protoc 2009;4:1073-1081.

22. Tavtigian SV, Deffenbaugh AM, Yin L, et al. Comprehensive statistical study of 452 BRCA1 missense substitutions with classification of eight recurrent substitutions as neutral. J Med Genet 2006;43:295-305.

23. Mathe E, Olivier M, Kato S, Ishioka C, Hainaut P, Tavtigian SV. Computational approaches for predicting the biological effect of p53 missense mutations: a comparison of three sequence analysis based methods. Nucleic Acids Res 2006;34:1317-1325.

24. Takimoto K, Yang EK, Conforti L. Palmitoylation of KChIP splicing variants is required for efficient cell surface expression of Kv4.3 channels. J Biol Chem 2002;277:26904-26911.

25. Duarri A, Teijido O, Lopez-Hernandez T, et al. Molecular pathogenesis of megalencephalic leukoencephalopathy with subcortical cysts: mutations in MLC1 cause folding defects. Hum Mol Genet 2008;17:3728-3739.

26. Duarri A, Lopez de HM, Capdevila-Nortes X, et al. Knockdown of MLC1 in primary astrocytes causes cell vacuolation: a MLC disease cell model. Neurobiol Dis 2011;43:228-238.

27. Strassle BW, Menegola M, Rhodes KJ, Trimmer JS. Light and electron microscopic analysis of KChIP and Kv4 localization in rat cerebellar granule cells. J Comp Neurol 2005;484:144-155.

28. Mezghrani A, Monteil A, Watschinger K, et al. A destructive interaction mechanism accounts for dominant-negative effects of misfolded mutants of voltage-gated calcium channels. J Neurosci 2008;28:4501-4511.

29. An WF, Bowlby MR, Betty M, et al. Modulation of A-type potassium channels by a family of calcium sensors. Nature 2000;403:553-556.

30. Wang H, Yan Y, Liu Q, et al. Structural basis for modulation of Kv4 K+ channels by auxiliary KChIP subunits. Nat Neurosci 2007;10:32-39.

31. Trimmer JS. Regulation of ion channel expression by cytoplasmic subunits. Curr Opin Neurobiol 1998;8:370-374.

32. Shibata R, Misonou H, Campomanes CR, et al. A fundamental role for KChIPs in determining the molecular properties and trafficking of Kv4.2 potassium channels. J Biol Chem 2003;278:36445-36454.

33. Hille B. Ionic Channels in Excitable Membranes. 3rd edition, Sinauer Associates, Sunderlands, MA, USA, 2001.

34. Hsu YH, Huang HY, Tsaur ML. Contrasting expression of Kv4.3, an A-type K+ channel, in migrating Purkinje cells and other post-migratory cerebellar neurons. Eur J Neurosci 2003;18:601-612.

35. Herrup K, Kuemerle B. The compartmentalization of the cerebellum. Annu Rev Neurosci 1997;20:61-90.

36. Covarrubias M, Bhattacharji A, De Santiago-Castillo JA, et al. The neuronal Kv4 channel complex. Neurochem Res 2008;33:1558-1567.

37. Rhodes KJ, Carroll KI, Sung MA, et al. KChIPs and Kv4 alpha subunits as integral components of A-type potassium channels in mammalian brain. J Neurosci 2004;24:7903-7915.

38. Hoffman DA, Magee JC, Colbert CM, Johnston D. K+ channel regulation of signal propagation in dendrites of hippocampal pyramidal neurons. Nature 1997;387:869-875.

39. Birnbaum SG, Varga AW, Yuan LL, Anderson AE, Sweatt JD, Schrader LA. Structure and function of Kv4-family transient potassium channels. Physiol Rev 2004;84:803-833.

40. Kim J, Jung SC, Clemens AM, Petralia RS, Hoffman DA. Regulation of dendritic excitability by activity-dependent trafficking of the A-type K+ channel subunit Kv4.2 in hippocampal neurons. Neuron 2007;54:933-947.

41. Jerng HH, Pfaffinger PJ, Covarrubias M. Molecular physiology and modulation of somatodendritic A-type potassium channels. Mol Cell Neurosci 2004;27:343-369.

42. Chen X, Yuan LL, Zhao C, et al. Deletion of Kv4.2 gene eliminates dendritic A-type K+ current and enhances induction of long-term potentiation in hippocampal CA1 pyramidal neurons. J Neurosci 2006;26:12143-12151.

43. Niwa N, Wang W, Sha Q, Marionneau C, Nerbonne JM. Kv4.3 is not required for the generation of functional Ito,f channels in adult mouse ventricles. J Mol Cell Cardiol 2008;44:95-104.

44. Spitzer NC. Electrical activity in early neuronal development. Nature 2006;444:707-712.

45. De Zeeuw CI, Yeo CH. Time and tide in cerebellar memory formation. Curr Opin Neurobiol 2005;15:667-674.

46. Jorntell H, Hansel C. Synaptic memories upside down: bidirectional plasticity at cerebellar parallel fiber-Purkinje cell synapses. Neuron 2006;52:227-238.

47. Doyle KM, Kennedy D, Gorman AM, Gupta S, Healy SJ, Samali A. Unfolded proteins and endoplasmic reticulum stress in neurodegenerative disorders. J Cell Mol Med 2011;15:2025-2039.

48. Roomans GM. Pharmacological treatment of the ion transport defect in cystic fibrosis. Expert Opin Investig Drugs 2001;10:1-19.

49. Giudicessi JR, Ye D, Tester DJ, et al. Transient outward current (I(to)) gain-of-function mutations in the KCND3-encoded Kv4.3 potassium channel and Brugada syndrome. Heart Rhythm 2011;8:1024-1032.

50. Browne DL, Gancher ST, Nutt JG, et al. Episodic ataxia/myokymia syndrome is associated with point mutations in the human potassium channel gene, KCNA1. Nat Genet 1994;8:136-140.

CHAPTER 4

Prodynorphin mutations cause the neurodegenerative disorder spinocerebellar ataxia type 23

Georgy Bakalkin,[1] Justyna Jezierska,[2,10] Hiroyuki Watanabe,[1,10] Cloë Depoorter,[2] Corien Verschuuren-Bemelmans,[2] Igor Bazov,[1] Konstantin A. Artemenko,[3] Tatjana Yakovleva,[1] Dennis Dooijes,[4] Bart P.C. Van de Warrenburg,[5] Roman A. Zubarev,[6] Berry Kremer,[7] Pamela Knapp,[8,9] Kurt F. Hauser,[9] Cisca Wijmenga,[2] Fred Nyberg,[1] Richard J. Sinke[2,4] & Dineke S. Verbeek[2]

[1]Division of Biological Research on Drug Dependence, Department of Pharmaceutical Biosciences, Uppsala University, Sweden, [2]Department of Genetics, University Medical Center Groningen, University of Groningen, Groningen, the Netherlands, [3]Division of Molecular Biometry, Institute for Cell and Molecular Biology, Uppsala University, Uppsala, Sweden, [4]Department of Medical Genetics, University Medical Center Utrecht, Utrecht, The Netherlands, [5]Department of Neurology, University Medical Center Nijmegen, Nijmegen, The Netherlands, [6]Division of Molecular Biometry, Department of Medicinal Biochemistry & Biophysics Department, Karolinska Institutet, Stockholm, Sweden, [7]Department of Neurology, University Medical Center Groningen, University of Groningen, Groningen, The Netherlands, [8]Department of Anatomy and Neurobiology, [9]Department of Pharmacology and Institute for Drug and Alcohol Studies, Virginia Commonwealth University, Richmond, Virginia

[10]These authors contributed equally to this work

Am J Hum Genet 2010; 87: 1-11

Abstract

Spinocerebellar ataxias (SCAs) are dominantly inherited neurodegenerative disorders characterized by progressive cerebellar ataxia and dysarthria. We have identified missense mutations in *prodynorphin* (*PDYN*) that cause SCA23 in four Dutch families displaying progressive gait and limb ataxia. PDYN is the precursor protein for the opioid neuropeptides, a-neoendorphin, and dynorphins A and B (Dyn A and B). Dynorphins regulate pain processing and modulate the rewarding effects of addictive substances. Three mutations were located in Dyn A, a peptide with both opioid activities and nonopioid neurodegenerative actions. Two of these mutations resulted in excessive generation of Dyn A in a cellular model system. In addition, two of the mutant Dyn A peptides induced toxicity above that of wild-type Dyn A in cultured striatal neurons. The fourth mutation was located in the nonopioid PDYN domain and was associated with altered expression of components of the opioid and glutamate system, as evident from analysis of SCA23 autopsy tissue. Thus, alterations in Dyn A activities and/or impairment of secretory pathways by mutant PDYN may lead to glutamate neurotoxicity, which underlies Purkinje cell degeneration and ataxia. PDYN mutations are identified in a small subset of ataxia families, indicating that SCA23 is an infrequent SCA type (~0.5%) in the Netherlands and suggesting further genetic SCA heterogeneity.

Introduction

The dominant spinocerebellar ataxias (SCAs) are a genetically heterogeneous group of neurodegenerative disorders characterized by progressive cerebellar ataxia, dysarthria, oculomotor abnormalities, and many additional symptoms.[1] The ataxia results from selective atrophy of the Purkinje cells in the cerebellum. To date, 31 different SCA loci have been described, but the causative mutation and corresponding gene has only been identified in 19 SCA types.[2,3] Nine of the 19 SCAs are caused by coding CAG repeat (SCA1–3, SCA6, SCA7, and SCA17; MIM #164400, MIM #183090, MIM #109150, MIM #183086, MIM #164500, and MIM #607136) or noncoding CAG, CTG, or ATTCT repeat expansions. These coding CAG (glutamine) repeat expansions lead to elongated polyglutamine tracts that subsequently cause misfolding of the corresponding proteins. The functional implication of the noncoding repeat expansions is suggested to induce RNA-mediated gain-of-function mechanisms, leading to neurotoxicity. However, the remainders of the known SCA types are due to missense mutations or chromosomal rearrangements (SCA5, SCA11, SCA13–15, SCA20, SCA27, SCA28, and SCA31; MIM #600224, MIM #604432, MIM #605259, MIM #605361, MIM #606658, MIM #608687, MIM #609307, MIM #610246, and MIM #117210).[2] The SCA genes involved play a role in a wide range of biological processes. Recent studies into the function of the disease proteins revealed the existence of common pathways leading to ataxia consisting of changes in gene transcription and RNA processing or synaptic transmission via calcium and glutamate signaling.[4,5]

Currently, only 70% of the Dutch SCA families can be diagnosed by mutation analysis of seven of the known SCA genes (SCA1–3, SCA6, SCA7, SCA12, and SCA14). The identification of causal mutations and novel genes in the group of genetically undiagnosed families will provide additional insights into the underlying pathological pathways leading to cerebellar neurodegeneration and will perhaps indicate therapeutic approaches.

We previously mapped the SCA23 locus (MIM #610245) to a 6 Mb region located on chromosomal region 20p12.3-p13 in a single, large Dutch ataxia family without mutations in the SCA genes that were recognized at the time.[6] MRI and neuropathological examination of SCA23 autopsy tissue revealed neuronal loss in the Purkinje cell layer, dentate nuclei, and inferior olivary nuclei. The patients showed a relatively slowly progressive, isolated, cerebellar ataxia. Additional neurological examination revealed dysarthria, oculomotor problems such as slowing saccades, and ocular dysmetria. Decreased vibration sense below the knee was observed in three affected individuals, hyperreflexia was observed in four patients, and two patients displayed Babinski's signs. Because no affected individuals of the first generation were still alive at the time of the assessment, clinical anticipation could not be confirmed. The SCA23 locus comprises 97 genes and transcripts, of which at least 54 are expressed in the cerebellum. Previous attempts to identify one or more mutations causing the disease did not yield any results.[6,7]

In the present study, we identified four missense mutations in *prodynorphin*, *PDYN* (MIM #131340), in the originally reported SCA23 family and in three families from a Dutch ataxia cohort. PDYN is the precursor protein for the opioid neuropeptides a-neoendorphin, Dyn A, and Dyn B, ligands for the k-opioid receptor (*OPRK1*; MIM #165196).[8] Neuropeptides constitute a large family of signaling molecules that mediate and modulate neuronal communication by acting on cell surface receptors and thus regulate diverse physiological functions and behavior.[9,10] Neuropeptides and their precursor molecules have not yet been identified as causative factors for neurodegenerative disorders.

Subjects and methods

Human subjects

The participants from the SCA23 family all gave informed consent, as approved by the Medical Ethical Committee of the University Medical Centre Utrecht. The 1100 ataxia patients (single index cases) screened in this study were obtained from the genetic diagnostic centers in Utrecht and Groningen in The Netherlands. All extended DNA analyses were performed in a diagnostic setting (accredited diagnostic DNA laboratory). Only DNA samples from patients who were referred for genetic testing for SCA were used and had no mutations in seven known SCA (SCA1–3, SCA6, SCA7, SCA12, and SCA14) genes. This cohort is comprised of 10% familial cases (8% dominant and 2% recessive) and 90% seemingly sporadic cases. The additional tests were thus performed in line with the original diagnostic request. Moreover, when the blood samples were taken, patients were asked whether they had objections to the use of their DNA for future (anonymous) studies to help develop or improve techniques. If they had objections, this was indicated on the original "Request for DNA Test" form, and the DNA was not used. The unrelated 500 control individuals were obtained from the Dutch blood bank.

Postmortem human specimens

SCA23 cerebellar tissues from the subject with a p.R138S mutation and from a control subject were obtained from the University Medical Center Nijmegen, Nijmegen, The Netherlands. Samples of the cerebellum (Cb), dorsolateral prefrontal cortex (PFC; Brodmann area 9), and nucleus accumbens (NAc) from three control subjects, all females of European descent (for demographic data, see **Table S6**), were collected at the Karolinska Institute, Stockholm, Sweden, by qualified pathologists. The collection was performed under full ethical clearance from the University Medical Center Nijmegen and the Stockholm Ethical Review Board. Informed written consent from the next of kin was also obtained.

PDYN sequencing

DNA was extracted from peripheral blood by a routine salting-out procedure. The genomic DNA of all participating subjects in this study was used to amplify the PDYN coding exons 3 and 4 (GenBank accession number:NM024411.3) by PCR. The resulting amplicons, including the intron-exon boundaries, were screened for mutations via Sanger sequencing on an ABI 3700 (Applied Biosystems). The PCR, primer sequences, and conditions are shown in **Table S7**.

Dynorphin radioimmunoassay

The radioimmunoassay (RIA) procedure was described elsewhere.[11,12] Briefly, cells were extracted in 1 M acetic acid, extracts were run through an SP-Sephadex ion exchange C-25 column, and peptides were eluted and analyzed by RIA.

Peptide synthesis

Dyn A peptides were synthesized at the Leiden University Medical Center, Leiden, The Netherlands, purified by reverse-phase chromatography and Superdex column, and analyzed by reverse-phase chromatography and MALDI-TOF MS. The purity of all peptides was ~98%.

Neuron-enriched cultures, peptide treatment and assessment of neuron viability

Neurons were isolated from E15–E16 imprinting control region CD-1 mouse striatum as published.13 Briefly, the tissue was enzymatically and mechanically dissociated and filtered through a 70 μm pore nylon mesh. Neurons were plated onto poly-L-lysine (Sigma-Aldrich) coated glass coverslips inserted into a 24-well multiwell plate (5 x 10^5 neurons suspended per well). Neurons were maintained in Neurobasal media with added B27 supplement (Invitrogen), antibiotics, 0.5 mM L-glutamine, and 0.025 μM glutamate (both Invitrogen) at 37°C in 5% CO_2 at ~95% humidity. Cultures matured for 1 week prior to the start of experiments and were almost exclusively neurons when assessed by immunostaining for either NeuN or MAP2a/b (glial contamination < 1%). Neurons were treated with wild-type or mutant Dyn A peptides (p.L211S, p.R212W, or p.R215C) at 100 nM for 60 hr.

Time-lapse digital images of the same neuron were recorded at 20 min intervals for 60 hr with a Zeiss AxioObserver Z.1 microscope equipped with an automated, computer-controlled stage encoder, digital camera (Zeiss MRm), and environmental control chamber (PeCon Instruments) at 37°C with 95% humidity and 5% CO_2. In each experiment, cells from 2–3 pups were pooled and distributed across treatments such that the neurotoxic effects of each peptide variant were directly compared in the same population of cells. Approximately 50 healthy neurons with welldefined dendritic and axonal arbors were identified within ≥8 overlapping fields (40x magnification; Mark&Find and Time Lapse modules Zeiss AxioVision 4.6) in each individual culture well prior to treatment (0 hr). Individual neurons were tracked throughout the experiment, and death was defined by the culmination of a series of events resulting in nuclear fragmentation and destruction of the cell body. Events preceding neuronal death included dendritic and axonal pruning, the dissolution of the Nissl substance, appearance of cytoplasmic swelling and vacuolization, nuclear damage and pyknosis, and eventual destruction of the cell body.[13,14] Death was confirmed by viability markers such as ethidium homodimer, ethidium monoazide, or trypan blue (data not shown). These markers all possess inherent cytotoxicity and cannot be used to monitor cells during the entire course of the experiment. The effect of each treatment on neuron survival (percent pretreatment value) was analyzed statistically at 4 hr intervals via one-way repeated-measures analysis of variance (ANOVA; Graphpad Prism software) and was reported as mean neuron survival 5 standard error of the mean (SEM) from n = 2–4 separate experiments (100–200 total neurons per treatment).

mRNA analysis by quantitative Real-time PCR using TaqMan low density arrays

RNA preparation was performed with RNeasy Lipid Tissue Mini Kit (QIAGEN). RNA was quantified with microspectrophotometry by Nanodrop. RNA Quality Indicator (RQI) was measured with Bio-Rad Experion. RNA samples with RQI values above 5.0 are generally considered to be suitable for qRT-PCR.[15–17] Average RQI was 7.28

± 1.55 (mean, standard deviation [SD]), demonstrating high quality of isolated RNA. cDNA was synthesized with the High-Capacity cDNA Archive Kit (Applied Biosystems). mRNA levels were quantified by TaqMan low-density arrays (Applied Biosystems). For each gene, every sample was run in triplicate on the same array. To measure the quantity of a given RNA species, we monitored the threshold cycles (Ct) by the Applied Biosystems 7900HT Fast Real-Time PCR System. mRNA levels were calculated by relative quantification by using a normalization factor (geometric mean of four reference genes: beta-actin, *ACTB*; ribosomal large P0, RPLP0; polymerase (RNA) II [DNA-directed) polypeptide A, POLR2A; and ubiquitin C, UBC) and the qBASE program for internal and external calibration and for easy care of large RT-PCR data sets.

Immunohistochemistry

The cerebellar tissue was obtained from an SCA23 patient with a p.R138S[6] and from a control subject via a rapid autopsy protocol with a warm postmortem interval of 4 or 5 hr (**Table S4**). The control subject was without cerebellar ataxia or other neurological disorders. Fresh-frozen cerebellar tissue samples were fixed in 4% phosphate-buffered paraformaldehyde, frozen, cut in 5 mm thick sections, and processed as described previously, with modifications.[18,19] Briefly, the sections were incubated with PBS/0.2% triton and 0.1 M sodium citrate buffer (pH = 4.5) exposed to microwave irradiation and incubated with rabbit polyclonal anti-PDYN, Dyn A, or Dyn B antibodies (IgG fraction)[12,19] or mouse monoclonal anti-SLC1A6 (alias EAAT4; MIM #600637) antibodies (Abcam). After incubation with peroxidase-labeled secondary antibodies (Santa Cruz Biotechnology), the staining was visualized by 3-amino-9-ethylcarbazole (AEC; Sigma-Aldrich) and counterstained with hematoxylin. The sections were analyzed with a bright-field microscope (Leica; DM3000).

Cell culture, transfection, and plasmids

RINm-5F cells were grown in RPMI-1960 (Invitrogen) supplemented with 10% fetal bovine serum (Invitrogen) in a 37°C incubator with 5% CO_2. Transfections were carried out with Lipofectamine (Invitrogen). pCMV4 empty plasmid was used for mock transfection. The wild-type pCMV4-fl-h-PDYN construct was described previously.[19] The p.R138S, p.L211S, p.R212W, and p.R215C mutations were introduced into the *PDYN* cDNA with the Quickchange II Site-Directed Mutagenesis kit (Stratagene). The mutagenesis primers that were used to generate the mutant PDYN constructs are listed in **Table S8**. Sequencing was performed to verify the presence of the mutations and to check *PDYN* cDNA sequence.

Western blot analysis

To enrich PDYN in extracts of the cerebellum characterized by low *PDYN* expression levels, we extracted the tissues with 1 M acetic acid followed by SEP-PAC C18 reverse-phase chromatography or with Buffer C, as described before.[12,19] Both procedures gave essentially the same results. Tissues for analysis of EAAT4 and calbindin (MIM #114050) and cell pellets for analysis of PDYN were extracted with 4% SDS buffer supplemented with DTT and Compete Inhibitor Cocktail (Roche), as described previously.[20] Protein concentration was determined with DC pro-

tein assay (Bio-Rad Laboratory). Proteins were resolved by SDS-PAGE on 10% Tricine gels, transferred onto nitrocellulose membranes (Schleicher and Schuell), and stained with MemCode reversible Protein Stain Kit (Pierce), as described previously.[12,19] Membranes blocked with 5% nonfat dry milk were probed with anti-PDYN, anti-Dyn B, and anti-EAAT4 antibodies (Santa Cruz Biotechnology) or anti-calbindin antibody (Sigma-Aldrich) and were incubated with peroxidase-conjugated anti-rabbit, anti-mouse (Bio-Rad Laboratory), and anti-goat secondary antibodies (Sigma-Aldrich). Densitometric analysis was performed with Image Gauge V3.12 (Fujifilm). Protein levels were calculated as the ratio of optical density (OD) of protein immunoreactivity to MemCode OD. Measurements of all proteins were performed within the linear range of detection. The correlation coefficient between protein immunoreactivity measured as OD and protein load measured as MemCode OD was 0.98 or higher.

Sample preparation for mass spectrometry analysis

Powdered brain tissue samples were sonicated in the extraction buffer (6Murea, 2Mthiourea, and 1% octyl-b-D-glucopyranoside [all Sigma-Aldrich] in 10 mM Tris-HCl) and further exchanged to 50 mM NH_4HCO_3 (Sigma-Aldrich) with PD SpinTrap G-25 columns (GE Healthcare). The protein was measured via the microBCA assay (Pierce). The samples were processed via a modification of protocol described elsewhere.[21] The samples were reduced with 15 mM 1,4-dithiothreitol (Roche), alkylated by incubation with 30 mM iodoacetamide (Sigma-Aldrich), and then processed on the 10 kDa cutoff filters (Millipore). Stepwise washing with 2% acetonitrile (Sigma-Aldrich) in 50 mM NH_4HCO_3, 50% acetonitrile in 50 mM NH_4HCO_3 and 50 mM NH_4HCO_3 was followed by incubation with trypsin (1 µg per 50 µg protein; Roche) for 20 hr at 37°C. Peptides were eluted from the filters with 0.1% formic acid (Sigma-Aldrich) and were dried on SpeedVac. The aliquots of each sample containing the same amount of protein (3 µg) were prepared by dilution in 0.1% trifluoroacetic acid.

High-performance liquid chromatography/tandem mass spectrometry and key-node analysis

Experiments were performed on an LTQ-FT Ultra mass spectrometer (ThermoFisher Scientific) used online with an Agilent 1100 nanoflow high-performance liquid chromatography and a nano electrospray ion source (Proxeon Biosystems). A 15 cm C_{18} nanocolumn (75 µM inner diameter, 375 µm outer diameter) was used for peptide elution at a flow of 200 nL/min with a gradient from 2% to 50% acetonitrile for 100 min. Mass spectrometric analysis was performed by recording of high-resolution (100,000) survey mass spectrum in Fourier transform mass spectrometry and consecutive low-resolution, collision-induced dissociation of up to five of the most abundant ions in the LTQ. Acquired data (.RAW files) were converted to the Mascot search engine (version 2.1.3, Matrix Science). Monoisotopic mass tolerance was set to 10 ppm, and for fragment ions it was ±0.9 Da. A protein was considered to be positively matched by using the stringent threshold of 27 for the Mowse score for all its peptides ($p \leq 0.05$). The Mascot htm output and .RAW files of each sample were used as input files for quantification with an in-housewritten program package (C++). The area of the chromatographic peak was taken as the peptide abundance. Sum of the abundances of all "bold red" nonidentical peptides was attributed to the protein expression level (≥1 peptide per protein). Protein expression data are shown in **Table S4**. Protein IDs and

protein abundances were loaded into ExPlain 2.4.1 tool (BIOBASE GmbH), where protein IDs were substituted by respective gene IDs. Then we searched upstream for the key nodes most relevant for the input gene products.[22] Key nodes are signaling molecules found on pathway intersections in the upstream vicinity of the genes from the input list. Each key node found was given a score reflecting its connectivity, i.e., how many input-list genes are reached and the proximities to those genes. The score calculation also included the abundances of the downstream proteins. Changes in the key node scores thus reflected the changes in the activation levels of the corresponding signaling networks.[22]

Results

We previously reported the mapping of the SCA23 locus to chromosomal region 20p12.3-p13.6 After excluding 32 prioritized genes via sequencing,[7] we identified a c.414G>T (p.R138S) transition resulting in a missense mutation in exon 4 of *PDYN* in all affected family members (n = 10), but not in unaffected relatives (n = 4) of the originally reported SCA23 family (**Fig. 1A and 1B**). To confirm a possible role of PDYN in cerebellar degeneration, we screened the coding region of *PDYN* in a panel of Dutch ataxia patients (n = 1100). The panel consists of ataxia patients who applied for regular DNA diagnostics and had no mutations in seven known SCA genes (SCA1–3, SCA6, SCA7, SCA12, and SCA14). Only in 10% of these cases was a clear familial history of the disease described (8% dominant and 2% recessive), and 90% seemed apparently sporadic.

We identified three additional missense mutations, c.632T>C (p.L211S), c.634C>T (p.R212W), and c.643C>T (p.R215C), among the 1100 screened Dutch ataxia patients (one familial case with dominant inheritance of the disease and two apparently sporadic cases with an unknown family history; **Fig. 1C–1E**).We were able to show segregation of the p.R215C substitution in two affected siblings (patients II-1 and II-2 in **Fig. 1E**). For the other two families (**Fig. 1C and 1D**), no additional family members were available. The man with the p.L211S mutation (**Fig. 1C**, patient II:3) suffered from progressive gait and upper limb ataxia, oculomotor abnormalities, distal sensory neuropathy, and pyramidal signs of the legs. In addition, subtle parkinsonian features were noted. The disease symptoms started at age 73. The family history was incomplete, and ataxia was not mentioned. The woman with the p.R212W mutation (**Fig. 1D**, patient II:3) displayed a slowly progressive cerebellar ataxia of the legs and arms, as well as a progressive mixed axonal polyneuropathy. The onset of the symptoms started at age 54, and the family history was negative for ataxia. An MRI scan of the brain, performed 4 months prior to death, revealed generalized cerebral cortical and subcortical atrophy, agenesis of the corpus callosum, and prominent atrophy of the cerebellar vermis, the pons, and the inferior olivary nucleus. The woman carrying the p.R215C mutation (**Fig. 1E**, patient II:1) was initially diagnosed with an essential tremor of head and postural arms. From about age 50 onward, memory and word finding deteriorated. A neurological exam at age 53 revealed slowed mental processes, slight dysarthria, mild ataxia of upper and lower limbs, postural arm tremor and a tremor of the head, proximal paresis of the legs with mild signs of sensory neuropathy, and a bilateral pes cavus. Her brother (**Fig. 1E**, patient II:2) was already considered clumsy at school age. Around age 54, mild gait impairment and slowing were noted. The neurological examination at age 56 revealed head tremor, fixation instability at neutral gaze,

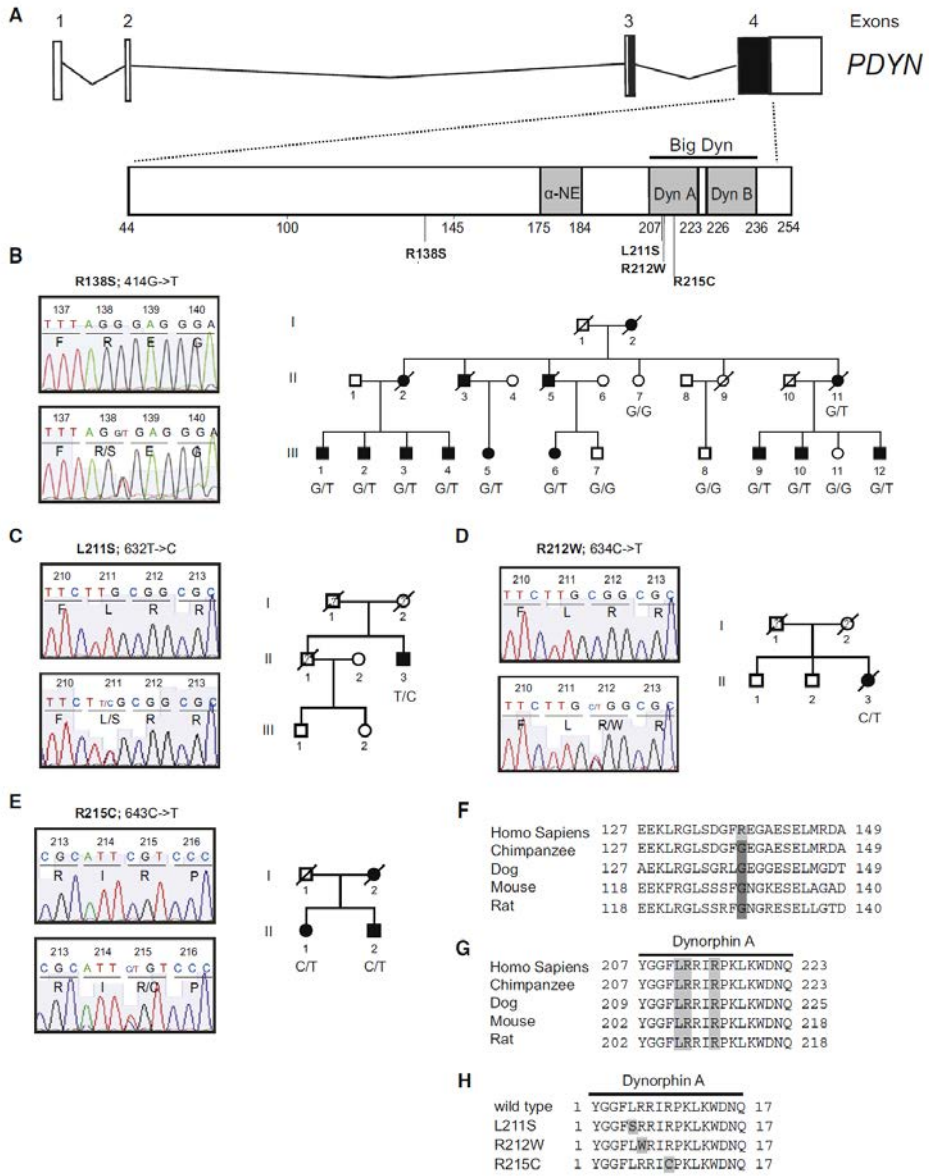

Fig. 1. *PDYN* **Mutations Causing SCA23**

(**A**) PDYN exons 3 and 4 encode PDYN, which gives rise to the opioid peptides a-neoendorphin (a-NE), dynorphin A (Dyn A), dynorphin B (Dyn B), and big dynorphin (Big Dyn), which encompasses Dyn A and Dyn B. DNA sequence analysis identified four missense mutations (c.414G>T, c.632T>C, c.634C>T, and c.643C>T) in SCA23 subjects. (**B**) Sequence electropherogram and pedigree of original Dutch SCA23 family. The c.414G>T; p.R138S mutation was identified in 10 affected individuals, but not in the four unaffected family members. (**C–E**) Sequence electropherograms and pedigrees of the patients with Dyn A mutations: c.632T>C; p.L211S, c.634C>T; p.R212W, and c.643C>T; p.R215C. At the moment, no DNA material of additional family members was available for mutation screening in the p.L211S and p.R212W families. The p.R215C mutation was identified in two affected siblings. Closed symbols denote affected; open symbols denote unaffected; ? denotes disease status unknown; / denotes deceased. (**F and G**) Conservation of the mutated amino acids. Arginine 138 is human specific; other species analyzed have Glycine 138. Leucine 211, Arginine 212, and Arginine 215 are conserved across species. (**H**) Localization of mutations in Dyn A.

very mild dysarthria, action tremor of the hands, and a subtle ataxia of the hands and arms. The mother of these two patients (not examined by us) suffered from mild late-onset ataxia and head and limb tremor since primary school, and her mother likely suffered from dementia. The clinical details are summarized in **Table S1**. All four mutations were absent in 1000 Dutch blood bank control chromosomes. In addition, three known SNPs (rs77155664, rs45469293, and rs6045819) were identified in exon 4, and no difference in their distribution was observed between ataxia cases and controls (data not shown).

Of the four altered amino acids, Arg^{138} is confined to humans (**Fig. 1F**), whereas Lys^{211}, Arg^{212}, and Arg^{215} were conserved across the vertebrate species examined (**Fig. 1G and 1H**). *In silico* analysis with four different bioinformatics programs (polyPhen, SIFT, SWAP, and Align GVD) predicted three (p.L211S, p.R212W, and p.R215C) of the four missense mutations to have damaging effects on protein structure and function, whereas the p.R138S mutation was predicted to be benign (**Table S2**). In addition, the p.R138S and p.L211S mutations were also predicted to increase PDYN phosphorylation levels by generating potential phosphorylation sites (**Table S3**).

Proprotein convertases 1 and 2 cleave PDYN at both paired and single basic residues, resulting in defined sets of neuropeptides.[8,23] The human-specific Arg^{138} is located in the nonopioid domain of PDYN and may affect N-terminal trimming of the 8 kDa and 10 kDa PDYN processing intermediates. The p.L211S, p.R212W, and p.R215C mutations in PDYN substitute amino acid residues Leu^5, Arg^6, and Arg^9 to Ser^5, Trp^6, and Cys^9, respectively, in the 17 amino acid Dyn A sequence (**Fig. 1H**). These changes may abrogate Dyn A conversion to Dyn A(1–8), Leu-enkephalin-Arg, or Leu-enkephalin; Dyn A is cleaved between the 8th and 9th, 6th and 7th, and 5th and 6th amino acid residues, and both Arg6 and Arg9 are critical for Dyn A processing.[23,24]

To examine whether the mutations affect PDYN synthesis and processing, we transfected the cDNA wild type (WT) or mutant PDYN cDNA into rat insulinoma RINm-5F cells. Protein and peptide products were analyzed by immunoblotting with anti-PDYN and Dyn B antibodies and by RIA for Dyn A, Dyn B, and the dynorphin conversion product Leu-enkephalin-Arg (**Fig. 2A–2D**).[19] RINm-5F cells do not produce endogenous PDYN and efficiently process ectopic PDYN into opioid peptides.[19] Analysis of cells transfected with PDYN plasmids demonstrated that WT and all mutants produced the 28 kDa PDYNs at similar levels (**Fig. 2A**). However, the efficiency of processing of these proteins to opioid peptides was dramatically affected by the mutations (**Fig. 2B–2D**). The levels of Dyn A produced by PDYN p.L211S and p.R212W were 10- to 18-fold elevated compared to WT, whereas the levels of Dyn B produced by PDYN p.R138S, p.R212W, and p.R215C, as well as the levels of Leu-enkephalin-Arg produced by PDYN p.R138S and p.R215C, were decreased approximately 2-fold. Thus, all three Dyn A mutants resulted in a 2- to 35-fold higher Dyn A production compared to Dyn B.

Previous studies have shown that Dyn A can induce toxicity and neuronal cell death.[25–27] To examine whether mutant Dyn A would be more neurotoxic, we analyzed effects of WT and mutant Dyn A peptides on the viability of striatal neurons via environmentally controlled timelapse imaging. Although mild toxic effects were induced by WT Dyn A, we observed marked increases in neuronal losses following exposure to p.R212W and p.R215C mutant Dyn A peptides compared to vehicle-treated controls or the WT peptide after 60 hr of exposure (**Fig. 2E and 2F**). No significant differences in cell viability were observed between control and the p.L211S Dyn

A-treated neurons. Thus, two mutations in Dyn A may enhance the intrinsic neurotoxicity of WT Dyn A.

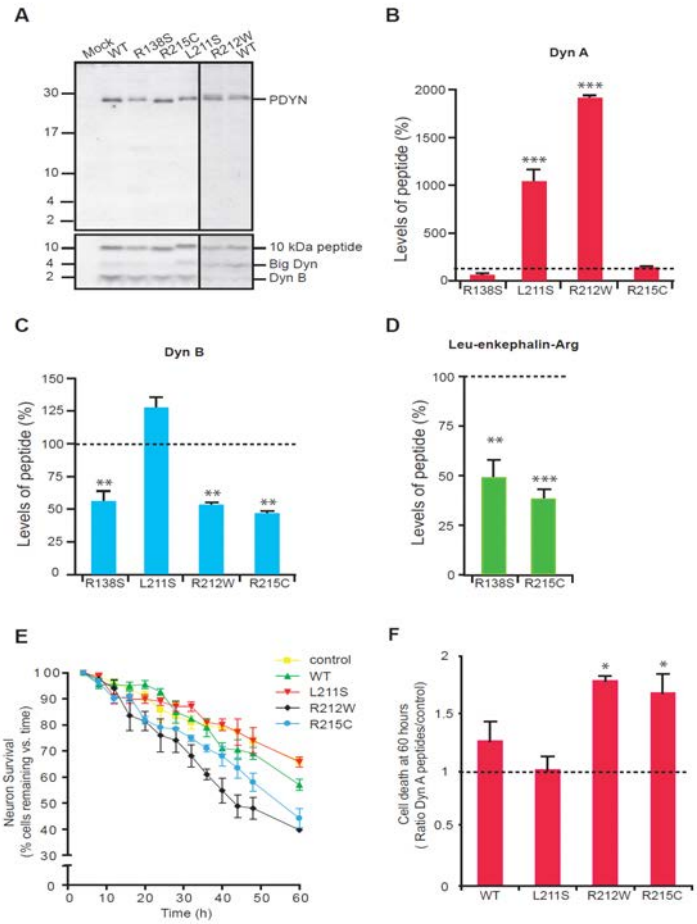

Fig. 2. SCA23 Mutations Affect PDYN Processing and Enhance Dyn A Toxicity

(**A**) Expression and processing of WTand mutant PDYNs in RINm-5F cells. Immunoblotting was performed with anti-PDYN (against C-terminal fragment; top) or anti-Dyn B (bottom) antibodies. Synthetic big dynorphin (a 32 amino acid peptide consisting of Dyn A and Dyn B) and Dyn B were loaded on the same gel as peptide markers and produced the 4 and 2 kDa bands identified by anti-Dyn B antibodies (data not shown; however, their positions are shown on the right). The 10, 4, and 2 kDa PDYN processing products were detected in RINm-5F cells transfected with PDYN expression plasmids. (**B–D**) Peptide levels in cells expressing WT PDYN were taken as 100%. One-way ANOVA followed by Dunnett's multiple comparison test; $^{**}p < 0.01$, $^{***}p < 0.001$; mutant versus wild-type. Data are shown as means ± SEM. (**B**) RINm-5F cells expressing PDYN p.L211S and p.R212W showed significant elevation in levels of Dyn A compared to cells expressing WT PDYN (ANOVA; $p < 0.001$). The Dyn A RIA was not hindered by the mutations because they did not affect the binding of the mutant peptides to the Dyn A antibodies. The antibodies were generated against the C-terminal Dyn A fragment.[12,19] (**C**) Dyn B levels showed significant decrease in cells expressing PDYN p.R138S, p.R212W, and p.R215C (ANOVA; $p < 0.001$). (**D**) PDYN p.R138S and p.R215C produced lower levels of Leu-enkephalin-Arg compared to WT PDYN (ANOVA; $p < 0.005$). Leu-enkephalin-Arg peptides derived from PDYN p.L211S and p.R212W were not analyzed by RIA because these two mutations are located within the Leu-enkephalin-Arg antigenic epitope and may hinder the binding of these mutant peptides to anti-Leu-enkephalin-Arg antibodies.[12,19] (**E and F**) Time-lapse imaging of striatial neurons treated with Dyn A peptides (100 nM) revealed marked loss of neuronal viability induced by Dyn A p.R212W and Dyn A p.R215C peptides compared to vehicle-treated control or WT Dyn A (one-way repeated-measures ANOVA; $p < 0.005$). Data are represented as the means ± SEM. (F) Neuronal death at 60 hr induced by mutant Dyn A peptides. The level of neuronal death as a result of excess WT Dyn A was considered as 1. Bonferroni's multiple correction test, $^{*}p < 0.05$. Data are represented as the means ± SD.

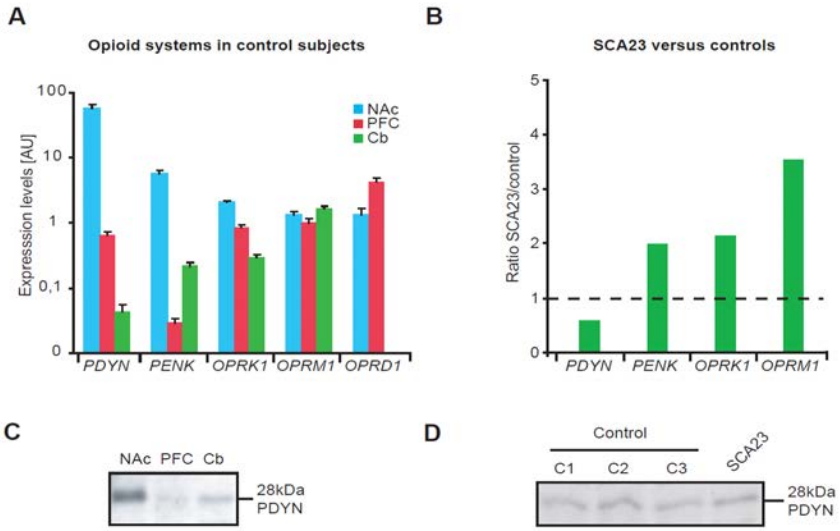

Fig. 3. Impact of the PDYN p.R138S Mutation on Expression of the Opioid Genes and PDYN Levels in Human Brain

(**A**) Levels of opioid mRNA in the nucleus accumbens (NAc), prefrontal cortex (PFC), and cerebellum (Cb) were quantified by TaqMan lowdensity arrays in postmortem samples from three control subjects. PDYN expression was substantially lower in Cb compared to NAc and PFC, the two brain areas with high and moderate gene expression. In the Cb, *PENK* showed high expression levels compared to the PFC but lower expression levels compared to the NAc. Both *OPRK1* and *OPRM1* are expressed in Cb, NAc, and PFC at similar levels, whereas *OPRD1* expression was not detectable in the Cb. Data bars represent the means ± SEM. (**B**) Comparison of mRNA levels in the Cb between three control and SCA23 cerebella. The data is shown as the ratio of levels in SCA23 to those in controls. Mean levels in controls were set to 1, as indicated by the dashed line. *PENK*, *OPRK1*, and *OPRM1* expression was 2- and 3.5-fold increased, whereas *PDYN* expression was slightly decreased in the SCA23 Cb compared to controls. (**C**) Analysis of PDYN in the human NAc, PFC, and Cb by immunoblot analysis. Tissue samples were pooled from three control subjects and purified on SEP-PAC reverse-phase columns prior to SDS-PAGE. PDYN levels in cerebellum are intermediate between those in NAc and PFC. (**D**) No differences were evident between PDYN levels in control (C1-3) and SCA23 cerebella.

The bias, based almost exclusively on data in mature rodents, is that the endogenous opioid peptides and their receptors are not produced and do not regulate neuronal activity in the cerebellum.[28] To gain insight into pathophysiological mechanisms of PDYN actions, we characterized these systems in three controls and SCA23 cerebella. Only a single brain of a SCA23 PDYN p.R138S subject was available for postmortem analysis.[6] Our results showed that *PDYN* was expressed in the human cerebellum, although at low levels compared to the nucleus accumbens (NAc) and prefrontal cortex (PFC; **Fig. 3A**). In contrast to animals, the κ- and μ- (*OPRM1*; MIM #600018) opioid receptors and proenkephalin (*PENK*; MIM #131330) were expressed in human cerebellum at levels that were comparable with those in the NAc and PFC, whereas the δ-opioid receptor (*OPRD1*) was not expressed (**Fig. 3A**).[29] In SCA23 tissue, cerebellar *OPRK1*, *OPRM1*, and *PENK* were 2- to 3.5-fold upregulated, whereas the level of *PDYN* mRNA was slightly lower than in controls (**Fig. 3B**). In contrast to mRNA, cerebellar PDYN levels were intermediate between those in PFC and NAc and were similar in controls and SCA23 (**Fig. 3C and 3D**). The high protein levels in relation to *PDYN* expression in cerebellum in comparison to NAc and PFC suggest slower processing of PDYN to mature peptides in this area.

To determine in which cell types PDYN, Dyn A, and Dyn B are localized in cerebellum, we performed immunohistochemistry. This analysis demonstrated that PDYN and its major peptide products are mainly located in the Purkinje cells in both control and SCA23 cerebellum (**Fig. 4A**). The SCA23 cerebellum showed significant loss of Purkinje cells and atrophic dendrites, as was described previously.[6] No marked differences in the localization and generation of PDYN and the Dyn A and B peptides were observed between control and SCA23 cerebella.

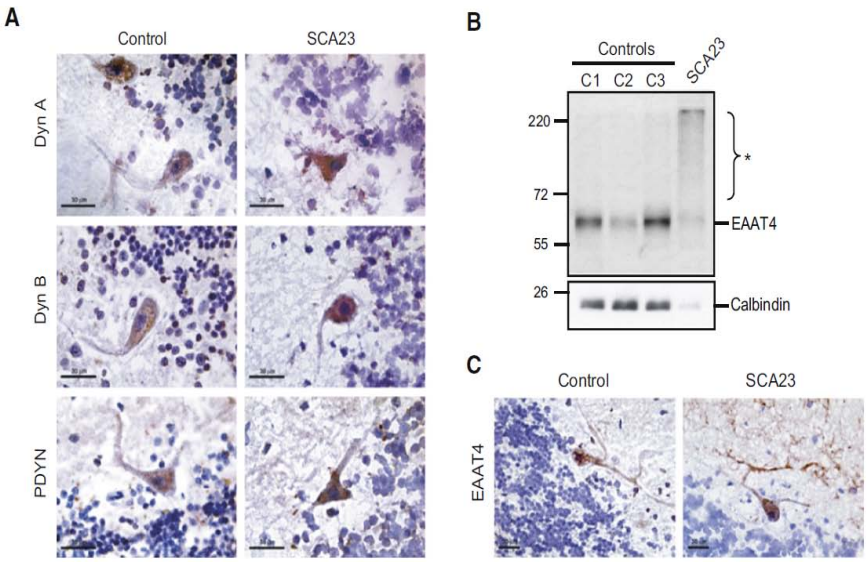

Fig. 4. Localization of PDYN and Dynorphins, and Analysis of the Purkinje Cell-Specific Excitatory Amino Acid Transporter, in SCA23 Cerebellum

(**A**) Immunohistochemistry of cerebellum from the PDYN p.R138S subject and a control individual without neurological disease. Immunoperoxidase labeling with anti-Dyn A, anti-Dyn B, or anti-PDYN antibodies was visualized by 3-Amino-9-ethylcarbazole as the chromogen and was counterstained with hematoxylin. (**B**) Immunoblot analysis of excitatory aminoacid transporter (EAAT4) and calbindin, both Purkinje cell markers. High molecular weight species were detected in the SCA23 cerebellum (*). (**C**) Immunoperoxidase labeling of EAAT4 in SCA23 and control cerebellum. Scale bars represent 30 mm (A and C).

Dyn A has been shown to induce neurodegeneration through a nonopioid mechanism that may involve glutamate receptors and acid-sensing ion channels.[9,30] To unravel cellular pathways affected by PDYN p.R138S, we performed shotgun proteomic analysis of control and SCA23 cerebella. Proteins involved in cell adhesion, synaptogenesis, secretory pathways, and signal transduction were up- or downregulated in SCA23 (**Fig. S1 and Table S4**). Key node molecules in cellular pathways affected in SCA23 cerebellum identified by pathway analysis include enzymes regulating glutamate cycling and proteins involved in neuroprotection, apoptosis, and signal transduction (**Table S5**). The solute carrier, SLC1A6 (alias EAAT4; excitatory amino acid transporter), a marker of Purkinje cells that has been previously found to be downregulated or aggregated in SCA1 and SCA5,[31,32] was decreased in the proteome of SCA23 PDYN p.R138S (**Table S4**). Immunoblotting confirmed a reduction in the 65 kDa EAAT4 in the SCA23 cerebellum by 3-fold (**Fig. 4B**). About 70% of EAAT4 was accumulated as aggregated or polyubiquitinated protein in SCA23 (**Fig. 4C**). EAAT4 showed strong staining in perikarya and dendrites of

the Purkinje cells in control and SCA23 cerebella (**Fig. 4C**). Calbindin is another protein marker of the Purkinje cells and was also found to be downregulated in SCA1 and SCA5 cerebella.[31,32] Although the proteomic analysis showed only marginal 1.6-fold decrease in calbindin levels in SCA23, further immunoblot analysis demonstrated substantial 7-fold downregulation of this protein in the pathological cerebellum (**Fig. 4B**).

Discussion

We have shown that missense mutations in PDYN cause a relatively slowly progressive, cerebellar ataxia with some distinctive features such as distal sensory neuropathy and pyramidal signs, proximal paresis of the legs, and tremors of the head and upper limbs. SCA23 was assumed to be a relatively pure cerebellar ataxia. However, our findings showed that the clinical phenotype of SCA23 can be highly variable and that no common starting symptom was present in our four different SCA23 families. Mutations in PDYN are identified here in a small subset of Dutch ataxia families (4 of 1100), indicating that SCA23 seems an infrequent SCA type (± 0.5%) in the Netherlands and suggesting further genetic heterogeneity. However, the syndromes present in our ataxia panel are phenotypically not well defined, which is reflected in the low success rate (~20%) to identify mutations in known SCA genes via diagnostic screening. This may explain why we have identified only 4 ataxia families exhibiting PDYN mutations in 1100 cases. Although we can only speculate about the frequency of SCA23 in a phenotypically better-defined cohort, we assume that SCA23 is a rare cause of ataxia and will not account for more than ~0.5% of the Dutch ataxia cases. To exclude the possibility that the PDYN p.R138S mutation would be a random sequence variation that cosegregates with the true disease mutation within the linkage interval, we sequenced 1000 unrelated blood bank control chromosomes in which this variation was not observed, and we did not identify any other additional coding sequence variation in 31 previously sequenced candidate genes that perfectly cosegregated with the disease phenotype in this family.7 In two families (PDYN p.R138S and p.R215C), we could confirm that the mutations segregated with the disease.

The *in silico* analysis predicts damaging effects of three Dyn A mutations (p.L211S, p.R212W, and p.R215C) on protein structure and possibly function, whereas the p.R138S mutation was assessed as benign. The negative prediction may be due to the insufficient sensitivity of the programs used in analysis, because they are based on similar algorithms and may have the same limitation. The analysis may also be hindered by the absence of any structural information for this class of proteins. Formation of an additional phosphorylation site in PDYN by the p.R138S mutation may affect processing or trafficking of mutant protein, thus representing an alternative mechanism of the pathogenic activity of PDYN.

Model cell experiments provided evidence that the PDYN mutations p.L211S (Leu^5) and p.R212W (Arg^6) result in enhanced Dyn A levels. This may be due to slow conversion of mutant Dyn A to short enkephalins. Indeed, conversion of Dyn A to short fragments generally occurs at di- and monobasic amino acid residues, including Leu^5 and Arg^9, that are substituted by Ser and Cys in mutant PDYN.[23] In addition, analysis of the effect of mutant Dyn A peptides on striatal neurons demonstrated high toxicity of Dyn A p.R212W and Dyn A p.R215C. The elevated neurotoxicity of Dyn A mutants compared to WT Dyn A suggests a dominant-negative effect of these mutations

rather than a loss of function. The increased stabilization of the mutant Dyn A peptides may not be the only factor underlying neurotoxicity, because Dyn A p.L211S, which is apparently resistant for conversion to a short fragment, does not induce any toxic response.

Immunohistochemical experiments revealed that PDYN, Dyn A, and Dyn B are mainly located in the Purkinje cells in both control and SCA23 cerebella. The absence of significant differences in PDYN and dynorphin localization and PDYN levels between control and PDYN p.R138S cerebella, observed by both the cell staining and immunoblotting, further argues against a possible loss of function and suggests that PDYN is strongly elevated in the Purkinje cells remaining in SCA23.

Further analysis of the endogenous opioid systems and the proteome in cerebellar autopsy tissue of the PDYN p.R138S subject revealed marked alterations in expression of crucial components of the opioid and glutamate systems. These alterations were evident for *OPRM1*, *OPRK1*, enzymes regulating glutamate cycling, and the excitatory amino acid transporter, *EAAT4*. These findings are consistent with previous observations demonstrating alterations in expression and localization of EAAT4 in SCA1 and SCA5 cerebella and provide additional evidence for the hypothesis that the dysfunction of glutamate signaling is a common downstream mechanism for SCA.[31,32]

Two putative mechanisms may be envisaged to explain the pathogenic effects of mutant PDYNs. First, modifications of nonopioid neurodegenerative and/or opioid activities of Dyn A or its longer pathological form, such as the 32 amino acid big dynorphin, may lead to alterations in glutamate signaling and excitotoxicity.[9,26,30,33] Several lines of evidence support this notion. Thus, Dyn A, but not other dynorphins, elicits various pathological effects, including neurological dysfunction and cell death. Intracerebroventricular injection of this peptide induces abnormal motor effects such as wild running, barrel rolling, and ataxia in mice, whereas intrathecal infusion produces allodynia, paralysis, and neuronal loss.[9,34–39] Consistently, increased production of Dyn A following trauma contributes to spinal cord injury and neuropathic pain.[9,37–39] Dyn A is also upregulated in aging rodent brain, contributing to age-related impairment of spatial learning and memory.[40] In the prefrontal cortex of Alzheimer disease patients, the elevated Dyn A levels correlate with neuritic plaque density.[41] Second, synthesis of mutant PDYNs may affect secretory pathways, inducing endoplasmic reticulum stress and impairing maturation and trafficking of glutamate transporters and other signaling proteins. Actions of mutant PDYNs accumulating over the years may ultimately lead to Purkinje cell degeneration. The p.R138S mutation located in the nonopioid PDYN domain supports the second hypothesis.

Neuropeptides are a large group of signaling molecules that regulate a wide variety of physiological and pathological processes.[9,10] A mutation that causes early-onset obesity and adrenal insufficiency had been found in proopiomelanocortin, the protein precursor to adrenocorticotropin, α-melanocyte-stimulating hormone, and β-endorphin.[42] Our findings demonstrate that mutations in a neuropeptide gene may cause an inherited neurodegenerative disorder. Neuropeptides usually exert their actions as ligands of G protein-coupled receptors. In the case of Dyn A, although physiological effects are largely mediated through the κ-opioid receptors, pathological effects may be generally mediated through direct action of this peptide on the plasma membrane, possibly by inducing pore formation and increased calcium influx in neurons.[9,43–45] Remarkably, three mutations identified in

SCA23 families alter the amino acid sequence of Dyn A in a domain associated with non-receptor-mediated, neurodegenerative actions. Two peptides with these mutations cause significant toxicity in cultured neurons, raising the possibility that some SCA23 degenerative processes are due to direct effects of mutant peptides on neurons. We may speculate that mutations in other neuropeptide precursor genes are involved in the etiology of cerebellar ataxia and that their identification will provide further insight into mechanisms of synaptic neurotransmission and neurodegeneration.

Acknowledgements

We thank the participating family members for their cooperation and all the members of the SpinoCerebellaire Ataxie Nederland working group for their input and help regarding this study. We acknowledge Henk Moorlag for preparing the cerebellar slides, Alexander Zubarev for protein quantification software, Henrik Druid, Kanar Alkash, and Pieter Wesseling for human brain samples, and Jackie Senior for improving the manuscript. This work was supported in part by a Rosalind Franklin Fellowship from the University of Groningen (D.S.V.) and a National Institute on Drug Abuse Independent Scientist Award (DA027374; K.F.H.), as well as by the Swedish Science Council, Swedish Institute, AFA Forsakring and Swedish Council for Working Life and Social Research (G.B.), and an Uppsala University Fellowship (H.W.).

Supplementary material and ***Web resources*** are available on: http://www.cell.com/AJHG/

References

1. Schols, L., Amoiridis, G., Bu¨ttner, T., Przuntek, H., Epplen, J.T., and Riess, O. (1997). Autosomal dominant cerebellar ataxia: Phenotypic differences in genetically defined subtypes? Ann. Neurol. 42, 924–932.

2. Matilla-Duen˜as, A., Sa´nchez, I., Corral-Juan, M., Da´valos, A., Alvarez, R., and Latorre, P. (2010). Cellular and molecular pathways triggering neurodegeneration in the spinocerebellar ataxias. Cerebellum 9, 148–166.

3. Sato, N., Amino, T., Kobayashi, K., Asakawa, S., Ishiguro, T., Tsunemi, T., Takahashi, M., Matsuura, T., Flanigan, K.M., Iwasaki, S., et al. (2009). Spinocerebellar ataxia type 31 is associated with "inserted" penta-nucleotide repeats containing (TGGAA)n. Am. J. Hum. Genet. 85, 544–557.

4. Schorge, S., van de Leemput, J., Singleton, A., Houlden, H., and Hardy, J. (2010). Human ataxias: A genetic dissection of inositol triphosphate receptor (ITPR1)-dependent signaling. Trends Neurosci. 33, 211–219.

5. Carlson, K.M., Andresen, J.M., and Orr, H.T. (2009). Emerging pathogenic pathways in the spinocerebellar ataxias. Curr. Opin. Genet. Dev. 19, 247–253.

6. Verbeek, D.S., van deWarrenburg, B.P.,Wesseling, P., Pearson, P.L., Kremer, H.P., and Sinke, R.J. (2004). Mapping of the SCA23 locus involved in autosomal dominant cerebellar ataxia to chromosome region 20p13-12.3. Brain 127, 2551–2557.

7. Verbeek, D.S. (2009). Spinocerebellar ataxia type 23: A genetic update. Cerebellum 8, 104–107.

8. Akil, H.,Watson, S.J., Young, E., Lewis, M.E., Khachaturian, H., and Walker, J.M. (1984). Endogenous opioids: Biology and function. Annu. Rev. Neurosci. 7, 223–255.

9. Hauser, K.F., Aldrich, J.V., Anderson, K.J., Bakalkin, G., Christie, M.J., Hall, E.D., Knapp, P.E., Scheff, S.W., Singh, I.N., Vissel, B., et al. (2005). Pathobiology of dynorphins in trauma and disease. Front. Biosci. 10, 216–235.

10. Ludwig, M., and Leng, G. (2006). Dendritic peptide release and peptide-dependent behaviours. Nat. Rev. Neurosci. 7, 126–136.

11. Christensson-Nylander, I., Nyberg, F., Ragnarsson, U., and Terenius, L. (1985). A general procedure for analysis of proenkephalin B derived opioid peptides. Regul. Pept. 11, 65–76.

12. Yakovleva, T., Bazov, I., Cebers, G., Marinova, Z., Hara, Y., Ahmed, A., Vlaskovska, M., Johansson, B., Hochgeschwender, U., Singh, I.N., et al. (2006). Prodynorphin storage and processing in axon terminals and dendrites. FASEB J. 20, 2124–2126

13. Singh, I.N., Goody, R.J., Dean, C., Ahmad, N.M., Lutz, S.E., Knapp, P.E., Nath, A., and Hauser, K.F. (2004). Apoptotic death of striatal neurons induced by human immunodeficiency virus-1 Tat and gp120: Differential involvement of caspase-3 and endonuclease G. J. Neurovirol. 10, 141–151.

14. Singh, I.N., El-Hage, N., Campbell, M.E., Lutz, S.E., Knapp, P.E., Nath, A., and Hauser, K.F. (2005). Differential involvement of p38 and JNK MAP kinases in HIV-1 Tat and gp120- induced apoptosis and neurite degeneration in striatal neurons. Neuroscience 135, 781–790.

15. Fleige, S., and Pfaffl, M.W. (2006). RNA integrity and the effect on the real-time qRT-PCR performance. Mol. Aspects Med. 27, 126–139.

16. Fleige, S., Walf, V., Huch, S., Prgomet, C., Sehm, J., and Pfaffl, M.W. (2006). Comparison of relative mRNA quantification models and the impact of RNA integrity in quantitative realtime RT-PCR. Biotechnol. Lett. 28, 1601–1613.

17. Stadler, F., Kolb, G., Rubusch, L., Baker, S.P., Jones, E.G., and Akbarian, S. (2005). Histone methylation at gene promoters is associated with developmental regulation and regionspecific expression of ionotropic and metabotropic glutamate receptors in human brain. J. Neurochem. 94, 324–336.

18. Waldvogel, H.J., Curtis, M.A., Baer, K., Rees, M.I., and Faull, R.L. (2006). Immunohistochemical staining of post-mortem adult human brain sections. Nat. Protoc. 1, 2719–2732.

19. Nikoshkov, A., Hurd, Y.L., Yakovleva, T., Bazov, I., Marinova, Z., Cebers, G., Pasikova, N., Gharibyan, A., Terenius, L., and Bakalkin, G. (2005). Prodynorphin transcripts and proteins differentially expressed and regulated in the adult human brain. FASEB J. 19, 1543–1545.

20. Okvist, A., Johansson, S., Kuzmin, A., Bazov, I., Merino-Martinez, R., Ponomarev, I., Mayfield, R.D., Harris, R.A., Sheedy, D., Garrick, T., et al. (2007). Neuroadaptations in human chronic alcoholics: Dysregulation of the NF-kappaB system. PLoS ONE 2, e930.

21. Wi_sniewski, J.R., Zougman, A., Nagaraj, N., and Mann, M. (2009). Universal sample preparation method for proteome analysis. Nat. Methods 6, 359–362.

22. Kel, A., Voss, N., Jauregui, R., Kel-Margoulis, O., and Wingender, E. (2006). Beyond microarrays: Find key transcription factors controlling signal transduction pathways. BMC Bioinformatics 7 (Suppl 2), S13.

23. Day, R., Lazure, C., Basak, A., Boudreault, A., Limperis, P., Dong, W., and Lindberg, I. (1998). Prodynorphin processing by proprotein convertase 2. Cleavage

at single basic residues and enhanced processing in the presence of carboxypeptidase activity. J. Biol. Chem. 273, 829–836.

24. Silberring, J., Castello, M.E., and Nyberg, F. (1992). Characterization of dynorphin A-converting enzyme in human spinal cord. An endoprotease related to a distinct conversion pathway for the opioid heptadecapeptide? J. Biol. Chem. 267, 21324–21328.

25. Hauser, K.F., Foldes, J.K., and Turbek, C.S. (1999). Dynorphin A (1-13) neurotoxicity in vitro: Opioid and non-opioid mechanisms in mouse spinal cord neurons. Exp. Neurol. 160, 361–375.

26. Tan-No, K., Cebers, G., Yakovleva, T., Hoon Goh, B., Gileva, I., Reznikov, K., Aguilar-Santelises, M., Hauser, K.F., Terenius, L., and Bakalkin, G. (2001). Cytotoxic effects of dynorphins through nonopioid intracellular mechanisms. Exp. Cell Res. 269, 54–63.

27. Goody, R.J., Martin, K.M., Goebel, S.M., and Hauser, K.F. (2003). Dynorphin A toxicity in striatal neurons via an alpha-amino-3-hydroxy-5-methylisoxazole-4-propionate/kainate receptor mechanism. Neuroscience 116, 807–816.

28. Mansour, A., Fox, C.A., Akil, H., and Watson, S.J. (1995). Opioid-receptor mRNA expression in the rat CNS: Anatomical and functional implications. Trends Neurosci. 18, 22–29.

29. Schadrack, J.,Willoch, F., Platzer, S., Bartenstein, P., Mahal, B., Dworzak, D., Wester, H.J., Zieglga¨nsberger, W., and To¨lle, T.R. (1999). Opioid receptors in the human cerebellum: Evidence from [11C]diprenorphine PET, mRNA expression and autoradiography. Neuroreport 10, 619–624.

30. Sherwood, T.W., and Askwith, C.C. (2009). Dynorphin opioid peptides enhance acid-sensing ion channel 1a activity and acidosis-induced neuronal death. J. Neurosci. 29, 14371–14380.

31. Lin, X., Antalffy, B., Kang, D., Orr, H.T., and Zoghbi, H.Y. (2000). Polyglutamine expansion down-regulates specific neuronal genes before pathologic changes in SCA1. Nat. Neurosci. 3, 157–163.

32. Ikeda, Y., Dick, K.A., Weatherspoon, M.R., Gincel, D., Armbrust, K.R., Dalton, J.C., Stevanin, G., Durr, A., Zuhlke, C., Burk, K., et al. (2006). Spectrin mutations cause spinocerebellar ataxia type 5. Nat. Genet. 38, 184–190.

33. Merg, F., Filliol, D., Usynin, I., Bazov, I., Bark, N., Hurd, Y.L., Yakovleva, T., Kieffer, B.L., and Bakalkin, G. (2006). Big dynorphin as a putative endogenous ligand for the kappa-opioid receptor. J. Neurochem. 97, 292–301.

34. Herman, B.H., Leslie, F., and Goldstein, A. (1980). Behavioral effects and in vivo degradation of intraventricularly administered dynorphin-(1-13) and D-Ala2-dynorphin-(1-11) in rats. Life Sci. 27, 883–892.

35. Walker, J.M., Moises, H.C., Coy, D.H., Baldrighi, G., and Akil, H. (1982). Nonopiate effects of dynorphin and des-Tyr-dynorphin. Science 218, 1136–1138.

36. Nakazawa, T., Ikeda, M., Kaneko, T., Yamatsu, K., Kitagawa, K., and Kiso, Y. (1989). Bestatin potentiates the antinociception but not the motor dysfunction induced by intracerebrally administered dynorphin-B in mice. Neuropeptides 13, 277–283.

37. Caudle, R.M., and Mannes, A.J. (2000). Dynorphin: Friend or foe? Pain 87, 235–239.

38. Lai, J., Ossipov, M.H., Vanderah, T.W., Malan, T.P., Jr., and Porreca, F. (2001). Neuropathic pain: The paradox of dynorphin. Mol. Interv. 1, 160–167.

39. Tan-No, K., Takahashi, H., Nakagawasai, O., Niijima, F., Sato, T., Satoh, S., Sakurada, S., Marinova, Z., Yakovleva, T., Bakalkin, G., et al. (2005). Pronociceptive role of dynorphins in uninjured animals: N-ethylmaleimide-induced nociceptive behavior mediated through inhibition of dynorphin degradation. Pain 113, 301–309.

40. Nguyen, X.V., Masse, J., Kumar, A., Vijitruth, R., Kulik, C., Liu, M., Choi, D.Y., Foster, T.C., Usynin, I., Bakalkin, G., and Bing, G. (2005). Prodynorphin knockout mice demonstrate diminished age-associated impairment in spatial water maze performance. Behav. Brain Res. 161, 254–262.

41. Yakovleva, T., Marinova, Z., Kuzmin, A., Seidah, N.G., Haroutunian, V., Terenius, L., and Bakalkin, G. (2007). Dysregulation of dynorphins in Alzheimer disease. Neurobiol. Aging 28, 1700–1708.

42. Krude, H., Biebermann, H., Luck, W., Horn, R., Brabant, G., and Gruters, A. (1998). Severe early-onset obesity, adrenal insufficiency and red hair pigmentation caused by POMC mutations in humans. Nat. Genet. 19, 155–157.

43. Marinova, Z., Vukojevic, V., Surcheva, S., Yakovleva, T., Cebers, G., Pasikova, N., Usynin, I., Hugonin, L., Fang, W., Hallberg, M., et al. (2005). Translocation of dynorphin neuropeptides across the plasma membrane. A putative mechanism of signal transmission. J. Biol. Chem. 280, 26360–26370.

44. Hugonin, L., Vukojevic, V., Bakalkin, G., and Graslund, A. (2006). Membrane leakage induced by dynorphins. FEBS Lett. 580, 3201–3205.

45. Hugonin, L., Vukojevic, V., Bakalkin, G., and Graslund, A. (2008). Calcium influx into phospholipid vesicles caused by dynorphin neuropeptides. Biochim. Biophys. Acta 1778, 1267–1273.

CHAPTER 5

Identification and characterization of novel *PDYN* mutations in dominant cerebellar ataxia cases

Justyna Jezierska[1], Giovanni Stevanin[2,3,4,5,6], Hiroyuki Watanabe[7] , Michiel Fokkens[1], Fabien Zagnoli[8], Jerome Kok[9], Jean-yves Goas[10], Pierre Bertrand[11], Christophe Robin[12], Alexis Brice[2,3,4,5], Georgy Bakalkin[7], Alexandra Durr[2,3,4,5] and Dineke S. Verbeek[1]

[1] Department of Genetics, University of Groningen, Groningen, University Medical Center Groningen, The Netherlands. [2] Université Pierre et Marie Curie-Paris, Centre de Recherche de l'Institut du Cerveau et de la Moelle épinière, Paris, France [3] INSERM, Paris, France. [4] CNRS, Paris, France [5] AP-HP, Hôpital de la Salpêtrière, Département de génétique et cytogénétique, Paris, France. [6] Ecole Pratique des Hautes Etudes, Paris, France. [7] Division of Biological Research on Drug Dependence, Department of Pharmaceutical Biosciences, Uppsala University, Uppsala, Sweden. [8] Hôpital d'Instruction des Armées, Service de Neurologie, Brest, France. [9] CMPPA, Bourg en Bresse, France. [10] CHU La Cavale Blanche, Service de Neurologie, Brest, France. [11] 46 avenue Moka, Saint Malo, France.[12] Groupe Hospilatier Général, 28 rue de Charlieu, Roanne, France.

J Neurol 2013; Volume 260, Issue 7 (2013), Page 1807-1812

Abstract

We have recently identified missense mutations in prodynorphin (*PDYN*), the precursor to dynorphin opioid peptides, to cause spinocerebellar ataxia (SCA23) in Dutch ataxia cases. Here, we screened *PDYN* for mutations in 371 cerebellar ataxia cases, with a positive family history and mostly of French origin. Sequencing revealed three novel putative missense mutations and one heterozygous two-base pair deletion in four independent SCA patients. These variants were absent in 400 matched controls and are located in the highly conserved dynorphin domain. To resolve the pathogenicity of the heterozygous variants, we assessed the peptide production of the mutant PDYN proteins. Two missense mutations raised dynorphin peptide levels, the two-base pair deletion terminated dynorphin synthesis, and one missense mutation did not affect PDYN processing. Given the outcome of our functional analysis, we may have identified at least two novel *PDYN* mutations in a French and Moroccan SCA patient. Our data corroborates recent work that also showed that *PDYN* mutations only account for a small percentage (~0.1%) of the European SCA cases.

Introduction

The spinocerebellar ataxias (SCA) are a large heterogeneous group of slowly progressive neurodegenerative disorders. All SCAs are characterized by selective neuronal loss in the cerebellum and/or the pons and patients suffer from motor coordination impairment, eye movement disorders, and dysarthria, but can exhibit as well several additional symptoms including pyramidal signs, peripheral neuropathy or cognitive impairment [1]. So far, 23 SCA disease genes have been reported [1-7]. Eight SCAs are caused by coding and non-coding CAG/CTG repeat expansions and three by extended intronic penta- and hexanucleotide repeats. The number of SCA types caused by conventional mutations including deletions, missense or frame-shift mutations is growing steadily, as yet twelve SCA types fall into this category.

Recently, missense mutations were identified in prodynorphin (*PDYN)* as causing SCA23 in Dutch ataxia families [2]. PDYN is the precursor protein for the opioid peptides α-neoendorphin, dynorphin A (Dyn A), and dynorphin B (Dyn B), ligands for the κ-opioid receptor [8]. Three of the four mutations were located in Dyn A, a peptide with both opioid and non-opioid neurodegenerative activities, and one missense mutation in the non-opioid domain of PDYN. Two mutations resulted in excessive generation of Dyn A and two resulted in enhanced intrinsic toxicity of the peptide [2]. To date, others reported one additional putative SCA23 mutation, without any functional support, in large UK, German and USA cohorts [9-11].

Here, we examined the prevalence of SCA23 in a large cohort of mostly French cerebellar ataxia cases with a positive family history, to define the range and pathogenicity of *PDYN* mutations and extend the clinical phenotype of SCA23 in Central Europe.

Subjects and Methods

Patients

As part of the SPATAX (SPastic paraparesis and/or ATAXia) network, we recruited 371 unrelated index cases with progressive cerebellar ataxia and a dominant family history. Most patients originated from France (n = 327) or from other countries in Europe (n = 23), North-Africa/Middle-East (n = 13), French West-Indies (n = 6) and China (n = 2). Pathogenic expansions were excluded for SCA1, 2, 3, 6, 7, 17 and DRPLA. Informed consent of all participants was obtained with the approval of the Comité Consultatif pour la Protection des Personnes et la Recherche Biomedicale Paris-Necker (approval No. 03-12-07) and all persons gave their informed consent prior to their inclusion in the study. The controls are spouses of affected family members, of whom mostly no clinical data is available. DNA was stored in the DNA and Cell Bank at the Pitié-Salpêtrière university hospital in Paris.

PDYN sequencing

Sequencing of the coding region and corresponding exon-intron boundaries of *PDYN* (NM_024411) was performed as described before [2]. The presence of the identified variants was assessed in 300 French and 100 North-African controls using small amplicon HiResolution melting (LightScanner; Bioke) using the following primers:

delGT-For 3'ACCTGTACAAACGCTATGG'5, delGT-Rev 3'CATAGCGCTTCTGGTTGTC'5, G227D-For: 3'CAAGCTCAAGTGGGACAAC'5, G227D-Rev: 3'CCAGAGTAAGCATTCGGAT'5, R206H/C-For: 3'GACCTGTACAAACGCTATG'5 and R206H/C-Rev: 3'CGCTTCTGGTTGTCCCAC'5. Aberrant melting curves were analyzed using Sanger sequencing.

Biological molecular analysis

The pCMV4-PDYN plasmid was described previously [12]. The mutations were introduced in the cDNA of *PDYN* using site-directed mutagenesis. RINm-5F cells that may process PDYN to mature opioid peptides were transiently transfected with plasmids using PEI reagent (Sigma). Western blot and RIA procedures were described elsewhere [13].

Results

We identified three novel heterozygous missense variants c.617G>A (p.R206H), c.616C>T (p.R206C), and c.680G>A (p.G227D), and one heterozygous two-base pair deletion c.658-659delGT (p.W220GfsX33) in four independent index cases (Fig. 1A). All variants were not detected in 400 ethnic matched controls and were not present in the Exome Variant Server, dbSNP and 1,000 genomes databases. The three missense variations affect 100% conserved aminoacids in all vertebrates in and around the two dynorphin peptides, Dyn A and B (data not shown). Additionally, all variants were *in silico* predicted to affect protein function using the programs PolyPhen, AlignGVGD, and Sift (data not shown). In addition, the two basepair deletion causes a frame-shift that introduces a premature stop codon, affecting the last 4 amino acids of Dyn A and leads to total loss of the Dyn B sequence. All variants were predicted not to affect splicing (data not shown). We did not screen *PDYN* for large deletions or duplications.

Co-segregation of the c.616C>T, c.680G>A, and c.658-659delGT variations with the disease phenotype was not tested because no family members were available for analysis. Surprisingly, mutational analysis did not detect the c.617G>A mutation in either mother or brother of the affected carrier (AAD-297), although they were also affected by frequent falls at older ages, mild to moderate gait problems, and mild cerebellar atrophy. Additionally, their clinical presentations differed from the index case by the absence of deafness and the later occurrence of the cerebellar deficit as well as the presence of normal reflexes. The main clinical features of the four index cases are shown in Table 1. The age at onset ranged from 15 to 54 years. The main presenting symptom was a slowly progressive cerebellar gait ataxia associated with a pyramidal syndrome in two patients; the first with spasticity in gait (c.616C>T, family AAD-745) and the second with bilateral extensor plantar reflexes (c.658-659delGT, family AAD-833). All patients had generalized increased reflexes. In addition, gait was impaired by altered sensory perception demonstrated by abolished vibration sense at ankles in two out of four patients. Brain MRIs showed cerebellar vermis and brainstem atrophy.

Table 1 Clinical data from the four index cases and relatives with *PDYN* variations

Family	AAD-745	AAD-297			AAD-833	AAD-751
Geographical origin	Swiss	France			France	Morocco
PDYN variation	c.616C>T; p.R206C	c.617G>A; p.R206H	-	-	c.658-659delGT; p.W220GfsX33	c.680G>A; p.G227D
Individual	Index	Index	Brother	Mother	Index	Index
Age at examination (years)	58	42	37	67	57	59
Age at onset (years)	50	15	28	45	45	54
Sign at onset (years)	Unsteadiness	Unsteadiness (15)	Unsteadiness (28)	Unsteadiness (45)	Unsteadiness	Unsteadiness
Functional handicap	Wheelchair	Wheelchair	Mild	Canes	Walking with help	Cannot run
Cerebellar ataxia	Moderate	Severe	Mild	Moderate	Moderate	Moderate
Dysarthria	Spastic and cerebellar	Cerebellar	Cerebellar	Cerebellar	Cerebellar	None
Nystagmus	Multi-directionel	Horizontal	None	None	None	None
Spastic gait	None	None	None	None	None	Moderate
Reflexes LL	Increased	Increased	Normal	Normal	Increased	Increased
Reflexes UL	Increased	Increased	Normal	Normal	Increased	Increased
Babinski sign	n.a.	None	None	None	Extensor	Indifferent
Wasting	None	None	None	None	None	LL prox. mild
Weakness	None	None	None	None	None	LL prox mild
Decreased vibration sense at ankles	Abolished	None	None	None	Abolished	Normal
Urinary symptoms	Incontinence	None	n.a.	n.a.	Urgency	None
Additional features	Tremor	Mild intellectual deficiency age 4, abnormal behavior, psychiatric symptoms at age 28 attention and memory deficit at age 32, bilateral sensory deafness	Psychiatric symptoms and neuroleptic treatment since age 22, attention difficulties, irritability, alcohol abuse	Mild intellectual deficiency since childhood	Cataract, head tremor	None
Cerebral MRI	n.a.	Cerebellar vermian atrophy	Cerebellar vermian atrophy	Cerebellar vermian atrophy	Normal	Cerebellar and brainstem atrophy

LL: lower limbs, UL: upper limbs, and n.a.: not assessed

To test for functional effects of the mutations, we analyzed processing of mutant PDYN proteins into opioid peptides. All mutant PDYN proteins were expressed with the exception of p.W220GfsX33 PDYN in a model cell line transfected with respective PDYN plasmids (**Fig. 1B and C**). Dyn A (2.0-2.7 fold), Dyn B (1.2-1.6 fold) and Leu-enkephalin-Arg (5-6 fold) levels were markedly elevated in p.R206H and p.G227D PDYN expressing cells compared to those producing wild type protein. No significant changes were detected for p.R206C PDYN, and no peptides were cleaved from p.W220GfsX33 PDYN. The peptide levels were normalized to PDYN content (**Fig. 1D**).

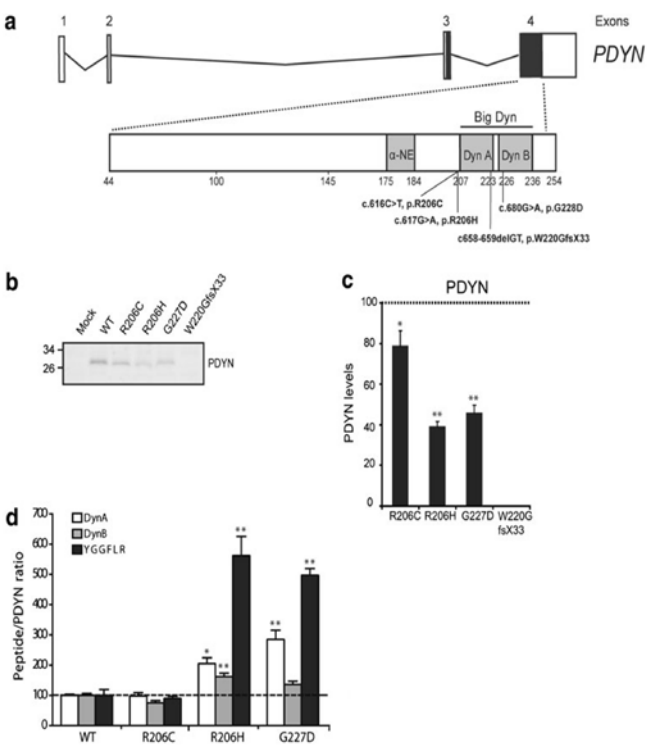

Fig. 1 The localization and the effect of the newly identified PDYN variations on PDYN expression and processing in RINm-5F cells.

a) Schematic representation of the *PDYN* transcript and the location of the identified bariations. The functional neuropeptides, α-neoendorphin, dynorphin A (Dyn A), and dynorphin B (Dyn B) are indicated in grey. The mutations identified in this study are shown in bold. b) Western blot analysis with anti-PDYN C-terminus-antibody identified the expected 28 kD protein in the WT, p.R206H, p.R206C, and p.G227D PDYN expressing RINm-5F cells. No protein was detected in the cells expressing p.W220GfsX33 PDYN. c) Quantification of Western blot data. PDYN immunoreactivity levels were normalized to total protein levels using Memcode staining. Shown are means ± SEM. obtained in three transfection experiments. WT protein levels were taken as 100%. d) Mature PDYN-derived opioid peptides Dyn A, Dyn B and Leu-enkephalin-Arg in RINm-5F cells transfected with WT and mutant PDYN plasmids measured using RIA. Peptide levels are normalized to the respective PDYN protein levels and are presented as % of those in WT PDYN expressing cells (Mean ± SEM.; n = 3 experiments). *Post-hoc* Dunnett's Multiple Comparison Test demonstrated a significant increase in Dyn A ($p < 0.05$ for p.R206H, $p < 0.01$ for p.G227D), Dyn B ($p < 0.01$ for p.R206H), and Leu-enkephalin-Arg ($p < 0.01$ for p.R206H and p.G227D) peptide levels. Processing of p.R206C PDYN did not yield major changes and no detectable peptides were processed from p.W220GfsX33 PDYN.

Discussion

We identified four novel heterozygous *PDYN* variations clustered in the Dyn A domain, c.617G>A (p.R206H), c.616C>T (p.R206C), and c.658-659delGT (p.W220GfsX33) or located in Dyn B, c.680G>A (p.G227D). None of these variations were detected in controls or any genetic database. The mutations affect amino acids that are 100% evolutionary conserved in all vertebrates. *In silico* analysis predicted the damaging effects of the mutations on the protein structure supporting the notion that they are pathogenic mutations rather than harmless polymorphisms. However, the two variants, c.617G>A and c.616C>T, that both modify the processing site just upstream of Dyn A at arginine 206 [14], might well be rare polymorphisms since the c.617G>A variation lacked co-segregation with the disease in family AAD-297, and the c.616C>T variant did not have any effect on processing of PDYN. Therefore, we cannot fully conclude that these variants exhibit pathogenic effects. On the other hand, the mother and brother may not suffer from the same disease as the index case from family AAD-297 and the c.616C>T variant might have functional consequences for the precursor for example by impairing trafficking rather than changing the peptide levels. The two other variants c.680G>A and c.658-659delGT showed either increased dynorphin and Leu-enkephalin-Arg levels or complete loss of Dyn A and Dyn B peptides. Since for both variants co-segregation could not be accessed, we can not completely exclude that those variants are rare polymorphisms. However, the c.658-659delGT variant leading to a truncated PDYN protein is very likely to be pathogenic and may be considered as disease-causing.

Notably, *PDYN* does not have a high degree of overall sequence variation, and a significant enrichment (Fisher's exact test, $p = 0.0238$) was observed for rare variations in *PDYN* in ataxia cases (4 variants in 371 cases) compared to EVS controls (27 variants in 6,500 individuals). Up to date, 5 out of 9 rare *PDYN* variations are located in Big Dynorphin (Big Dyn) consisting of Dyn A and Dyn B, which is the most pathological neuropeptide compared to other dynorphin peptides [15-17]. Four of these 5 directly affect the Dyn A sequence, of which one also destroys the Dyn B sequence and the fifth mutation changes the Dyn B sequence. The number of missense variations in Big Dyn including its arginine processing sites in this ataxia cohort (n = 371) or all sampled ataxia cases (n = 2246) compared to 6,500 controls in the EVS database, is significantly higher than that found in the remaining coding region of *PDYN* (Fisher's exact test, 2-tail; $p = 0{,}0067$ and $p = 0{,}0025$), which strongly suggests that the dynorphin/Big Dyn domain is a hotspot for rare variations and SCA23 mutations in ataxia cases.

Altogether, our data suggest that SCA23 mutations could enhance the dynorphin opioid function, or may have dominant negative effects inducing non-opioid neurodegenerative actions. In addition, complete loss of dynorphin peptides due to the truncating c.658-659delGT mutation strongly indicates that loss of function or haploinsufficiency can also contribute to the pathogenesis of SCA23.

Our study confirms that SCA23 is a rare type in Caucasians and accounts for ~0.1% of the tested SCA cases. The clinical phenotype of the newly identified SCA23 patients showed progressive cerebellar ataxia associated with pyramidal features with a relatively late age of onset. The apparent heterogeneous disease etiology will not help to preselect SCA23 cases for diagnostic screening. Although, the contribution of SCA23 to the European ataxia population appears to be limited, we believe that it is advisable to include screening of *PDYN* in diagnostic

settings, and to analyze co-segregation followed by functional analysis for verification of pathogenicity for the newly identified *PDYN* variants.

Acknowledgements

We thank the participating family members for their cooperation, Sylvie Forlani, Fabien Lesne, Kamila Karpinska, and Bianca van Wijk for technical assistance. This work was supported by a Rosalind Franklin Fellowship from the University of Groningen and the Swedish Science Council, Swedish Council for Working Life and Social Research, the European Union 6th PCRD (to the EUROSCA consortium), the association Connaitre les Syndrome cérébelleux (to the SPATAX network) and an Uppsala University Fellowship.

Financial disclosure: The authors report no disclosures.

References

1. Durr A (2010) Autosomal dominant cerebellar ataxias: polyglutamine expansions and beyond. Lancet Neurol 9:885–894

2. Bakalkin G, Watanabe H, Jezierska J, Depoorter C, Verschuuren-Bemelmans C, Bazov I, Artemenko KA, Yakovleva T, Dooijes D, van de Warrenburg BP, Zubarev RA, Kremer B, Knapp PE, Hauser KF, Wijmenga C, Nyberg F, Sinke RJ, Verbeek DS (2010) Prodynorphin mutations cause the neurodegenerative disorder spinocerebellar ataxia type 23. Am J Hum Genet 87:593–603

3. Kobayashi H, Abe K, Matsuura T, Ikeda Y, Hitomi T, Akechi Y, Habu T, Liu W, Okuda H, Koizumi A (2011) Expansion of intronic GGCCTG hexanucleotide repeat in NOP56 causes

SCA36, a type of spinocerebellar ataxia accompanied by motor neuron involvement. Am J Hum Genet 89:121–130

4. Wang JL, Yang X, Xia K, Hu ZM, Weng L, Jin X, Jiang H, Zhang P, Shen L, Guo JF, Li N, Li YR, Lei LF, Zhou J, Du J, Zhou YF, Pan Q, Wang J, Li RQ, Tang BS (2010) TGM6 identified as a novel causative gene of spinocerebellar ataxias using exome sequencing. Brain 133:3510–3518

5. Hekman KE, Yu GY, Brown CD, Zhu H, Du X, Gervin K, Undlien DE, Peterson A, Stevanin G, Clark HB, Pulst SM, Bird TD, White KP, Gomez CM (2012) A conserved eEF2 coding variant in SCA26 leads to loss of translational fidelity and increased susceptibility to proteostatic insult. Hum Mol Genet 21:5472–5483

6. Duarri A, Jezierska J, Fokkens M, Meijer M, Schelhaas HJ, den Dunnen WF, van Dijk F, Verschuuren-Bemelmans C, Hageman G, van de Vlies P, Kusters B, van de Warrenburg BP, Kremer B, Wijmenga C, Sinke RJ, Swertz MA, Kampinga HH, Boddeke E, Verbeek DS (2012) Mutations in potassium channel KCND3 cause spinocerebellar ataxia type 19. Ann Neurol 72:870–880

7. Lee YC, Durr A, Majczenko K, Huang YH, Liu YC, Lien CC, Tsai PC, Ichikawa Y, Goto J, Monin ML, Li JZ, Chung MY, Mundwiller E, Shakkottai V, Liu TT, Tesson C, Lu YC, Brice A, Tsuji S, Burmeister M, Stevanin G, Soong BW (2012) Mutations in KCND3 cause spinocerebellar ataxia type 22. Ann Neurol 72:859–869

8. Akil H, Watson SJ, Young E, Lewis ME, Khachaturian H, Walker JM (1984) Endogenous opioids: biology and function. Annu Rev Neurosci 7:223–255

9. Fawcett K, Mehrabian M, Liu YT, Hamed S, Elahi E, Revesz T, Koutsis G, Herscheson J, Schottlaender L, Wardle M, Morrison PJ, Morris HR, Giunti P, Wood N, Houlden H (2012) The frequency of spinocerebellar ataxia type 23 in a UK population. J Neurol [Epub ahead of print]

10. Fogel BL, Lee JY, Lane J, Wahnich A, Chan S, Huang A, Osborn GE, Klein E, Mamah C, Perlman S, Geschwind DH, Coppola G (2012) Mutations in rare ataxia genes are uncommon causes of sporadic cerebellar ataxia. Mov Disord 27:442–446

11. Schicks J, Synofzik M, Beetz C, Schiele F, Schols L (2011) Mutations in the PDYN gene (SCA23) are not a frequent cause of dominant ataxia in Central Europe. Clin Genet 80:503–504

12. Nikoshkov A, Hurd YL, Yakovleva T, Bazov I, Marinova Z, Cebers G, Pasikova N, Gharibyan A, Terenius L, Bakalkin G (2005) Prodynorphin transcripts and proteins differentially expressed and regulated in the adult human brain. Faseb J 19:1543–1545

13. Yakovleva T, Bazov I, Cebers G, Marinova Z, Hara Y, Ahmed A, Vlaskovska M, Johansson B, Hochgeschwender U, Singh IN, Bruce-Keller AJ, Hurd YL, Kaneko T, Terenius L, Ekstrom TJ, Hauser KF, Pickel VM, Bakalkin G (2006) Prodynorphin storage and processing in axon terminals and dendrites. Faseb J 20:2124–2126

14. Day R, Akil H (1989) The posttranslational processing of prodynorphin in the rat anterior pituitary. Endocrinology 124:2392–2405

15. Kuzmin A, Madjid N, Terenius L,Ogren SO, BakalkinG(2006) Big dynorphin, a prodynorphin-derived peptide produces NMDA receptor-mediated effects on memory, anxiolytic-like and locomotor behavior in mice. Neuropsychopharmacology 31:1928–1937

16. Marinova Z, Vukojevic V, Surcheva S, Yakovleva T, Cebers G, Pasikova N, Usynin I, Hugonin L, Fang W, Hallberg M, Hirschberg D, Bergman T, Langel U, Hauser KF, Pramanik A, Aldrich JV, Graslund A, Terenius L, Bakalkin G (2005) Translocation of dynorphin neuropeptides across the plasma membrane. A putative mechanism of signal transmission. J Biol Chem 280:26360–26370

17. Tan-No K, Takahashi H, Nakagawasai O, Niijima F, Sato T, Satoh S, Sakurada S, Marinova Z, Yakovleva T, Bakalkin G, Terenius L, Tadano T (2005) Pronociceptive role of dynorphins in uninjured animals: N-ethylmaleimide-induced nociceptive behavior mediated through inhibition of dynorphin degradation. Pain 113:301–309

CHAPTER 6

Elevated Dynorphin A levels lead to Purkinje cell loss in spinocerebellar ataxia type 23 mice

Justyna Jezierska[1,2], Cleo Smeets[1,2], Anna Duarri[1], Hiroyuki Watanabe[3] ,Georgy Bakalkin[3], Jan van Deursen[4], Harm H. Kampinga[5] Bart van de Sluis[6] and Dineke S. Verbeek[1]

[1] Department of Genetics, University of Groningen, University Medical Center Groningen, Groningen, the Netherlands

[2] these authors contributed equally

[3] Division of Biological Research on Drug Dependence, Department of Pharmaceutical Biosciences, Uppsala University, Uppsala, Sweden

[6] Faculty of Medical Sciences, Department of Pathology and Medical Biology, University of Groningen, University Medical Center Groningen, Groningen, the Netherlands

[4]Department of Pediatric and Adolescent Medicine, Mayo Clinic, Rochester, Minnesota, USA

[5] Department of Cell Biology, University Medical Center Groningen, University of Groningen, Groningen, the Netherlands

Submitted

Summary

Spinocerebellar ataxia type 23 (SCA23) is caused by mutations in *PDYN*, which encodes for the opioid neuropeptide precursor protein, prodynorphin. PDYN is processed into alfa-neoendorphin, Dynorphin (Dyn) A and B peptides, which participate in pain signalling and addiction via opioid-receptor mediated actions at physiological concentrations. However, the cerebellar non-opioid neurodegenerative function of PDYN or Dyn peptides is largely unknown. We have generated a conditional transgenic mouse model, expressing human PDYN, either wild type or carrying the SCA23-mutation R212W, and analyzed its motor performance and cerebellar morphology over a time-course of 12 months. We found that heterozygous PDYN-R212W mice reproduced the clinical features of SCA23 starting with gait deficits at three months of age, progressive loss of motor coordination and balance, and Purkinje cell loss by the age of 12 months. These findings correlated with pathologically elevated Dyn A levels in the cerebellum and reduced climbing fiber-Purkinje cell synapse distribution. Therefore, the elevated Dyn A levels probably underlie the etiology of SCA23 and affect climbing fiber-Purkinje cell synapse function. This results in synaptic alterations and Purkinje cell loss, leading to motor dysfunction.

Introduction

Spinocerebellar ataxia type 23 (SCA23) is a slowly progressive autosomal dominant neurodegenerative disorder caused by mutations in prodynorphin gene (*PDYN*) [1]. SCA23 patients suffer from a relatively slowly progressive motor coordination impairment and a generally isolated cerebellar ataxia due to Purkinje cell (PC) death in the cerebellum [1, 2]. PDYN is the precursor protein for the opioid neuropeptides α-neoendorphin, Dynorphin (Dyn) A, and Dyn B, which are endogenous ligands of the opioid receptors, and function in pain processing and addiction control [3]. Yet, the cerebellar function of these peptides is largely unknown. Notably, Dyn A exhibits neurotoxic effects, as pathologically increased levels caused pronounced cell death through mechanisms mediated by *N*-methyl-$_{D}$-aspartate receptors (NMDARs) [4] or α-amino-3-hydroxy-5-methylisoxazole-4-propionate receptors (AMPARs) [5]. Moreover, Dyn A was shown to directly bind NMDARs and potentiate their glutamate-induced currents [6].

Interestigly, the majority of SCA23 mutations are located in the highly conserved Dyn A-coding region and lead to enhanced levels of Dyn A *in vitro* [1, 7]. These SCA23-mutant Dyn A peptides displayed elevated intrinsic neurotoxic properties in cultured striatal neurons [1]. However, the exact mechanism through which mutant Dyn A induces neuronal cell death has to be resolved.

To further study the cerebellar role of PDYN and SCA23 disease pathology, we generated heterozygous conditional transgenic mice expressing PDYN-wt or SCA23-mutant PDYN-R212W. PDYN-R212W mice showed highly increased Dyn A levels in the cerebellum, which correlated with characteristic features of cerebellar ataxia including mild, but progressive motor coordination impairment, gait and balance abnormalities, and PC loss. Therefore, PDYN-R212W mice are a novel model for spinocerebellar ataxia, and our work suggests that pathologically elevated Dyn A levels in the cerebellum of SCA23-mutant mice are responsible for the ataxic phenotype and subsequent PC loss, recapitulating disease symptoms in humans.

Animals, materials and Methods

Animals

All animal experiments were performed according to the guidelines of the University of Groningen and Mayo Clinic College of Medicine. The experimental protocols were approved by Animal Welfare Committee of the University of Groningen. All efforts were made to reduce the number of animals and minimize their suffering. To generate heterozygous conditional transgenic mice carrying *PDYN*-wt or SCA23-mutant *PDYN*-R212W under Cre-recombinase control, the human *PDYN* cDNA was cloned into the pCALL2 plasmid downstream of a neomycin-resistance gene and transcription STOP signal (three tandemly arranged polyadenylation sites) flanked by *loxP* sites. Embryonic stem cell electroporation and clone selection was described previously [8, 9]. The blastocyst injections were performed at the Mayo Clinic College of Medicine, Rochester, Minnessota. For both, PDYN-wt and PDYN-R212W, two transgenic lines were generated, but the data is shown only for one line of each. To express PDYN, heterozygous transgene-inactive (Ti) *PDYN*-wt/R212W$^{(Ti)}$ males were crossed with *HPRT*^{Cre} females.

The same cross also produced wild type (WT) mice and Ti mice. The genotypes were assessed by PCR using the following primers:
PDYN-For 5'-TAGCAGTGGCGTTCATTTTG-3', and PDYN-Rev 5'-TCTGAGCTCCTCTTGGGGTA-3' and the *loxP* recombination was confirmed using the primers: For 5'-TCACTGCATTCTAGTTGTGGT-3', and Rev 5'-CTTATCGATACCGTCGACCT-3'.
All mice used for the experiments have a mixed 129Sv/E x C57Bl/6 genetic background. Four independent cohorts of 10-12 transgene-active (Ta) PDYN-wt/R212W$^{(Ta)}$, (and 12 WT/Ti control littermates) were aged for 3, 6, 9 and 12 months. Each cohort contained equal numbers of female and male mice.

Reverse transcription PCR and quantitative real-time PCR
Total RNA was isolated from snap-freezed mice cerebella using Trizol reagent (Invitrogen). The cDNA was generated using oligo-d(T) primers and RevertAid cDNA Kit (Fermentas). Quantitative real-time expression analysis was performed using SYBR-Green Mix (Life technologies, Applied Biosystems) and primer pairs listed below on Taqman ABI7900HT (Applied Biosystems) employing Standard Curve Quantification method and GAPDH as a reference gene. The primers used were:
GAPDH- For 5'-AGGCCGGTGCTGAGTATGTC-3', and GAPDH-Rev 5'-TGCCTGCTTCACCACCTTCT-3';
PDYN- For 5'-GCCTGCCTCCTCATGTTCC-3', and PDYN-Rev 5'-CCTTCCCCAACCGACTTGC-3';
pdyn-For 5'-GTGCAGTGAGGATTCAGGATGGG-3', and pdyn-Rev 5'-GAGCTTGGCTAGTGCACTGTAGC-3'.
List of primers for genes from opioid pathway and others are presented in **Suppl. Table 1**. All procedures were performed according to provided manufacturers' protocols.

Protein extraction and Western blotting
Proteins were isolated from snap-freezed mice organs. Organs were homogenized in ice-cold isolation buffer (320 mM sucrose, 1 mM EDTA and 10 mM Tris-HEPES, pH7.4) supplemented with complete protease inhibitor cocktail (Roche, Woerden, the Netherlands). Protein concentrations were determined using the Pierce BCA Protein Assay Kit (Thermo Scientific, Etten-Leur, the Netherlands), sample buffer (12% SDS, 30% glycerol, 6% β-merkaptoethanol) was added to proteins and equal amounts were loaded on SDS-PAGE gels. After electrophoresis, the proteins were transferred to the Polyvinylidene difluoride (PVDF) membrane (Life technologies) and blocked with 5% bovine serum albumin (BSA, Sigma-Aldrich) in TBS-Tween. The blots were analyzed with primary antibodies against human PDYN (rabbit, 1: 500, kindly provided by G. Bakalkin), Dyn A (rabbit, 1:300, Abcam), VGlut2 (rabbit, 1:1000, Synaptic Systems), EAAT4 (rabbit, 1:500, Alpha Diagnostics) or Calbindin (mouse, 1:500, Abcam). Secondary antibodies were conjugated with horseradish peroxidase (goat, 1:10 000, Jackson ImmunoResearch Laboratories).

Radioimmunoassay
Proteins were extracted in 1 M acetic acid and gel filtration was performed in order to separate the peptides using

an SP-Sephadex ion exchange C-25 column. The radioimmunoassay procedure was performed as described before [10].

Histology, immunofluorescent stainings and microscopy

For immunofluorescent stainings, brains were dissected and fixed overnight in 15% picric acid, 4% paraformaldehyde and 0.05% gluteraldehyde in 0.1 M phosphate buffer (PB). After fixation, brains were cryopreserved in 10% and 20% sucrose solutions in PB overnight, and then frozen on dry ice. Sectioning was performed on a HM550 microm cryostat (Thermo Scientific). Full cerebella were cut into 8 series of 30 µm-thick coronal sections. All stainings were performed free floating. For overall morphology studies, sections were stained with 1% Toluidine Blue (Sigma) for 2 min, washed with water, and mounted in Faramount mounting medium (Dako). For fluorescent stainings, sections were blocked with 3% normal donkey serum (Jackson ImmunoResearch Laboratories) for 30 min, after which antigen retrieval was carried out in 10 mM citric acid buffer (pH 6) at 90°C for 20 min. Sections were incubated with primary antibody overnight at 4°C and subsequently with secondary antibodies for 1h at room temperature, followed by Sudan Black B incubation to eliminate autofluorescence (0.1% in 70% ethanol; Sigma), washing with PB + 0.02% Tween, and mounting (BrightMount mounting medium, Abcam). Primary antibodies were against: hPDYN (rabbit, 1:300, [1]), Dyn A (rabbit, 1:300, Abcam), VGlut2 (rabbit, 1:1000, Synaptic Systems), EAAT4 (rabbit, 1:500, Alpha Diagnostics) and α-Calbindin (mouse, 1:500, Abcam). Secondary anti-rabbit antibodies were conjugated with Alexa488 and anti-mouse with Cy3 (both: donkey, 1:250, Jackson ImmunoResearch Laboratories). Sections were imaged using a AxioObserver Z1 fluorescence microscope (Zeiss) and Leica TCS SP8 confocal microscope, and the images were analysed using the ImageScope (Aperio e-pathology solutions, http://www.aperio.com) and Fiji software (National Institutes of Health, NIH, http://fiji.sc/).

Motor performance analyses

Ledge and hindlimb clasping tests were performed according to the protocol described previously [11]. The scoring was performed three times by two independent researchers. Footprint patterns were analyzed using a runway (80 cm by 10.5 cm wide) with white paper at the bottom. Mice paws were deeped in non-toxic, water-soluble ink (black for hind paws and magenta for front paws; Liquitex). Five consecutive strides were measured for each animal [12]. To assess motor performance the accelerating rotarod test was used (3-cm-diameter rotating cylinder; IITC). The training session contained 3 runs at stable 20 rpm at day 1, followed by a 2 day training session (each 3 runs per day) at accelerating speed (from 4 to 30 rpm within 180 seconds, and maximal 600 seconds at 30rpm). The actual experiment was done on day 4,identically to day 2 and 3. The minimal interval time in between the runs was 15 min [12]. All tests were performed without genotype information.

Cerebellar examinations: Purkinje cell count, molecular layer thickness measurements and climbing fiber distribution

PCs were counted and averaged over 200 µm and the CF distribution was quantified by measuring the height of VGlut2 staining in the molecular layer relative to Calbindin staining in the same region. The PC length was

measured as the distance from the top of PC soma to the tip of PC dendrite, and the CF distribution in the molecular layer was measured from the top of PC soma to the tip of CF arbor. In addition, the molecular layer thickness was measured. For molecular layer thickness and CF distribution, at least 10 measurements per section were taken in specific cerebellar regions. All images used for measurements were obtained using an AxioObserver Z1 fluorescence microscope (Zeiss) that scanned the full section. One series of cerebellar sections per animal and two animals per genotype (WT/Ti, hPDYN^{Ta}-wt and hPDYN^{Ta}-R212W) were used for one staining. Full cerebellar regions (including lobules II, IV/V, VI, and IX, paramedian lobule, paraflocculus, sim and crus) were present in different sections and two to five sections per region were analyzed. All measurements were done using Fiji software (NIH).

Statistical analysis

All data are expressed as mean ± standard error of the mean (SEM), unless stated otherwise. We used one-way ANOVA, followed by *post-hoc* multiple testing Bonferroni correction and Tukey's Honestly Significant Difference (HSD) tests, to determine the significance of the observed differences between the groups ($p < 0.05$ is considered statistically significant).

Results

Generation of conditional transgenic PDYN-wt and PDYN-R212W mice

We generated conditional transgenic mice carrying *PDYN*-wt or SCA23-mutant *PDYN*-R212W downstream of a transcription STOP signal flanked by *loxP* sites (**Fig. 1a**). To express *PDYN*-wt/R212W, heterozygous *PDYN*-wt/R212W Ti males were crossed with *HPRT*^{Cre} females, generating heterozygous PDYN-wt/R212W Ta mice that ubiquitously express the transgenes. The heterozygous PDYNwt/R212W Ta progeny was identified by PCR analysis (see Materials and Methods), and will be reffered to as PDYN-wt or PDYN-R212W.

First, *PDYN* expression in the cerebellum was assessed by quantitative real-time PCR. Both PDYN-wt and SCA23-mutant PDYN-R212W mice lines showed similar *PDYN* mRNA levels (**Fig. 1b**) and expression of *PDYN* did not change the levels of endogenous mouse *pdyn* (**Fig. 1c**). Overall, around 2-fold increase in *PDYN* mRNA levels was detected compared to *pdyn* mRNA in both lines (**Suppl Fig. 1a**). Western blot analysis confirmed higher expression of PDYN in the PDYN-wt mice, whereas PDYN-R212W mice showed decreased levels of PDYN protein in the cerebellum (**Fig. 1d**), despite similar transcript levels in both lines. Reduced PDYN levels were detected also in brain of PDYN-R212W mice compared to PDYN-wt (**Suppl. Fig. 1b**). These results suggest that PDYN-R212W is more processed into peptides or is more rapidly degraded than PDYN-wt in the neuronal tissue. Additionally, the expression of PDYN was confirmed also in liver and kidney of PDYN-wt and PDYN-R212W mice and similar protein levels were seen in both lines (**Suppl. Fig. 1c and d**).

To reveal the effect of expression of *PDYN* on the levels of its opioid peptides, we determined the amount of Dyn A, Dyn B and Arg-Leu-enkephalin (Leu-ENK-Arg6) in PDYN-wt and PDYN-R212W cerebella using radioimmunoassay and peptide-specific antibodies. While Leu-ENK-Arg6 levels were not changed (**Fig. 1e**),

expression of *PDYN* led to higher levels of Dyn A and B peptides in the cerebella of both PDYN-wt and PDYN-R212W mice (**Fig. 1f and g**). A 2-3-fold increase in Dyn A levels was observed in SCA23-mutant PDYN-R212W cerebella compared to PDYN-wt (**Fig. 1g**). Altogether, these experiments indicate that SCA23-mutant PDYN-R212W is more rapidly processed to opioid peptides than PDYN-wt, and its Dyn A peptides (carrying SCA23 mutation) are more stable, resulting in an increase of mutant Dyn A concentration in cerebellar tissue.

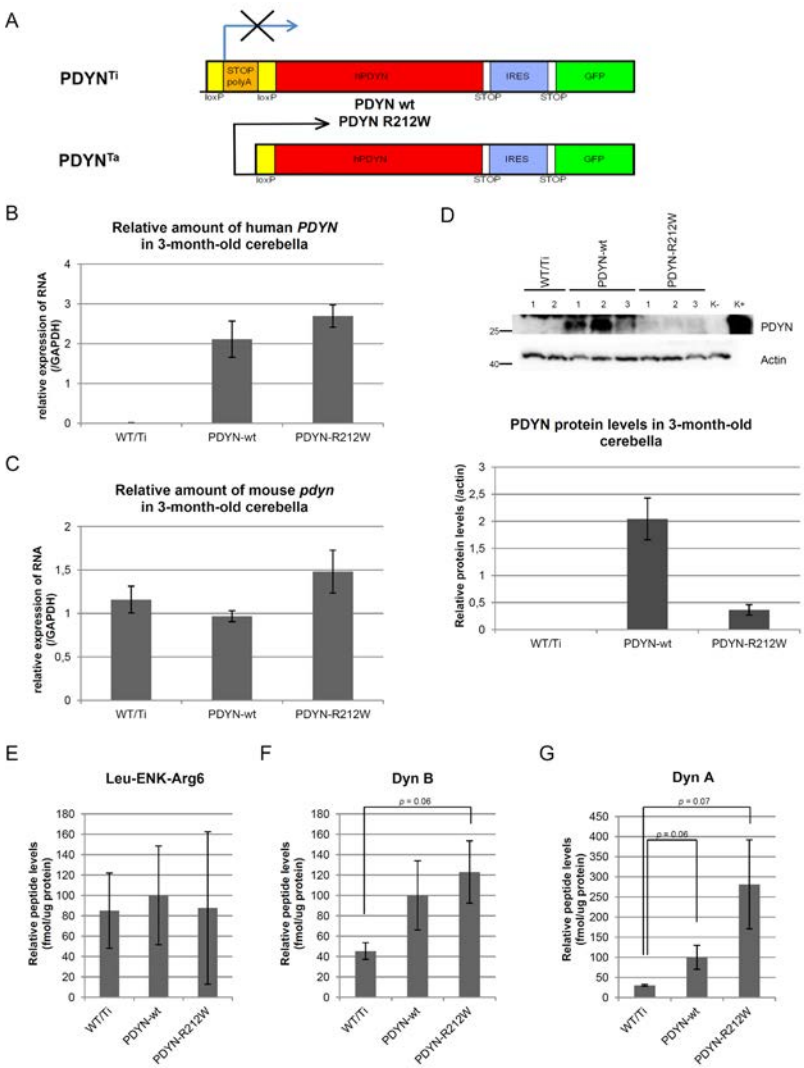

Fig. 1 Characterization of a conditional transgenic mouse model for SCA23.

(**A**) The transgene-inactive casette contained the full *PDYN* cDNA downstream of two *loxP* sites flanking a transcription STOP signal (three consecutively arranged polyadenylation sites). In addition, the IRES system was employed, enabling GFP expression whenever *PDYN* transgene is expressed without direct fusion of the two proteins. After crossing with *HPRT*^{Cre} mice expressing Cre-recombinase in the oocytes, the transgene was expressed. (**B**) Relative amount of *PDYN* mRNA in the cerebella of 3-month-old controls littermates (WT/Ti), PDYN-wt, and PDYN-R212W mice (n = 5 per genotype), and approximately equal expression levels were observed. (**C**) Relative amount of endogenous (mouse) *pdyn* mRNA in the cerebella of 3-month-old transgenic mice and control littermates (n = 5 per genotype). Expression of the transgene did not affect *pdyn* levels. (**D**) Representative immunoblot and quantification graph of relative PDYN protein levels in cerebella of 3-months-old mice (n = 6 per genotype). PDYN-wt and PDYN-R212W mice expressed 2.04 ± 0.38 and 0.36 ± 0.09 of PDYN (mean ± SEM), respectively. (**E**, **F**, **G**) Relative peptide levels in the mice cerebella at the age of 3-months (n = 2 per genotype), including Leu-ENK-Arg6 (**E**), Dyn B (**F**), and Dyn A (**G**). Peptide levels in the cerebella of WT/Ti, PDYN-wt and PDYN-R212W mice were 85.02 ± 36.97, 100.00 ± 48.52, and 87.66 ± 74.81 fmol/µg protein (**E**), 45.43 ± 8.21, 100.00 ± 33.98, and 122.92 ± 30.56 (**F**), and 30.34 ± 2.15, 100.00 ± 29.74, and 281.36 ± 110.61 (**G**), respectively. The data is expressed as relative (to protein levels in the samples) mean ± SEM, and normalized by PDYN-wt.

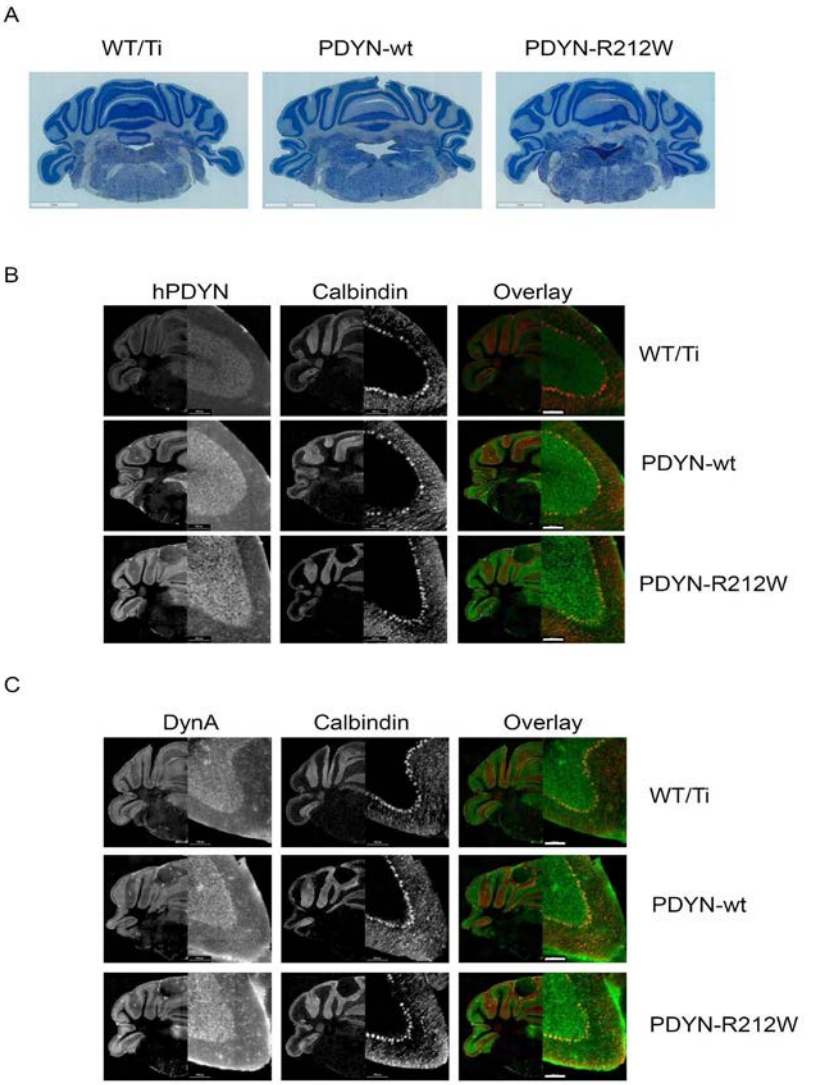

Fig. 2 Cerebellar morphology of SCA23-mutant PDYN-R212W mice at the age of 3 months.

(**A**) Photomicrographs of toluidine blue-stained cerebellar coronal sections, comprising of the molecular, PC, and granule cell layers, showed no differences in size between PDYN-wt, and PDYN-R212W mice and control littermates. Scale bar, 2 mm. (**B, C**) Immunofluorescence revealed ubiquitous PDYN (**B**) and Dyn A (**C**) expression in cerebella of PDYN-wt, and PDYN-R212W mice and not in control littermates. Robust expression of PDYN and Dyn A was detected in the soma of PCs and dendritic trees as was seen by co-localization with the PC-specific marker Calbindin (overlay). Photomicrographs of cerebellar overall morphology and 20x magnification, scale bar, 100 µm.

Additionally, no significant changes were detected in expression of genes of opioid receptors, including *Oprk1*, *Oprm1* and *Oprd1*, in PDYN-wt and PDYN-R212W mice compared to control littermates (**Suppl. Fig. 2a and b**).

Histological examination using toluidine blue staining showed unchanged cerebellar size in both PDYN-wt and PDYN-R212W at the age of 3 months (**Fig. 2a**). Clear expression of PDYN and Dyn A was detected by immunofluorescence in the cerebella using specific anti-human PDYN and anti-Dyn A antibodies (**Fig. 2b and c**, respectively) and strong co-localization was observed in the PC soma with the PC-specific marker Calbindin. Additionally, Dyn A was localized more to the dendritic trees in the molecular layer than PDYN.

Thus, we have generated viable transgenic mice that ubiquitously express PDYN-wt or PDYN-R212W. Moreover, SCA23-mutant PDYN-R212W mice showed highly elevated Dyn A levels that seem to be a direct consequence of enhanced precursor processing as low PDYN levels were detected in these mice.

PDYN-R212W causes cerebellar ataxia

To assess an effect of SCA23-mutation on motor coordination in PDYN-R212W mice, first, a ledge test was performed in 3- to 12-month-old mice. Defects in balance, hindlimb gait, and coordination were scored using a scale from 0 to 3 (3 for severe impairment; described previously [11]). Already at the age of 3 months, PDYN-R212W mice performed significantly worse on the ledge than PDYN-wt and WT/Ti control littermates, and this progressed in time, reaching the score of 2 at the age of 12 months (**Fig. 3a**). However, PDYN-R212W mice exhibited a relatively mild motor impairment, as a score of 3 was not reached. Mild age-related motor coordination deficits were also detected in the WT/Ti controls by the age of 12 months.

The progression of cerebellar motor impairment was scored in the hindlimb clasping test (again, scored from 0 to 3; [11]). At the 3 months of age, SCA23-mutant mice PDYN-R212W showed retracted hindlimbs to the abdomen more often than PDYN-wt mice and WT/Ti controls, reflected by a higher clasping score, and it worsened in time-course of disease (**Fig. 3b**). In this test again, at the age of 12 months, age-related deficits were also observed in the control littermates.

To further study the ataxic phenotype, footprint patterns were analyzed for differences in stride length, base width, and overlap between front and hind paws (**Fig. 3c**). No differences were found in stride length (data not shown). Hindlimb base of PDYN-R212W mice was significantly wider compared to PDYN-wt and WT/Ti mice (**Fig. 3d**). Moreover, significant loss of overlap was detected in the footprint pattern of SCA23-mutant PDYN-R212W mice starting at 6 months of age in contrast to PDYN-wt and WT/Ti mice, which did not display this effect (**Fig. 3e**).

Finally, to determine motor performance, the accelerating rod test (max. 30 rpm) was performed (see Materials and Methods for details). No significant differences between the genotype groups were detected at 3 to 9 months of age (**Fig. 3f**). Only at 12 months of age, PDYN-R212W mice spent significantly less time on the accelerating rod than PDYN-wt and control littermates (**Fig. 3f**). We were not able to study motor function decline in this particular test, as the PDYN-R212W mice only showed a detectable deficits during the last time point of the analysis. Moreover, defects in motor performance were not due to body size variation as there was no significant difference in body weight per genotype group (**Suppl. Fig. 3**).

Altogether, these data clearly show that SCA23-mutant PDYN-R212W mice exhibit a mild and slowly progressive motor coordination impairment reflecting ataxic features of SCA23 patients, including motor dysfunction with deficits in balance and step alterations. This is in contrast to the mouse models of polyglutamine-related SCA, such as SCA1 [13], that show a severe and rapid disease progression, but is similar to the mouse models for other SCAs caused by conventional mutations, including SCA5 [14].

Loss of Purkinje cells and climbing fiber innervation in PDYN-R212W mice

To reveal whether the ataxic symptoms were caused by PC loss and cerebellar neurodegeneration, the cerebellar morphology and PC layer integrity were determined in mice at 12 months of age. No molecular layer thinning was detected, however, changes between the genotypes may be missed due to the variability in molecular layer

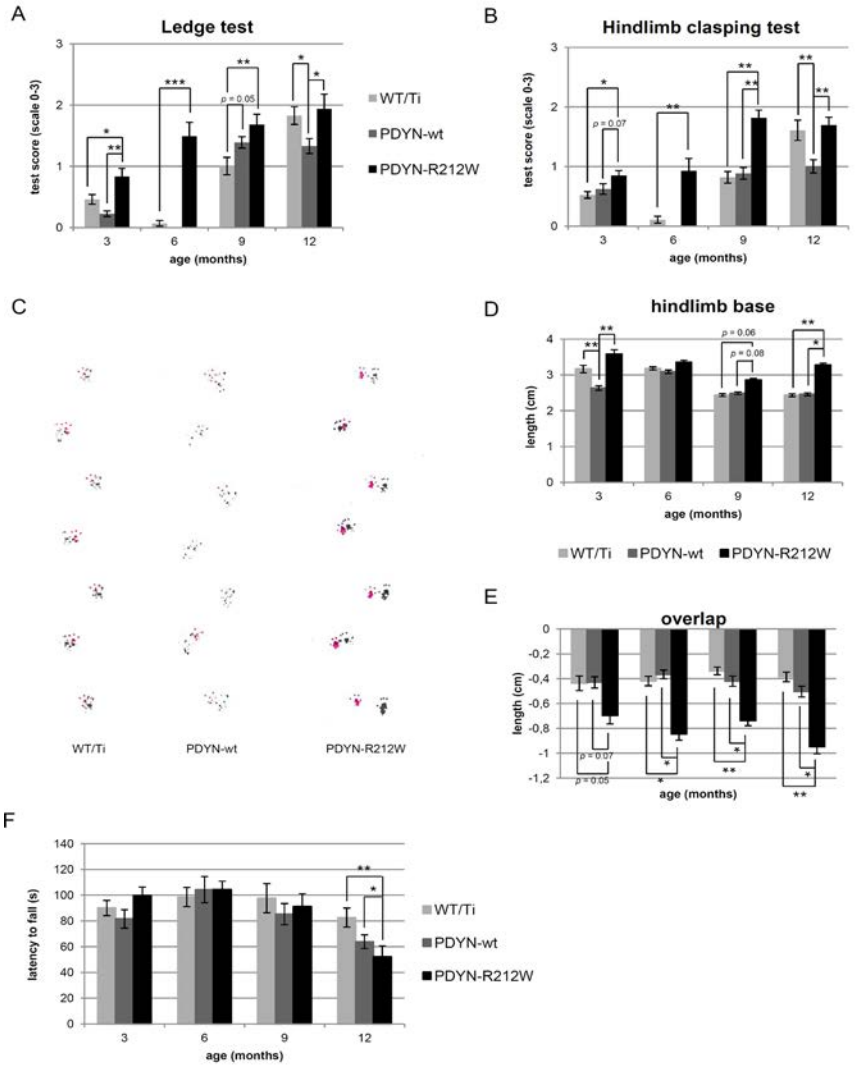

Fig. 3 Cerebellar ataxia in PDYN-R212W mice.

(**A**) Quantification of the ledge tests in time using a scoring scale from 0 (no phenotype) to 3 (severe ataxic phenotype). At the age of 3 months, PDYN-R212W mice performed significantly worse on the ledge than PDYN-wt and WT/Ti control littermates (0.83 ± 0.13 versus 0.22 ± 0.04 and 0.46 ± 0.07, respectively). Their motor impairment progressed in time as a score of 1.94 ± 0.24 was reached at the age of 12 month, while PDYN-wt mice scored 1.33 ± 0.12. Significant differences, * $p < 0.05$, ** $p < 0.001$, and *** $p < 10^{-5}$. (**B**) Quatification of hindlimb clasping in time using scoring scale from 0 (no clasping) to 3 (severe hindlimb retraction to the abdomen). Already at the age of 3 months, PDYN-R212W mice showed significantly higher clasping scores (0.85 ± 0.08) than PDYN-wt (0.62 ± 0.09) and WT/Ti controls (0.52 ± 0.05). Significant differences, * $p < 0.005$, and ** $p < 10^{-5}$. (**C**) Representative footprint patterns of 12-month-old WT/Ti controls, PDYN-wt, and SCA23-mutant PDYN-R212W mice. Hind paws are in black, and front paws in magenta. (**D**) Quantification of the hindlimb base from footprint patterns showed a significantly wider base for PDYN-R212W mice (3.2 ± 0.046 cm) than PDYN-wt and control littermates (2.45 ± 0.041 cm and 2.43 ± 0.039 cm) at 12 months of age. Significant differences, * $p < 0.01$, and ** $p < 0.005$. (**E**) Quantification of the front and hind paws overlap from footprint patterns showed significant loss of overlap in PDYN-R212W mice starting at 6 months of age, which was not observed in PDYN-wt and control littermates (-0.84 ± 0.05 cm versus -0.36 ± 0.03 cm and -0.41 ± 0.04 cm, respectively). Significant differences, * $p < 0.005$, and ** $p < 10^{-5}$. (**F**) Quantification of latency to fall from the accelerating rotarod for the three genotypes at experimental day 4. Only at 12 months of age, PDYN-R212W showed decreased latency to fall (52.18 ± 8.38 seconds) comparing to PDYN-wt mice (63.84 ± 5.38 seconds) and control littermates (82.63 ± 7.42 seconds). Significant differences, * $p < 0.05$, and ** $p < 0.005$. Data is expressed as mean ± SEM. Significance of results was tested using One-way ANOVA, followed by HSD tests.

thickness between or within the various lobules of the cerebellum (Fig. 4a). Nonetheless, clearly reduced PC numbers were detected in lobules II, VI and IX, paraflocculus and paramedian lobule of PDYN-R212W mice comparing to PDYN-wt and WT/Ti, but not in cerebellar regions sim and crus (Fig. 4b). This was not reflected in clear loss of Calbindin levels by Western blot analysis (Fig. 4c). Interestingly, we observed an increase in PC number in lobules IV-V in PDYN-R212W mice (Fig. 4b), suggesting potential compensatory effects for PC loss in other vermal regions.

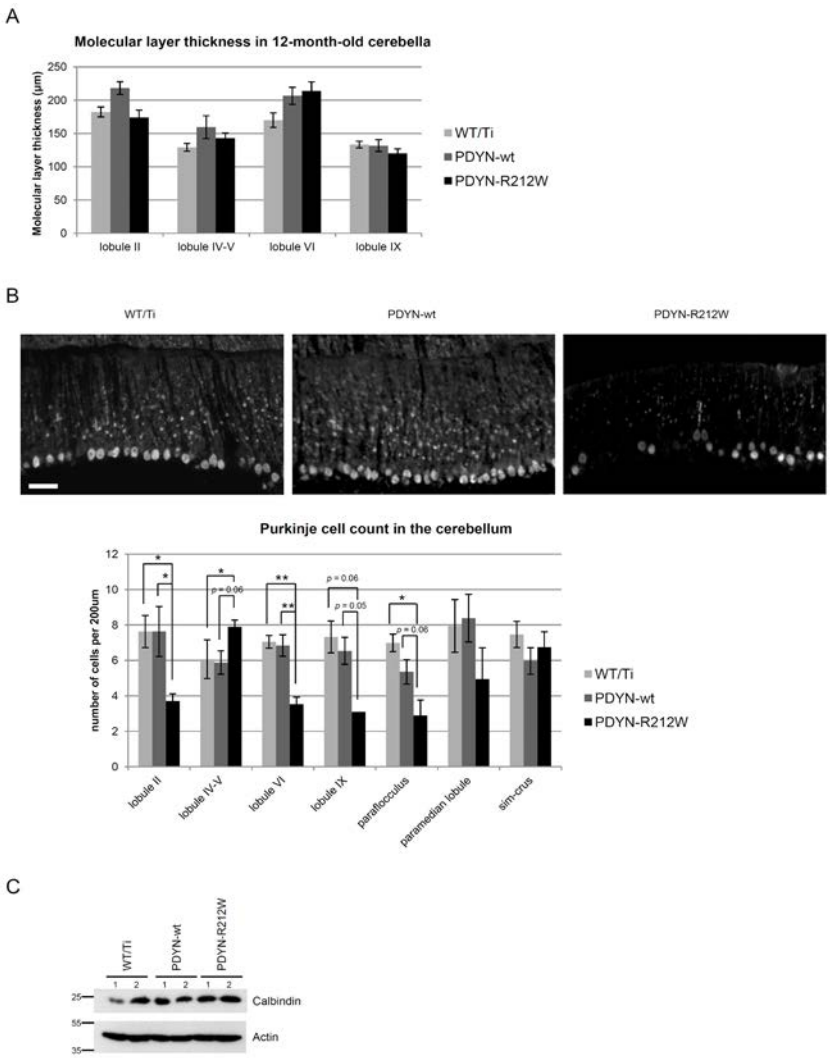

Fig. 4 Purkinje cell loss in 12-month-old PDYN-R212W mice.

(**A**) Quantification of the molecular layer thickness in different vermal regions of 12-month-old mice cerebella did not reveal any significant differences between the genotypes. High variability in molecular layer thickness was seen between and within the lobules. (**B**) Representative photomicrographs of immunofluorescence of the cerebellar lobule VI, using anti-Calbindin antibody, showing the PC and molecular layer in 12-month-old mice (control littermates WT/Ti, PDYN-wt, and PDYN-R212W). Scale bar, 80 µm. PC numbers were quantified in lobules II, IV-V, VI and IX, paraflocculus, paramedian lobule, and sim and crus among the genotypes and averaged per 200 µm. Approximately 50% of PCs were lost in PDYN-R212W compared to PDYN-wt and WT/Ti controls. Data is expressed as mean ± SEM. Significance of results was tested using One-way ANOVA, followed by HSD tests. Significant differences, * $p < 0.01$, and ** $p < 0.0005$. (**C**) Western blot analysis of cerebellar extracts did not reveal alterations in Calbindin levels.

To assess morphological alterations that could precede PC loss in PDYN-R212W cerebella, we analyzed the expression and localization of the glutamate transporter EAAT4, as marked alterations in EAAT4 levels and distribution were seen in SCA5 and SCA23 human postmortem material [1, 15]. No changes in EAAT4 localization

or expression were detected between the genotypes at 3 and 12 months of age (**Suppl. Fig 4a and b**). However, already at 3 months of age, PDYN-R212W mice exhibited marked loss of climbing fiber (CF) synapses on PC dendrites in lobules II, VI and IX, paramedian lobule, and paraflocculus (**Fig. 5a**), which progressed during the course of disease (**Fig. 5b and Suppl. Fig. 5**). Loss of CF innervation was previously seen in SCA1 and SCA7 mice [16, 17]. Notably, highly variable VGlut2 levels were measured in cerebellar extracts among the genotypes by Western blot analysis (data not shown). The progressive loss of CF innervation suggests active elimination of CF-PC synapses and preceded PC loss in PDYN-R212W cerebella, indicating that alterations in synaptic transmission may underlie ataxic phenotype.

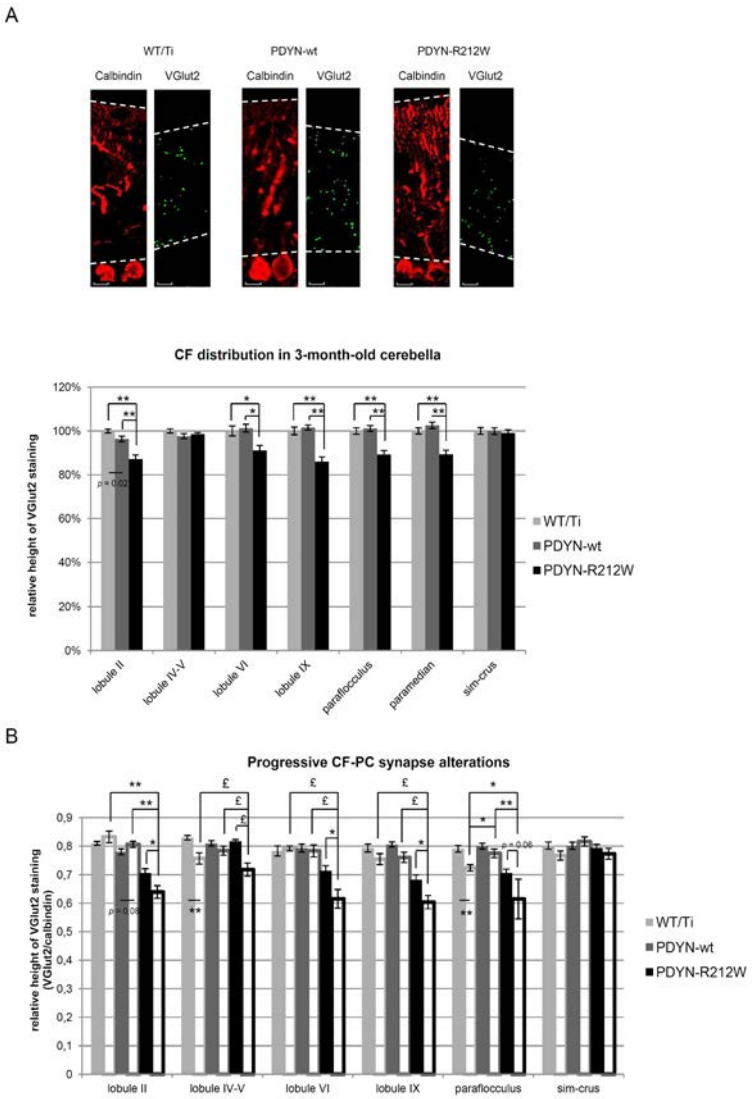

Fig. 5 Reduced climbing fiber synapse innervation at PC dendrites in PDYN-R212W mice.

(**A**) Representative photomicropgraphs of immunofluorescence analysis of the mice cerebella at 3 months of age stained with anti-Calbindin antibody to visualize the PC dendritic trees, and anti-VGlut2 antibody for CF detection. The measured height of VGlut2 and Calbindin stainings over the dendritic tree is indicated in the molecular layers. Scale bar, 10µm. Quantification of the relative height of VGlut2 staining (to Calbindin) in lobules II, IV-V, VI and IX, paramedian lobule, flocculus and paraflocculus of 3-months-old mice shows decreased CF distribution in SCA23-mutant PDYN-R212W mice of approximately 10% in the affected regions. Data is expressed as mean ± SEM, normalized to WT/Ti control littermates. Significance of results was tested using 1-way ANOVA, followed by HSD tests, * $p < 0.01$, and ** $p < 0.0005$. (**B**) Quantification of loss of CF synapses between genotypes in 3- (full bars) and 12-month-old (empty bars) mice. PDYN-R212W mice showed progressive decrease in CF innervation in the affected vermal regions (lobule II, VI, and IX) comparing to PDYN-wt and WT/Ti mice. Data is expressed as mean ± SEM (VGlut2/Calbindin). Significant differences (One-way ANOVA, followed by HSD tests), * $p < 0.05$, ** $p < 0.005$, and £ $p < 10^{-4}$.

Discussion and conclusions

We have generated for the first time a conditional transgenic mouse model for SCA23 expressing PDYN-R212W, that mimicks many characteristics of SCA23 human disease, including mild, but progressive balance and gait abnormalities, motor dysfunction, and cerebellar PC loss. This work confirms that R212W mutation in *PDYN* underlies the pathology of SCA23. Consistent with our previous *in vitro* work (Bakalkin et al., 2010), we found 2-3-fold higher Dyn A levels in the cerebella of PDYN-R212W mice comparing to PDYN-wt, despite similar transcript levels in both lines. This suggests that SCA23-mutant PDYN-R212W protein undergoes enhanced processing into Dyn peptides or that the SCA23-mutant Dyn A is more stable than wt, and cannot be processed efficiently to Leu-ENK-Arg6, thus accumulates in the tissue. The mouse model generated by us could provide mechanistic insights into the non-opioid neurodegenerative actions of Dyn A peptides.

Increased concentration or prolonged exposure of Dyn A have already been found to be neurotoxic and caused cell death through non-opioid mechanisms via activation of ionotropic glutamate receptors, including NMDARs or AMPARs [5, 6]. AMPAR-mediated excitotoxicity was proposed as the underlying mechanism of PCs loss in SCA5 [14]. Moreover, Dyn A binds NMDARs and potentiate their currents [6], which may lead to excitotoxicity. PCs death through excitotoxic mechanism was linked to CF hyperexcitability before [18, 19]. Our results are in line with the hypothesis that Dyn A may cause excitotoxicity acting through ionotropic glutamate receptors, either NMDARs or AMPARs, on the CF-PC synapse and cause PCs death. CF-PC synapse elimination might be the compensatory mechanism to prevent the hyperexcitability of CF due to elevated Dyn A levels that potentiates glutamate currents.

While the most prominent deficits were observed in PDYN-R212W mice, some age-related motor decline was seen in PDYN-wt and control littermates. Notably, at the age of 12 months, PDYN-wt mice performed significantly better than PDYN-R212W and control littermates in the ledge and clasping tests, suggesting protective role of PDYN or opioid peptides. Potential neuroprotective effects of Dyn A were already suggested to be mediated through κ-opioid receptor (KOR; encoded by *Oprk1*) [20], as KOR activation reduces intracellular calcium concentrations and may therefore prevent excitotoxicity [21-23]. Slightly reduced *Oprk1* levels were detected in PDYN-R212W mice at 12 months of age. This could imply that next to pathologically elevated Dyn A levels, loss of KOR expression might contribute to the disease pathology. However, since the excitotoxic effects of pathologically elevated Dyn A were suggested to be much more potent than the negative effects on opioid signalling [20], it is unlikely that loss of KOR is a major component of the etiology of SCA23. Altogether, we believe that pathologically elevated Dyn A levels may cause excitotoxicity leading to PC loss and cerebellar ataxia in PDYN-R212W mice.

We found mild motor deficits in PDYN-R212W mice preceding the PCs loss that coincided with reduced CF innervation of PCs dendrites. Loss of CF innervation progressed in time and this suggests active elimination of CF-PC synapses, rather than developmental problems of the molecular layer in PDYN-R212W mice. Since loss of CF-PC synapses preceded PC loss and coexisted with the first signs of ataxic symptoms, alterations in synaptic transmission might underlie the motor impairment in SCA23 pathology. Decreased CF-PC synapse distribution seems to be common in SCA pathology and was reported also in mouse models of SCA1 and SCA7 [16, 17, 24].

Additionally, in PDYN-R212W mice, the loss of CF termini and PCs was mostly restricted to particular lobules of the cerebellar vermis, correlating with a relatively mild pure cerebellar ataxic phenotype. Similarly, in the human postmortem SCA23 material atrophy was most pronounced in the frontotemporal region and the vermis of the cerebellum [2]. Interestingly, the CF synapses in the anterior lobules IV-V of PDYN-R212W mice were not affected at 3 months of age, and only mildly at 12 months, which correlated with an increase in PC number. These observations suggest compensatory mechanisms of these lobules to take over motor tasks of the affected regions. The regional degeneration is a direct consequence of functional topography of the cerebellum, and is consistent with the recent reports that PCs can display different excitability and firing properties within various cerebellar regions controlling different tasks [25, 26]. It is noteworthy that SCAs caused by conventional mutations usually show a milder disease manifestation and slower disease progression than polyglutamine-related SCA types and this is reflected in selective cerebellar degeneration versus widely-spread brainstem degeneration, respectively [27-29].

In conclusion, the PDYN-R212W mouse described here is a new model for ataxia and is the first mouse model for SCA23. These SCA23-mutant mice display many disease symptoms seen in SCA23 patients, including mild and progressive ataxic phenotype and PCs loss, due to pathologically elevated Dyn A levels, providing convincing evidence that the PDYN-R212W mouse model is suitable to study the etiology of SCA23. The elevated Dyn A levels in SCA23-mutant mice seem to be responsible for the initiation and progression of the disease via excitotoxic damage through CF-PC synapses. Additionally, the PDYN-R212W mice develop symptoms slowly, which provides a possibility to study in detail the progression of pure, isolated cerebellar ataxia over time, and display elevated Dyn A levels which may be a useful model for studying not only SCA23, but also other Dyn A-controlled mechanisms such as pain processing or addiction control.

References

1. Bakalkin G, Watanabe H, Jezierska J et al. Prodynorphin Mutations Cause the Neurodegenerative Disorder Spinocerebellar Ataxia Type 23. *Am J Hum Genet* 2010.
2. Verbeek DS, van de Warrenburg BP, Wesseling P, Pearson PL, Kremer HP, Sinke RJ. Mapping of the SCA23 locus involved in autosomal dominant cerebellar ataxia to chromosome region 20p13-12.3. *Brain* 2004; 127: 2551-2557.
3. Schwarzer C. 30 years of dynorphins--new insights on their functions in neuropsychiatric diseases. *Pharmacol Ther* 2009; 123: 353-370.
4. Tan-No K, Cebers G, Yakovleva T et al. Cytotoxic effects of dynorphins through nonopioid intracellular mechanisms. *Exp Cell Res* 2001; 269: 54-63.
5. Singh IN, Goody RJ, Goebel SM et al. Dynorphin A (1-17) induces apoptosis in striatal neurons in vitro through alpha-amino-3-hydroxy-5-methylisoxazole-4-propionate/kainate receptor-mediated cytochrome c release and caspase-3 activation. *Neuroscience* 2003; 122: 1013-1023.
6. Woods AS, Kaminski R, Oz M et al. Decoy peptides that bind dynorphin noncovalently prevent NMDA receptor-mediated neurotoxicity. *J Proteome Res* 2006; 5: 1017-1023.
7. Jezierska J, Stevanin G, Watanabe H et al. Identification and characterization of novel PDYN mutations in dominant cerebellar ataxia cases. *J Neurol* 2013.
8. Baker DJ, Dawlaty MM, Wijshake T et al. Increased expression of BubR1 protects against aneuploidy and cancer and extends healthy lifespan. *Nat Cell Biol* 2013; 15: 96-102.
9. van Ree JH, Jeganathan KB, Malureanu L, van Deursen JM. Overexpression of the E2 ubiquitin-conjugating enzyme UbcH10 causes chromosome missegregation and tumor formation. *J Cell Biol* 2010; 188: 83-100.
10. Christensson-Nylander I, Nyberg F, Ragnarsson U, Terenius L. A general procedure for analysis of proenkephalin B derived opioid peptides. *Regul Pept* 1985; 11: 65-76.
11. Guyenet SJ, Furrer SA, Damian VM, Baughan TD, La Spada AR, Garden GA. A simple composite phenotype scoring system for evaluating mouse models of cerebellar ataxia. *J Vis Exp* 2010.
12. Brooks SP, Dunnett SB. Tests to assess motor phenotype in mice: a user's guide. *Nat Rev Neurosci* 2009; 10: 519-529.
13. Burright EN, Clark HB, Servadio A et al. SCA1 transgenic mice: a model for neurodegeneration caused by an expanded CAG trinucleotide repeat. *Cell* 1995; 82: 937-948.
14. Perkins EM, Clarkson YL, Sabatier N et al. Loss of beta-III spectrin leads to Purkinje cell dysfunction recapitulating the behavior and neuropathology of spinocerebellar ataxia type 5 in humans. *J Neurosci* 2010; 30: 4857-4867.
15. Ikeda Y, Dick KA, Weatherspoon MR et al. Spectrin mutations cause spinocerebellar ataxia type 5. *Nat Genet* 2006; 38: 184-90.
16. Duvick L, Barnes J, Ebner B et al. SCA1-like disease in mice expressing wild-type ataxin-1 with a serine to aspartic acid replacement at residue 776. *Neuron* 2010; 67: 929-935.
17. Furrer SA, Waldherr SM, Mohanachandran MS et al. Reduction of mutant ataxin-7 expression restores motor function and prevents cerebellar synaptic reorganization in a conditional mouse model of SCA7. *Hum Mol Genet* 2013; 22: 890-903.
18. O'Hearn E, Molliver ME. The olivocerebellar projection mediates ibogaine-induced degeneration of Purkinje cells: a model of indirect, trans-synaptic excitotoxicity. *J Neurosci* 1997; 17: 8828-8841.
19. O'Hearn E, Molliver ME. Degeneration of Purkinje cells in parasagittal zones of the cerebellar vermis after treatment with ibogaine or harmaline. *Neuroscience* 1993; 55: 303-310.
20. Hauser KF, Aldrich JV, Anderson KJ et al. Pathobiology of dynorphins in trauma and disease. *Front Biosci* 2005; 10: 216-235.
21. Bausch SB, Esteb TM, Terman GW, Chavkin C. Administered and endogenously released kappa opioids decrease pilocarpine-induced seizures and seizure-induced histopathology. *J Pharmacol Exp Ther* 1998; 284: 1147-1155.
22. Husain S, Abdul Y, Potter DE. Non-analgesic effects of opioids: neuroprotection in the retina. *Curr Pharm Des* 2012; 18: 6101-6108.
23. Wagner JJ, Caudle RM, Chavkin C. Kappa-opioids decrease excitatory transmission in the dentate gyrus of the guinea pig hippocampus. *J Neurosci* 1992; 12: 132-141.

24. Ebner BA, Ingram MA, Barnes JA et al. Purkinje cell ataxin-1 modulates climbing fiber synaptic input in developing and adult mouse cerebellum. *J Neurosci* 2013; 33: 5806-5820.

25. Stoodley CJ, Schmahmann JD. Evidence for topographic organization in the cerebellum of motor control versus cognitive and affective processing. *Cortex* 2010; 46: 831-844.

26. Kim CH, Oh SH, Lee JH, Chang SO, Kim J, Kim SJ. Lobule-specific membrane excitability of cerebellar Purkinje cells. *J Physiol* 2012; 590: 273-288.

27. Durr A. Autosomal dominant cerebellar ataxias: polyglutamine expansions and beyond. *Lancet Neurol* 2010; 9: 885-94.

28. Whaley NR, Fujioka S, Wszolek ZK. Autosomal dominant cerebellar ataxia type I: a review of the phenotypic and genotypic characteristics. *Orphanet J Rare Dis* 2011; 6: 33.

29. Fujioka S, Sundal C, Wszolek ZK. Autosomal dominant cerebellar ataxia type III: a review of the phenotypic and genotypic characteristics. *Orphanet J Rare Dis* 2013; 8: 14.

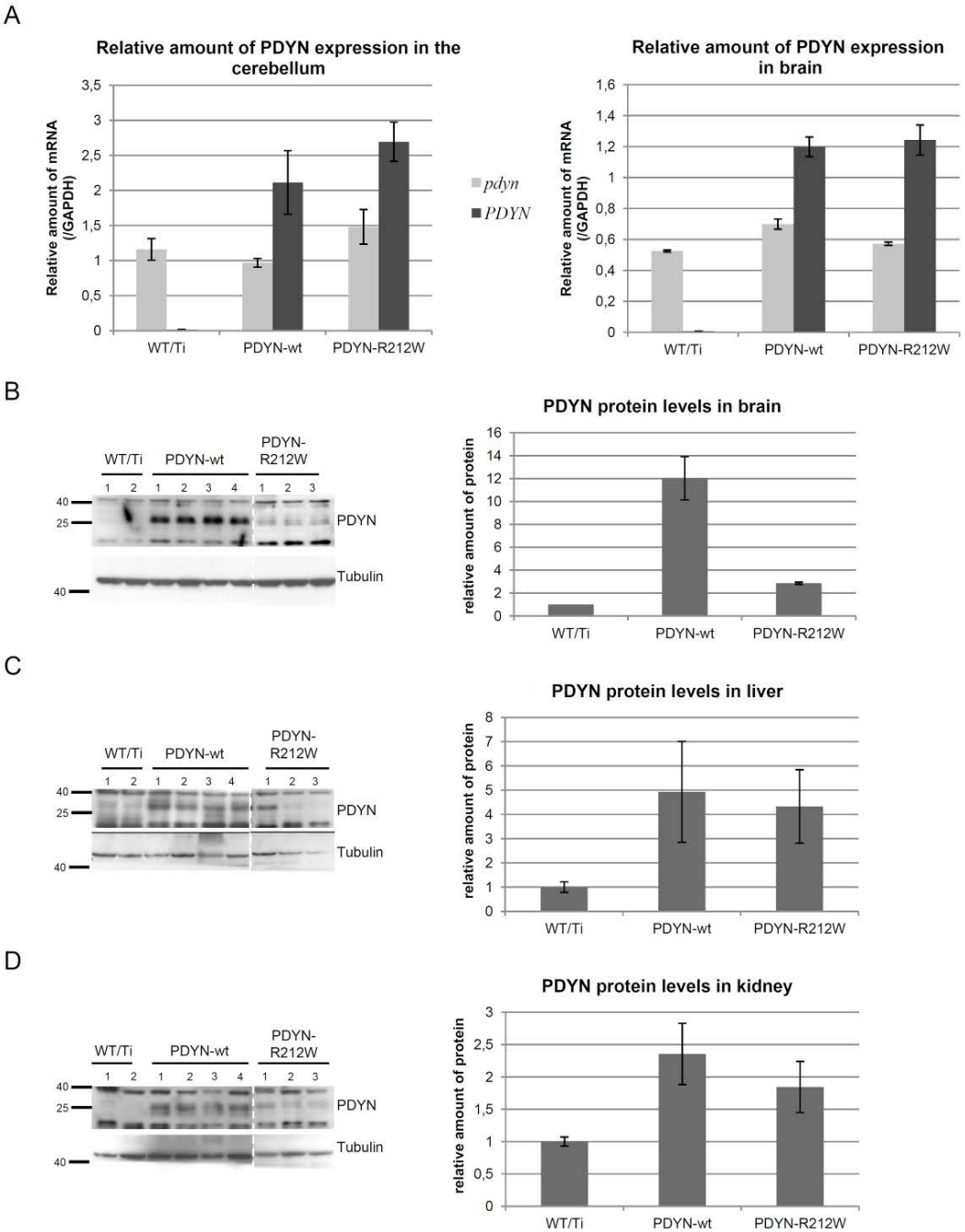

Suppl. Fig. 1

(**A**) Relative amount of *PDYN* mRNA, both mouse and human, in cerebellar and brain tissue of 3-month-old WT/Ti controls, PDYN-wt, and PDYN-R212W mice (n = 5 per genotype, mean ± SEM). (**B-D**) Representative immunoblots and quantifications of relative PDYN protein levels in brain (**B**), liver (**C**) and kidney (**D**) of 3-months-old mice (n = 3 per genotype, mean ± SD, relative to Tubulin and normalized by WT/Ti). PDYN-wt and PDYN-R212W mice expressed 12.02 ± 0.93 and 2.86 ± 0.04 of PDYN (**B**), 4.93 ± 2.08 and 4.33 ± 1.51 (**C**), 2.36 ± 0.47 and 1.84 ± 0.39 (**D**), respectively.

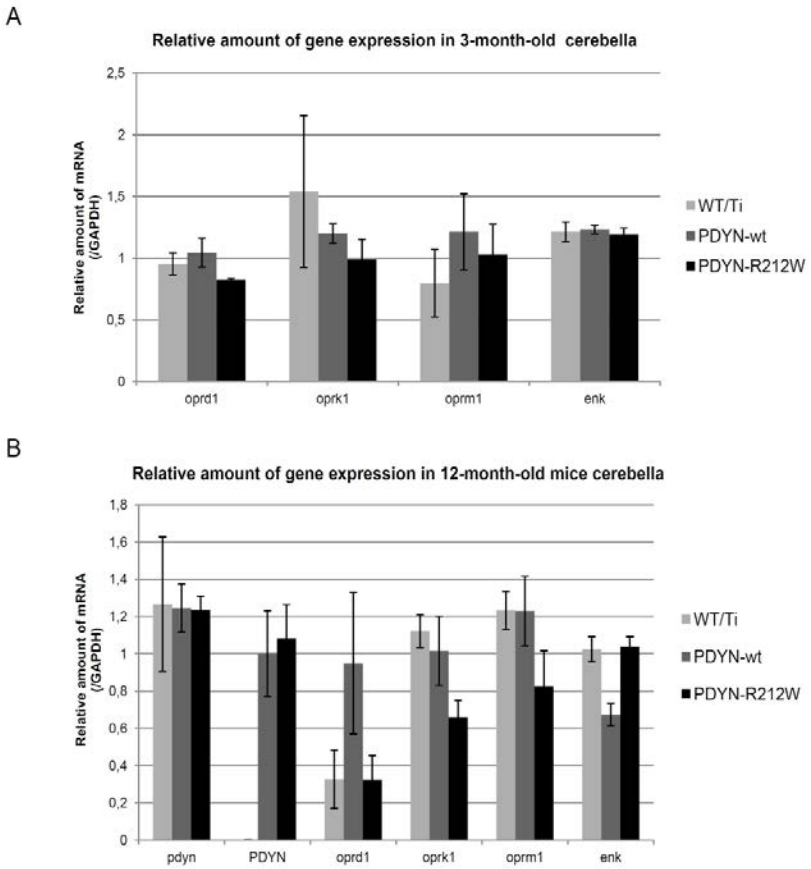

Supplementary Figure 2

(**A**, **B**) Relative expression of opioid system in the cerebella of 3-month-old (**A**) and 12-months-old (**B**) WT/Ti controls, PDYN-wt, and PDYN-R212W mice. Data is expressed as mean ± SEM (n = 5 per genotype). No significant results were found. oprd1 = δ-opioid receptor, oprk1 = κ-opioid receptor, oprm1 = μ-opioid receptor, enk = proenkephalin-A

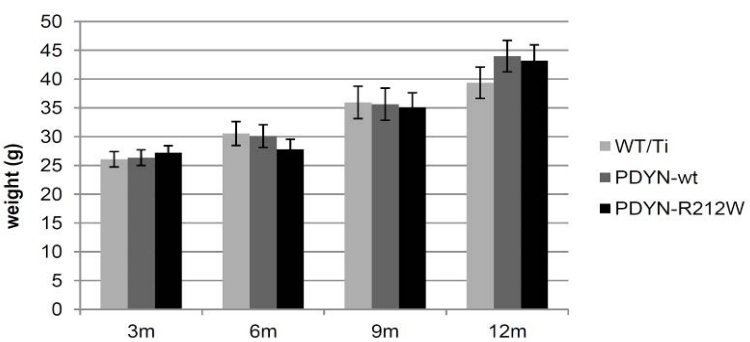

Suppl. Fig. 3

Average body weight of WT/Ti controls, PDYN-wt, and SCA23-mutant PDYN-R212W mice in time, showing no significant differences that could explain defects in motor performance. Data is expressed as mean ± SEM.

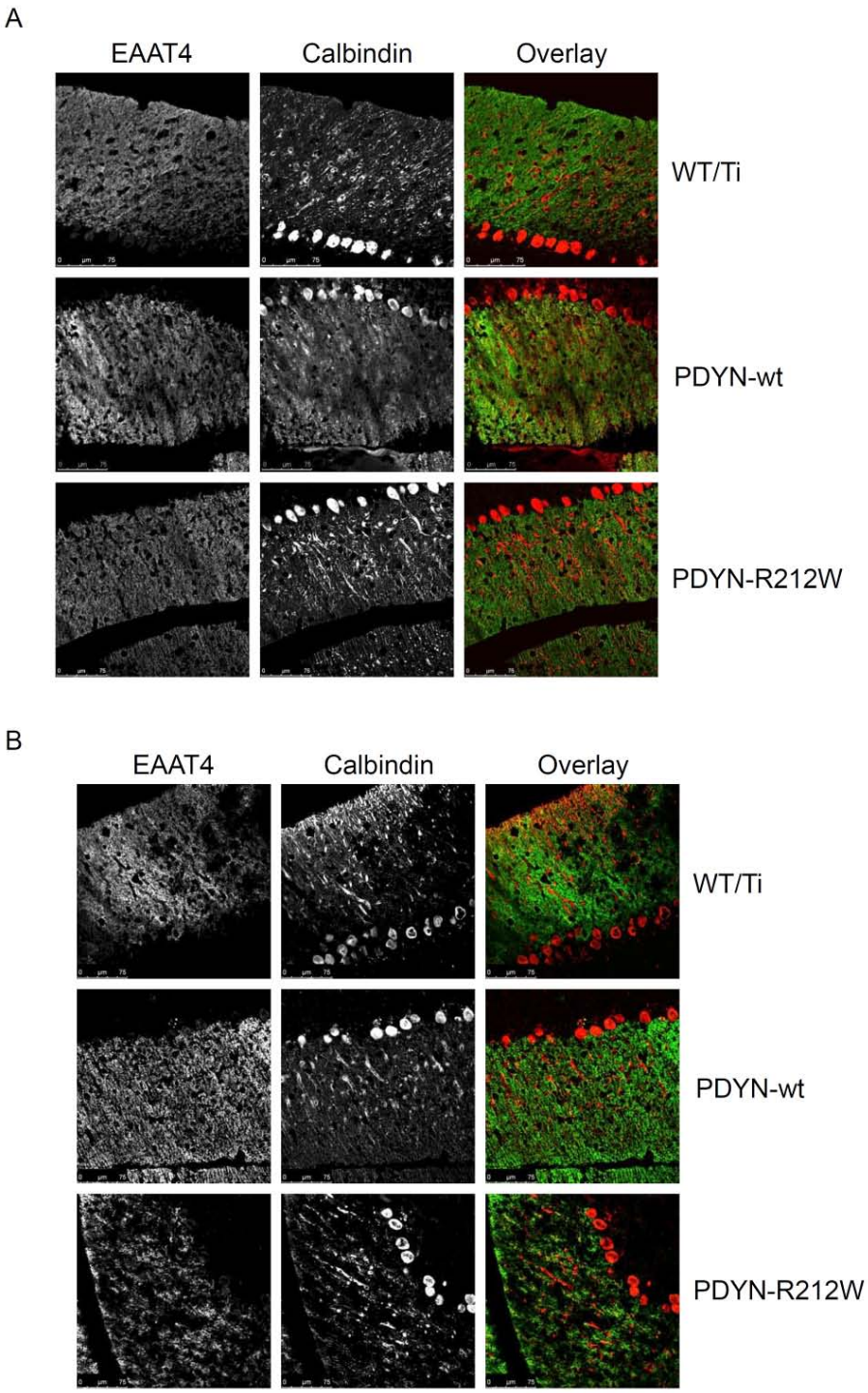

Suppl. Fig. 4

Representative photomicrographs of immunofluorescence analysis of 3-month-old (**A**) and 12-month-old (**B**) mice cerebella, using anti-Calbindin and anti-EAAT4 antibodies, that showed no differences in EAAT4 levels or distribution in the molecular layer between the genotypes. Scale bar, 75 µm.

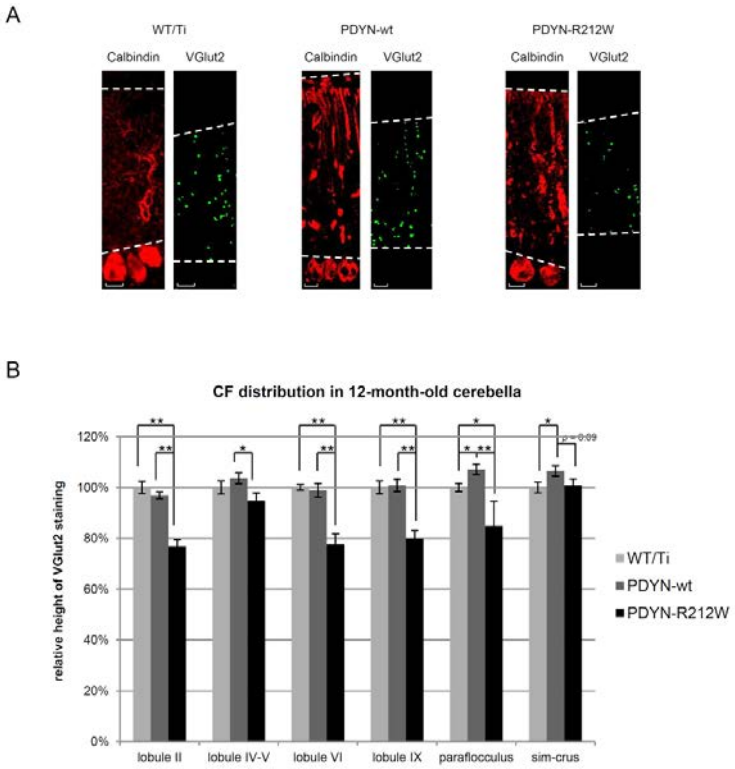

Suppl. Fig. 5

(**A**) Representative photomicrographs of 12-months-old cerebella of WT/Ti controls, PDYN-wt, and hPDYN-R212W mice, analyzed with anti-VGlut2 and anti-Calbindin antibodies, showing relative CF distribution in molecular layer. Scale bar, 10µm. (**B**) Quantification of the relative height of VGlut2 staining (to Calbindin) in lobules II, IV-V, VI and IX, paramedian lobule, flocculus and paraflocculus of 12-months-old mice shows decreased CF distribution in SCA23-mutant PDYN-R212W mice of approximately 20% in the affected regions. Data is expressed as relative to WT/Ti mean ± SEM. Significance of results was tested using One-way ANOVA, followed by HSD tests, * $p < 0.05$, and ** $p < 0.005$.

Supplementary Table 1

Primer list used for quantitative real-time PCR for expression analysis of opioid signalling proteins

Primer name	Primer sequence
mOprk1__RT_For	GTTGCGGTCTTCATCTTCGT
mOprk1_RT_Rev	ATCCCTGTTATCATCACCGC
mOprd1_RT_For	ATGTAGATGTTGGTGGCGGT
mOprd1_RT_Rev	GCTCTACTCGGCTGTGTGC
mEnk_RT_For	CTAAATGCACGTACCGCCTGGTT
mEnk_RT_Rev	CGATGTTATCCCAAGGGAACTCG
mOprm1_RT_For	GCTCAAAGACAAGGGACAGG
mOprm1_RT_Rev	GCAAAACTCTGCTCGAATCC

CHAPTER 7

SCA23-mutant Dynorphin A peptides cause cell death via non-opioid excitotoxic mechanisms

J. Jezierska[1], C. Smeets[1], M.N. Melo[2], A. Stargardt[3], C. Dooley[4], G. Bakalkin[5], J. McLaughlin[4], S. Marrink[2], H.H. Kampinga[6], E.A Reits[3], and D.S. Verbeek[1]

[1] Dept of Genetics, University Medical Center Groningen, University of Groningen, The Netherlands

[2] Groningen Biomolecular Sciences and Biotechnology Institute, Centre for Life Sciences, University of Groningen, The Netherlands

[3] Dept of Cell Biology and Histology, Academic Medical Center, Amsterdam, The Netherlands

4Torrey Pines Institute for Molecular Studies, Port St Lucie, USA

5Division of Biological Research on Drug Dependence, Dept of Pharmaceutical Biosciences, Uppsala University, Sweden

[6] Dept of Cell Biology, University Medical Center Groningen, University of Groningen, The Netherlands

Manuscript in preparation

Abstract

Spinocerebellar ataxia type 23 (SCA23) is caused by missense mutations in the prodynorphin, *PDYN,* gene, which is the precursor protein for the opioid neuropeptides α-neoendorphin, Dynorphin (Dyn) A, and Dyn B. Dyn A acts on opioid receptors to induce pain reduction in the spinal cord, but its cerebellar function is largely unknown. Increase in Dyn A concentrations or prolonged exposure is neurotoxic mediated through non-opioid mechanisms as these deleterious effects cannot be blocked by opioid antagonists. Dyn A peptides bind *N*-methyl-$_D$-aspartate receptors (NMDARs) potentiating glutamate currents, that may cause excitotoxicity. We previously showed that SCA23 mutations cause elevated Dyn A peptide levels and enhance the intrinsic toxicity of wild type Dyn A. In the present study, we investigated the disease mechanisms underlying SCA23-mutant Dyn A peptides. SCA23 mutations disrupted the secondary structure of Dyn A, fully ablating the α-helical structure, similarly to Dyn A-Y1del (2-17), that correlated with decreased κ-opioid receptor affinity, altered peptide degradation and aggregation. Additionally, the mutant peptides induced NMDAR-mediated cell death in differentiated NG108 cells. We propose that the pathology of SCA23 results from converging mechanisms of loss of opioid signaling and NMDA-induced excitotoxicity.

Introduction

Missense mutations in prodynorphin (*PDYN*) gene cause spinocerebellar ataxia type 23 (SCA23), in which patients suffer from relatively slowly progressive motor coordination impairment due to Purkinje cells death in the cerebellum [1, 2]. PDYN is the precursor protein for opioid neuropeptides α-neoendorphin, Dynorphin (Dyn) A, and Dyn B, which are inhibitory neurotransmitters and function in pain processing and addition control [3]. Dyn A peptide acts on opioid receptors and preferentially binds to κ-opioid receptor (KOR) [3]. While Dyn A role has been extensively studied regarding the pain and addiction, the cerebellar function of this peptide, by which SCA23-mutant Dyn A can mediate ataxic phenotype, is largely unknown.

There is growing evidence that pathophysiological changes in Dyn A production, concentration or processing can contribute to maladaptive neuroplastic changes and neurodegeneration (reviewed in [4]). The deleterious effect of Dyn A seen in secondary neuronal injury is mediated through non-opioid mechanisms as it cannot be blocked by opioid antagonists [5]. The finding that MK801, specific blocker of *N*-methyl-$_D$-aspartate receptor (NMDAR) is able to prevent negative consequences of Dyn A elevated concentrations or prolonged exposure indicates that non-opioid mechanisms of Dyn A are mediated through this receptor [6]. Dyn A peptides were shown to bind NMDARs and potentiate their glutamate currents [7]. Dyn A peptides may have dichotomous actions as the peptide can be neuroprotective acting via opioid receptors and can be neurotoxic through NMDARs [6]. The neuroprotection mediated through Dyn A interaction with KOR might be the consequenc of reduced intracellular calcium concentrations upon KOR activation by Dyn A [8, 9]. Whereas neurodegenerative actions of Dyn A via NMDAR activation probably involve a pathological intracellular calcium increase in neurons leading to excitotoxicity.

Dyn A, a 17-aminoacid-long peptide, displays a stable N-terminal α-helical structure, which spreads from Phe^4 to Pro^{10}, and C-terminal β-turn, formed by aminoacids Trp^{14} to Gln^{17} [10]. However, Dyn A structurize only in the membrane environment and in the aquaous solution it is unfolded [11]. Moreover, structure-activity analyses indicated that Tyr^1, Leu^5 and Arg^6-Lys^{11} are important for KOR binding [12, 13].

Previously, we showed that three SCA23 mutations located in Dyn A-coding region lead to enhanced levels of the Dyn A peptide in transiently transfected cells (with precursor PDYN cDNA). Additionally, two of these mutations, R6W and R9C, increased the intrinsic toxicity of wild type Dyn A in cultured striatal neurons, whereas in contrast L5S did not [2], suggesting different underlying mechanism for the various mutant Dyn A peptides.

Here, we aimed to unravel the disease mechanisms underlying the SCA23-mutant Dyn A peptides L5S, R6W, and R9W. We showed that all SCA23-mutant Dyn A peptides displayed altered secondary structures that correlated with lower peptide binding efficiencies to KOR. Dyna A-R6W and Dyn A-R9W peptides were more resistant to degradation, whereas in contrast Dyn A-L5S was very rapidly degraded. This finding coincided with increased aggregation kinetics for the Dyn A-R6W and Dyn A-R9C peptides, that was absent in Dyn A-L5S. Notably, all peptides exhibited NMDAR-mediated neurotoxic effects leading to enhanced NG108 cell death. We hypothesize that the Dyn A-R6W and Dyn A-R9C peptides display a toxic gain of function, whereas loss-of-function may underlie Dyn A-L5S pathology. Moreover, the pathology of SCA23 may result from a convergence of two mechanisms: loss of opioid signaling-mediated neuroprotection and NMDAR activation leading to excitotoxicity.

Material and Methods

Modeling of the secondary structure and interaction of Dyn A with POPC membranes

The interaction of Dyn A mutants with palmitoyl-oleyl phosphatidylcholine (POPC) membranes was simulated using the GROMACS software package version 4.5, the GROMOS43A1 force field, and parameters for the phospholipids adapted from Berger *et al*. [14, 15]. Simulations were carried out for at least 200 ns. The systems were composed by a single peptide molecule, a 104 POPC membrane patch, 3428 water molecules and either 3 or 4 countering chloride ions, depending on the formal charge of the mutant. Prior to production runs, the system with the wild type (wt) Dyn A peptide was equilibrated for 5 µs using the MARTINI coarse-grain force field [16]. Mutations were also performed at the (more robust) coarse-grain level, after which the system was again briefly equilibrated for 2 ns before being converted to a fine grain representation following a procedure described elsewhere [17]. At the fine grain level the systems were energy-minimized and then equilibrated for 0.5 ns at a 0.5 fs time step and pressure coupling time of 0.5 ps, and then again for 1 ns at 1 fs time step with a pressure coupling time of 0.05 ps. Secondary structure analysis was done using the DSSP tool (CMBI version of April 4, 2000; [18]). Visualization was done using the VMD package [19].

Peptide synthesis

SCA23-mutant and wt Dyn A peptides were synthesized by solid phase strategies using an automated multiple peptide synthesizer (SyroII, MultiSyntech). For the quenched Dyn A peptides, a Cystein was inserted to Dyn A sequence in between two Glycines at the N-terminus and a fluorescein (Fl) was introduced by covalent coupling of fluorescein-5-iodoacetamide (5-IAF, Fluka) to the Cysteine. Quenching of Fl fluorescence was performed by a dabcyl group that had been introduced in the peptide by coupling of Fmoc-L-Lys (Dabcyl)-OH (NeoMPS). Peptides were purified by size exclusion chromatography and Reversed phase (RP)-HPLC (>95% pure) and showed the expected molecular mass as determined by mass spectrometry (Maldi Tof, Voyager, ABI). Peptides were dissolved in 100% 1,1,1,3,3,3-hexafluoro-2-propanol (HFIP; Sigma), aliquoted, dried under vacuum in a SpeedVac (Eppendorf) and stored at -20°C.

KOR competitive binding assay

The competitive binding assay of Dyn A peptides to KOR was performed as described before [20]. Briefly, Dyn A binding was assessed in the presence of radioactively labeled U50,488 in cerebellar membrane fractions using different concentrations of Dyn A peptide. Unlabeled U50,488 was used to decrease unspecific binding and generate standards. Bound radioactivity was counted on a Wallac Beta-plate Liquid Scintillation Counter (Piscataway, NJ). Non-linear regression analysis of the competition curves fitted best by using a two sites analysis, of which the high affinity site represents the KOR.

Quenched Dyn A peptide degradation assay

The degradation assay was performed as described before [21]. In short, HFIP-treated aliquots of Dyn A peptides

were resuspended in DMSO followed by sonication for 10 minutes, immediately before addition to 5 µg protein from the mouse cerebellum extracts or human liquor in KMH buffer (110 mM KAc, 2 mM MgAc and 20 mM Hepes-KOH, pH 7.2) to a total volume of 50 µl. Degradation of the peptide was analyzed at 37°C using a fluorescence plate reader (FLUOstar OPTIMA, BMG Labtec.).

Electron microscopy

Dyn A peptide (150 ng/ml in water) preparations were adsorbed on 300-mesh formar/copper grids for 2 minutes and excess of fluid was filtered off. Upon staining with 2.5% uranyl acetate for 2 minutes, grids were analyzed with a transmission electron microscope (Tecnai-12 G2, FEI).

Cell culturing

Neuroblastoma-glioma NG108 cells were cultured in high-glucose Dulbecco's modified Eagle's medium (DMEM, Gibco, Bleiswijk, the Netherlands) implemented with 10% fetal bovine serum (FBS) and 5% penicillin (100 U/ml) and streptomycin (100 mg/ml). The cultures were maintained at 37°C in an atmosphere of 5% CO_2. The cells were detached using trypsinization and same number of cells were plated in 96-well plates. The differentiation was conducted by addition of 50 µM 3-Isobutyl-1-methylxanthine (IBMX, Sigma) and 100 µM 5'-N-ethyl-carboxamide-adenosine (NECA, Sigma) in the low-FBS medium for at least 5 days, until long protrusions were seen.

Peptide-induced toxicity assay

The differentiated NG108 cells were cultured in 96-well plates in presence of propidium iodide (PI; 5 µg/ml) and stimulated with various Dyn A peptides at different concentrations. Cell death was measured by following enhanced fluorescence of PI upon its incorporation into nuclei of dying cells. The PI fluorescence was monitored for 72 hours after addition of Dyn A peptides using a fluorescence plate reader (Synergy HT, BioTEK). As negative controls NG108 cells without peptide stimulation were used, and cells stimulated with 0.25% Triton X-100, 15 mM EDTA, or poly-D-Lysine (all purchased from Sigma) were used as positive controls.

Statistical analysis

All data are expressed as the mean of at least three independent experiments. The statistical significance were tested using unpaired Student's *t*-test.

Results

SCA23 mutations interfere with the secondary structure of Dyn A peptides

To gain insight into the mechanism underlying SCA23 mutations in Dyn A-coding region, we first examined the impact of the L5S, R6W, and R9C mutations on the secondary structure of Dyn A by computational modeling of these mutant peptides in the presence of membrane. The simulation was carried out for at least 200 ns enabling us to follow the stability of peptide secondary structures in time. Our data confirmed the N-terminal α-helix in

the secondary structure of Dyn A-wt upon interaction with POPC membranes (**Fig. 1A, Suppl. Fig. 1A**), validating our modeling approach. The Dyn A-wt secondary structure was stable across the whole simulation. All mutations resulted in a loss of α-helical structures in the Dyn A peptides (**Fig. 1 B-D, Suppl. Fig. 1B-D**), suggesting that these aminoacids are important for the α-helix formation. Moreover, Dyn A-R6W showed a relatively stable β-bridge between aminoacids Arg^{9} and Lys^{13} in its secondary structure (**Fig. 1C, Suppl. Fig. 1C**). Additionally, a membrane in-depth profile of each peptide was generated upon interaction with POPC membranes that showed no marked differences between the SCA23 mutants and wt profiles, reflecting only little alteration in positioning of the peptides in the membrane (**Fig. 2**). Altogether, these data show that SCA23 mutations disrupt the native conformation of Dyn A peptides, but do not markedly change the positioning in the membrane.

SCA23-mutant Dyn A peptides exhibit reduced κ-opioid receptor (KOR) affinities

Since Tyr^{1}, Leu^{5} and Arg^{6}-Lys^{11} are important for KOR binding as indicated by structure-activity analyses of Dyn A peptide [12, 13], we hypothesized that SCA23-mutant Dyn A peptides may exhibit decreased receptor affinity. To test this hypothesis, we analyzed the κ-opioid receptor binding affinities of the various mutant Dyn A peptides *in vitro* in a competitive binding assay using the selective KOR antagonist (U50,488) as a competitor (**Fig. 3**). The competition analysis showed that all mutant Dyn A peptides have 5-10 times lower KOR affinity than Dyn A-wt (IC_{50} values: L5S: 2,59 nM, R6W: 4.91 nM, and R9C: 3.12 nM versus wt: 0,63 nM, respectively), indicating that partial loss of KOR-mediated neuroprotection might contribute to SCA23.

As the SCA23-mutant Dyn A peptides clearly displayed lower KOR affinities and loss of α-helical secondary structure, we hypothesized that the formation of the α-helix in Dyn A peptide may be important for KOR interaction. Therefore, we modeled the secondary structure of Dyn A-Y1del, lacking Tyr^{1}, that is known to have no affinity for opioid receptors, including KOR, and exhibit only non-opioid functions [22]. Our results showed that Dyn A-Y1del also did not display the α-helical structure at the N-terminus (**Fig. 4**), similarly as was observed for the various SCA23-mutant Dyn A peptides (**Fig. 1, Suppl. Fig. 1**). This indicates that the α-helical structure in Dyn A is important for KOR interaction, but it is not the sole determinant of this interaction as the SCA23-mutant peptides still showed quite some KOR interaction. Additionally, the membrane positioning of the Dyn A-Y1del peptide also did not change much compared to Dyn A-wt, suggesting that other mechanisms must underlie the complete loss of KOR interaction for this peptide (**Suppl. Fig. 2**).

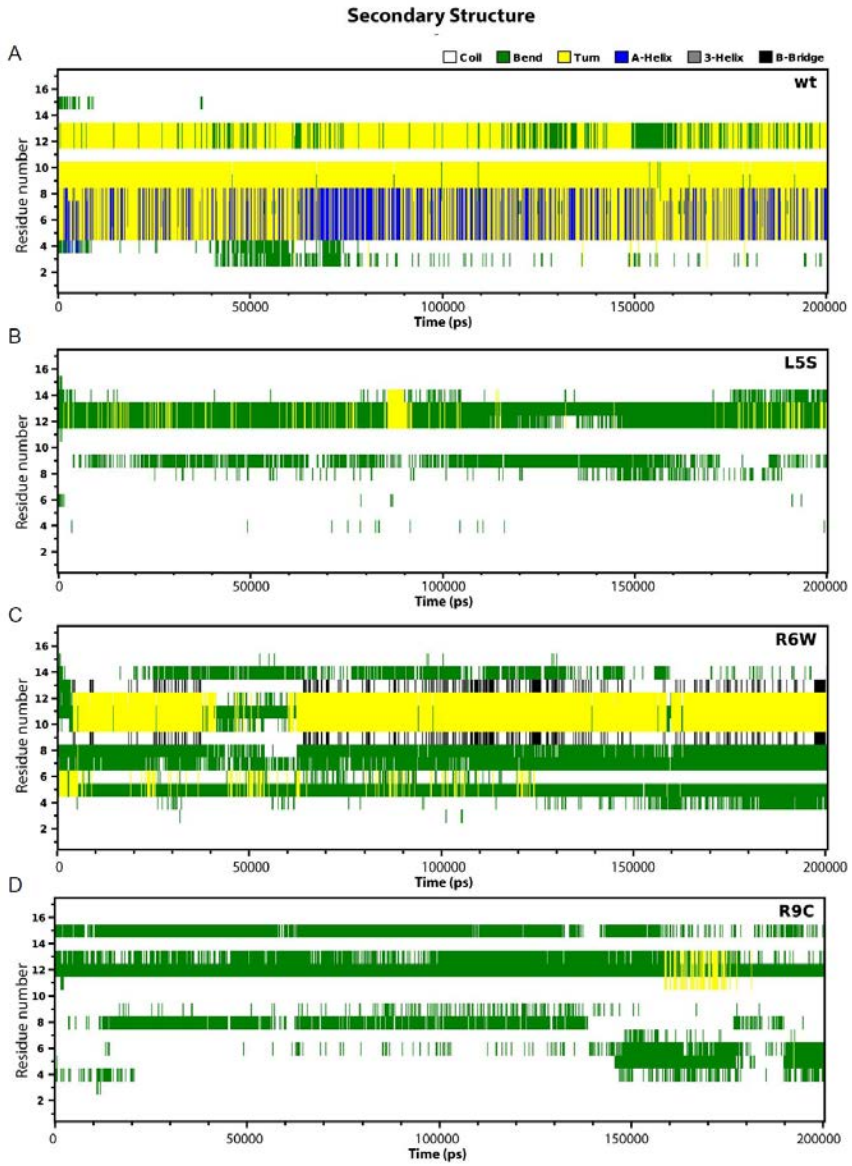

Fig. 1 Secondary structures of SCA23-mutant Dyn A peptides upon interaction with POPC membranes over time.

(**A**) Dyn A-wt exhibits α-helical conformation between aminoacids 4 and 9, that is relatively stable in time. (**B-D**) Conversely, the mutations L5S, R6W, and R9C caused loss of the α-helix and the resulting mutant structures were overall extended, though β-bridge stabilization was occasionally observed in one case (**C**).

The graphs show adopted secondary structures per aminoacid residue (Y axis) in time (X axis). Computational modeling of various Dyn A peptides interacting with a POPC membrane was conducted for at least 200 ns after the different mutations were performed.

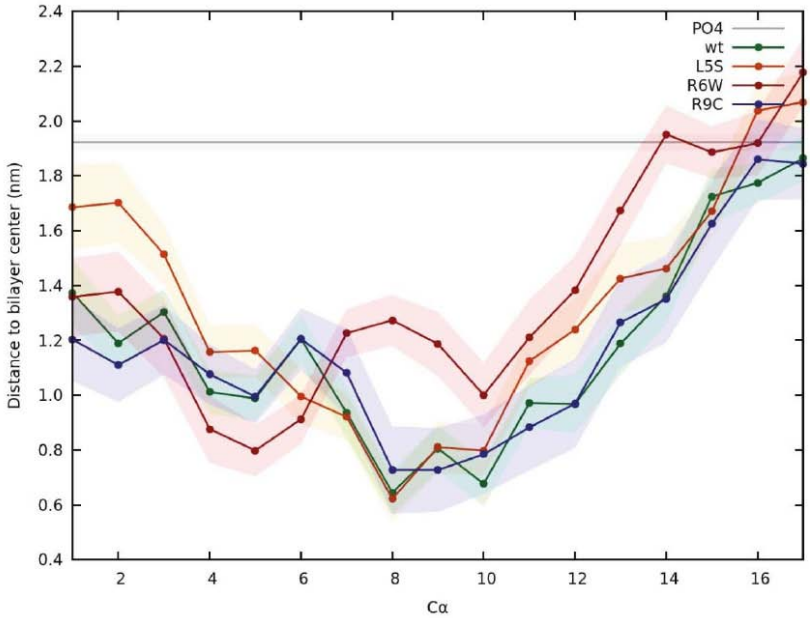

Fig. 2 SCA23-mutant Dyn A peptides position in membrane.

The graph represents averaged distance of Cα carbons of each residue of wild type and SCA23-mutant Dyn A peptides to the center of the POPC bilayer. The simulation was carried out for 80 ns. The gray line indicates the average depth of the phosphate groups. The insertion depth of SCA23-mutant peptides seems to be little affected during the studied time scale.

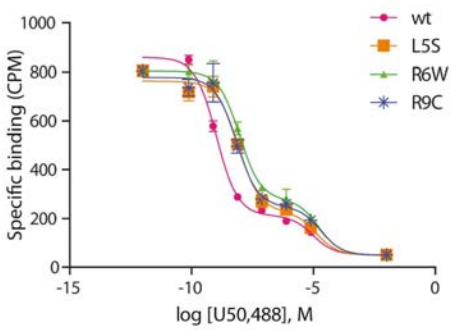

Table 1: Binding affinities of various Dyn A peptides for kappa

Sample	Ki	nM	STD
Dyn A-wt	6,30E-10	0,63	2,72E-10
Dyn A-L5S	2,58E-09	2,59	1,10E-09
Dyn A-R6W	4,91E-09	4,91	1,00E-09
Dyn A-R9C	3,12E-09	3,12	1,2E-09

Fig. 3 Binding affinity of SCA23-mutant Dyn A peptides to KOR.

The quantification graph of competitive binding assays for various Dyn A peptides and the highly selective KOR antagonist U52,488. All SCA23-mutant Dyn A peptides exhibited lower potential to displace the antagonist from the high affinity binding site compared to Dyn A-wt. Data is shown as a mean of four independent experiments (± SD). The table shows binding affinities (Ki) of the wild type and SCA23-mutant Dyn A peptides and the half maximal inhibitory concentration in nM.

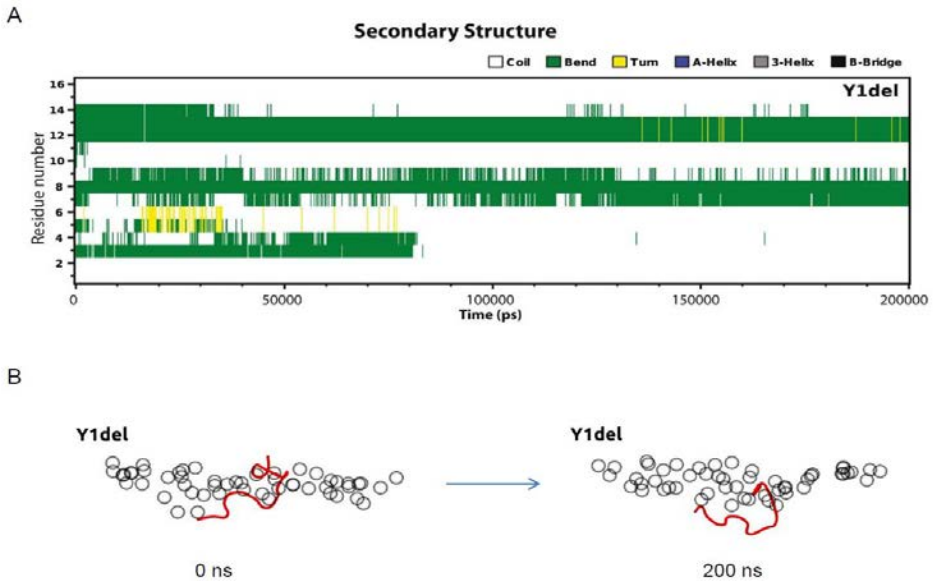

Fig. 4

(**A-B**) Deletion of the first tyrosine in Dyn A peptide also leads to loss of the α-helical structure. For complete legend see **Fig. 1** and **Suppl. Fig. 1**.

SCA23 mutations affect the degradation efficiency of Dyn A peptides

We previously observed highly elevated SCA23-mutant Dyn A levels *in vitro* [2], and since SCA23 mutations disrupt the native conformation of Dyn A peptide, we hypothesized that alterations in the secondary structure of the SCA23-mutant Dyn A peptides affect proper peptide degradation. To test this idea, we determined breakdown of the mutant Dyn A peptides in mouse cerebellar extracts and human liquor in real time. For this purpose, we generated Dyn A peptides with a small fluorescent group at the N-terminus and a quenching dabcyl group introduced to medial/C-terminal part of Dyn A peptides [23]. The quenched Dyn A peptides become fluorescent upon separation of the fluorophore and quencher due to degradation of the peptide. Upon addition of the peptides to cerebellar extracts, a marked increase in fluorescence signal for Dyn A-wt and Dyn A-L5S was detected in time, but in contrast almost no fluorescence signal was observed for Dyn A-R6W and Dyn A-R9C (**Fig. 5A and C**). Notably, Dyn A-L5S was much more rapidly degraded than Dyn A-wt.

To further study the breakdown of the SCA23-mutant Dyn A peptides, we also determined their stability in human liquor, which contains many metabolic enzymes including hydrolases and peptidases. In these conditions, the degradation of Dyn A-wt and Dyn A-L5S was less rapid than in cerebellar extract, but similar profiles were generated and again Dyn A-L5S exhibited elevated fluorescence signals, and once more strongly reduced fluorescence signals were observed for Dyn A-R6W and Dyn A-R9C (**Fig. 5B and D**).

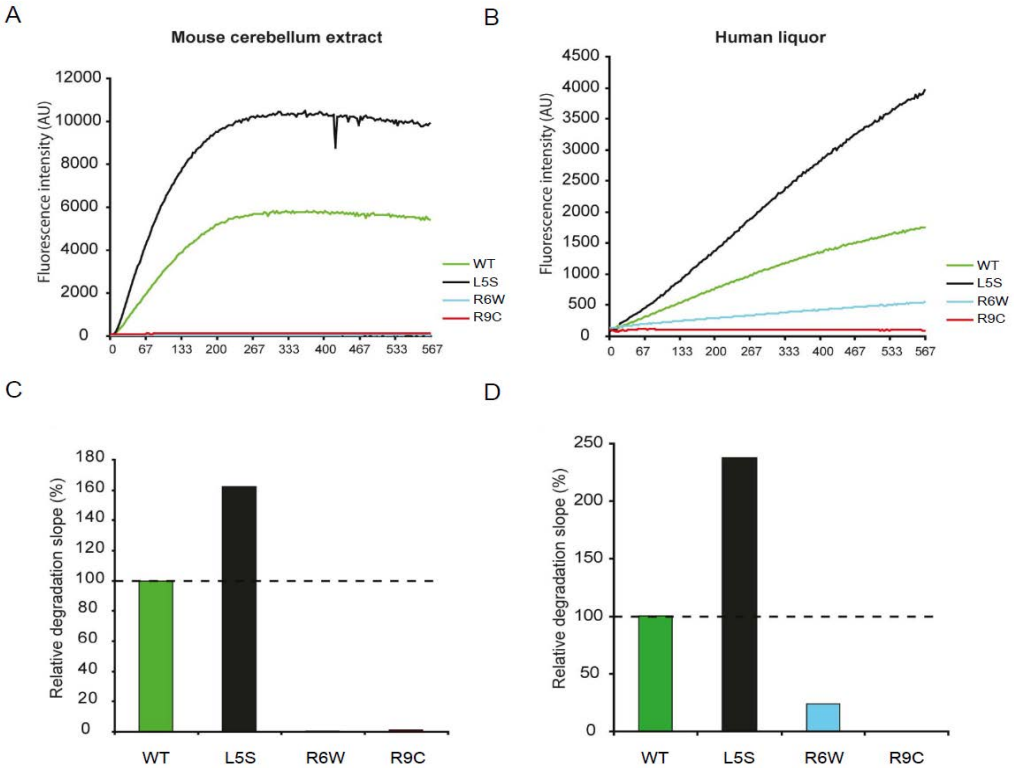

Fig. 5 Degradation rate of SCA23-mutant Dyn A peptides.

(**A-B**) Degradation curves of wild type and SCA23-mutant Dyn A peptides in time as measured by the increase in fluorescence intensity upon separation of the quencher and fluorophore. The assay was carried out in mouse cerebellar extract (**A**) or in human liquor (**B**) for 200 cycles of 5 minutes. (**C-D**) Quantification of the degradation slope of SCA23-mutant Dyn A peptides relative to Dyn A-wt (100%) in the lysates of mouse cerebellar tissue (**C**) and human liquor (**D**). The data is expressed as a mean of three independent experiments.

These data clearly show that the R6W and R9C mutations impair proper Dyn A degradation, whereas L5S seems to increase Dyn A breakdown. The degradation of Dyn A-wt and Dyn A-L5S peptides were more efficient in cerebellar extract compared to human liquor, suggesing the presence of cerebellar-specific peptidases that can degrade Dyn A with high efficiency.

As we observed higher stability of Dyn A-R6W and Dyn A-R9C, we wondered if these mutants could assemble into oligomeric structures that may decrease their degradation rate. Therefore, we investigated the *in vitro* oligomerization of the SCA23-mutant Dyn A peptides *in vitro* at various time points by electron microscopy. Dyn A-wt formed some oligomeric structures after 4 hours of incubation in aquaous solution (**Fig. 6**), but a marked increase in oligomerization was observed for Dyn A-R6W and Dyn A-R9C compared to Dyn A-wt, but not for Dyn A-L5S. All SCA23-mutant peptides assembled into oligomeric structures faster than Dyn A-wt .

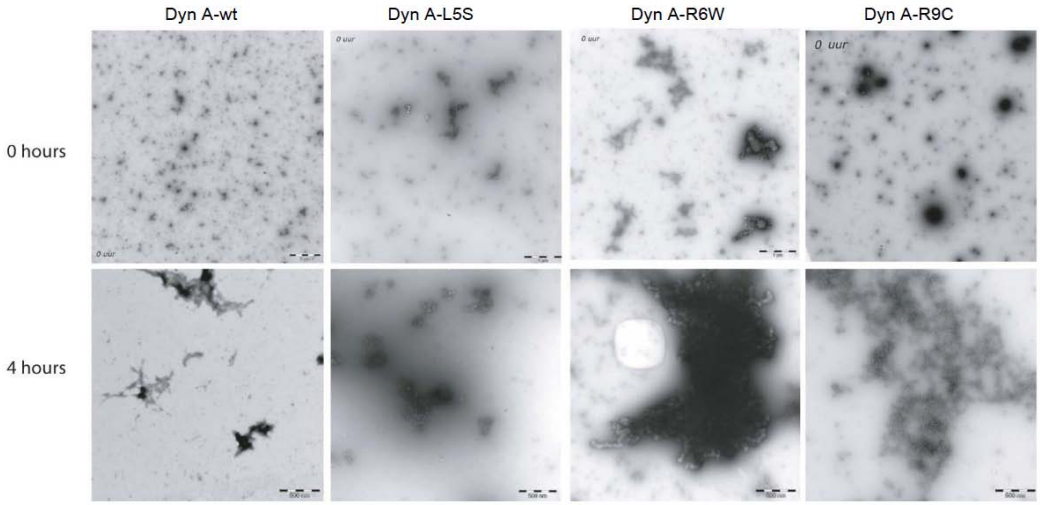

Fig. 6 Oligomerization of SCA23-mutant Dyn A peptides in time.

Electron microscopy images showing increased oligomerization of Dyn A-R6W and Dyn A-R9C comparing to Dyn A-wt at 37°C in time (0 and 4 hours), whereas in contrast no large oligomeric structures were observed for Dyn A-wt and Dyn A-L5S. Scale bars are 1 µm (upper panel; 0 hours) and 500 nm (lower panel; 4 hours).

Altogether, these data indicate that the R6W and R9C mutations increase the half-life of Dyn A, that could cause enhanced oligomerization. The very rapid degradation of L5S suggests a loss of this particular peptide and indicates that not all SCA23 mutations display the same underlying disease mechanism.

SCA23-mutant Dyn A exhibit increased neurotoxic effects via the NMDAR

Recent work has shown that Dyn A non-covalently binds NMDAR and can potentiate its excitatory currents [7]. Additionally, high concentrations or prolonged exposure of Dyn A has been shown to cause neuronal cell death via non-opioid mechanisms [5, 6]. Given the elevated Dyn A levels in SCA23 pathology, we hypothesized that the mutant peptides may induce neurotoxicity through NMDAR activation leading to enhanced cell death.

To test this hypothesis, the various Dyn A peptides were added to differentiated NG108 cells and cultured with propidium iodide (PI; 5 µg/mL), enabling cell death measurements in time. In this assay, Dyn A-wt was not toxic for the differentiated NG108 cells, but SCA23-mutant Dyn A peptides showed marked concentration-dependent toxicity reflected by increased cell death (**Fig. 7A and B**). Forty-eight hours after addition of 1 µM peptide, Dyn A-L5S and Dyn A-R9C caused a 2-fold increase in cell death (2.3 ± 0.10 and 1.97 ± 0.76 versus 1.04 ± 0.10) and Dyn A-R6W a 9-fold (8.9 ± 0.38) increase compared to Dyn A-wt (**Fig. 7A**). This effect was even more pronounced at 72 hours after cell exposure to peptides. The toxicity of all mutant Dyn A peptides was concentration-dependent as 100 nM peptide was not toxic to differentiated NG108 cells in time and 10 µM Dyn A peptides caused more pronounced cell death than 1 µM (**Fig. 7B**).

A

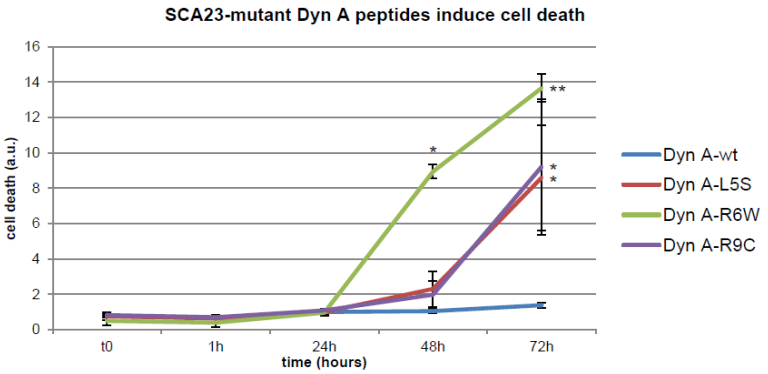

B

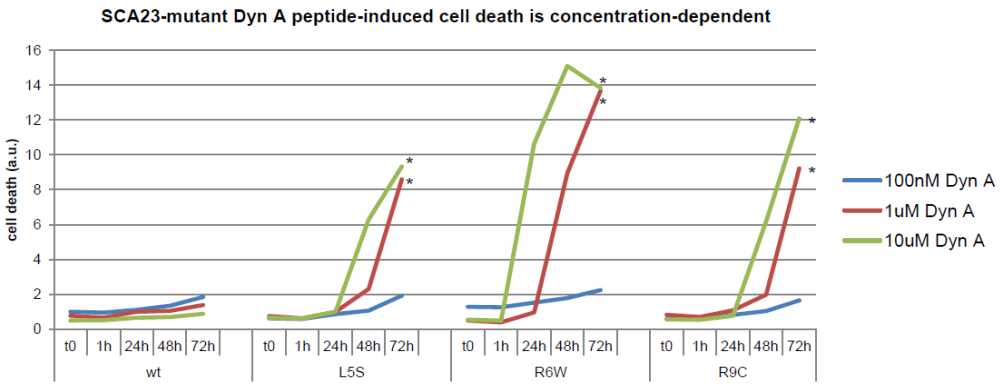

Fig. 7 Toxicity induced by SCA23-mutant Dyn A peptides.

(**A-B**) Quantification of cell death og differentiated NG108 cells in the presence of various Dyn A peptides in time. The analysis showed high toxicity of SCA23-mutant peptides compared to Dyn A-wt after 48h and 72h after addition of peptides. (**A**) Cell death induced by various Dyn A peptides (1uM). Dyn A-R6W showed the highest toxicity. The data is presented as mean ± SEM. Significant differences (unpaired *t*-test) are indicated as * $p < 0.05$, ** $p < 0.005$ (**B**) Induction of cell death by SCA23-mutant Dyn A is concentration-dependent. * $p < 0.005$.

To test whether mutant Dyn A caused neurotoxicity and cell death via NMDAR activation, cell death was measure in differentiated NG108 cells upon treatment with (1μM) wt or SCA23-mutant Dyn A peptides and NMDA (50 μM). The specific stimulation of NMDARs by NMDA caused more pronounced cell death in presence of SCA23-mutant peptides than peptides treatment alone , especially in case of Dyn A-R6W, and this effect was completely blocked by the NMDAR antagonist, MK801 (**Fig. 8A and B**). MK801 also partially blocked SCA23-mutant peptide induced toxicity as cells treated with MK801 (added 24 hours after peptide) showed decreased PI fluorescence than cells treated with peptide only (**Fig 8B**). These data confirms that Dyn A peptides exhibit neurotoxicity through NMDAR activation as it could be blocked by MK801, indicating that excitotoxicity may underlie the Dyn A-induced pathology in SCA23.

Additionally, we stimulated NMDARs with the co-agonists, Glycine or D-Serine, in the presence of 100 nM (non-toxic concentrations) Dyn A peptide. High concentrations (10 mM) of these co-agonists are able to

activate different subunits of NMDAR [24], D-Ser (like NMDA) acts mainly on synaptic NMDARs (containing NR2A), and Glycine on extra-synaptic NMDARs (containing NR2B) [25]. Only 10 mM D-Serine in the presence of mutant Dyn A resulted in markedly increased cell death compared to Glycine activation. This indicates that synaptic rather than extra-synaptic NMDARs contribute to SCA23 neurotoxicity (Fig. 8C).

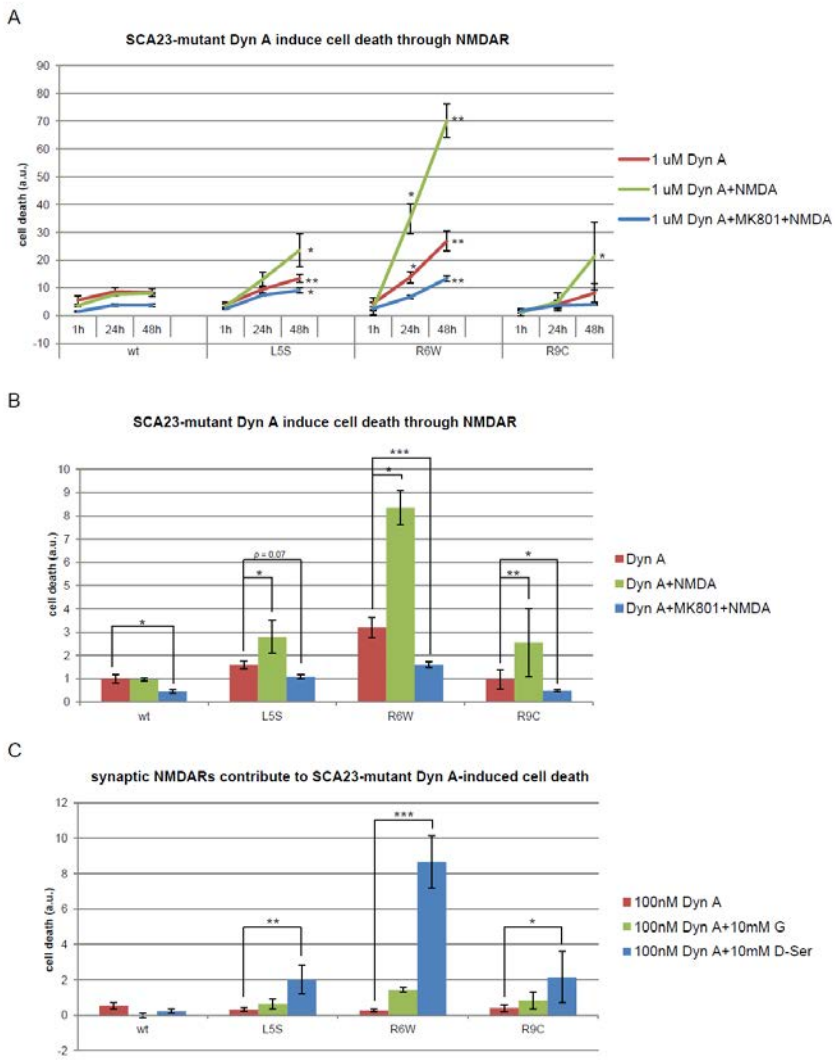

Fig. 8 Toxic effects of SCA23-mutant Dyn A mediated through NMDAR pathway. (**A-B**) Time-course of the cell death of differentiated NG108 cells cultured with PI in the presence of various 1 μM Dyn A peptides, stimulated with 50 μM NMDA with or without specific NMDAR antagonist, MK801 (10 μM). Co-stimulation with SCA23-mutant peptides and NMDA led to a significant increase in cell death, that could be completely blocked by the addition of MK801. Again, Dyn A-R6W showed the highest toxicity. MK801 was added 20 minutes before NMDA to effectively block NMDA receptors. Significant differences (unpaired *t*-test) are indicated as (**A**) * $p < 0.05$, ** $p < 0.005$, between SCA23-mutant peptides and Dyn A-wt, (**B**) * $p < 0.05$, ** $p < 0.01$, *** $p < 0.005$. (**C**) Quantification of toxicity caused by NMDARs stimulation in the presence of the various Dyn A peptides at non-toxic concentrations (100 nM) in time. NMDAR stimulation was conducted at high concentration of co-agonists (10 mM), by which Glycine targets extra-synaptic NMDARs and D-Serine – synaptic NMDARs. Significant differences (unpaired *t*-test) are indicated as * $p < 0.05$, ** $p < 0.01$, *** $p < 0.005$. G – Glycine, D-Ser – D-Serine.
The data is presented as mean ± SEM. Stimulation with NMDA or Glycine and D-Serine was conducted 24 hours after addition of Dyn A peptides.

To study the effect of SCA23-mutant Dyn A peptides on opioid signaling-mediated neuroprotection, we treated differentiated NG108 cells with 100 nM Dyn A peptides (non-toxic concentration) and blocked opioid or NMDAR pathways using specific antagonists, naloxone and MK801 (respectively), and followed cell death in time. Interestingly, after 72 hours of naloxone treatment markedly decreased cell viability in presence of 100 nM mutant peptides was observed, which was the most pronounced for Dyn A-R6W (15.52 ± 0.92 versus 0.00 ± 0.08 for Dyn A-wt; **Fig. 9**). These findings further support the hypothesis that the opioid pathway may play a crucial role in modulating the SCA23 pathology via neuroprotection.

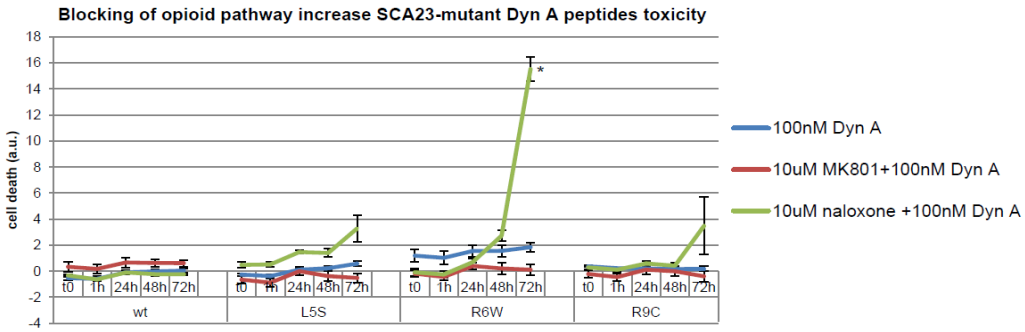

Fig. 9 Toxicity of SCA23-mutant Dyn A peptides during inhibition of opioid pathway.
The quantification graph shows the cell death of differentiated NG108 cells cultured with PI induced by 10 μM naloxone (antagonist of opioid receptors) and by 10 μM MK801 in the presense of in non-toxic Dyn A concentrations (100 nM). Naloxone clearly induced strong cell death after 4 to 72 hours of stimulation. The strongest effect was observed in the presence of Dyn A-R6W. Naloxone and MK801 were added 20 minutes before peptides. The data is presented as mean ± SEM.

Discussion and conclusions

In the present study we showed that SCA23 mutations located in Dyn A disrupt the peptide secondary structure that is important for KOR binding, and lead to non-opioid neurotoxic actions of Dyn A via the NMDAR.

All SCA23 mutations disrupted the formation of the N-terminal α-helix, similarly to Dyn A-Y1del mutant, suggesting that these aminoacids take part in α-helix formation. This loss of helical structure correleted with reduced KOR affinity. Additionally, Tyr^1, Leu^5, Arg^6, and Arg^9 were already shown to be important for KOR binding in structure activity analyses [12, 13]. Thus, the α-helix at the N-terminus is important for KOR binding, but it cannot be the sole determinant for proper KOR interaction, as the SCA23-mutant Dyn A peptides were still able to bind to KOR.

Furthermore, the data obtained by us support the hypothesis of opioid signaling neuroprotection, as SCA23-mutant Dyn A peptides showed lower affinity to KOR and blocking of opioid signaling in differentiated NG108 cells markedly increased toxicity of SCA23-mutant Dyn A peptides. These data indicate that partial loss of neuroprotection through opioid signaling may contribute to the pathogenesis of SCA23.

A clear hallmark of SCA23 in our previous work was the increase in mutant Dyn A levels [2]. This could be the consequence of slower degradation of the Arginine-mutant Dyn A peptides, R6W and R9C, that also

formed stable oligomeric structures *in vitro*. Stable β-bridge in Dyn A-R6W secondary structure or introduced Cysteine in Dyn A-R9C, which may form disulfide bonds, might contribute to increased oligomerization seen for these mutants. Yet, physiological relevance of this findings is hard to assess, as the oligomerization assays were performed in aquaous solution, without presence of membranes. It, however, may suggest that Arg-mutant Dyn A peptides may form additional interactions, either accumulating in higher molecular weight species or interacting with unknown partners.

We proved that the SCA23-mutant peptides are toxic in our cell model system in a concentration-dependent manner and confirmed that Dyn A-R6W is the most pathogenic peptide, as seen before [2]. Moreover, the mutant Dyn A toxicity was mediated through NMDAR, as neuronal cell death could be blocked with NMDAR-specific antagonist. Additionally, our results suggest that synaptic NMDARs contribute more to toxicity than extra-synaptic receptors. Still, further work need to show the direct interaction between Dyn A and NMDARs of various composition or that blocking of the Dyn a toxicity can be achieved by the use of subunit-specific antagonists. Taking into account that Dyn A can potentiate glutamate-evoked currents of NMDARs [7] and the increased cell death upon NMDA stimulation in presence of SCA23-mutant Dyn A peptides observed in this study, we suggest that Dyn A toxicity in SCA23 is caused by excitotoxic mechanism through NMDAR.

Notably, Dyn A-wt did not display toxic effects in differentated NG108 cells. Maybe these immortalized cells are more resistant to Dyn A peptide-induced toxicity than primary neuronal cultures as has been used before, and higher concentrations or longer exposure of Dyn A-wt may be needed to observe the cell death. However, we cannot exclude that Dyn A toxicity in SCA23 is specific for particular populations of neurons, and different effects would be seen for striatal neurons and neuronal-like cell lines, and physiologically relevant Purkinje cells.

We provide further evidence that the Arginine mutations in Dyn A (R6W and R9C) have different mechanism of pathology than L5S. The Arginine-mutant Dyn A peptides were more resistant to degradation and formed oligomeric structures compared to DynA-wt and L5S, supporting our hypothesis that these mutations exhibit gain-of-function mechanism. Dyn A-L5S was rapidly degraded, and did not oligomerize that fast. Thus in case of L5S mutations, loss of Dyn A function rather than toxic gain of function might underlie the disease pathology, which is in line with mild ataxic phenotype that started at the age of 73, compared to the R6W and R9C mutations that were correlated with a more severe phenotype and younger age of onset [2].

In conclusion, we showed that SCA23-mutant Dyn A peptides have disrupted secondary structures, which may lead to decreased affinity to KOR and loss of opioid receptors-mediated neuroprotection. The mutant peptides exhibited marked toxicity through NMDAR pathway, probably by excitotoxic actions of SCA23-mutant Dyn A peptides on these receptors.

Acknowledgements

This work was supported by Rosalind Franklin Fellowship and Jan Kornelius de Cock Stichting, from the University Medical Center Groningen, University of Groningen. We thank Marcel Raspe for his help with the Dyn A degradation assay.

References

1. Verbeek DS, van de Warrenburg BP, Wesseling P, Pearson PL, Kremer HP, Sinke RJ. Mapping of the SCA23 locus involved in autosomal dominant cerebellar ataxia to chromosome region 20p13-12.3. *Brain* 2004; 127: 2551-2557.
2. Bakalkin G, Watanabe H, Jezierska J et al. Prodynorphin Mutations Cause the Neurodegenerative Disorder Spinocerebellar Ataxia Type 23. *Am J Hum Genet* 2010.
3. Schwarzer C. 30 years of dynorphins--new insights on their functions in neuropsychiatric diseases. *Pharmacol Ther* 2009; 123: 353-370.
4. Hauser KF, Aldrich JV, Anderson KJ et al. Pathobiology of dynorphins in trauma and disease. *Front Biosci* 2005; 10: 216-235.
5. Tan-No K, Cebers G, Yakovleva T et al. Cytotoxic effects of dynorphins through nonopioid intracellular mechanisms. *Exp Cell Res* 2001; 269: 54-63.
6. Hauser KF, Knapp PE, Turbek CS. Structure-activity analysis of dynorphin A toxicity in spinal cord neurons: intrinsic neurotoxicity of dynorphin A and its carboxyl-terminal, nonopioid metabolites. *Exp Neurol* 2001; 168: 78-87.
7. Woods AS, Kaminski R, Oz M et al. Decoy peptides that bind dynorphin noncovalently prevent NMDA receptor-mediated neurotoxicity. *J Proteome Res* 2006; 5: 1017-1023.
8. Przewlocki R, Parsons KL, Sweeney DD et al. Opioid enhancement of calcium oscillations and burst events involving NMDA receptors and L-type calcium channels in cultured hippocampal neurons. *J Neurosci* 1999; 19: 9705-9715.
9. Wagner JJ, Caudle RM, Chavkin C. Kappa-opioids decrease excitatory transmission in the dentate gyrus of the guinea pig hippocampus. *J Neurosci* 1992; 12: 132-141.
10. Sankararamakrishnan R, Weinstein H. Molecular dynamics simulations predict a tilted orientation for the helical region of dynorphin A(1-17) in dimyristoylphosphatidylcholine bilayers. *Biophys J* 2000; 79: 2331-2344.
11. Hassan SA, Mehler EL, Zhang D, Weinstein H. Molecular dynamics simulations of peptides and proteins with a continuum electrostatic model based on screened Coulomb potentials. *Proteins* 2003; 51: 109-125.
12. Lapalu S, Moisand C, Mazarguil H, Cambois G, Mollereau C, Meunier JC. Comparison of the structure-activity relationships of nociceptin and dynorphin A using chimeric peptides. *FEBS Lett* 1997; 417: 333-336.
13. Schlechtingen G, DeHaven RN, Daubert JD et al. Structure-activity relationships of dynorphin a analogues modified in the address sequence. *J Med Chem* 2003; 46: 2104-2109.
14. Pronk S, Pall S, Schulz R et al. GROMACS 4.5: a high-throughput and highly parallel open source molecular simulation toolkit. *Bioinformatics* 2013; 29: 845-854.
15. Berger O, Edholm O, Jahnig F. Molecular dynamics simulations of a fluid bilayer of dipalmitoylphosphatidylcholine at full hydration, constant pressure, and constant temperature. *Biophys J* 1997; 72: 2002-2013.
16. Marrink SJ, Risselada HJ, Yefimov S, Tieleman DP, De Vries AH. The MARTINI force field: coarse grained model for biomolecular simulations. *J Phys Chem B* 2007; 111: 7812-7824.
17. Rzepiela AJ, Schafer LV, Goga N, Risselada HJ, De Vries AH, Marrink SJ. Reconstruction of atomistic details from coarse-grained structures. *J Comput Chem* 2010; 31: 1333-1343.
18. Joosten RP, te Beek TA, Krieger E et al. A series of PDB related databases for everyday needs. *Nucleic Acids Res* 2011; 39: D411-D419.
19. Humphrey W, Dalke A, Schulten K. VMD: visual molecular dynamics. *J Mol Graph* 1996; 14: 33-38.
20. Dooley CT, Ny P, Bidlack JM, Houghten RA. Selective ligands for the mu, delta, and kappa opioid receptors identified from a single mixture based tetrapeptide positional scanning combinatorial library. *J Biol Chem* 1998; 273: 18848-18856.
21. Stargardt A, Reits E. Kinetic studies of cytoplasmic antigen processing and production of MHC class I ligands. *Methods Mol Biol* 2013; 960: 41-51.
22. Walker JM, Moises HC, Coy DH, Baldrighi G, Akil H. Nonopiate effects of dynorphin and des-Tyr-dynorphin. *Science* 1982; 218: 1136-1138.
23. Reits E, Neijssen J, Herberts C et al. A major role for TPPII in trimming proteasomal degradation products for MHC class I antigen presentation.

Immunity 2004; 20: 495-506.

24. Newell DW, Barth A, Ricciardi TN, Malouf AT. Glycine causes increased excitability and neurotoxicity by activation of NMDA receptors in the hippocampus. *Exp Neurol* 1997; 145: 235-244.

25. Papouin T, Ladepeche L, Ruel J et al. Synaptic and extrasynaptic NMDA receptors are gated by different endogenous coagonists. *Cell* 2012; 150: 633-646.

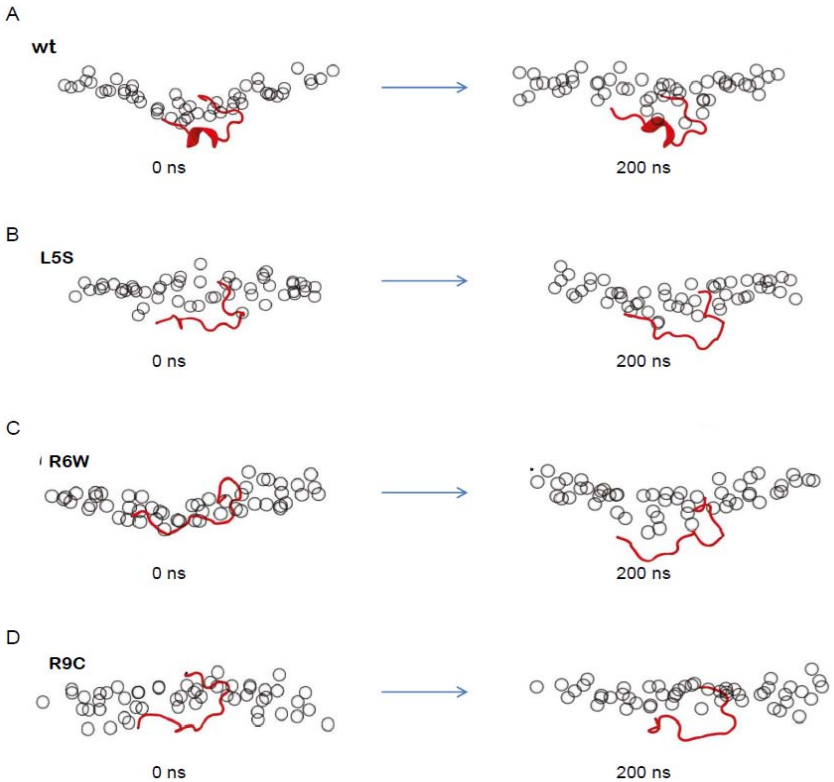

Suppl. Fig. 1 Representative configurations of wild type and SCA23-mutant Dyn A peptides interacting with a POPC membrane at 0ns and 200ns.

The backbone residues of various Dyn A peptides, including (**A**) Dyn A-wt, (**B**) Dyn A-L5S, (**C**) Dyn A-R6W, and (**D**) Dyn A-R9C, are drawn according to a ribbon representation of a DSSP-assigned structure and the top leaflet phosphate groups are depicted as translucid spheres. It is clear that the wild-type peptide retains its secondary structure whereas the rest of the mutants depart from it. However, the insertion profile into the membrane seems hardly affected by the mutations during the studied time scale.

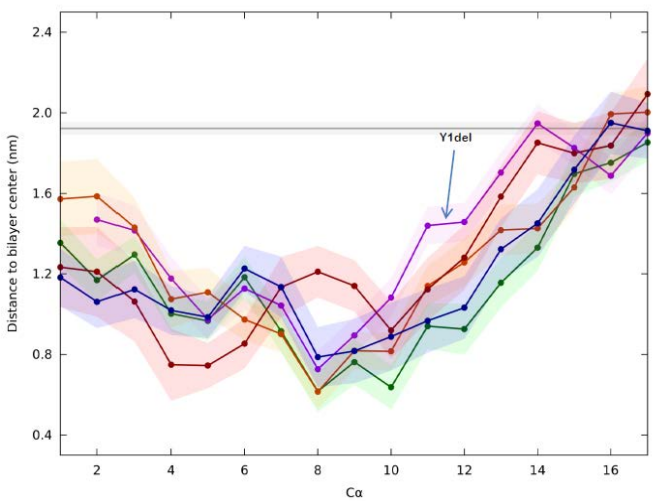

Suppl. Fig. 2 Dyn A-Y1del peptide position at the membrane.

For complete legend see **Fig. 2**.

CHAPTER 8

Conclusions, General Discussion and Future Perspectives

Gene/mutation identification in unknown SCA types

Currently, only 70% of the Dutch SCA families can be diagnosed by mutation analysis of the eight known SCA genes (SCA1-3, 6, 7, 12, 14 and 17) that are relatively more common. The identification of causal mutations and novel genes in the group of families who cannot be diagnosed genetically would not only help to improve the diagnostic possibilities for these patients, but would also provide more insight into the underlying pathological pathways leading to cerebellar neurodegeneration and SCA disease.

The genetic diagnosis of SCA is complicated because there are 32 known SCA types, some of which are very rare, and not all the SCA genes have yet been identified for each reported disease locus. The rarer SCA types, like SCA11, 23, or 28, or the new SCAs for which the prevalence has not yet been established (e.g. SCA19, SCA36), are not usually included in the diagnostic testing due to the relatively high cost of screening and the low probability of identifying mutations. One could also ask if it is really worth including the rare SCA types in the DNA diagnostic tests. It would be preferable to have a tool with lower screening costs that could test every SCA gene, independent of the SCA type frequency. The best alternative would be to generate a custom-made capturing array that would include all the known SCA genes, followed by high-throughput sequencing (next-generation sequencing (NGS) approach). With the falling cost of NGS, this method is now affordable and has already proven useful for diagnosing cardiomyopathies [1]. However, NGS data analysis can be difficult for dominant disorders, as the variants that occur in one allele are relatively common in the genome. Nonetheless, it can also be successful, as shown in **Chapter 3** and [2, 3], especially when using a family-based NGS approach in which the sequencing results can be validated by studying co-segregation of the phenotype with the variants identified in the family. The success rate of NGS also depends on whether the disease locus has already been mapped, as in the case of SCA19 (**Chapter 3**). The SCA19 locus was large, ~32 Mbp in size and contained approximately 500 genes [4], and we did not identify the mutation responsible for SCA19 using Sanger sequencing of the candidate genes (**Chapter 3**). However, for linkage regions containing a reasonable number of genes, Sanger sequencing can be successful, as we showed for SCA23 (**Chapter 4**). SCA23 locus was mapped to chromosomal region 20p12.3-p13 and was ~6.1 Mbp in size, containing 97 genes [5], of which 54 are expressed in the cerebellum. After excluding 32 prioritized genes by Sanger sequencing [6], we identified the causative mutation as localized in *PDYN*. However, our prioritization of candidate genes for mutation screening based on known and common underlying mechanisms did not help because SCA23 was, to our knowledge, the first to be reported as linking neuropeptides to a SCA disorder. For the first time, mutated neuropeptide precursor protein was shown to be directly responsible for the neurodegeneration. Therefore, it may be better to use a hypothesis-free approach as the outcome might be surprising (as in the case of SCA23). In conclusion, at the moment, NGS is the best, unbiased and most efficient method to identify new mutations/genes without prioritizing them first, and it yields data in a hypothesis-free manner.

The rare SCAs caused by conventional mutations are growing in number as new platforms for gene/mutation identification are being developed and large, multi-centre studies are being performed. In the last decade, the causative mutations were identified in SCA5, 13, 14, 19/22 (**Chapter 3**), 20, 23 (**Chapter 4**), 26,

28, and 35 [2, 3, 7-11]. Some remaining questions are: how many more types of SCAs are there? Will we be able to identify them all? Are all SCA types the same disease or are different biological routes involved in their aetiology? Common underlying pathomechanisms for SCAs have already been suggested by multiple reports [12-15], and our studies imply that problems with synaptic transmission underlie the pure cerebellar SCAs caused by conventional mutations (see discussion below). One of the current challenges is to identify the disease genes/mutations in small families and in isolated ataxia cases. With the outcome of our work, an array capturing all the synapse-associated genes – with a special focus on the CF-PC synapse, but also including other synaptic and extra-synaptic proteins that are important for neuronal transmission – could be generated and used in research and diagnostics in order to find new mutations responsible for SCA.

Mechanisms underlying Purkinje cell death in SCAs

Despite more than two decades of research, the mechanisms underlying SCA disease have still not been solved. As the neurological phenotype of the various SCAs is quite homogenous, there may well be common disease mechanisms underlying the genetically different SCA types. In contrast to other SCA types, the SCAs caused by conventional mutations, like SCA14 (**Chapter 2**), SCA19 (**Chapter 3**) and SCA23 (**Chapter 4-7**), usually exhibit a purer, more isolated cerebellar phenotype, with neuronal loss restricted to the cerebellum. Therefore, this group presents a more accurate model for studying the pathomechanisms underlying selective PC loss. Alterations in neuronal signalling leading to Ca^{2+} imbalance represent one of the possibilities proposed; they seem to be common in SCAs caused by mutations with different genetic mechanisms, including coding polyQ expansions and conventional mutations. Since PC loss is the pathology shared by all the SCAs, Ca^{2+} imbalance may be a key in the pathomechanism specifically underlying PC death and cerebellar degeneration, rather than other accompanying symptoms. In this thesis, all the SCA genes studied encode for neuronal signalling proteins, including PKCγ in SCA14 (**Chapter 2**), K_v4.3 in SCA19 (**Chapter 3**) and PDYN in SCA23 (**Chapters 4-7**).

SCA14

PKCγ is abundantly expressed in PCs [16] and phosphorylates many targets, including ionotropic glutamate receptors and potassium channels [17-19], leading to their inactivation or internalization. Moreover, Purkinje cell dendritic development critically depends on the activity of PKCγ, which triggers functional changes as well as anatomical maturation of the PC dendritic tree during cerebellar development at different time levels [20]. SCA14 is caused by missense mutations in *PRKCG* encoding for PKCγ. One of the hallmarks of SCA14 is PKCγ protein insolubilization, due to a changed structure of the mutant protein that leads to impaired protein processing (**Chapter 2**). This suggests that loss of functional kinase from the soluble pool may underlie the disease pathology. However, it is possible that SCA14-mutant PKCγ has a dominant-negative effect on wt-PKCγ and causes its insolubilization as well [21]. Moreover, the loss of PKCγ kinase activity was shown for other SCA14 mutants earlier [22]. Altogether, these data imply that loss of active kinase in PCs underlies SCA14.

Moreover, SCA14-mutant PKCγ causes PC malfunction by disrupting the elimination of CF synapses

during development, which leads to altered synaptic transmission [21]. Problems with developmental synapse elimination caused increased numbers of CF synapses in the proximal dendrites and soma of PCs, which may result in PC overexcitation and cell death due to excitotoxicity. Additionally, aberrant PKCγ signalling due to SCA14 mutations, leading to reduced phosphorylation of targets such as the Ca^{2+} channel TRPC3, was associated with elevated intracellular Ca^{2+} concentrations *in vitro* [19, 22]. Loss of TRPC3 phosphorylation would lead to sustained Ca^{2+} influx and altered intracellular Ca^{2+} homeostasis [19].

However, we cannot exclude the possibility that SCA14-mutant PKCγ causes oxidative stress, as PKCγ can also be activated by reactive oxygen species (direct oxidation of the C1B domain by H_2O_2) and subsequently phosphorylates connexins, resulting in disassembly of gap junctions between cells [23]. SCA14-mutant PKCγ proteins carrying mutations in the C1B domain lack the ability to respond to H_2O_2 and increase cell susceptibility for H_2O_2-induced apoptosis in lens due to oxidative damage [24, 25].

SCA19

Voltage-gated potassium channels participate in fast spiking of PCs and modulate their action potential firing [26, 27]; they therefore also play a crucial role in motor control. $K_v4.3$, a subunit of the voltage-gated potassium channel, is highly expressed in the cerebellum and is thought to be important for cerebellar development [28]. SCA19 mutations in *KCND3* encoding for $K_v4.3$ cause impaired channel trafficking, reduced protein stability, and affect channel activity, leading to formation of inactive (or highly reduced activity of) channel complexes if located at the plasma membrane (**Chapter 3**). Altogether, these data suggest that loss of $K_v4.3$ function may underlie SCA19. However, *KCND3* knock-out mice have been generated and they did not display any neurological impairment or motor coordination deficiency [29], probably due to redundancy of other K_v4 family members. This suggests that the SCA19-mutant $K_v4.3$ must have a dominant negative effect on the maturation or activity of the wild type $K_v4.3$ subunit or on other K_v4 α subunits such as $K_v4.1$ and $K_v4.2$. Loss of functional K_v4 channel complexes on the plasma membrane would abrogate neuronal repolarization leading to longer duration of action potentials. This could change intracellular Ca^{2+} homeostasis and may trigger PC death. Additionally, SCA19-mutant Kv4.3 subunits, trapped in ER, may lead to ER stress and induction of the unfolded protein response, contributing to PC death.

SCA23

The cerebellar function of neuropeptide Dyn A, or its precursor PDYN, is largely unknown. They were previously studied only in relation to pain processing and addiction [30]. Although at physiological levels the actions of Dyn A are mainly mediated through opioid receptors, elevated Dyn A levels can display cytotoxic and neurodegenerative effects, which cannot be inhibited by opioid antagonists [31]. Interestingly, these neurotoxic effects can be prevented by NMDAR-specific antagonists [32], suggesting a role of these receptors in non-opioid actions of Dyn A peptides. Dyn A can interact directly with the NMDAR and potentiate their currents [33]. Enhanced stimulation of NMDARs may cause excitotoxicity leading to neuronal cell death (reviewed in [34]).

SCA23 mutations were identified in the *PDYN*, and resulted in elevated Dyn A peptide levels and toxicity

in vitro (Chapters 4 and 5). Increased levels of Dyn A were also detected in the SCA23 mouse model that we developed and were found to correlate with PC loss and cerebellar ataxia (Chapter 6). Moreover, SCA23-mutant Dyn A was found to be more resistant to degradation, probably due to changes in its secondary structure (Chapter 7). Specific stimulation of NMDARs caused more pronounced cell death in the presence of SCA23-mutant peptides (Chapter 7), which is in line with the finding that Dyn A is able to potentiate NMDAR glutamate currents [33]. These findings support the hypothesis of an excitotoxic mechanism underlying SCA23.

In addition, it was implied that Dyn A actions through κ-opioid receptor (KOR) are neuroprotective [35], as Dyn A interaction with KOR decreases intracellular Ca^{2+} concentrations [36, 37], preventing excitotoxicity. Our results support this hypothesis, as blocking of the opioid pathway increased the toxicity of SCA23-mutant Dyn A peptides (Chapter 7).

The importance of glutamate/Ca^{2+} homeostasis in dynorphin signalling in the cerebellum is underscored by altered EAAT4 glutamate transporter insolubilization, which was found in material from SCA23 patients (Chapter 4). Reduced expression of EAAT4 transporters on the membrane of the PC would lead to synaptic accumulation of glutamate and may contribute to excitotoxic damage. Although, we did not detect altered EAAT4 distribution in SCA23-mutant mice (Chapter 6), we did observe decreased CF-PC synapses that may cause deficits in movement control leading to ataxic phenotype. However, as loss of CF innervation may account for alterations in PC glutamatergic signalling and ataxia, it cannot fully explain the PC death and progressiveness of the disease. Since it was reported that PC death correlates with CF hyperexcitability [38, 39] and Dyn A potentiates glutamate currents of NMDARs [33], elevated Dyn A levels in our SCA23 mouse model may cause excitotoxic damage at CF-PC synapses and PC death. The progressive elimination of CF-PC synapses during the course of the disease would serve as a compensatory mechanism.

Alternatively, loss of PDYN or haploinsufficiency might also underlie SCA23 as we identified a truncating mutation leading to complete loss of Dyn peptides (Chapter 5). The identification of the R138S mutation, localized to the non-opioid region of *PDYN*, also suggests that the precursor protein PDYN, and not only its peptide derivatives, may have an unknown cerebellar function that is also important for PC survival.

Clearly, additional studies are needed to assess the pathological actions of SCA23-mutant Dyn A, as well as the PDYN-dependent neurodegenerative mechanism, but a comprehensive model of neurotoxic, non-opioid Dyn A actions in SCA23 is now emerging. Future research will show if SCA23 Dyn A peptides are able to over-stimulate NMDARs and cause excitotoxicity that can be rescued by anti-excitotoxicity compounds or subunit-specific NMDAR blockers. The latter would also prove which NMDAR subunit is responsible for Dyn A-mediated current potentiation.

Excitotoxicity as a common pathology underlying SCAs

Taken together, a common pathology of aberrant glutamate/Ca^{2+} signalling leading to excitotoxicity is emerging (summarized in Fig. 1). Pathological increase in intracellular Ca^{2+} concentrations cause activation of various enzymes leading to fragmentation of DNA, cytoskeleton and membranes components, and subsequently cell death.

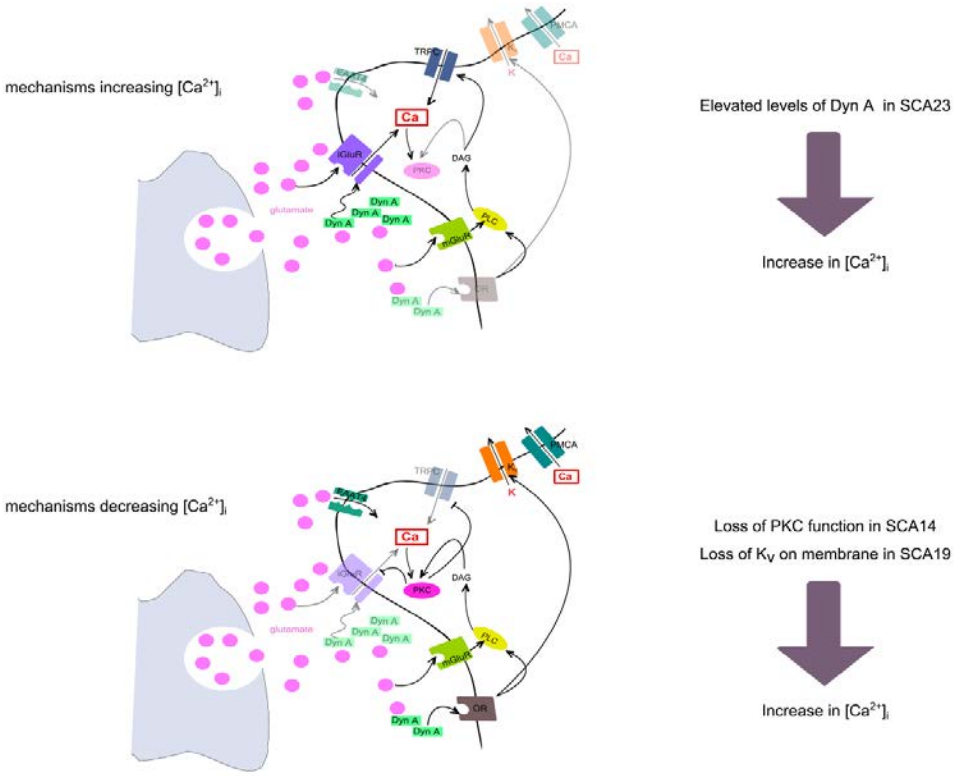

Figure 1 Neuronal mechanisms possibly leading to excitotoxicity in Purkinje cells.

TRPC = transient receptor potential channel, iGluR = ionotropic glutamate receptor, mGluR = metabotropic glutamate receptor, K_V = voltage-gated potassium channel, PLC = phospholipase C, PMCA = plasma membrane calcium ATPase, DAG = diacylglycerol, OR = opioid receptor

Similarly to SCA14, impaired elimination of CF synapses during development was reported in a SCA1 mouse model [40]. Moreover, sustained CF excitation causes PC neurodegeneration [38, 39], suggesting that increased CF innervation of PCs may lead to excitotoxicity.

Impairment of glutamate re-uptake from the synaptic cleft, due to reduced expression of glutamate transporters at the PC membrane (analogous to SCA23), has been implicated in SCA5 [23], and also in the polyQ-related SCA types SCA1 and SCA7 [41, 42]. Decreased glutamate re-uptake would lead to extensive activation of glutamate receptors leading to increased intracellular Ca^{2+} influx and activation of apoptotic pathways [43]. Mutations in the gene encoding for the plasma membrane Ca^{2+} ATP-ase PMCA3 were recently associated with X-linked cerebellar ataxia [44]. Loss-of-function mutations disrupted the PMCA3 channel function and may lead to elevated intracellular Ca^{2+} levels in neuronal cells. Moreover, the Ca^{2+} stabilizer, dantrolene, was capable of mitigating the motor deficits observed in SCA2 and SCA3 mouse models, indicating that maintaining balanced intracellular Ca^{2+} concentrations prevents dysfunctional Ca^{2+} signalling and subsequent PC degeneration in these mice [45, 46].

Furthermore, SCA13 mutations in *KCNC3*, a gene encoding for $K_v3.3$ subunit of potassium channel and required for the high-frequency firing of action potentials in PCs and Ca^{2+} spike termination [47, 48], result in non-functional $K_v3.3$ subunits [49]. Similarly to SCA19, these mutant subunits act with a dominant-negative effect on other subunits of the K_v3 family, leading to a loss of K_v3 channels function [50]. *KCNC3* knock-out mice display a marked increase in the duration of PC action potential and a disrupted function of the olivo-cerebellar circuit, leading to mild motor coordination problems [51].

Together, these findings underscore the importance of Ca^{2+} homeostasis in PCs and imply a common mechanism for PC degeneration in the genetically different SCA types that involves defects in glutamate/Ca^{2+} synaptic transmission and excitotoxic damage, leading to PC death and subsequent cerebellar ataxia. Future research will prove if excitotoxicity is a common underlying mechanism of all SCA types.

Therapeutic strategies in SCAs

Although the first SCA was discovered in 1993 [52, 53], and enormous research efforts have been made since then to understand the molecular pathomechanism underlying different SCAs, the disease remains incurable. The currently available treatments only reduce symptoms and no effective cure exists that can prevent the disease or modify its progression (reviewed in [54]). Some benefits regarding alleviation of ataxic symptoms were reported in SCA2 and SCA3 patients who took NMDAR modulators or antagonists, or dopaminergic and anticholinergic drugs that decrease tremor or dystonia (reviewed in [54]). Benzodiazepines and β-blockers are used in ameliorating tremor, and magnesium, chinine or mexiletine are used to reduce muscle cramps in SCA1, 3, and 7 [54]. Lithium carbonate improved motor function and neuronal morphology in a SCA1 mouse model [55], and clinical trials were recently conducted in SCA1, 2 and 3 (NCT00683943, NCT00998634, and NCT01096082, respectively; http://clinicaltrials.gov, National Institutes of Health, USA). These trials showed that lithium carbonate was safe and improved the quality of life for ataxic patients, reducing neurological symptoms, ataxia and depression. A follow-up study is underway. Additionally, Ca^{2+} signalling blockers, including specific antagonists of NMDAR subunit NR2B, mGluR5 or IP_3R, or Ca^{2+} stabilizers such as dantrolene have proved partially beneficial in treating neurological symptoms in various SCA types [45, 46].

These treatments may relieve patients' ataxic symptoms, but they do not provide a cure for the disease. In gene therapy, the disease gene can be replaced by the wild-type gene or the mutant allele can be specifically silenced (reviewed in [56]). This approach is feasible for monogenic disorders such as the SCAs. In SCA1, an RNA interference (RNAi) approach has been tested to downregulate the mutated allele and inhibit neurodegeneration. Viral injections of RNAi constructs targeting the mutant allele improved movement control, cerebellar morphology, and protein misfolding in a SCA1 mouse model [57]. Similar effects were seen upon mutant allele silencing in SCA3 rats [58]. However, these promising results from animal models have not yet been followed up by clinical trials in humans. This might be due to the fact that the delivery of the RNAi constructs by viral vectors carries the risk of a sustained immunological response and off-target effects, as interference with the expression of unknown, possibly important, targets can be anticipated. This innovative approach therefore needs to be tested further for

intrinsic toxicity. The major advantage of gene therapy is that it targets the primary problem, the gene mutation, without requiring a full knowledge of the molecular mechanisms underlying the disease. This is in contrast to drug-based therapies which target specific molecular pathways.

Given our results, the drugs against excitotoxicity may prove useful to treat and cure SCAs. Agents inducing anti-excitotoxic effects, like riluzole, partially alleviated ataxic symptoms in patients with cerebellar ataxias [59] and are currently being tested in clinical trials (recruiting phase; NCT01104649, http://clinicaltrials.gov, National Institutes of Health, USA).

The current therapies focus on the more frequent SCA types, namely the polyQ-related SCAs, but neglect the rare SCAs caused by conventional mutations. However, the progress being made in learning more about the common molecular pathologies that underlie the genetically different types of SCA will contribute greatly to the development of therapeutic interventions that can target all the SCA types.

References

1. Sikkema-Raddatz B, Johansson LF, de Boer EN et al. Targeted Next-Generation Sequencing can Replace Sanger Sequencing in Clinical Diagnostics. *Hum Mutat* 2013; 34: 1035-1042.
2. Hekman KE, Yu GY, Brown CD et al. A conserved eEF2 coding variant in SCA26 leads to loss of translational fidelity and increased susceptibility to proteostatic insult. *Hum Mol Genet* 2012; 21: 5472-5483.
3. Wang JL, Yang X, Xia K et al. TGM6 identified as a novel causative gene of spinocerebellar ataxias using exome sequencing. *Brain* 2010; 133: 3510-3518.
4. Verbeek DS, Schelhaas JH, Ippel EF, Beemer FA, Pearson PL, Sinke RJ. Identification of a novel SCA locus (SCA19) in a Dutch autosomal dominant cerebellar ataxia family on chromosome region 1p21-q21. *Hum Genet* 2002; 111: 388-393.
5. Verbeek DS, van de Warrenburg BP, Wesseling P, Pearson PL, Kremer HP, Sinke RJ. Mapping of the SCA23 locus involved in autosomal dominant cerebellar ataxia to chromosome region 20p13-12.3. *Brain* 2004; 127: 2551-2557.
6. Verbeek DS. Spinocerebellar ataxia type 23: a genetic update. *Cerebellum* 2009; 8: 104-107.
7. Ikeda Y, Dick KA, Weatherspoon MR et al. Spectrin mutations cause spinocerebellar ataxia type 5. *Nat Genet* 2006; 38: 184-90.
8. Waters MF, Minassian NA, Stevanin G et al. Mutations in voltage-gated potassium channel KCNC3 cause degenerative and developmental central nervous system phenotypes. *Nat Genet* 2006; 38: 447-51.
9. Chen DH, Brkanac Z, Verlinde CL et al. Missense mutations in the regulatory domain of PKC gamma: a new mechanism for dominant nonepisodic cerebellar ataxia. *Am J Hum Genet* 2003; 72: 839-49.
10. Knight MA, Hernandez D, Diede SJ et al. A duplication at chromosome 11q12.2-11q12.3 is associated with spinocerebellar ataxia type 20. *Hum Mol Genet* 2008; 17: 3847-53.
11. Di BD, Lazzaro F, Brusco A et al. Mutations in the mitochondrial protease gene AFG3L2 cause dominant hereditary ataxia SCA28. *Nat Genet* 2010; 42: 313-321.
12. La Spada AR, Taylor JP. Repeat expansion disease: progress and puzzles in disease pathogenesis. *Nat Rev Genet* 2010; 11: 247-258.
13. Takahashi T, Katada S, Onodera O. Polyglutamine diseases: where does toxicity come from? what is toxicity? where are we going? *J Mol Cell Biol* 2010; 2: 180-191.
14. Matilla-Duenas A, Sanchez I, Corral-Juan M, Davalos A, Alvarez R, Latorre P. Cellular and molecular pathways triggering neurodegeneration in the spinocerebellar ataxias. *Cerebellum* 2010; 9: 148-66.
15. Carlson KM, Andresen JM, Orr HT. Emerging pathogenic pathways in the spinocerebellar ataxias. *Curr Opin Genet Dev* 2009; 19: 247-253.
16. Barmack NH, Qian Z, Yoshimura J. Regional and cellular distribution of protein kinase C in rat cerebellar Purkinje cells. *J Comp Neurol* 2000; 427: 235-254.
17. Patten SA, Roy B, Cunningham ME, Stafford JL, Ali DW. Protein kinase Cgamma is a signaling molecule required for the developmental speeding of alpha-amino-3-hydroxyl-5-methyl-4-isoxazole-propionate receptor kinetics. *Eur J Neurosci* 2010; 31: 1561-1573.
18. Desai R, Kronengold J, Mei J, Forman SA, Kaczmarek LK. Protein kinase C modulates inactivation of Kv3.3 channels. *J Biol Chem* 2008; 283: 22283-22294.
19. Adachi N, Kobayashi T, Takahashi H et al. Enzymological analysis of mutant protein kinase Cgamma causing spinocerebellar ataxia type 14 and dysfunction in Ca2+ homeostasis. *J Biol Chem* 2008; 283: 19854-19863.
20. Metzger F, Kapfhammer JP. Protein kinase C: its role in activity-dependent Purkinje cell dendritic development and plasticity. *Cerebellum* 2003; 2: 206-214.
21. Shuvaev AN, Horiuchi H, Seki T et al. Mutant PKCgamma in spinocerebellar ataxia type 14 disrupts synapse elimination and long-term depression in Purkinje cells in vivo. *J Neurosci* 2011; 31: 14324-14334.
22. Verbeek DS, Goedhart J, Bruinsma L, Sinke RJ, Reits EA. PKC gamma mutations in spinocerebellar ataxia type 14 affect C1 domain accessibility and kinase activity leading to aberrant MAPK signaling. *J Cell Sci* 2008; 121: 2339-2349.

23. Lin D, Takemoto DJ. Oxidative activation of protein kinase Cgamma through the C1 domain. Effects on gap junctions. *J Biol Chem* 2005; 280: 13682-13693.

24. Lin D, Shanks D, Prakash O, Takemoto DJ. Protein kinase C gamma mutations in the C1B domain cause caspase-3-linked apoptosis in lens epithelial cells through gap junctions. *Exp Eye Res* 2007; 85: 113-122.

25. Lin D, Barnett M, Lobell S et al. PKCgamma knockout mouse lenses are more susceptible to oxidative stress damage. *J Exp Biol* 2006; 209: 4371-4378.

26. Hille B. Ionic channels in excitable membranes. Current problems and biophysical approaches. *Biophys J* 1978; 22: 283-294.

27. Serodio P, Rudy B. Differential expression of Kv4 K+ channel subunits mediating subthreshold transient K+ (A-type) currents in rat brain. *Nat Rev Neurosci J Neurophysiol* 1998; 79: 1081-1091.

28. Hsu YH, Huang HY, Tsaur ML. Contrasting expression of Kv4.3, an A-type K+ channel, in migrating Purkinje cells and other post-migratory cerebellar neurons. *Eur J Neurosci* 2003; 18: 601-612.

29. Niwa N, Wang W, Sha Q, Marionneau C, Nerbonne JM. Kv4.3 is not required for the generation of functional Ito,f channels in adult mouse ventricles. *J Mol Cell Cardiol* 2008; 44: 95-104.

30. Schwarzer C. 30 years of dynorphins--new insights on their functions in neuropsychiatric diseases. *Pharmacol Ther* 2009; 123: 353-370.

31. Tan-No K, Cebers G, Yakovleva T et al. Cytotoxic effects of dynorphins through nonopioid intracellular mechanisms. *Exp Cell Res* 2001; 269: 54-63.

32. Hauser KF, Knapp PE, Turbek CS. Structure-activity analysis of dynorphin A toxicity in spinal cord neurons: intrinsic neurotoxicity of dynorphin A and its carboxyl-terminal, nonopioid metabolites. *Exp Neurol* 2001; 168: 78-87.

33. Woods AS, Kaminski R, Oz M et al. Decoy peptides that bind dynorphin noncovalently prevent NMDA receptor-mediated neurotoxicity. *J Proteome Res* 2006; 5: 1017-1023.

34. Arundine M, Tymianski M. Molecular mechanisms of calcium-dependent neurodegeneration in excitotoxicity. *Cell Calcium* 2003; 34: 325-337.

35. Hauser KF, Aldrich JV, Anderson KJ et al. Pathobiology of dynorphins in trauma and disease. *Front Biosci* 2005; 10: 216-235.

36. Przewlocki R, Parsons KL, Sweeney DD et al. Opioid enhancement of calcium oscillations and burst events involving NMDA receptors and L-type calcium channels in cultured hippocampal neurons. *J Neurosci* 1999; 19: 9705-9715.

37. Wagner JJ, Caudle RM, Chavkin C. Kappa-opioids decrease excitatory transmission in the dentate gyrus of the guinea pig hippocampus. *J Neurosci* 1992; 12: 132-141.

38. O'Hearn E, Molliver ME. The olivocerebellar projection mediates ibogaine-induced degeneration of Purkinje cells: a model of indirect, trans-synaptic excitotoxicity. *J Neurosci* 1997; 17: 8828-8841.

39. O'Hearn E, Molliver ME. Degeneration of Purkinje cells in parasagittal zones of the cerebellar vermis after treatment with ibogaine or harmaline. *Neuroscience* 1993; 55: 303-310.

40. Ebner BA, Ingram MA, Barnes JA et al. Purkinje cell ataxin-1 modulates climbing fiber synaptic input in developing and adult mouse cerebellum. *J Neurosci* 2013; 33: 5806-5820.

41. Custer SK, Garden GA, Gill N et al. Bergmann glia expression of polyglutamine-expanded ataxin-7 produces neurodegeneration by impairing glutamate transport. *Nat Neurosci* 2006; 9: 1302-1311.

42. Lin X, Antalffy B, Kang D, Orr HT, Zoghbi HY. Polyglutamine expansion down-regulates specific neuronal genes before pathologic changes in SCA1. *Nat Neurosci* 2000; 3: 157-163.

43. Rasheva VI, Domingos PM. Cellular responses to endoplasmic reticulum stress and apoptosis. *Apoptosis* 2009; 14: 996-1007.

44. Zanni G, Cali T, Kalscheuer VM et al. Mutation of plasma membrane Ca2+ ATPase isoform 3 in a family with X-linked congenital cerebellar ataxia impairs Ca2+ homeostasis. *Proc Natl Acad Sci U S A* 2012; 109: 14514-14519.

45. Liu J, Tang TS, Tu H et al. Deranged calcium signaling and neurodegeneration in spinocerebellar ataxia type 2. *J Neurosci* 2009; 29: 9148-9162.

46. Chen X, Tang TS, Tu H et al. Deranged calcium signaling and neurodegeneration in spinocerebellar ataxia type 3. *J Neurosci* 2008; 28: 12713-12724.

47. Akemann W, Knopfel T. Interaction of Kv3 potassium channels and resurgent sodium current influences the rate of spontaneous firing of Purkinje neurons. *J Neurosci* 2006; 26: 4602-4612.

48. Martina M, Yao GL, Bean BP. Properties and functional role of voltage-dependent potassium channels in dendrites of rat cerebellar Purkinje neurons. *J Neurosci* 2003; 23: 5698-5707.

49. Waters MF, Pulst SM. Sca13. *Cerebellum* 2008; 7: 165-169.

50. Figueroa KP, Minassian NA, Stevanin G et al. KCNC3: phenotype, mutations, channel biophysics-a study of 260 familial ataxia patients. *Hum Mutat* 2010; 31: 191-196.

51. Hurlock EC, Bose M, Pierce G, Joho RH. Rescue of motor coordination by Purkinje cell-targeted restoration of Kv3.3 channels in Kcnc3-null mice requires Kcnc1. *J Neurosci* 2009; 29: 15735-15744.

52. Orr HT, Chung MY, Banfi S et al. Expansion of an unstable trinucleotide CAG repeat in spinocerebellar ataxia type 1. *Nat Genet* 1993; 4: 221-6.

53. Chung MY, Ranum LP, Duvick LA, Servadio A, Zoghbi HY, Orr HT. Evidence for a mechanism predisposing to intergenerational CAG repeat instability in spinocerebellar ataxia type I. *Nat Genet* 1993; 5: 254-258.

54. Marmolino D, Manto M. Past, present and future therapeutics for cerebellar ataxias. *Curr Neuropharmacol* 2010; 8: 41-61.

55. Watase K, Gatchel JR, Sun Y et al. Lithium therapy improves neurological function and hippocampal dendritic arborization in a spinocerebellar ataxia type 1 mouse model. *PLoS Med* 2007; 4: e182.

56. Lim F, Diaz-Nido J. Gene therapy approaches to ataxias. *Curr Gene Ther* 2009; 9: 1-8.

57. Xia H, Mao Q, Eliason SL et al. RNAi suppresses polyglutamine-induced neurodegeneration in a model of spinocerebellar ataxia. *Nat Med* 2004; 10: 816-820.

58. Alves S, Nascimento-Ferreira I, Auregan G et al. Allele-specific RNA silencing of mutant ataxin-3 mediates neuroprotection in a rat model of Machado-Joseph disease. *PLoS One* 2008; 3: e3341.

59. Ristori G, Romano S, Visconti A et al. Riluzole in cerebellar ataxia: a randomized, double-blind, placebo-controlled pilot trial. *Neurology* 2010; 74: 839-845.

PODSUMOWANIE

SAMEVALUING

SUMMARY

Podsumowanie

Rozdział 1 zawiera opis ataksji rdzeniowo-móżdżkowych (ang. spinocerebellar ataxia, SCA), które są chorobami neurodegeneracyjnymi dziedziczonymi autosomalnie dominująco i charakteryzują się atrofią komórek Purkiniego w móżdżku. Ataksje rdzeniowo-móżdżkowe są spowodowane mutacjami o różnym mechanizmie genetycznym, którymi są: ekspansje ciągu poliglutaminowego, niekodujące ekspansje ciągów powtórzeń oraz mutacje klasyczne (mutacje niesynonimiczne, delecje itp.). Do tej pory odkryto 32 rodzaje ataksji rdzeniowo-móżdżkowych, jednak tylko dla 22-óch typów zostały znalezione mutacje sprawcze. Badania mające na celu identyfikację nowych mutacji odpowiedzialnych za ataksje rdzeniowo-móżdżkowe o nieodkrytym do tej pory podłożu genetycznym nie tylko poszerzają możliwości diagnostyczne ataksji, ale również prowadzą do szerszego zrozumienia mechanizmów komórkowych odpowiedzialnych za tę chorobę i odkrycia możliwych terapii.

W **Rozdziale 2** zostały przedstawione badania wpływu mutacji V138E na aktywację i dezaktywację kinazy PKCγ w kontekście ataksji rdzeniowo-móżdżkowej typu 14 (SCA14), która wywoływana jest mutacjami w genie kodującym PKCγ. Mutacja V138E prowadziła do zmiany konformacji kinazy PKCγ, powodując deficyt w jej defosforylacji oraz degradacji, i w konsekwencji wewnątrzkomórkową akumulację PKCγ. Wyniki naszych badań sugerują, że ilościowy deficyt aktywnej kinazy PKCγ w rozpuszczalnej frakcji komórkowej jest przyczyną ataksji SCA14 oraz że białka modyfikujące rozpuszczalność oraz aktywację/dezaktywację PKCγ, takie jak PDK1, mogą w przyszłości przyczynić się do stworzenia terapii dla ataksji SCA14.

Rozdział 3 opisuje identyfikację trzech mutacji w genie KCND3 odpowiedzialnych za ataksję SCA19. Pierwsza mutacja została zidentyfikowana z użyciem sekwencjonowania nowej generacji dla próbek DNA od dwóch pacjentów z tej samej rodziny. Pozostałe dwie mutacje zostały znalezione metodą denaturacji DNA z wysoką rozdzielczością (ang. high-resolution melting) w grupie 230 pacjentów z ataksją o nieznanym podłożu genetycznym. Gen KCND3 koduje kanał potasowy Kv4.3, odpowiedzialny za aktywny transport potasu na zewnątrz komórki podczas przesyłania potencjału czynnościowego (impulsu elektrycznego) w układzie nerwowym. Kv4.3 występuje w komórkach móżdżku w dużej ilości i bierze udział w wyciszaniu potencjału czynnościowego w dendrytach komórek Purkiniego. Badania morfologii móżdżku pacjenta z ataksją SCA19 ujawniły wyraźną atrofię komórek Purkiniego w regionie vermis, który jest najsilniej zaatakowany również w innych ataksjach spowodowanych mutacjami klasycznymi (SCA13, SCA15/16, SCA23, and SCA28). Zmutowane białka Kv4.3 w ataksji SCA19, niosące różne mutacje, były zlokalizowane głównie w retikulum endoplazmatycznym i nie docierały do błony. Wykazywały również obniżoną stabilność proteolityczną oraz bardzo ograniczoną zdolność do transportu jonów potasowych (gdy były zlokalizowane w błonie). Nasze wyniki wykazują, że brak kanału potasowego w błonie może być przyczyną degeneracji móżdżku i ataksji.

W **Rozdziałach 4, 5 i 6** znajduje się opis badań in vitro oraz in vivo nad ataksją SCA23. Jako pierwsi zidentyfikowaliśmy mutację odpowiedzialną za ataksję SCA23 w genie PDYN (kodującym białko prodynorfinę, PDYN) w sprzężonym z chorobą regionie położonym na chromosomie 20 (20p13) z użyciem sekwencjonowania metodą Sangera (**Rozdział 4**). Badania przesiewowe grupy 800 pacjentów z ataksją o nieznanym podłożu genetycznym doprowadziły do identyfikacji kolejnych trzech mutacji w regionie kodującym peptyd dynorfinę (Dyn) A. PDYN

jest prekursorem neuropeptydów opioidowych, między innymi Dyn A, które regulują odczuwanie bólu oraz biorą udział w szlakach metabolicznych prowadzących do uzależnień. Funkcja peptydów opioidowych w móżdżku jest jednak nieznana. W przeprowadzonych przez nas doświadczeniach mutacje zlokalizowane w regionie kodującym Dyn A powodowały zwiększoną ilość oraz toksyczność tego peptydu w kulturach pierwszorzędowych komórek nerwowych prążkowia. Dodatkowo, jedna mutacja została zidentyfikowana w regionie niekodującym peptydów opioidowych i prowadziła do zmian w ekspresji składników szlaku opioidowego oraz glutaminianowego. Analiza białkowa tkanki nerwowej pacjenta z ataksją SCA23 wykazała między innymi zmniejszoną ilość transportera glutaminianu EAAT4 w błonie komórkowej oraz patologiczną wewnątrzkomórkową akumulację tego białka. Brak działających poprawnie cząsteczek EAAT4, których główną funkcją jest usuwanie nadmiaru glutaminianu ze szczeliny synaptycznej, prowadziłby do zwiększenia stężenia glutaminianu i w konsekwencji do nadmiernej aktywacji neuronów, zwanej ekscytotoksycznością. Wyniki naszych badań są zgodne z poprzednimi doniesieniami o zmianach w ekspresji i lokalizacji transportera EAAT4 w ataksjach SCA1 i SCA5, a także wskazują na wspólny mechanizm patologii w ataksjach z rodzaju SCA (autosomalnych dominujących).

W celu zbadania częstotliwości ataksji SCA23 w Europie przeprowadzone zostały badania przesiewowe w grupie pacjentów z ataksją o nieznanym podłożu genetycznym (**Rozdział 5**). Choroba ta okazała się bardzo rzadka, odpowiadając jedynie za 0,1% przypadków wśród ataksji z rodzaju SCA. Podczas badań przesiewowych zidentyfikowaliśmy w genie PDYN dodatkowe trzy substytucje oraz jedną delecję prowadzącą do przesunięcia ramki odczytu i pojawienia się przedwczesnego kodonu stop. Dwie z wykrytych substytucji prowadziły do zwiększonej ilości peptydu Dyn A. Jednakże analiza kosegregacji choroby z substytucjami nie była jednoznaczna, dlatego nie byliśmy w stanie dowieść patologii tych zmian i wykazać czy substytucje są mutacjami czy tylko polimorfizmami. Z kolei delecja znaleziona u jednej rodziny prowadziła do całkowitego zaniku ekspresji peptydów Dyn A, co wskazuje na to, że utrata funkcji przez białko PDYN lub jego niedobór (w wyniku braku jednego allelu) mogą również powodować ataksję SCA23. Dodatkowo wyniki naszych badań sugerują, że region kodujący Dyn A może być tzw. gorącym miejscem (ang. hot-spot) dla mutacji SCA23.

Chcąc dowieść patologii znalezionych przez nas mutacji in vivo oraz zbadać mechanizmy komórkowe odpowiadające za ataksję SCA23, stworzyliśmy model zwierzęcy tej choroby – mysz transgeniczną posiadającą jeden allel ludzkiego genu PDYN z mutacją R212W (**Rozdział 6**). Mutacja ta wykazywała najbardziej toksyczne efekty w naszych wcześniejszych badaniach in vitro. Analiza modelu ataksji SCA23 w czasie (1 rok) potwierdziła patogenność mutacji R212W. Myszy PDYN-R212W wykazywały objawy typowe dla ataksji SCA23 u ludzi, włącznie z wolno postępującymi, łagodnymi problemami z koordynacją ruchową i chodzeniem oraz zanikiem komórek Purkiniego w móżdżku w późniejszym stadium choroby. Zaraz po wystąpieniu pierwszych objawów choroby wykryliśmy zwiększoną ilość peptydu Dyn A w móżdżkach myszy PDYN-R212W, która była powiązana ze spadkiem ilości zakończeń nerwowych CF (ang. climbing fiber) na komórkach Purkiniego. Ta zmiana postępowała w czasie przebiegu choroby, wskazując na aktywną eliminację zakończeń CF, a nie na problemy w rozwoju embrionalnym układu nerwowego w modelu SCA23. Biorąc pod uwagę zwiększoną ilość Dyn A w móżdżku oraz doniesienia, że Dyn A może zwiększać aktywność receptorów glutaminianowych, zaproponowaliśmy hipotezę, według której zmutowane

peptydy Dyn A powodują nadmierną aktywację komórek Purkiniego i ekscytotoksyczność, prowadzącą do atrofii komórek móżdżku i ataksji.

Żeby zweryfikować tę hipotezę i poznać mechanizmy, za pośrednictwem których Dyn A powoduje śmierć komórek, użyliśmy modelowej linii komórkowej NG108 zróżnicowanej do neuronów oraz zbadaliśmy wpływ mutacji zlokalizowanych w regionie kodującym Dyn A na strukturę i funkcję tego peptydu (Rozdział 7). Zmutowane peptydy Dyn A wykazywały zmienioną strukturę drugorzędową na błonach, podobną do struktury peptydu Dyn A-Y1del, który nie oddziałuje z receptorami opioidowymi. Peptydy Dyn A niosące mutacje SCA23 wiązały się z receptorami opioidowymi, ale oddziaływanie to było osłabione. Dodatkowo dwie z trzech mutacji powodowały podwyższoną stabilność peptydów Dyn A, co mogłoby wyjaśniać zwiększoną ilość Dyn A w naszych poprzednich badaniach in vitro i in vivo. Zmutowane peptydy Dyn A powodowały śmierć modelowych komórek nerwowych, wykazując toksyczność zależącą od stężenia. Toksyczność zmutowanych peptydów DynA wynikała głównie z ich oddziaływania na receptory glutaminianowe NMDA, gdyż użycie specyficznych antagonistów tych receptorów blokowało ten efekt. Ponadto nasze wyniki potwierdziły hipotezę, że szlak opioidowy jest potrzebny do utrzymywania homeostazy i jego aktywacja ma właściwości neuroprotekcyjne, gdyż blokowanie tego szlaku doprowadziło do śmierci modelowych komórek nerwowych w obecności nietoksycznych stężeń peptydów Dyn A. Dlatego też zaproponowaliśmy , że zmutowane peptydy Dyn A mogą powodować neurotoksyczność poprzez dwa mechanizmy: zmniejszoną aktywność neuroprotekcyjnego szlaku opioidowego oraz ekscytotoksyczność poprzez oddziaływanie na receptory glutaminianowe NMDA.

Rozdział 8 obejmuje dyskusję na temat wspólnych mechanizmów komórkowych prowadzących do śmierci komórek Purkiniego w ataksjach z rodzaju SCA. Z naszych badań wynika, że jednym z tych mechanizmów może być ekscytotoksyczność, czyli nadmierna aktywacja receptorów glutaminianowych. Prowadzi ona do zwiększenia wewnątrzkomórkowego stężenia jonów wapnia, aktywujących liczne enzymy, w tym fosfolipazy, endonukleazy i proteazy, które uszkadzają struktury komórkowe, poprzez fragmentację składników cytoszkieletu, błon komórkowych oraz DNA. Z tego powodu, związki blokujące ekscytotoksyczność lub aktyrujące anty-ekscytotoksyczne szlaki np. będący na etapie prób klinicznych riluzol (ang. riluzole), stanowią obiecujące źródło terapii ataksji.

Podsumowując, ataksje typu SCA tworzą grupę chorób o różnym podłożu genetycznym, jednakże podobne objawy choroby sugerują wspólne podłoże molekularne/komórkowe. W tej pracy doktorskiej opisane zostały trzy rodzaje ataksji typu SCA spowodowane mutacjami klasycznymi w różnych genach. Ataksje typu SCA spowodowane mutacjami klasycznymi stanowią bardziej odpowiedni model do badania tej choroby, ponieważ pierwotna atrofia neuronów ogranicza się do móżdżku, a inne regiony mózgu nie są zaatakowane (jak w rodzajach ataksji typu SCA o innym podłożu genetycznym). Z naszych badań wynika, że ekscytotoksyczność może być wspólnym patologicznym mechanizmem w ataksjach SCA14, SCA19 i SCA23, w których zmutowane białka prowadzą do problemów w przewodnictwie synaptycznym, powodując zwiększenie stężenia jonów wapnia w komórkach nerwowych. Szersze zrozumienie mechanizmów prowadzących do ekscytotoksyczności i śmierci komórek Purkiniego może się przyczynić do wynalezienia terapii ataksji typu SCA.

Samenvatting

In **Hoofdstuk 1**, presenteer ik een korte inleiding over spinocerebellar ataxias (SCAs). Dit zijn autosomaal dominante neurodegeneratieve aandoeningen, gekarakteriseerd door atrophie van Purkinje cellen in het cerebellum. Ik review de onderliggende genetische en moleculaire mechanismen van SCA, die uit drie genetische verschillende groepen bestaan: polyglutamine repeat expansies, niet-coderende repeat expansies of conventionele mutaties. Tot nu toe zijn 32 SCA types bekend, die gelokaliseerd zijn op verschillende genetische loci. Voor 22 types zijn de ziekte veroorzakende genen en mutaties geïdentificeerd. Het vinden van de causale mutaties in de groep van SCA families zonder genetische diagnose verbeterd niet alleen de diagnostische mogelijkheden voor deze patiënten maar levert ook verdere inzichten in de onderliggende pathologische wegen van SCA dat bijdraagt aan nieuwe therapeutische ontwikkelingen.

In **Hoofdstuk 2** wordt de impact van de V138E mutatie op de levenscyclus van PKCg bestudeerd in de context van SCA14, dat veroorzaakt wordt door missense mutaties in het gen coderend voor protein kinase C gamma, PKCg. We observeerden dat SCA14-mutant PKCg een veranderd eiwit structuur heeft, wat leidt tot verminderde defosforylatie en afbraak en ophoping van de mutante moleculen in de Triton-onoplosbare cellulaire fractie. Ons werk suggereert dat verminderde hoeveelheden van actief PKCg kinase in de oplosbare cellulaire fractie de SCA14 pathologie veroorzaakt. Moleculen die de verwerking van PKCg beïnvloeden, zoals PDK1, die het verlies tegengaan van actief en gefosforyleerde PKCg eiwitten in de onoplosbare pool, zijn potentiële kandidaten voor een nieuwe therapeutische interventie voor SCA14.

In **Hoofdstuk 3** werden missense mutaties in *KCND3* geïdentificeerd die SCA19 veroorzaakten via exoom sequencing in twee aangedane personen van de als eerste gerapporteerde SCA19 familie. *KCND3* codeert voor Kv4.3, een voltage-gereguleerd kalium kanaal die de kortdurende, naar buiten gerichte kalium stromen in zenuwcellen reguleert. Kv4.3 komt hoog tot expressie in het cerebellum en draagt bij aan het verminderen van post-synaptische potentialen in de dendrieten van Purkinje cellen. Het screenen van twee honderd en dertig ataxie patiënten, zonder mutaties in de bekende SCA genen, voor mutaties in KCND3 via High-Resolution Melting, zorgde voor de identificatie van 2 nieuwe mutaties. SCA19 autopsie materiaal liet duidelijke degeneratie zien van Purkinje cellen in de cerebellaire vermis, net zoals de pathologie in andere SCA typen veroorzaakt door conventionele mutaties (SCA13, 15/16, 23 en 28). Alle SCA19-mutante Kv4.3 subunits zaten in het endoplasmatisch reticulum (ER) door verminderd transport, wat verminderde plasma membraan lokalisatie en verminderde eiwit stabiliteit veroorzaakte. De regulaire subunit KChIP2 redde de lokalisatie afwijkingen en de eiwit stabiliteit in 2 van de 3 mutante Kv4.3 kanaal complexen. Echter, hiermee werd slechts gedeeltelijk of helemaal niet de kanaal functie hersteld. Onze resultaten laten zien dat verlies van Kv4.3 kanalen, die alleen nodig zijn om de snelle repolarisatie van neuronen tegen te gaan, genoeg is om cerebellaire neurodegeneratie te veroorzaken.

De **Hoofdstukken 4, 5 en 6** beschrijven de identificatie van mutaties die SCA23 veroorzaken gevolgd door *in vitro* en *in vivo* studies. De eerste SCA23 mutatie was geïdentificeerd in prodynorphin, *PDYN*, via Sanger sequencen van kandidaat genen in het linkage interval op de chromosomale regio 20p13-12.3 (**Hoofdstuk 4**). Het screenen van het Nederlandse ataxie cohort (n = 800) leidde tot de ontdekking van drie andere missense

mutaties, die zich in het neuropeptide Dynorphin (Dyn) A bevonden. PDYN is een voorloper eiwit voor de opioid neuropeptides a-neoendorphin, Dyn A and B. Dynorphins reguleren pijn verwerking en moduleren het beloning gevoel van verslavende middelen via opioid signalering, maar hoe Dyn A neurodegeneratie in het cerebellum kan veroorzaken is niet bekend. De SCA23 mutaties in Dyn A leiden tot verhoogde peptide niveaus en twee van de drie mutaties verhoogde de intrinsieke toxiciteit van normaal (gezond) Dyn A in gekweekte striatale zenuwcellen. Eén mutatie bevond zich in het niet-opioid gerelateerde domein van PDYN en kwam overeen met veranderde expressie van componenten van het opioid en glutamaat systeem zoals EAAT4, zoals duidelijk werd na proteoom analyse van SCA23 autopsie materiaal. Verlies van EAAT4 functie op de Purkinje cel membraan kan leiden tot ophoping van excitatoir glutamaat in de synaptische groeve en zal bijdragen aan excitotoxische schade. Onze bevindingen komen overeen met eerdere werk waarin veranderingen in expressie en lokalisatie van EAAT4 in SCA1 en SCA5 gerapporteerd werden, en duiden erop dat de acties van Dyn A kunnen leiden tot veranderingen in glutamaat en/of calcium signalering wat SCA23 kan veroorzaken.

Om de SCA23 ziekte frequentie in Europa te bepalen, werden dominante cerebellaire ataxie patiënten, van voornamelijk Franse achtergrond, gescreend voor mutaties in *PDYN* (**Hoofdstuk 5**). Variaties in *PDYN* bleken zeldzaam te zijn in Kaukasische ataxie patiënten. We identificeerden drie nieuwe missense variaties en een afkappende mutatie (een 2 basenpaar deletie) wat leidde tot een vervroegd stop codon. Twee missense variaties kwamen overeen met verhoogde Dyn A niveaus waarvan één niet co-segregeerde met het ziektebeeld en voor de ander kon co-segregatie niet worden vast gesteld. Daarom konden we niet concluderen dat deze missense variaties ziekte veroorzakend zijn. Geheel verlies van de Dynorphin peptides door de afkappende mutatie geeft een sterke aanwijzing dat haploïnsufficientie of verlies van functie ook SCA23 kan veroorzaken. Verder lijkt Dyn A een "hotspot" te zijn voor SCA23 mutaties, wat het belang van Dyn A's functie onderstreept in het cerebellum.

Om de rol van PDYN te kunnen bestuderen in cerebellaire neurodegeneratie en ataxie en om inzichten te krijgen in de ziekte mechanismen van SCA23, werd er een voorwaardelijk transgeen muismodel gemaakt die overal menselijk PDYN-R212W tot expressie brengt (**Hoofdstuk 6**). Deze mutatie liet de ernstigste pathogene effecten zien in ons eerdere *in vitro* werk. We bevestigden dat PDYN-R212W cerebellaire ataxie veroorzaakt *in vivo*, als de transgene muizen de ziekte symptomen lieten zien van SCA23 patiënten zoals langzaam verergerende motor coördinatie en loopgang afwijkingen en Purkinje cel verlies op de leeftijd van 12 maanden. De SCA23-mutante transgene muizen hadden verhoogde Dyn A niveaus in het cerebellum dat gekoppeld leek te zijn met verminderde klimvezel innervatie van de Purkinje cellen. Dit tekort in klimvezel synaps distributie begon al vroeg in het ziekte proces en verergerde in tijd, wat suggereert dat deze vezels actief verwijderd worden in plaatst van problemen in de aanleg tijdens de ontwikkeling. Gezien het verhoogde Dyn A niveau, dat N-methyl-D-Aspartaat (NMDA) receptoren stromen kan potentiëren, veronderstelden wij dat SCA23 wordt veroorzaakt door Dyn A gedreven excitoxische schade via NMDA receptor activatie.

Om de neurodegeneratieve mechanismen aangestuurd via de SCA23-mutante Dyn A peptiden te onderzoeken, bestudeerden we de effecten van de SCA23 mutaties op de secondaire structuur van Dyn A, opioid receptor affiniteit, en celdood gebruik makend van selectieve antagonisten en agonisten voor zowel opioid als

NMDA receptoren (**Hoofdstuk 7**). Alle SCA23-mutante Dyn A peptiden lieten sterke veranderingen zien in hun secondaire structuur in de aanwezigheid van membranen. Dit kwam overeen met de secondaire structuur van Dyn A-Y1del, een peptide dat niet meer interacteert met k-opioid receptoren. Voor twee van de drie mutaties leidde de veranderingen in de secondaire structuur tot stabielere peptiden die bijna geheel immuun waren tegen peptidase afbraak en lieten *in vitro* verhoogde oligomerisatie zien. SCA23-mutant Dyn A veroorzaakte duidelijk dosis afhankelijke neurotoxiciteit in gedifferentieerde NG108 cellen, dat hoofdzakelijk veroorzaakt werd via NMDA receptoren als specifieke antagonisten in staat waren om deze effecten te verminderen. Tevens vonden we bewijs voor de hypothese dat opioid signalering beschermend kan zijn voor zenuwcellen, als naloxone, een opioid receptor anagonist in de aanwezigheid van niet-toxisch SCA23-mutant Dyn A peptides ernstige celdood veroorzaakte. Dus SCA23-mutant Dyn A peptiden hebben dichotome neurotoxische activiteiten, als eerste via verlies van bescherming van neuronen gereguleerd via opioid receptoren en als tweede via excitotoxische acties aangestuurd door NMDA receptoren.

Hoofdstuk 8 bevat de discussie over de gemeenschappelijke ziekte mechanismen van de verschillende SCA types, met als focus die SCAs veroorzaakt door conventionele mutaties zoals SCA14, SCA19 en SCA23. Onze data samenvattend lijkt excitotoxiciteit de gemeenschappelijke noemer te zijn die Purkinje celdood veroorzaakt in SCA. Excitotoxiciteit is gekoppeld met de pathologische activatie van ionotrofe glutamaat receptoren (zoals NMDA receptoren), wat een verhoging van de intracellulaire calcium concentratie veroorzaakt en tot activatie leidt van verschillende enzymen zoals endonucleasen, fosfolipasen en proteasen wat DNA, cytoskelet en membraan component fragmentatie veroorzaakt. Verbindingen die excitotoxiciteit blokkeren kunnen bruikbaar zijn in toekomstige therapieën voor SCA. Anti-excitatoire drugs zoals riluzole lieten al gedeeltelijke vermindering zien van de ataxtische symptomen in patiënten met cerebellaire ataxie en worden momenteel getest in klinische trials.

In conclusie, de SCAs vormen een genetisch heterogene groep van ziekten maar toch lijkt er een gemeenschappelijke moleculaire pathologie te zijn sinds patiënten van verschillende SCA typen een overeenkomstig ziektebeeld laten zien. In dit proefschrift werden SCA14, SCA19 en SCA23 bestudeerd, allen veroorzaakt door conventionele mutaties in verschillende en schijnbaar functioneel niet-gerelateerde genen. SCA typen veroorzaakt door conventionele mutaties laten meestal een puur, wat meer geïsoleerd cerebellair fenotype zien, met beperkt zenuwcel verlies in het cerebellum. Daarom is deze groep een beter en meer nauwkeuriger model dan de andere SCA typen om de ziekte mechanismen achter het selectieve Purkinje cel verlies te bestuderen. Ons werk wijst naar excitoxiciteit als gemeenschappelijke pathologie voor SCA14, SCA19 en SCA23, als de mutante eiwitten betrokken zijn bij defecten in de synaptische signaal overdracht dat verhoogde intracellulaire calcium niveaus en vervolgens celdood veroorzaakt. Beter begrip van de excitotoxische mechanismen veroorzaakt door de verschillende mutante SCA eiwitten zal bijdragen aan toekomstige therapeutische interventie.

Summary

In **Chapter 1**, I present a brief background on spinocerebellar ataxias (SCAs), which are autosomal dominant neurodegenerative disorders, characterized by atrophy of Purkinje cells in the cerebellum. I review the underlying genetic and molecular mechanisms of SCAs, consisting of three genetically different groups: caused by polyglutamine repeat expansions, non-coding repeat expansions or conventional mutations. Up to date, 32 types of SCAs are known, each mapped to a different genetic locus. For 22 of them the disease causing genes and mutations were identified. The identification of the causal mutations in the group of genetically undiagnosed SCA families does not only improve the diagnostic possibilities for these patients, but also provides additional insights into the underlying pathological pathways of SCA disease contributing to new therapeutic developments.

In **Chapter 2**, the impact of the V138E mutation on PKCγ lifecycle in context of SCA type 14 was studied, which is caused by missense mutations in the gene encoding for protein kinase C γ, PKCγ. We observed that SCA14-mutant PKCγ-V138E exhibited a changed protein structure, resulting in impaired dephosphorylation and degradation that led to accumulation of the mutant molecules in the Triton-insoluble fraction. Our work suggests that decreased levels of active PKCγ kinase in the soluble cellular fraction underlies the SCA14 pathology. Additionally, modifiers of PKCγ processing, like PDK1, are potential candidates to prevent the loss of active and still phosphorylated PKCγ proteins in the insoluble pool and present new therapeutic opportunities for SCA14.

In **Chapter 3**, missense mutations in *KCND3* were identified to cause SCA19, using exome sequencing in two affected members of the originally reported SCA19 family. *KCND3* encodes for $K_v4.3$, a voltage-gated potassium channel, which regulates the transient outward potassium current in the neurons. $K_v4.3$ is highly expressed in the cerebellum and participates in decreasing the postsynaptic potentials in dendrites of Purkinje cells. Screening of two hundred and thirty ataxia patients, without mutations in known SCA genes, for mutations located in *KCNC3* using high-resolution melting led to identification of two additional mutations. SCA19 brain autopsy material showed pronounced degeneration of Purkinje cells in the cerebellar vermis, similarly to the pathology seen in other SCA types caused by conventional mutations (SCA13, 15/16, 23 and 28). All SCA19-mutant $K_v4.3$ subunits exhibited endoplasmatic reticulum retention, due to impaired trafficking, leading to loss of plasma membrane localization and reduced protein stability. The regulatory subunit KChIP2 was able to rescue localization deficits and the stability of two of the three mutant Kv4.3 channel complexes, however, this did not restore channel function or only partially. Our results show that loss of $K_v4.3$ channels, only required to prevent the fast repolarization of neurons, is sufficient to cause cerebellar neurodegeneration.

The **Chapters 4, 5 and 6** describe the identification of mutations underlying SCA23, and following *in vitro*, and *in vivo* studies. The first SCA23 mutation was identified in prodynorphin, *PDYN*, by Sanger sequencing of candidate genes in the linkage interval located at chromosomal region 20p13-12.3 (**Chapter 4**). Screening of the Dutch ataxia cohort (n = 800) led to the discovery of three additional missense mutations, located in the neuropeptide Dynorphin (Dyn) A. PDYN is a precursor protein for the opioid neuropeptides α-neoendorphin, Dyn A and B. Dynorphins regulate pain processing and modulate the rewarding effects of addictive substances via opioid signaling, but the mechanisms by which Dyn A can mediate neurodegeneration in the cerebellum are unknown. The SCA23

mutations in Dyn A-coding region led to enhanced peptide levels and two of the three mutations enhanced the intrinsic toxicity of wild-type Dyn A in cultured striatal neurons. One mutation was located in the non-opioid region of PDYN and correlated with altered expression of components of the opioid and glutamate system, including EAAT4, as was evident from proteomic analysis of SCA23 autopsy tissue. Lack of EAAT4 function on the Purkinje cell membrane may cause the accumulation of excitatory glutamate in the synaptic cleft contributing to excitotoxic damage. Our findings are consistent with previous reports demonstrating alterations in expression and localization of EAAT4 in SCA1 and SCA5, and indicate that mutant Dyn A actions may lead to changes in glutamate/calcium signaling that results in SCA23 pathology.

To reveal the SCA23 disease frequency in Europe, dominant cerebellar ataxia patients of mostly French origin were screened for mutations in *PDYN* (**Chapter 5**). *PDYN* variations turned out to be rare in Caucasian ataxia cases. We identified three novel missense variations and a truncating mutation (heterozygous 2 bp deletion), leading to premature stop codon. Two missense variations correlated with enhanced Dyn A levels of which one did not co-segregated with the disease and for the other co-segregation could not be established. Therefore we could not conclude that these missense variations are indeed pathogenic. The complete loss of the Dynorphin peptides in case of the truncating mutation strongly suggests that haploinsufficiency or loss of function may also underlie SCA23. Additionally, Dyn A-coding region seems to be a hotspot for SCA23 mutations, underlining the importance of Dyn A function in the cerebellum.

To study the role of PDYN in cerebellar neurodegeneration and ataxia and to get insights into the disease mechanisms underlying SCA23, a conditional transgenic mouse model was generated that ubiquitously expresses human PDYN-R212W (**Chapter 6**). This mutation showed the most pathogenic effects in our previous *in vitro* work. We confirmed that PDYN-R212W causes cerebellar ataxia *in vivo*, as the transgenic mice displayed the disease symptoms of SCA23 patients including slowly progressive, mild motor coordination and gait deficits, and Purkinje cell loss at the age of 12 months. The SCA23-mutant transgenic mice exhibited elevated Dyn A levels in the cerebellum that seemed to be associated with decreased climbing fiber innervation of the Purkinje cells. This deficiency in climbing fiber synapses distribution started early in the course of disease and progressed in time, suggesting active elimination of climbing fiber synapses rather than developmental problems. Given the increased levels of Dyn A, which can potentiate N-methyl-D-aspartate (NMDA) receptors currents, we hypothesize that SCA23 is caused by Dyn A-mediated excitotoxic damage via NMDA receptors activation.

To further investigate the neurodegenerative mechanisms mediated by SCA23-mutant Dyn A peptides, we studied the effects of SCA23 mutations on secondary structure of Dyn A, opioid receptor affinity and cell death using selective antagonists and agonists for opioid and NMDA receptors (**Chapter 7**). All SCA23-mutant Dyn A peptides displayed marked changes of the secondary structure in the presence of membranes, mimicking the structure of Dyn A-Y1del, a peptide that does not interact with κ-opioid receptors. The SCA23-mutant peptides still interacted with κ-opioid receptor but showed reduced affinity. Additionally, for two out of three mutations, changes in the secondary structure led to more stable peptides that were almost resistant for peptidase degradation, and showed enhanced oligomerization *in vitro*. SCA23-mutant Dyn A caused marked dose-dependent

neurotoxicity in differentiated NG108 cells, mainly mediated via NMDA receptors, as specific antagonists were able to reverse these effects. We also found evidence supporting the hypothesis that opioid signaling could be neuroprotective as naloxone, an opioid receptors antagonist, in the presence of non-toxic SCA23-mutant Dyn A peptide concentrations caused pronounced cell death. Thus SCA23-mutant Dyn A peptides may exhibit dichotomous neurotoxic effects, the first through loss of neuroprotection mediated by opioid receptors, and second by excitotoxic actions via NMDA receptors.

Chapter 8 contains the discussion of the common pathomechanisms underlying the different types of SCAs, with a main focus on SCAs caused by conventional mutations such as SCA14, SCA19, and SCA23. Taken together all our results, excitotoxicity appears as a common mechanism underlying Purkinje cell death in SCA. Excitotoxicity is associated with pathological activation of ionotropic glutamate receptors (like NMDA receptors), which cause an increase of intracellular calcium concentrations that activates various enzymes, such as endonucleases, phospholipases, and proteases, resulting in fragmentation of DNA, and cytoskeleton and membranes components. Compounds blocking excitotoxicity may be useful in future therapies of SCAs. Anti-excitotoxic drugs like riluzole already have been shown to partially alleviate ataxic symptoms in patients with cerebellar ataxias and are currently being tested in clinical trials.

To conclude, the SCAs form a genetically heterogeneous group of diseases; however, a common molecular pathology may exist as patients with different SCA types display similar disease phenotypes. In this thesis, SCA14, SCA19 and SCA23 were studied, all caused by conventional mutations, but in different, and seemingly functionally non-related genes. The SCAs caused by conventional mutations usually exhibit purer, more isolated cerebellar phenotype, with neuronal loss restricted only to the cerebellum. Therefore, this group is a more accurate model to study pathomechanisms underlying selective Purkinje cell loss than other SCA types. Our work points into excitotoxicity as a common pathology underlying SCA14, SCA19 and SCA23, as all mutant proteins are associated with defects in synaptic transmission that may lead to elevated intracellular calcium concentrations and subsequent neuronal cell death. Better understanding of the excitotoxic mechanisms caused by various mutant SCA proteins will contribute greatly to future therapeutic interventions.

Acknowledgements

I would like to acknowledge all the people who helped me during the PhD period, including: i) Ataxia group, collegues from the lab and collaborators for nice working environment, ii) friends and family in Poland for their support and 'being there for me', and iii) housemates and friends in the Netherlands for lots and lots of fun, all the trips and psychotherapy ;)

Special thanks to my supervisor, Dineke, who took care of me, trained me, and made me a better, more independent scientist.

Also, many thanks to Richard and Harrie for being my promotors, helping me out with the thesis, and for lively discussions along the way; and to Prof.dr H. van Bokhoven, Prof.dr H.P.H. Kremer, and Prof.dr O.C.M. Sibon for being a part of the assessment committee for my thesis, for taking the time to read it and for giving their approval for the defense. And I also thank Lovebird and Eikon for taking the burden of the thesis design, edition and printing from me!

I am very grateful for all the friendships that I've made during my PhD. Special thanks to Tonka, Paulina and Łukasz, Ba'ra, Aśka, Marcin, Nika, Sylwia, Kamila, Gosia, Reto, Aga, Andrius, and Ania for sharing everyday life with me. Również, dzięki wielkie za bycie moimi paranimfami, girls! ;) Also, thanks to Thomas, Marta, Genia, Gimon, Juha, Anna P., Olga, Marcus, Jesse, and other GRASP/Gopher members for fun time, not only during board meetings ;) I've enjoyed our bowling, drinking, BBQs and trips. Also, many, many, many thanks to Roy and Plaza Danza, Martin, Marta, Eelco, Luc, Jesse, Kees, UDC and USVA for the dance and the dancing along the way ;)

And last but not least, thanks to my best'ies and family. Wiem, że nie muszę wymieniać Was z imienia i nazwiska ;) Jestem wdzięczna za każdą chwilę, każdego maila, każde odwiedziny i fakt, że mimo odległości i prawie braku czasu dla siebie nic się nie zmieniło w naszych stosunkach i nadal z Wami czuję się 'jak w domu'. Buziaki i ściski :*